Exploration of Dissolved Inorganic Carbon and Dissolved Organic Carbon in Hot Springs within Yellowstone National Park

by

Tanner Barnes

A Thesis Presented in Partial Fulfillment
of the Requirements for the Degree
Master of Science

Approved June 2023 by the
Graduate Supervisory Committee:

Everett Shock, Chair
D'Arcy Meyer-Dombard
Hilairy Hartnett

ARIZONA STATE UNIVERSITY

December 2023

ABSTRACT

Dissolved inorganic carbon (DIC) and dissolved organic carbon (DOC) are crucial nutrients for autotrophic and heterotrophic microbial life, respectively, in hydrothermal systems. Biogeochemical processes that control amounts of DIC and DOC in Yellowstone hot springs can be investigated by measuring carbon abundances and respective isotopic values. A decade and a half of field work in 10 regions within Yellowstone National Park and subsequent geochemical lab analyses reveal that sulfate-dominant acidic regions have high DOC (Up to 57 ppm C) and lower DIC (up to 50 ppm C) compared to neutral-chloride regions with low DOC (< 2 ppm C) and higher DIC (up to 100 ppm C). Abundances and isotopic data suggest that sedimentary rock erosion by acidic hydrothermal fluids, fresh snow-derived meteoric water, and exogenous carbon input allowed by local topography may affect DOC levels. Evaluating the isotopic compositions of DIC and DOC in hydrothermal fluids gives insight on the geology and microbial life in the subsurface between different regions. DIC $\delta^{13}C$ values range from -4‰ to +5‰ at pH 5-9 and from -10‰ to +3‰ at pH 2-5 with several springs lower than -10‰. DOC $\delta^{13}C$ values parkwide range from -10‰ to -30‰. Within this range, neutral-chloride regions in the Lower Geyser Basin have lighter isotopes than sulfate-dominant acidic regions. In hot springs with elevated levels of DOC, the range only varies between -20‰ and -26‰ which may be caused by local exogenous organic matter runoff. Combining other geochemical measurements, such as differences in chloride and sulfate concentrations, demonstrates that some regions contain mixtures of multiple fluids moving through the complex hydrological system in the subsurface. The mixing of these

fluids may account for increased levels of DOC in meteoric sulfate-dominant acidic regions. Ultimately, the foundational values of dissolved carbon and their isotopic composition is provided in a parkwide study, so results can be combined with future studies that apply different sequencing analyses to understand specific biogeochemical cycling and microbial communities that occur in individual hot springs.

ACKNOWLEDGMENTS

I have received great support from many individuals throughout my research toward this master's degree. First and foremost, I thank my advisor Everett Shock for believing in me and providing support throughout the completion of this degree. I was presented with countless opportunities, and I was able to complete field work in Yellowstone due to Everett's support. I would also like to acknowledge my other committee members, D'Arcy Meyer-Dombard and Hilairy Hartnett, who have made a great contribution to my career and have given me advice.

Next, I would like to acknowledge past and present members of the GEOPIG lab. Specifically, Jordyn Robare and Randall "Vince" Debes for their immense support in helping me get on my feet within the lab. I also would like to thank the Yellowstone Park Service for allowing us to complete research in Yellowstone and none of this would be possible without their protection.

Lastly, I would like to acknowledge my family and friends for their support throughout my journey in graduate school. None of this would have been possible without their constant loving support.

TABLE OF CONTENTS

Page

CHAPTER Page

LIST OF TABLES

Table Page

LIST OF FIGURES

Figure Page

Figure Page

Figure Page

Figure Page

Figure Page

CHAPTER 1

INTRODUCTION

Yellowstone National Park is home to over 10,000 unique thermal features and a vast diversity of wildlife and organisms. Thermal features in Yellowstone are powered primarily by meteoric water that has infiltrated the subsurface over varying temporal scales and circulating at depths of 100-550m (Fournier 1989; Lowenstern and Hurwitz 2008). While conventional meteoric infiltration typically yields ponds and rivers, the presence of an underlying volcanic structure within Yellowstone National Park leads to a unique phenomenon where water becomes superheated and infused with volcanic gases, giving rise to distinctive thermal features such as the hot spring compared with a pond in Figure 1.1. Ponds and hot springs share geologic, geochemical, hydrologic and biological processes, and hot springs are affected by additional contributions of the underlying hydrothermal system.

The precise extent to which each volcanic process influences the composition of thermal fluids in individual hot springs remains an ongoing investigation. Traditionally, the characterization of fluid in hot springs has relied on the plotting of sulfate (SO_4^{-2}) concentration against chloride (Cl^-) concentration (Nordstrom et al., 2009). This approach suggests that an increase in SO_4^{-2} concentration signifies heightened volcanic gas input, while an elevation in Cl^- concentration indicates greater water-rock interaction as illustrated in Figure 1.2. Lower concentrations tend to mirror those of rain or snow samples that have yet to be influenced by the thermal hydrological system. Nonetheless, an exclusive reliance on SO_4^{-2} and Cl^- concentration profiles to elucidate the primary

processes influencing a given hot spring proves to be inadequate. Multiple dynamic factors, including gas injection, boiling and evaporation, water-rock interactions, and varying degrees of fluid mixing, can all conspire to modify the measured levels of SO_4^{-2} and Cl^-.

As illustrated in Figure 1.3, there are many combinations of processes that can lead to a point where different histories of fluids undergoing distinct processes may produce identical values in the SO_4^{-2} vs. Cl^- concentration plot. Hypothetical case 1 shows a mixture, represented by the star, made from a fluid that has undergone a large gas addition increasing sulfate with another fluid that has undergone deep boiling with water-rock interactions increasing the concentration of chloride. The same concentrations of sulfate and chloride can be reached for hypothetical case number 2 representing a fluid that has undergone boiling and evaporation with some gas additions. These are just two scenarios among infinite possibilities of mixtures between different processes to reach identical concentrations of sulfate and chloride with different fluid histories. Consequently, the opportunity arises to incorporate additional variables into the analytical framework that can facilitate more nuanced and comprehensive understandings of the dominant processes at play in each hot spring.

As demonstrated in this thesis, dissolved inorganic carbon (DIC) and organic carbon (DOC) serve as invaluable metrics for helping to unravel the dynamic processes occurring within thermal fluids. Concentration of DIC is helpful in gauging the extent of gas injection similar to the role of sulfate (SO_4^{-2}) in quantifying the influence of the volcanic system below. On the other hand, DOC concentrations are useful due to their

capacity to signify the presence of meteoric infiltration in a hot spring, which represents the influence of the system at the surface. Elevated DOC concentrations indicate a greater influence of meteoric water, while lower concentrations point to the dominance of deeply sourced, thermally altered organic carbon. Combining DIC and DOC concentrations can help to quantify both the subsurface and the surface influences on the surrounding hydrothermal system responsible for individual springs.

Isotopic measurements of both DIC and DOC further enrich our understanding of the various processes at play. The $\delta^{13}C$ versus VPDB values of inorganic carbon sourced from the mantle range from −5‰ to -8‰ (Deines, 2002), while values can exhibit a broader range of +5‰ to −35‰ in a typical pond system (Campeau, 2017). Consequently, this wide range makes it imperative to isolate the processes affecting $\delta^{13}C$ signature to avoid misinterpretation. As an example, if the $\delta^{13}C$ values are heavier than the mantle signature, this could signify the dominance of boiling or evaporation within a given hot spring. If values $\delta^{13}C$ are lighter than mantle sources in the area, microbiology may be influencing these values through oxidation of isotopically light DOC. In the case of DOC, the $\delta^{13}C$ values become a potent tool for distinguishing the type of water present in the system, as they can be compared to the isotopic signatures of the surrounding vegetation. Meteoric fluid typically exhibits a photosynthetic signature depending on if nearby plants are dominantly C_3 (-20‰ to -37‰) or C_4 (-10‰ to -16‰). Nearly all known taxa (97%) within Yellowstone National Park uses the C_3 photosynthetic pathway (Feranec, 2007). In contrast, thermal alteration of DOC in deeply sourced fluids can

display an enriched $\delta^{13}C$ signature relative to DOC derived from local vegetation (Kirkels, 2022).

The combination of these approaches, in conjunction with the SO_4^{-2} and Cl^- concentrations, furnishes a robust methodology for inferring the underlying processes influencing thermal fluids in distinct hot springs as documented here.

Within this study, DIC and DOC concentrations and their respective $\delta^{13}C$ values are explored in 10 regions of Yellowstone with data from 2005-2019. This introduction provides insights into the geologic setting of Yellowstone National Park, prior literature pertaining to Yellowstone, an overview of hot spring features, and conceptual models elucidating the role of both DIC and DOC.

Geological History of Yellowstone

Yellowstone hot springs are powered by a mantle plume under the North American tectonic plate. This mantle plume arose ~16 million years ago under present day Oregon (Pierce et al., 2009). Plate movement occurred over time resulting in the plume beneath Yellowstone National Park by about 2 Ma. The Yellowstone Plateau itself reflects the persistent upwelling of volcanic activity associated with the hot spot, characterized by the emission of rhyolitic lavas and tuffs. Rhyolite, being notably nutrient-poor, plays a pivotal role in sustaining the lodgepole pine forests that thrive in the region.

Signature features of mantle plumes are large caldera eruptions. The most recent significant eruption occurred approximately 640,000 years ago, marking the formation of

the most recent major caldera within Yellowstone. This event resulted in the creation of a vast depression, measuring approximately 40 by 65 kilometers, which became filled with rhyolitic lava flows (Christiansen, 2001; Stelten, 2023).

How hot springs form

Yellowstone National Park features a variety of hot springs, which are mixtures of groundwaters of varying ages that have circulated to different depths as well as local meteoric water. Groundwater is sourced from local precipitation and becomes hydrothermal fluid as it travels deep underground through porous rhyolite tuff, heating up to 350-450°C (Fournier, 1989). Along this journey, hydrothermal fluids accumulate chloride, leading to a distinctive chloride signature in hot springs dominated by the deep hydrothermal system. Some hot springs also have elevated sulfate levels, indicating a strong influence of volcanic gases (Nordstrom et al., 2009). This distinction leads to the categorization of Yellowstone's hot springs into two groups: acid-sulfate dominant and neutral-chloride abundant hot springs. In this study I explore these groups and their impact on dissolved inorganic carbon (DIC) and dissolved organic carbon (DOC) levels based on the specific hydrothermal processes involved.

Neutral-chloride hydrothermal fluids sourced from groundwater reservoirs contain notable chloride levels (300-600 mg/L) and are heated to temperatures between 180-270°C at depths ranging from 100-550 meters below the surface (Fournier, 1977). Analyzing chloride levels in hot springs provides insights into the intricacies of subsurface hydrology and the primary water-rock influence. Hot springs rich in chloride originate from deeper reservoirs, and often exhibit minimal variations in geochemical

measurements over time. These systems remain geochemically consistent including nutrient availability for local microorganisms. Many neutral-chloride springs are found in the Upper, Midway, and Lower Geyser Basins and often have substantial siliceous sinter deposits. This study focuses on springs matching this profile, occurring in Sentinel Meadows, White Creek, Geyser Creek, and other thermal areas.

Acid-sulfate dominance arises from hydrothermal boiling beneath the surface, generating vapor. This vapor, along with volcanic gases, is transported through vertical fractures in the rock to the surface. It is hypothesized that this steam heats local groundwater aquifers, which are supplied by meteoric water, and directly charges them with hydrothermal gases (Fournier, 1989). Consequently, these aquifers have low chloride levels, as chloride is not transported through the vapor phase, and water-rock interaction is limited. The influx of volcanic gas rich in SO_2 disproportionates as it enters hot water. Sulfate is generated as sulfuric acid which renders the pH of these hot springs acidic (Nordstrom et al., 2009).

DIC data can contribute to efforts to understand the processes leading to neutral chloride springs and acid sulfate springs since the major sources of DIC and sulfate are the underlying volcanic system. In turn, DOC values can reveal mixing of shallow water with hydrothermal fluid to characterize the history of complex fluid pathways by quantifying the amount of surface influence on specific hot springs, as shown in Chapter 3. DOC concentrations in hot springs are influenced by connections to the local meteoric groundwater system as well as alteration or consumption by microbes.

A comprehensive comparison of DIC and DOC concentrations, combined with $\delta^{13}C$ values, across a diverse array of Yellowstone's hot springs has not been conducted at a large scale. This research described in this thesis establishes baseline values for various Yellowstone regions, providing essential context for future studies on DIC and DOC signatures. Additionally, concentrations and isotopic signatures of DIC and DOC are linked in this study with other geochemical measurements and techniques, offering a robust foundation for formulating hypotheses about hydrology and biological processes in specific hot springs. Furthermore, outlier hot springs, which are now of particular interest for future investigations, are identified. In the remainder of this introductory chapter, several scenarios are presented for interpreting DIC and DOC concentrations and isotopic compositions that illustrate processes of delivery to hot springs.

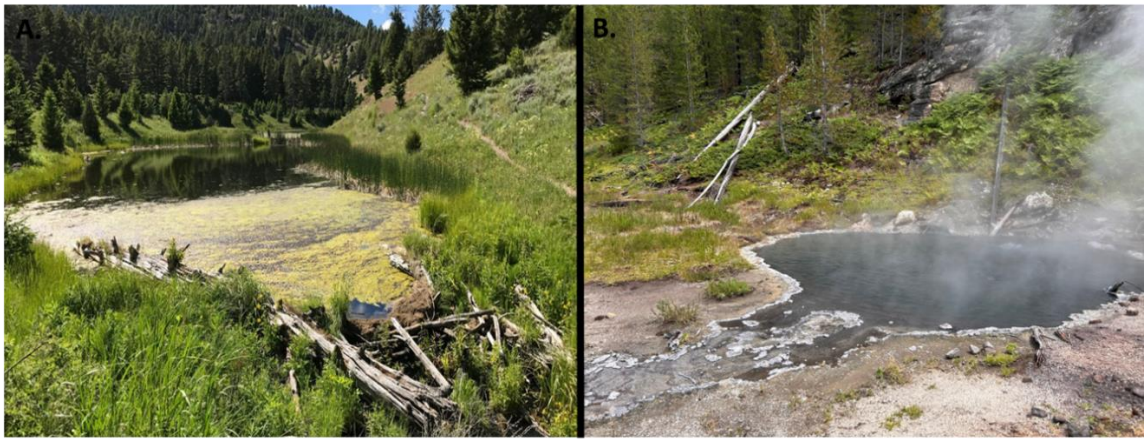

Figure 1.1: This figure displays a picture of (left) a pond in a forest at Beaver Pond Trail (USGS), compared with a hot spring (right), both located in Yellowstone National Park (right image taken under Permit YELL-SCI-5434).

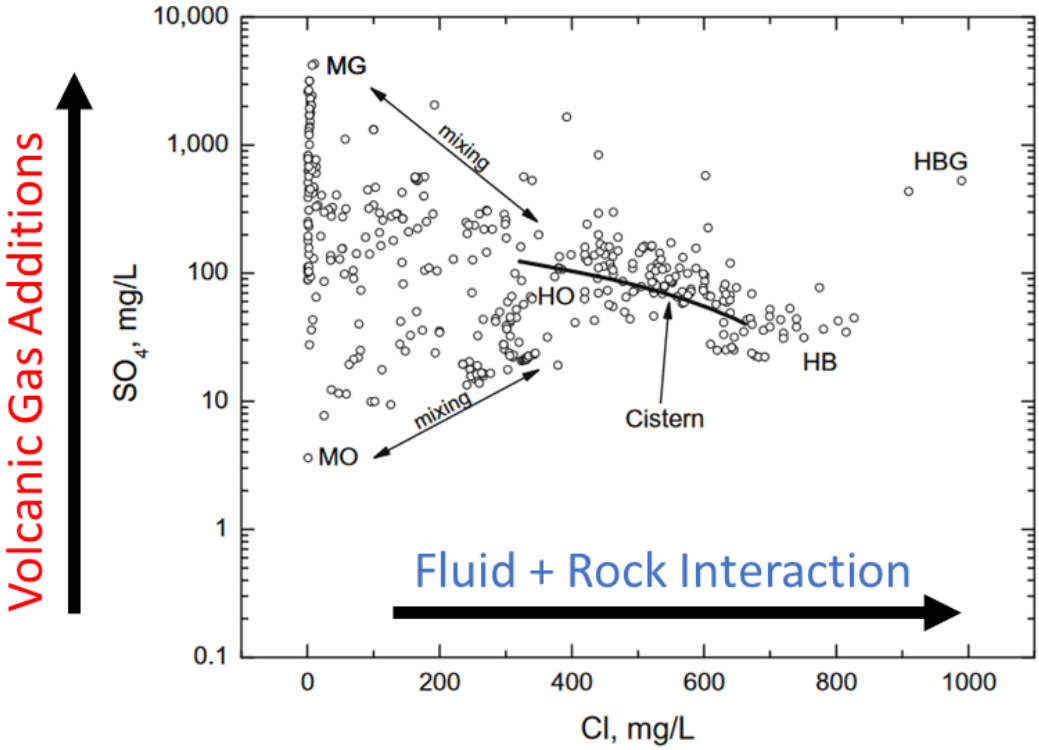

Figure 1.2: This is a modified figure from Nordstrom et al. (2009) with arrows added to indicate inferred trends of response to geochemical processes.

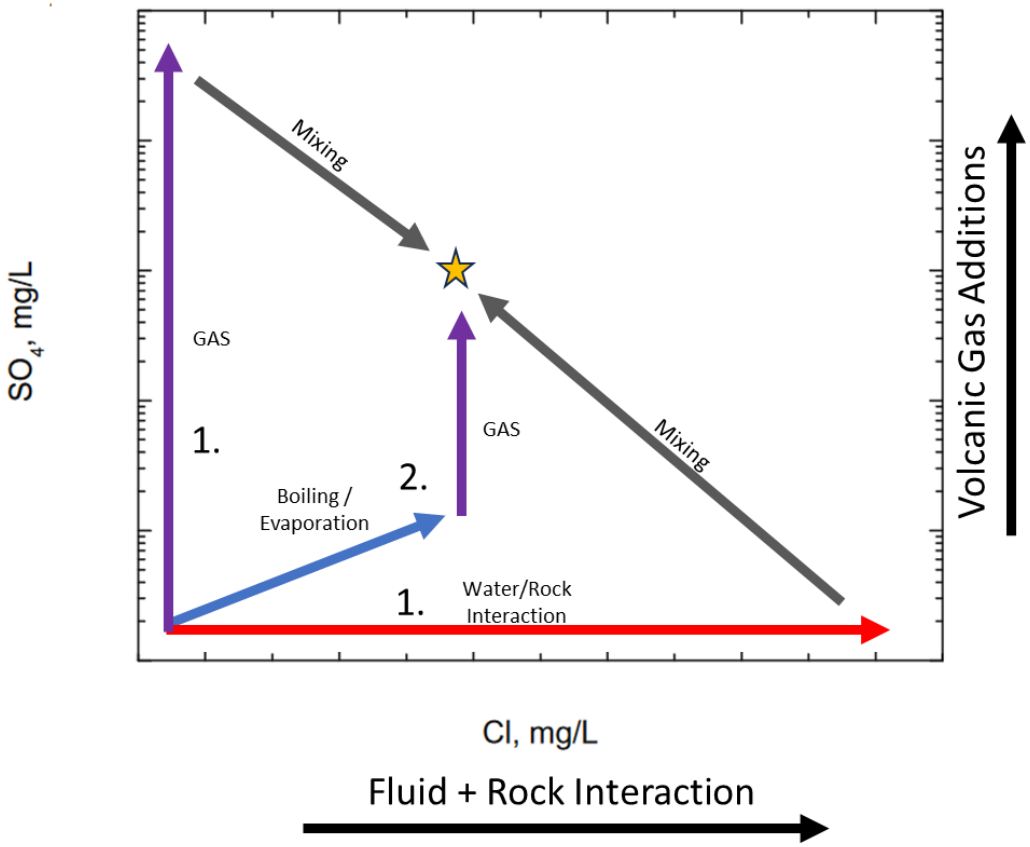

Figure 1.3: A plot of SO_4^{-2} vs. Cl^- depicting two scenarios through which different fluid pathways lead to the same composition. The first possibility is that two fluids with widely divergent histories mix. The second path is a combination of processes affecting a single fluid. Sulfate and chloride concentrations alone cannot distinguish among such scenarios.

DIC Pathways

Dissolved inorganic carbon (DIC) in hydrothermal systems influences fluid chemistry, mineral precipitation, and, ultimately, the environmental conditions that can support diverse forms of life. In solution, DIC speciates into various forms, such as bicarbonate (HCO_3^-), carbonate (CO_3^{2-}), and carbonic acid ($CO_{2\,(aq)}$), depending on

factors like pH and temperature as shown in Fig. 1.4. The curves in this figure separate fields of relative predominance of these three forms of DIC.

As alluded to by Fig 1.1, several processes that affect concentrations of DIC in are shared by surface aquatic systems such as ponds and hot springs. Therefore, a direct comparison can help to identify those processes unique to hot spring systems. The left panel of Fig 1.5 shows a typical groundwater system supporting a pond in a forested ecosystem. Dominant processes affecting how DIC circulates in the system are atmospheric exchange (A), infiltration (B), and respiration of organic matter in the pond itself. The infiltration process can transport DIC derived from water-rock reactions and microbial respiration in surrounding soil. The gold stars in Figure 1.5 indicate that microbial activity that can produce and consume DIC is present in the pond, hot spring, and within the surrounding soil.

The right panel of Fig 1.5 shows the increased complexity of sources and delivery processes affecting DIC when a magmatic source is introduced into the system. In this case, DIC is sourced from CO_2 in the atmosphere (A), microbiological production through the oxidation of DOC in both the hot spring and surrounding soil (B), and CO_2 released at depth from the crystalizing magma (C). Another potential source may be from underlying sedimentary rocks encountered by the deeply circulating fluid. Figure 1.5 also contains schematic diagrams showing predictions of effects on concentration of DIC from several delivery processes.

Effects on DIC concentrations

Ways in which various processes can affect the concentration of DIC in hot springs are illustrated schematically in the lower panel of Fig 1.5. Processes I, II and III are unique to hot springs, while processes IV and V would affect both ponds and hot springs. Distinct rock types possess the capacity to release inorganic carbon into the fluid; however, Yellowstone's predominant rock type rhyolite is notably carbon poor. Therefore, DIC contains little if any carbon extracted directly from the rhyolite during hydrothermal alteration. However, gases associated with rhyolitic silicate melts contain H_2O, CO_2, SO_2 and many other volatile species at lower abundances (Lowenstern, 2015). Volcanic CO_2 can be added to hydrothermal fluids from magma degassing, including the processes of magma solidification and crystallization in which volatiles like CO_2 are expelled. Degassed CO_2 can then contribute to water-rock reactions (I) as carbonic acid appearing in solution as DIC speciated as shown in Fig 1.3. In addition, sedimentary rocks could be present in some areas where carbonate minerals could release DIC through water-rock reactions. Deeply circulating fluids driven by heat flow can transport this DIC upward through the system. In a neutral-chloride spring this will increase the amount of DIC mainly in the form of bicarbonate in the fluid. Processes in acidic springs can be more complicated because CO_2 is a constituent of the volcanic gases (III) that drive fluids to low pH, and deep additions of CO_2 can escape into the atmosphere from acidic springs. Hydrothermal fluids can undergo varying degrees of boiling and evaporation (II) leading to an increase in the overall concentration of DIC in neutral-

chloride springs. Conversely, in acidic springs, boiling and evaporation will reduce DIC concentration, as DIC will transform into CO_2, departing as a gas.

Processes influencing DIC content of both ponds and hot springs include the diffusion of atmospheric CO_2 across the surface, and atmospheric exchange of CO_2 in local water, which can have the effect of increasing the concentration of DIC in the water depending on pH (not depicted in lower part of Fig 1.5). In addition, microbial processes within a pond or hot spring can consume or produce DIC (IV). Autotrophy, including chemotrophy and photosynthesis if conditions allow, involves uptake of CO_2 and can lead to a decrease in DIC. Meanwhile, heterotrophs in a hot spring or pond uptake organic carbon and can release CO_2, contributing to DIC. In the case of Yellowstone, the effectiveness of microbial processes may not predominate when compared to the input from the volcanic system beneath, depending on relative rates. Infiltrating water contains DIC from atmospheric exchange as well as DIC from microbial productivity in soils that affect local groundwater. As a result, infiltration (V) can cause an increase in DIC depending on the amount of water that flows into the system and internal rates of microbial activity.

Effects on $\delta^{13}C$ of DIC

The processes affecting DIC delivery induce alterations and transformations, which can be assessed through examination of the DIC $\delta^{13}C$. The $\delta^{13}C$ signature of the mantle, primarily -5‰, is believed to be universally consistent, with a smaller extent of

input ranging from -22‰ to -26‰ (Deines, 2002). In 2023, atmospheric CO_2 currently carries a $\delta^{13}C$ signature of -8‰, with a concentration of 424 ppm, and its total concentration is increasing due to fossil fuel combustion, depleting ^{13}C (NOAA,2023).

Figure 1.6 outlines projected trends in DIC $\delta^{13}C$ values in response to various hydrothermal processes. The red arrow (I) illustrates the influence of increasing water-rock interactions on DIC $\delta^{13}C$ values. Notably, the carbon-poor nature of rhyolite has minimal impact on this signature. The dashed line signifies the potential interaction of fluids with sedimentary rocks, as observed in specific Yellowstone regions containing ancient, buried sediments (Fouke, 2011). Such interactions result in a depleted DIC $\delta^{13}C$ signature, given the biogenic origin and processing of many sedimentary carbonates.

Elevated levels of boiling introduce a slight enrichment in DIC $\delta^{13}C$ values, attributed to ^{12}C entering the vapor phase faster than ^{13}C; this trend is indicated by the purple arrow (II). A similar enrichment occurs in biological carbon fixation pathways, which show preferences for ^{12}C. This topic is explored further below in the autotrophic section of the DOC pathway. The yellow arrow (III) indicates that DIC $\delta^{13}C$ can be influenced by both autotrophic consumption and heterotrophic production of CO_2. The degree to which production affects the DIC $\delta^{13}C$ signature remains unclear, denoted by a dashed line.

These small fractionations combined with varying degrees of mixing will lead to distinct isotopic signatures of DIC in the system. It is unclear to what extent these small fractionations impact the overall signature, so it is important to try and identify and separate out each possible process to avoid misinterpretation. Plotting concentrations of

DIC concentration versus chloride can be useful for identifying various processes like boiling and dilution (Hearn, 1990). Specifically, increasing chloride levels alongside decreasing DIC concentrations indicate springs that have undergone boiling, resulting in the release of steam at depth. Boiling causes the removal of CO_2, limiting bicarbonate formation, and leads to an increase in chloride concentration. The combined effects of chloride, boiling, and evaporation are predicted in Figures 1.5 and 1.6, and the findings are discussed in Chapter 3 when comparing DIC concentrations across specific regions.

The unique $\delta^{13}C$ signature observed in each hot spring results from a complex interplay of delivery pathways, further influenced by the fractionation of carbon isotopes during local microbial metabolism. In essence, the concentration and isotopic values of DIC serve as tracers, revealing the influence of the underlying volcanic system on the groundwater dynamics. To understand the entirety of this system, the subsequent section will elucidate the various processes affecting DOC, serving as a proxy to quantify the impacts of surface and shallow subsurface influences.

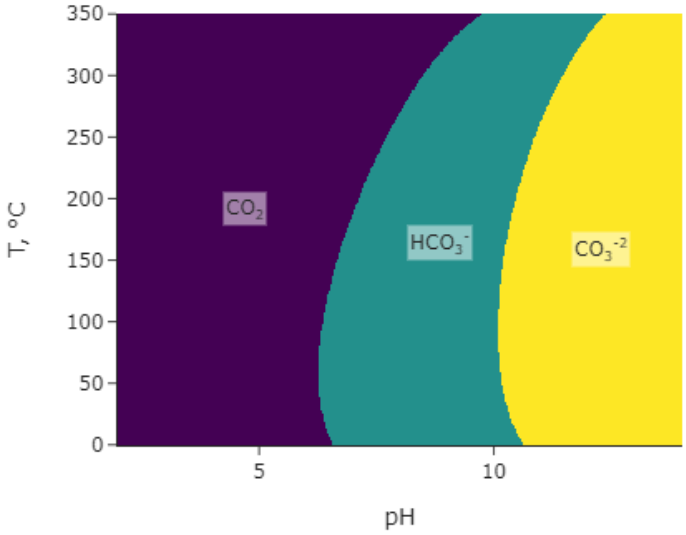

Figure 1.4: This relative stability diagram shows what species are dominant in the fluid when H_2O and CO_2 are reacting at different pH and Temperatures. The shaded regions indicate which species are dominant. This figure was generated in WORM (Boyer, 2021).

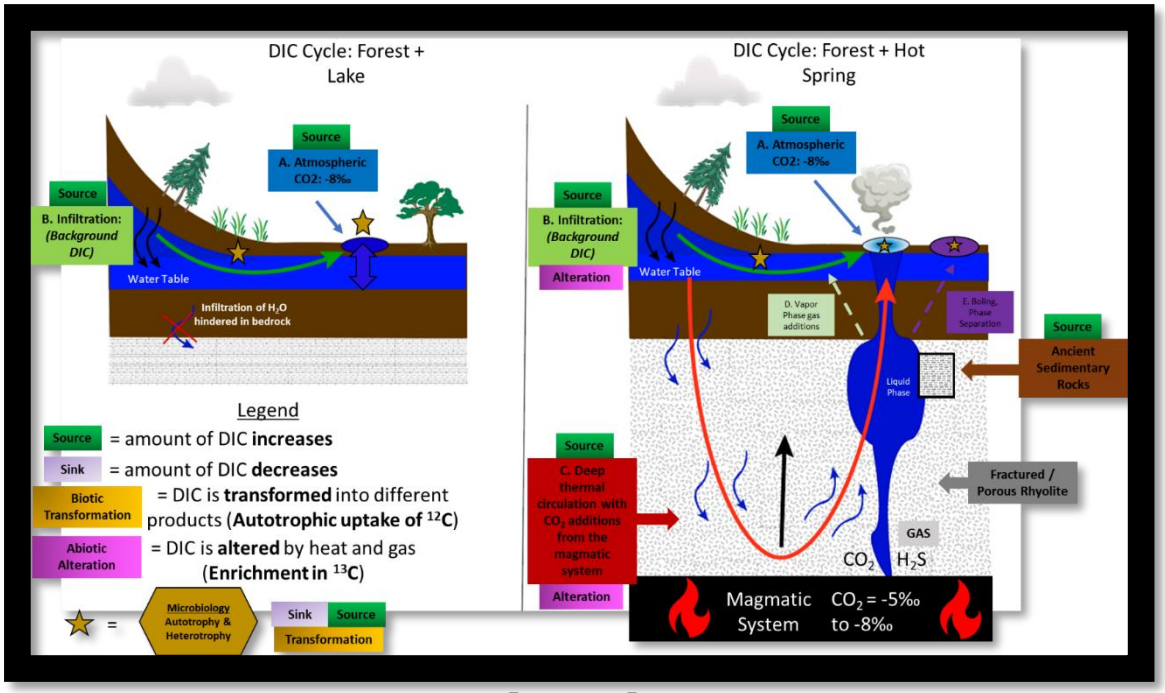
DIC Cycle: Forest + Lake
Source
A. Atmospheric CO2: -8‰
Source
B. Infiltration: (Background DIC)
Water Table
Infiltration of H2O hindered in bedrock
Legend
Source = amount of DIC increases
Sink = amount of DIC decreases
Biotic Transformation = DIC is transformed into different products (Autotrophic uptake of 12C)
Abiotic Alteration = DIC is altered by heat and gas (Enrichment in 13C)
Microbiology Autotrophy & Heterotrophy
Sink
Source
Transformation
DIC Cycle: Forest + Hot Spring
Source
A. Atmospheric CO2: -8‰
Source
B. Infiltration: (Background DIC)
Alteration
Water Table
D. Vapor Phase gas additions
E. Boiling, Phase Separation
Source
Ancient Sedimentary Rocks
Liquid Phase
Source
C. Deep thermal circulation with CO2 additions from the magmatic system
Fractured / Porous Rhyolite
GAS
CO2
H2S
Alteration
Magmatic System
CO2 = -5‰ to -8‰

[DIC]

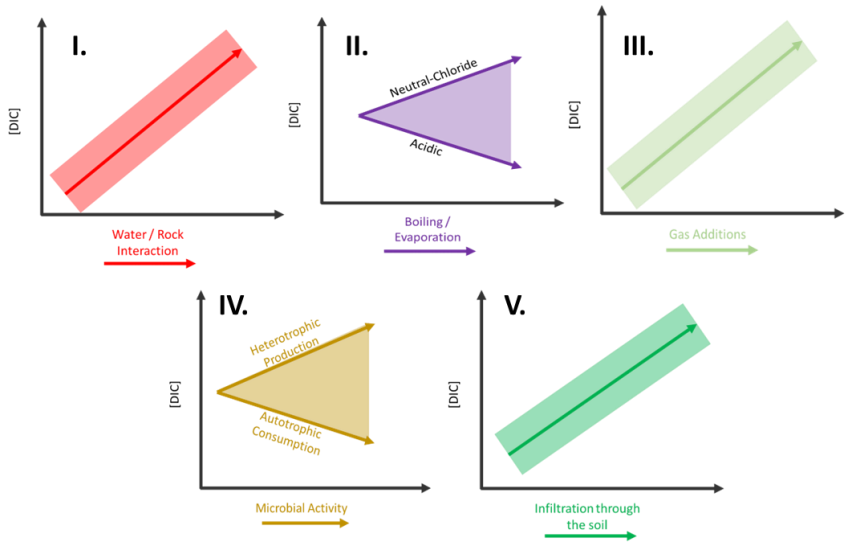
I.
[DIC]
Water / Rock Interaction
II.
Neutral-Chloride
Acidic
[DIC]
Boiling / Evaporation
III.
[DIC]
Gas Additions
IV.
Heterotrophic Production
Autotrophic Consumption
[DIC]
Microbial Activity
V.
[DIC]
Infiltration through the soil

Figure 1.5: Schematic depiction of DIC pathways by contrasting a pond with a hot spring system. Below the schematic are arrows depicting how the concentration of DIC will be affected by different processes in either a neutral-chloride or acidic hot spring.

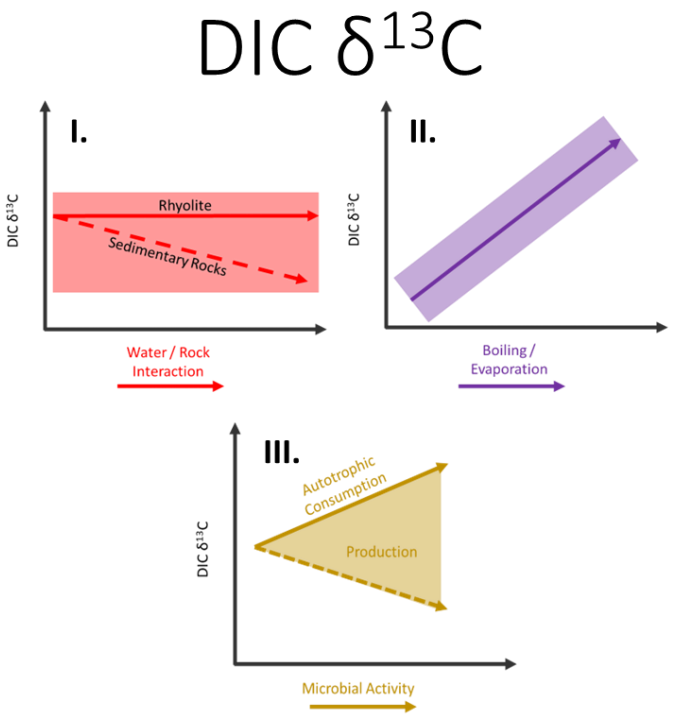

Figure 1.6: General trends of DIC $\delta^{13}C$ as results of various processes affecting the isotopic concentration of carbon. These processes are those shown schematically in Figure 1.5.

DOC Pathways

The main source of dissolved organic carbon (DOC) to either a pond or a hot spring is the surface environment, as illustrated in Fig 1.7. DOC in a typical system is regulated by photosynthetic plant material that is contributed to soils where it is a nutrient for local microbiology and altered/transformed. DOC derived from decomposing plant

material can then be transported through shallow groundwater flow. Additions of DOC by shallow transport through the soil to a pond or a hot spring are possible when there is rain or snowmelt. Occasional storms can add pulses of DOC and may even induce overland flow allowing material to be moved throughout the surface and subsurface (either panel of Fig 1.7)

However, when a hydrothermal system is introduced, additional new processes drive increases or decreases in DOC concentration as illustrated in the right panel of Figure 1.7. As a consequence, DOC can be sourced, altered, and transformed in hot spring systems differently than in ponds. As in a pond system, DOC is primarily sourced in hot springs from surrounding photosynthetic material and biological processing to create organic compounds. The derived DOC is transported along pathways shown in Fig 1.7: A. Direct Delivery, B. Infiltration: Surface Derived Vegetation, C. Deep Thermal Circulation with Water/Rock Interactions. These delivery processes have consequences for the concentration of DOC. In addition, hydrothermal influences can also affect the $\delta^{13}C$ signature of DOC. The combination of these isotopic and concentration changes allows the use of DOC as a sensitive tracer of fluid history.

Other processes summarized in Fig 1.7 also lead to the alteration and transformation of DOC including: D./E. Phase Separation, and F. Microbiological Processing. Each of these processes can affect both concentration of DOC and its $\delta^{13}C$ signature further expanding the potential of DOC as a tracer of fluid history.

In the following discussion a conceptual model of processes affecting DOC is developed with the goal of identifying hot springs and thermal regions that are dominated

by specific subsets of hydrothermal processes. Linkages are proposed between processes affecting DOC and the response of DOC concentrations and isotopic composition. Particular detail is devoted to how to identify these processes though data analysis. Mixing among various pathways produced complex DOC responses in many thermal areas, which complicates interpretation of the data. By focusing on effects of each process, evidence can be found in DOC data that allow hot spring fluid pathways/histories to be separated from one another as shown in Chapter 3. These techniques are useful to understand how the local environment affects each hot spring.

Direct Delivery

Direct Delivery, depicted by the blue arrow (A) in the right panel of Figure 1.7, involves the introduction of freshly produced organic carbon from local vegetation, similar to a hydrological system affecting a typical pond. The environmental resemblance between hot springs and ponds, as seen in Figure 1.1, highlights the parallel nature of their surroundings. Direct Delivery to hot springs can occur through physical disturbances, such as fallen trees, or via overland delivery due to weather events that transport exogenous organic carbon. Yellowstone experiences approximately 150 inches (380 cm) of annual snowfall, together with rain and wind. Taken together, these weather events can introduce local exogenous carbon into hot springs through overland flow. The extent of this introduction hinges on various factors, including the local vegetation types, local topography surrounding hot springs, and the magnitude of the weather events. The effects of Direct Delivery are therefore seasonally tied to precipitation and vary with each

event. This concept is intricately linked to Yellowstone's weather system and is independent of the volcanic source below. Hot springs influenced by this delivery method may exhibit a diverse array of life, owing to the variability in nutrients they receive. It should be noted that hot springs reliant on “Direct Delivery” for DOC may respond rapidly to climate fluctuations due to this proposed reliance on exogenous carbon and energy.

“Direct Delivery” influences the isotopic composition, resulting in a $\delta^{13}C$ - depleted DOC due to the inflow of photosynthetic material. Therefore, the isotopic composition will be noticeably depleted in a hot spring that typically has an enriched ^{13}C signature. However, a hot spring with a dominant photosynthetic $\delta^{13}C$ signature will not change due to a storm event as more depleted photosynthetic material is washed into the hot spring (see Fig. 1.8: I.) There will however be a change in concentration that could be noticeable in this case (see Fig. 1.7: I.)

A single precipitation event can perturb these systems for several days, a phenomenon explored further in Chapter 4 of this thesis, including specific examples before and after different weather events showing how both [DOC] and $\delta^{13}C$ values are affected indicating additional exogenous carbon into the hot spring system.

Infiltration: DOC from Surface-Derived Vegetation

Infiltration, as classified in this model, refers to DOC derived from organic material from the surface ecosystem that has entered the soil, been altered, and

subsequently circulated within the subsurface hydrology and groundwater system. This material is older and more processed than the material from Direct Delivery, having at least started the decomposition process. Much like Direct Delivery, this process is ongoing in any hydrological system transporting organic material through the groundwater system. In this conceptual model, as infiltration increases there is a corresponding rise in the concentration of DOC (see Figure 1.7: I.). The influx of photosynthetic organic carbon through infiltration can lead to a depletion of ^{13}C isotopes in the system (see Figure 1.8: I.).

However, this material can also undergo some alteration from volcanic gases in two distinct processes. Phase separation is the process where gaseous species divulge from the fluid in the subsurface and gas injection is where volcanic gas is increased due to the crystallizing magma. Phase separation and vapor injections of gas are actively affecting hydrothermal fluid, ultimately heating the organic carbon in the shallow subsurface. While gas additions do not alter the DOC concentration, the heat associated with volcanic gas can diminish the organic carbon concentration (see Figure 1.7: II.). This alteration also affects the $\delta^{13}C$ signature by enriching the fluid in ^{13}C (see Figure 1.8: II.).

Additionally, DOC can be produced and consumed by microorganisms in the surrounding soil and added through infiltration, in the heated subsurface, or in the hot spring itself. This means that changes in concentration result from combinations of these processes occurring simultaneously, adjacently, or juxtaposed (see Figure 1.7: III.). The $\delta^{13}C$ DOC signature influenced by microbiology will also reflect a mixture of processes

(see Figure 1.8: III.). The preferential uptake of ^{12}C by autotrophic organisms leads to DOC being enriched in ^{13}C. The consumption of organic carbon by heterotrophs may or may not impact the isotopic composition of DOC.

These diverse combinations render the effects of infiltration complex and challenging to measure. As a result, it occupies a position intermediate between the endmembers of direct delivery and thermal alteration. Some hot springs will be more affected by infiltration than others. I hypothesize that hot springs depositing sinter will be significantly less impacted by infiltration than other springs. The formation of sinter creates a lower-permeability armored tube that inhibits the penetration of groundwater from the shallow subsurface (see Figure 1.9). Sinter-clad hot springs displaying the phenomenon of low infiltration are discussed further in Chapter 3.

Deep Thermal Circulation with Water/Rock Interactions

The process of Thermal Alteration primarily affects DOC that has undergone prolonged processing and has traveled deep into the subsurface. This DOC is subjected to high temperatures and pressures, has witnessed extensive water-rock reactions, and is dissolved in water to which volcanic gases may have been added, all leading to compositional alterations. At elevated temperatures and pressures organic carbon can be fully oxidized or reduced to gaseous products that may be lost from the dissolved phase (see Figure 1.7: IV. and V.). These products include carbon dioxide, methane, and various light hydrocarbons (Clifton et al., 1990; McCollom et al., 1999, 2001; Seewald, 2003; Hawkes et al., 2015; Nye, 2020). With increasing water-rock interaction at depth, the $\delta^{13}C$ signature becomes enriched (see Figure 1.8: V.).

High temperatures also induce boiling and evaporation, resulting in an ultimate increase in DOC relative to the fluid (see Figure 1.7: IV.). This same trend is observed for boiling and evaporation due to the heat additions; ^{13}C bonds, being slightly stronger, remain in the fluid longer, ultimately enriching the fluid (see Figure 1.8: IV.). Separating these various processes into trends aids in data interpretation, and these interpretations will be empirically tested in Chapter 3.

It is worth noting that thermally altered DOC has been found in other studies to contain numerous molecular formulas specific to Yellowstone. As an example, Gonsoir et al. (2018) found that around 80% of these formulas contain sulfur. While that study focused on four hot springs within Yellowstone, a recent study by Nye (2020) characterized 222 hot springs using fluorescence spectroscopy. Nye employed an Excitation Emission Matrix (EEM) to create a novel PARAFAC model identifying a five-component system displaying unique fluorescence characteristics in Yellowstone National Park. Notably, there is a component unique to acidic hot springs that can be correlated with samples isotopically enriched in ^{13}C. The EEM analysis, in combination with complementary samples from the dataset in this thesis, adds an additional variable for predicting fluid paths, elaborated upon in Chapter 5 with in-depth examples of DOC delivery.

Microbiological Processing of DOC

Hot spring fluids harbor autotrophic microorganisms that exploit chemical sources of energy to use CO_2 and other solutes from the fluid to generate organic compounds. The study of autotrophy and carbon isotopes in Yellowstone hot springs was

pioneered by Estep (1984), who revealed a wide range of isotopic fractionation in carbon. Subsequent research has further characterized carbon fractionation in biofilms in Yellowstone hot springs (van der Meer et al., 2000a; Jahnke et al., 2001; van der Meer et al., 2003; Zhang et al., 2004; van der Meer et al., 2005; van der Meer et al., 2007; Havig et al., 2011). Carbon isotopes undergo fractionation differently depending on the dominant carbon fixation pathway used by microorganisms (Havig et al., 2011). Production and consumption of organic carbon, which is subsequently utilized by autotrophic and heterotrophic microorganisms residing within the hot spring, are indicated by the yellow star in Figure 1.5 and 1.7 and the yellow schematic below (III.). Importantly, microbial production elevates DOC concentration and ultimately enriches the DIC in ^{13}C due to uptake of isotopically lighter CO_2 for organic carbon production. The degree of enrichment varies depending on the dominant carbon fixation pathway.

Heterotrophy is the process by which organisms utilize organic material for energy and for synthesis of biomolecules. Heterotrophy is complex, as these organisms may employ organic material produced by neighboring autotrophs, incoming fresh organic carbon, and/or thermally altered organic compounds present in the spring. Heterotrophy varies between hot springs based on the dominant energy source for these organisms and the composition of the microbiome of the spring (Meyer-Dombard et al., 2011; Schubotz et al., 2013; 2015). Heterotrophy in Yellowstone hot springs has been studied for decades, starting from the hypothesis that overland flow and local topography influence the growth of heterotrophic communities within the hot spring (Swingley et al., 2012; Schubotz et al., 2013). According to results of field experiments described by

Schubotz et al. (2015), streamer biofilm communities can transition between autotrophy and heterotrophy based on substrate availability. Heterotrophy can lead to a reduction in DOC concentration due to microbial uptake of organic compounds (see Figure 1.7: IV). It remains unclear whether the consumption of organic carbon affects the $\delta^{13}C$ signature, as there is no clear evidence detectable in the samples of heterotrophs exhibiting an isotopic preference (see Figure 1.8: III).

YNP DATA 2005-2019

Testing the conceptual models summarized in Figs 1.5 through 1.8 is made possible with DIC and DOC data from Yellowstone National Park collected by GEOPIG researchers. Over the period spanning 2005-2019, 707 samples were collected and analyzed across 10 hydrothermal regions as shown in Fig. 1.10. Among the 10 regions discussed in this study, three regions, Geyser Creek, Norris, and Sylvan are located outside the caldera that resulted from the 0.64 Ma eruption. In addition, Washburn is located outside the inner ring fracture. The remaining six regions are situated within the caldera. Consequently, there could be geological differences outside the caldera, meaning that DIC and DOC data could possibly be influenced by their proximity to the caldera.

Sulfate and chloride data for all 707 samples are shown in in two plots in Fig 1.11 with the goal of providing insights into the types of fluids within each region. Data are overlain directly on the corresponding plot from Nordstrom et al. (2009) in Fig 1.11 A. It can be seen that a substantial number of data points align along the vertical axis of this figure prompting the creation of Fig 1.11 B, which uses logarithmic scales. Modified

arrows from Nordstrom et al. (2009) and Nye (2020) illustrate the hydrothermal processes impacting sulfate and chloride concentrations.

In the classification scheme of Nordstrom et al. (2009), hot springs with less than 5 mg/L chloride are classified as "Meteoric Only." In this thesis, they are termed "Meteoric Dominant (MD)" because, although they are dilute, they contain more chloride than fresh meteoric snow in Yellowstone (see Figure 1.11). MD waters may also interact with volcanic gases rising towards the surface, altering the chemistry and isotopic composition of DOC. These springs are classified as "Meteoric Gas Dominant (MGD)," (>100 mg/L SO_4^{-2}) as illustrated in Figure 1.11 (A). This classification helps identify hot springs influenced by the hydrologic system that is driven by meteoric water. For instance, Rabbit Creek South is categorized as "meteoric dominant," while Washburn is classified as "meteoric gas dominant."

In contrast, regions like Geyser Creek, GOPA, and Sylvan host hot springs with compositions that vary by orders of magnitude in sulfate and chloride. These regions are excellent candidates for test how adding additional variables helps to elucidate the processes responsible for the compositional complexity among features that are often in close proximity. As developed in more detail in Chapter 3, incorporating DIC and DOC concentrations, along with their respective isotopic signatures, offers further insights into fluid pathways in areas characterized by complex mixing patterns.

As depicted in Figure 1.7, it is anticipated that gas additions leading to heat increases in DOC will affect the isotopic signature, resulting in ^{13}C enrichment. This prediction aligns with the data differentiating MD and MGD hot springs. As shown in

Figure 1.12, MD-classified hot springs exhibit $\delta^{13}C$ signatures ranging from -23‰ to -28‰. In contrast, MGD-classified hot springs ($Cl^- < 5$ mg/L, $SO_4^{-2} > 100$ mg/L owing to gas injection), can display $\delta^{13}C$ values enriched in ^{13}C compared to meteoric-dominant fluids. It is important to note that the MDG fluids overlap the MD fluids in Fig 1.12, which means that the evaporation explanation cannot be applied universally. Further evidence of active processes can be deduced from the observation that DOC $\delta^{13}C$ values are enriched conductivity increases.

Conductivity is a valuable parameter as it links thermal alteration to a quantifiable value. Conductivity values (in µS/cm) are reported as specific conductivity, temperature-compensated to 25°C (Hamilton et al., 2011). In Figure 1.13 DOC $\delta^{13}C$ VPDB (‰) is plotted against conductivity for all hot spring samples from 2005-2019 used in this study. Although there is considerable scatter in the data, it can be seen that with increasing conductivity, a stronger correlation emerges, indicating that DOC $\delta^{13}C$ values become more enriched in ^{13}C. Increasing conductivity could be attributed to increased evaporation and boiling, which could also explain the isotopic data as $^{12}CO_2$ can enter the vapor phase more rapidly than $^{13}CO_2$, creating a slight isotopic difference. Conductivity can serve as an indicator of evaporation if ions become concentrated in solution. However, this effect is not uniform across all regions, as depicted in Figure 1.14, where isotopic data from two regions exhibit varying slopes with increasing conductivity. This variability may be due to mixing between waters, one of which may have experienced deep thermal circulation, which is represented as process C, indicated by the red arrow in Figure 1.7. As discussed above, increasing thermal alteration results in ^{13}C enrichment.

This process-driven approach effectively differentiates MD and MGD data by introducing additional variables, providing alternative perspectives on fluid paths. This approach of introducing additional variables is tested in Chapter 3 while examining four regions characterized by distinct fluid types: meteoric, deep hydrothermal, meteoric mixing and phase separation, and complex meteoric and deep hydrothermal mixing with large gas additions. But first, methods used in this study are summarized in Chapter 2.

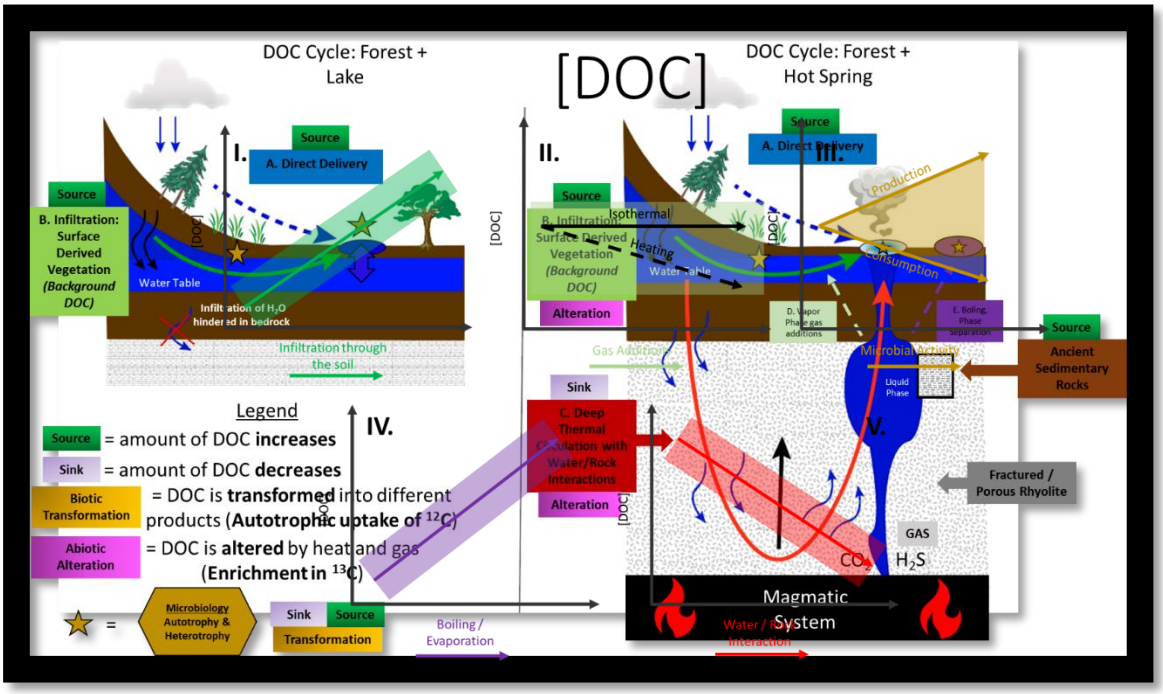

Figure 1.7: Schematic depiction of processes affecting DOC in a lake and hot spring system. The processes affecting DOC in a lake would also be present at a hot spring, where additional processes would be involved. Below the schematic cross-sections are arrows depicting how concentration of DOC will be affected by various processes.

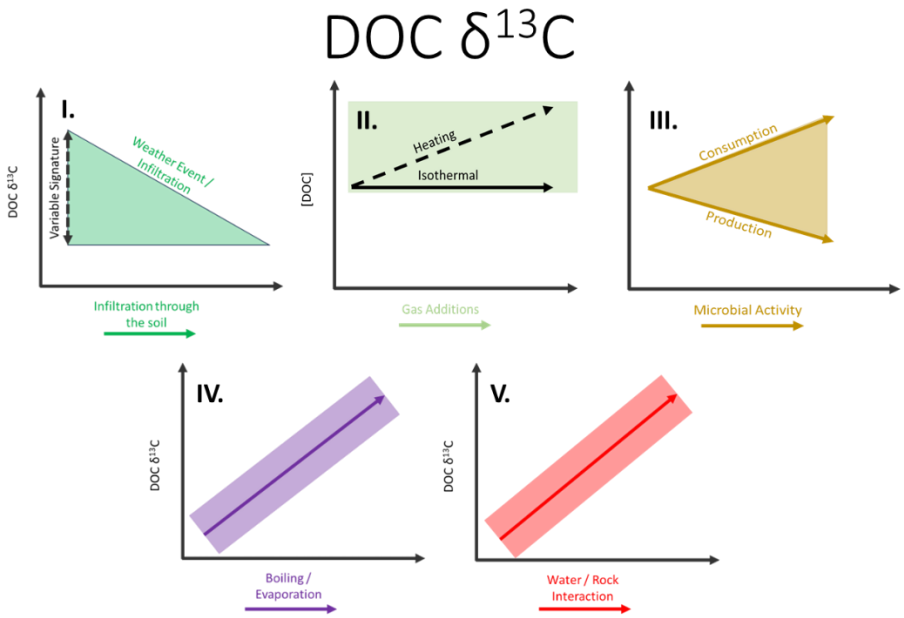

Figure 1.8: General trends of how various processes affect the isotopic concentration of carbon (DOC $\delta^{13}C$). These processes are related to those shown in the lower panel of Figure 1.7.

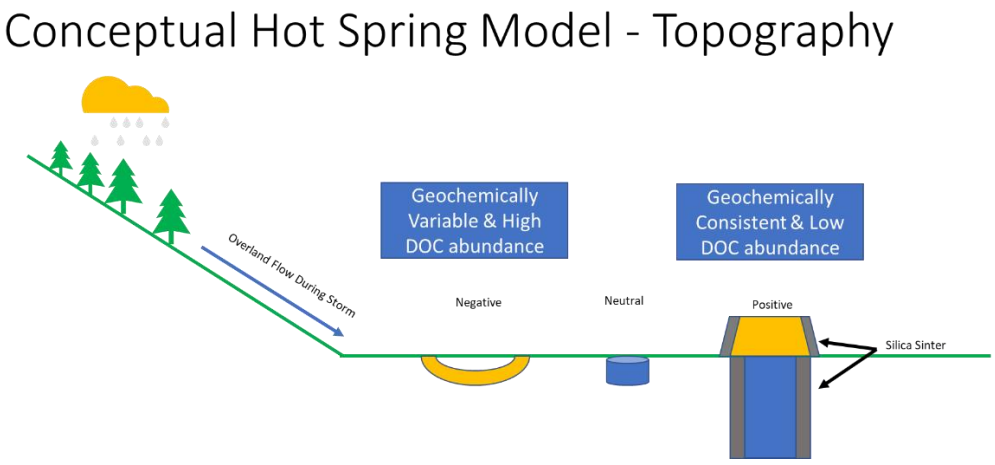

Figure 1.9: Conceptual Hot Spring Model – Topography: Negatively classified hot springs are topographically low compared to the surrounding environment. Positive Hot

Springs are topographically higher due to silica sinter precipitation limiting exogenous input. Neutral springs are classified as a mixture of positive and negative attributes.

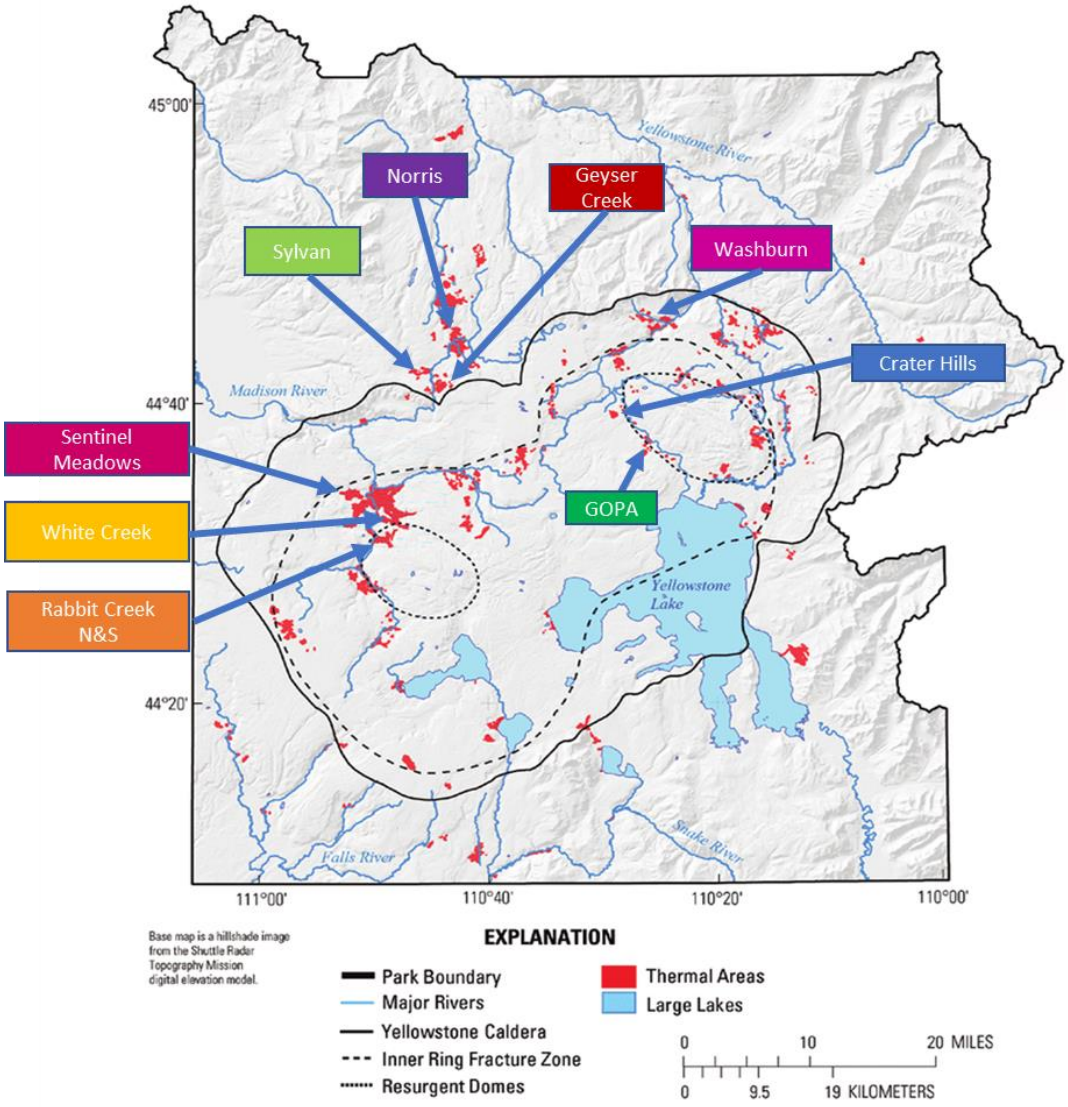

Figure 1.10: Map of Yellowstone National Park adapted from Vaughn (2014) overlain with the 10 thermal regions sampled in this study.

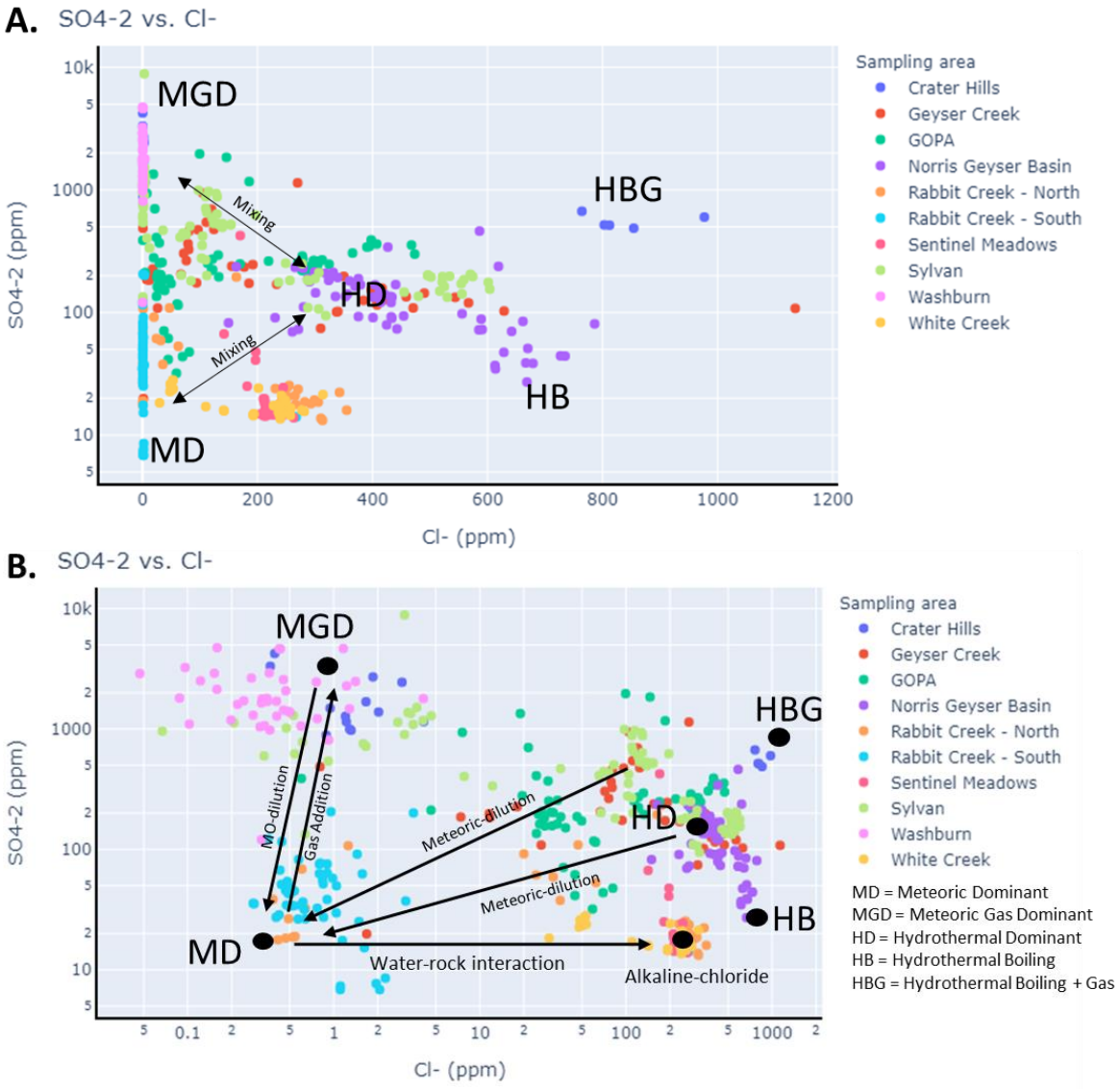

Figure 1.11: (A) Plot of sulfate vs. chloride for all samples in this study using axes as adopted by Nordstrom et al. (2009) and Nye (2020). (B) The same data using logarithmic scales for both solutes. Arrows show the compositional consequences of various processes affecting hot springs and leading to their distinct signatures.

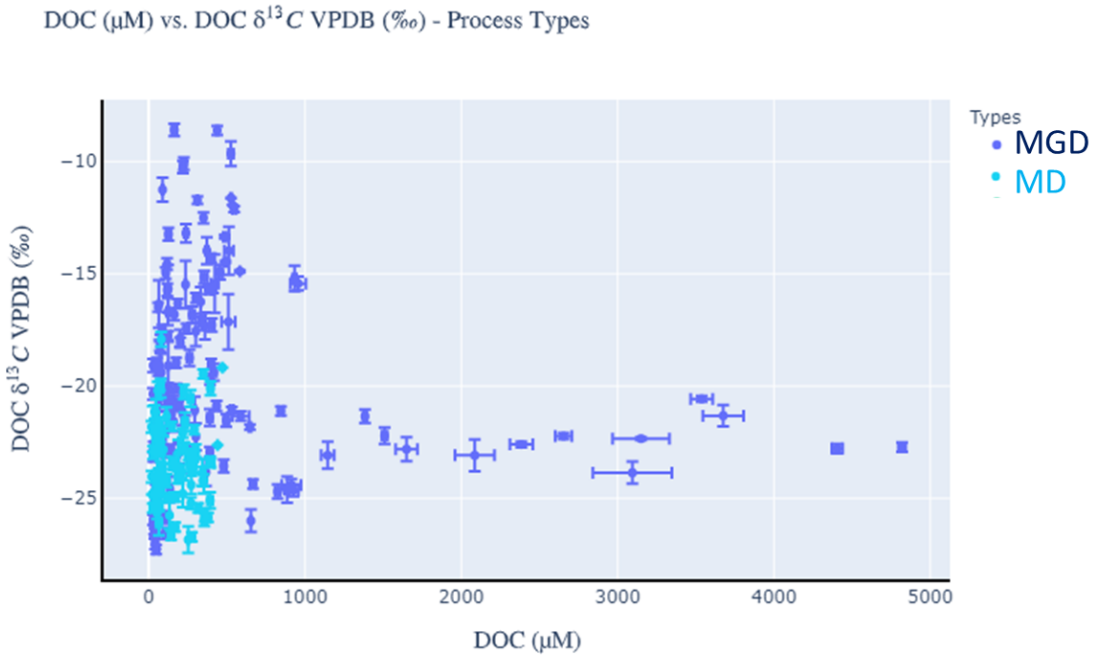

Figure 1.12: DOC $\delta^{13}C$ vs. DOC concentration for hot springs classified by process as in Nordstrom et al. (2009). Meteoric Dominant (MD): less than 5 mg/L chloride and less than 100 mg/L sulfate. Meteoric Gas Dominant (MGD): less than 5 mg/L chloride and more than 100 mg/L sulfate.

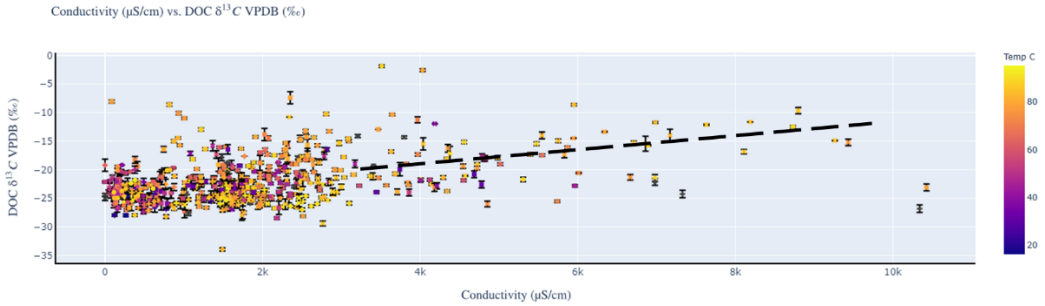

Figure 1.13: DOC $\delta^{13}C$ vs. conductivity for all hot spring samples used in this study. Color indicates temperature in °C as indicated by the scale on the right. The dashed line represents a suggested trend of enrichment in $\delta^{13}C$ correlating positively with an increase in conductivity. At conductivities below 5000 this trend is not strong.

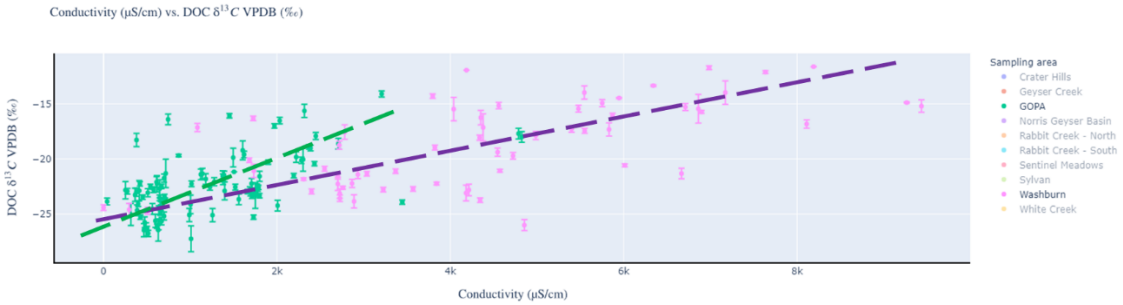

Figure 1.14: DOC $\delta^{13}C$ vs. conductivity for all GOPA and Washburn hot spring samples. The dashed lines represent suggested trends of enrichment in $\delta^{13}C$ correlating positively with increasing conductivity. Note that slopes of such correlations appear to differ depending on thermal area.

REFERENCES

Boyer, G., Robare, J., Ely, T., & Shock, E. (2021). AqEquil: Python package for aqueous geochemical speciation (0.13.4). Zenodo. https://doi.org/10.5281/zenodo.5768107

Campeau, A., Wallin, M. B., Giesler, R., Löfgren, S., Mörth, C. M., Schiff, S., ... & Bishop, K. (2017). Multiple sources and sinks of dissolved inorganic carbon across Swedish streams, refocusing the lens of stable C isotopes. *Scientific Reports*, *7*(1), 9158.

Christiansen, R. L. (2001), The Quarternary and Pliocene Yellowstone Plateau volcanic field of Wyoming, Idaho, and Montana, U.S. Geol. Surv. Prof. Pap. 729-G, Menlo Park, Calif.

Clifton, C., Walters, C., and Simoneit, B. (1990); Hydrothermal petroleums from Yellowstone National Park, Wyoming, U.S.A. Applied Geochemistry 5(1-2), pp. 169–191, doi:10.1016/0883-2927(90)90047-9.

Deines, P. (2002). The carbon isotope geochemistry of mantle xenoliths. *Earth-Science Reviews*, *58*(3-4), 247-278.

Feranec, R. S. (2007). Stable carbon isotope values reveal evidence of resource partitioning among ungulates from modern C3-dominated ecosystems in North America. *Palaeogeography, Palaeoclimatology, Palaeoecology*, *252*(3-4), 575-585.

Fouke, B. W. (2011). Hot-spring Systems Geobiology: abiotic and biotic influences on travertine formation at Mammoth Hot Springs, Yellowstone National Park, USA. Sedimentology, 58(1), 170-219.

Fournier, R. (1977); Chemical geothermometers and mixing models for geothermal systems. Geothermics 5(1-4), pp. 41–50, doi:10.1016/0375-6505(77)90007-4.

Fournier, R. O. (1989); Geochemistry and dynamics of the Yellowstone National Park hydrothermal system. Annual Review of Earth and Planetary Sciences 17(1), pp. 13–53, doi:10.1146/annurev.ea.17.050189.000305.

Gonsior, M., Hertkorn, N., Hinman, N., Dvorski, S. E.-M., Harir, M., Cooper, W. J., and Schmitt-Kopplin, P. (2018); Yellowstone hot springs are organic chemodiversity hot spots. Scientific Reports 8(1), p. 14155, doi:10.1038/s41598-018-32593-x

Hawkes, J. A., Rossel, P. E., Stubbins, A., Butterfield, D., Connelly, D. P., Achterberg, E. P., Koschinsky, A., Chavagnac, V., Hansen, C. T., Bach, W., and Dittmar, T. (2015); Efficient removal of recalcitrant deep-ocean dissolved organic matter

during hydrothermal circulation. Nature Geoscience 8, pp. 856–860, doi: 10.1038/ngeo2543.

Havig, J. R., Raymond, J., Meyer-Dombard, D. A. R., Zolotova, N., & Shock, E. L. (2011). Merging isotopes and community genomics in a siliceous sinter-depositing hot spring. *Journal of Geophysical Research: Biogeosciences*, *116*(G1).

Hamilton, T.L., Boyd, E.S., Peters, J.W. (2011), Environmental constraints underpin the distribution and phylogenetic diversity of nifH in the Yellowstone geothermal complex. Microbial Ecology 61, 860–870.

Hearn, E. H., Kennedy, B. M., & Truesdell, A. H. (1990). Coupled variations in helium isotopes and fluid chemistry: Shoshone Geyser Basin, Yellowstone National Park. *Geochimica et Cosmochimica Acta*, *54*(11), 3103-3113.

Jahnke, L. L., W. Eder, R. Huber, J. M. Hope, K. Hinrichs, J. M. Hayes, D. J. des Marais, S. L. Cady, and R. E. Summons (2001), Signature lipids and stable carbon isotope analysis of Octopus Spring hyperthermophilic communities compared with those of Aquificales representatives, Appl. Environ. Microbiol., 67, 5179–5189, doi:10.1128/AEM.67.11.5179– 5189.2001.

Kirkels, F. M., De Boer, H. J., Concha Hernández, P., Martes, C. R., Van Der Meer, M. T., Basu, S., ... & Peterse, F. (2022). Carbon isotopic ratios of modern C 3 and C 4 vegetation on the Indian peninsula and changes along the plant–soil–river continuum–implications for vegetation reconstructions. *Biogeosciences*, *19*(17), 4107-4127.

Lowenstern, J. B., Bergfeld, D., Evans, W. C., & Hunt, A. G. (2015). Origins of geothermal gases at Yellowstone. *Journal of Volcanology and Geothermal Research*, *302*, 87-101.

Lowenstern, J. B., & Hurwitz, S. (2008). Monitoring a supervolcano in repose: Heat and volatile flux at the Yellowstone Caldera. *Elements*, *4*(1), 35-40.

McCollom, T., Seewald, J., and Simoneit, B. (2001); Reactivity of monocyclic aromatic compounds under hydrothermal conditions. Geochimica et Cosmochimica Acta 65(3), pp. 455–468, doi:10.1016/S0016-7037(00)00533-0.

McCollom, T. M., Ritter, G., and Simoneit, B. R. T. (1999); Lipid synthesis under hydrothermal conditions by Fischer-Tropsch-type reactions. Origins of Life and Evolution of the Biosphere 29(2), pp. 153–166, doi:10.1023/A:1006592502746.

Meyer-Dombard, D. R., Swingley, W., Raymond, J., Havig, J., Shock, E. L., and Summons, R. E. (2011). Hydrothermal ecotones and streamer biofilm communities in the Lower Geyser Basin, Yellowstone National Park. Environ. Microbiol. 13, 2216–2231. doi: 10.1111/j.1462-2920.2011. 02476.x

NOAA Terrestrial Climate Data Records was accessed on 5/15/2023 from https://registry.opendata.aws/noaa-cdr-terrestrial.

Nordstrom, D. K., McCleskey, R. B., & Ball, J. W. (2009). Sulfur geochemistry of hydrothermal waters in Yellowstone National Park: IV Acid–sulfate waters. *Applied Geochemistry*, *24*(2), 191-207.

Nye, J. (2020). *Fluorescent Dissolved Organic Matter in Yellowstone National Park Hot Springs* (Doctoral dissertation, Arizona State University).

Pierce, K. L. & Morgan, L. A. Is the track of the Yellowstone hotspot driven by a deep mantle plume? — Review of volcanism, faulting, and uplift in light of new data. Journal of Volcanology and Geothermal Research 188, 1–25, https://doi.org/10.1016/j. jvolgeores.2009.07.009 (2009).

Schubotz, F., Hays, L. E., Meyer-Dombard, D. A. R., Gillespie, A., Shock, E. L., & Summons, R. E. (2015). Stable isotope labeling confirms mixotrophic nature of streamer biofilm communities at alkaline hot springs. *Frontiers in microbiology*, *6*, 42.

Schubotz, F., Meyer-Dombard, D. R., Bradley, A. S., Fredricks, H. F., Hinrichs, K.- U., Shock, E. L., et al. (2013). Spatial and temporal variability of biomarkers and microbial diversity reveal metabolic and community flexibility in Streamer Biofilm Communities in the Lower Geyser Basin, Yellowstone National Park. Geobiology 11, 549–569. doi: 10.1111/gbi.12051

Seewald, J. S. (2003); Organic-inorganic interactions in petroleum-producing sedimentary basins. Nature 426(6964), pp. 327–333, doi:10.1038/nature02132

Stelten, M. E., Thomas, N., Pivarunas, A., & Champion, D. (2023). Spatio-temporal clustering of post-caldera eruptions at Yellowstone caldera: implications for volcanic hazards and pre-eruptive magma reservoir configuration. *Bulletin of Volcanology*, *85*(10), 1-17.

Swingley, W. D., Meyer-Dombard, D. R., Shock, E. L., Alsop, E. B., Falenski, H. D., Havig, J. R., et al. (2012). Coordinating environmental genomics and geochemistry reveals metabolic transitions in a hot spring ecosystem. PLoS ONE 7:e38108. doi: 10.1371/journal.pone.0038108

van der Meer, M. T. J., S. Schouten, J. W. de Leeuw, and D. W. Ward (2000a), Autotrophy of green nonsulfur bacteria in hot spring microbial mats: Biological explanations for isotopically heavy organic carbon in the geological record, Environ. Microbiol., 2, 428–435.

van der Meer, M. T. J., S. Schouten, J. S. S. Damste, J. W. de Leeuw, and D. W. Ward (2003), Compound-specific isotopic fractionation patterns suggest different

carbon metabolisms among chloroflexus-like bacteria in hot-spring microbial mats, Appl. Environ. Microbiol., 69, 6000– 6006, doi:10.1128/AEM.69.10.6000–6006.2003.

van der Meer, M. T. J., S. Schouten, M. M. Bateson, U. Nubel, A. Wieland, M. Kuhl, J. W. de Leeuw, J. S. S. Damste, and D. M. Ward (2005), Diel variations in carbon metabolism by green nonsulfur-like bacteria in alkaline siliceous hot spring microbial mats from Yellowstone National Park, Appl. Environ. Microbiol., 7 1, 3978 –3986, doi:10.1128/ AEM.71.7.3978–3986.2005.

van der Meer, M. T. J., S. Schouten, J. S. S. Damste, and D. M. Ward (2007), Impact of carbon metabolism on 13C signatures of cyanobacteria and green non-sulfur-like bacteria inhabiting a microbial mat from an alkaline siliceous hot spring in Yellowstone National Park (USA), Environ. Microbiol., 9, 482–491, doi:10.111/j.1462–2920.2006.01165.x.

Zhang, C. L., B. W. Fouke, G. T. Bonheyo, A. D. Peacock, D. C. White, Y. Huang, and C. S. Romanek (2004), Lipid biomarkers and carbon- isotopes of modern travertine deposits (Yellowstone National Park, USA): Implications for biogeochemical dynamics in hot-spring systems, Geochim. Cosmochim. Acta, 68, 3157–3169, doi:10.1016/j.gca. 2004.03.005.

CHAPTER 2

METHODS

This chapter contains descriptions of sample collection, meter measurements performed in the field, ion chromatography methodology, DOC/DIC methodology, and elemental analysis methodology for all the samples analyzed in this thesis. Figure 2.1 displays the sampling pipeline used to characterize hydrothermal fluid that are relevant to this thesis.

Sample Collection

Data used in this thesis comes from samples collected during fieldwork in various regions of Yellowstone conducted between 2005 and 2019 by several GEOPIG teams. The hot spring locations were chosen based upon ongoing research projects throughout these years. Many different regions have been sampled, but this work encompasses the geochemical, DIC, and DOC data of 10 regions in Yellowstone National Park that were sampled the most during the 15-year period. The 10 regions are: Crater Hills, Geyser Creek, Greater Obsidian Pool Area (GOPA), Norris Geyser Basin, Rabbit Creek North, Rabbit Creek South, Sentinel Meadows, Sylvan Springs, Washburn Springs, and White Creek.

Initial pH and temperature measurements were taken in the field using a WTW 330i meter and probe. Conductivity measurements were performed using a YSI 30 conductivity meter. Water was collected from hot springs using long-handled polyethylene scoops. These scoops have a 500 mL beaker attached to the pole. Prior to collection the scoops are rinsed three times with hot spring water before taking a sample.

The water is filtered with 0.8/0.2 µm Supor syringe filters. Filtered water is then used for various sampling methods. Ion chromatography (IC) samples are used to detect major anions and cations. The filtered water for IC samples is put into 60 mL Nalgene bottles and stored in a refrigerator until analysis. Anion analysis is carried out using a Dionex DX 600 Dual IC System and cation analysis is done using a Dionex DX 120 IC System. Samples for DOC and DIC analysis were collected in 40 mL amber borosilicate vials with silicone Teflon-lined septa. DOC bottles are pretreated with 1 mL H_3PO_4 for DIC removal as CO_2 gas. These samples are filled rapidly to eliminate any headspace and reduce contamination. Biofilm and sediment samples were collected using 150 mm long, milled Teflon tweezers. The tweezers were rinsed with nitric acid and washed with deionized water. They were also rinsed downstream with hot spring water prior to sample collection. These samples were collected in both Whirl-Pak bags and 15 mL centrifuge tubes and stored on ice until transported to the lab refrigerator.

IC Methodology

Using conductivity measurements taken in the field, IC samples are diluted in the lab before analysis with 18.2MΩ deionized water to ensure measurements are made within the calibration ranges. Certified standards used are Alltech Multicomponent Certified Anion Standard Mix 6 and Dionex Combined 6 cations Standard II. Standard deviation is determined by replicating injections of the sample.

DOC/DIC Methodology

DOC and DIC concentrations are analyzed using an OI Analytical Model 1010 Wet Oxidation TOC Analyzer. Isotope analyses are generated after converting the DIC to CO_2 by acidification with phosphoric acid or chemical oxidation of the DOC to CO_2 using sodium persulphate. The resulting CO_2 is coupled with a continuous gas flow to a Thermo Delta Plus Advantage mass spectrometer. Sampling loops of 1ml, 5ml, and 25ml sizes were used first to analyze carbon content. In recent years, the procedure only uses 1ml and 10 ml loops, as this is sufficient to measure carbon content in most Yellowstone hot springs based on experience in the GEOPIG research group. If a sample was below the detection limit (0.16 µM), it was rerun with a larger loop to produce an analyzable CO_2 peak. Loops are determined based upon previous data for hot springs with multiple samples over multiple years. Three glycine organic standards were used (Low, Mid, High) to normalize the data. The isotopic values are as follows: Glycine Low ($\delta^{13}C$ =-39.64 ‰), Glycine Mid ($\delta^{13}C$ =-8.36 ‰), and Glycine High ($\delta^{13}C$ =15.67 ‰). The glycine standards are characterized using USGS40 and USGS41 to verify isotope values (Havig, 2011). To estimate the measurement uncertainty for C, glycine values throughout the run are combined to determine the %RSD.

Elemental Analysis Methodology

Biofilm and sediment samples were taken out of the freezer and immediately freeze dried using a lyophilizer. After freeze-drying, the samples were homogenized using a ceramic mortar and pestle. The powdered samples for C and N analysis were then weighed in 5x9mm tin capsules. Samples analyzed for organic carbon were weighed and placed into silver capsules where they were fumigated with 100 mL of hydrochloric acid

(HCl) for 18 hours. This is the recommended period before capsule degradation (Harris, 2001). A small amount of deionized water was added to each capsule to wet the sample powder. After acid treatment the samples were put into an oven at 60°C overnight. The samples were then stored in a desiccator while they cooled to room temperature. The silver capsules were then wrapped in tin capsules and ready for analysis. A premade soil standard with known concentration of organic carbon was used as a control to confirm the acid treatment was successful due to all acid-treated samples were within 5% of untreated samples.

Elemental analyses were processed via an Elemental Analyzer Isotope Ratio Mass Spectrometer (EA-IRMS). Samples were combusted in the EA into measurable quantities of gas (CO_2) that are measured in the IRMS to determine concentration and isotopic signature. C mass for samples is reported as percent of dry weight of sample. This data was standardized using the same glycine standards reported above for DIC/DOC and the detection limit is also 0.16 µM because both analyses are connected to the same IRMS. To estimate the measurement uncertainty for weight % C, glycine values throughout the run are combined to determine the %RSD.

Simplified Hot Spring Structure

Hot springs vary greatly by size, discharge of fluid, local topography, and local geochemistry among different thermal regions and within the same region. Hot springs range from nearly stagnant pools to actively outflowing. Local topography plays a major and yet undetermined role in the input of exogenous material into a hot spring system. Some hot springs have considerable silica sinter built up around the edge of the pool and

along the outflow channels, which can actively limit exogenous material from entering the system (Fig. 1.9). However, some springs do not have this sinter armor, allowing the local surroundings to directly interact and provide nutrients and toxins into the system. As a result, there can be differences in biofilms between these two different hot spring types. Biofilms within hot spring systems are influenced by the hot spring fluid and any input from the surrounding environment. Therefore, changes in the fluid or the surrounding environment can induce changes in hot spring biofilms. Data from biofilm samples in this thesis are used to explore the effects of fluid compositions and input from surrounding environments.

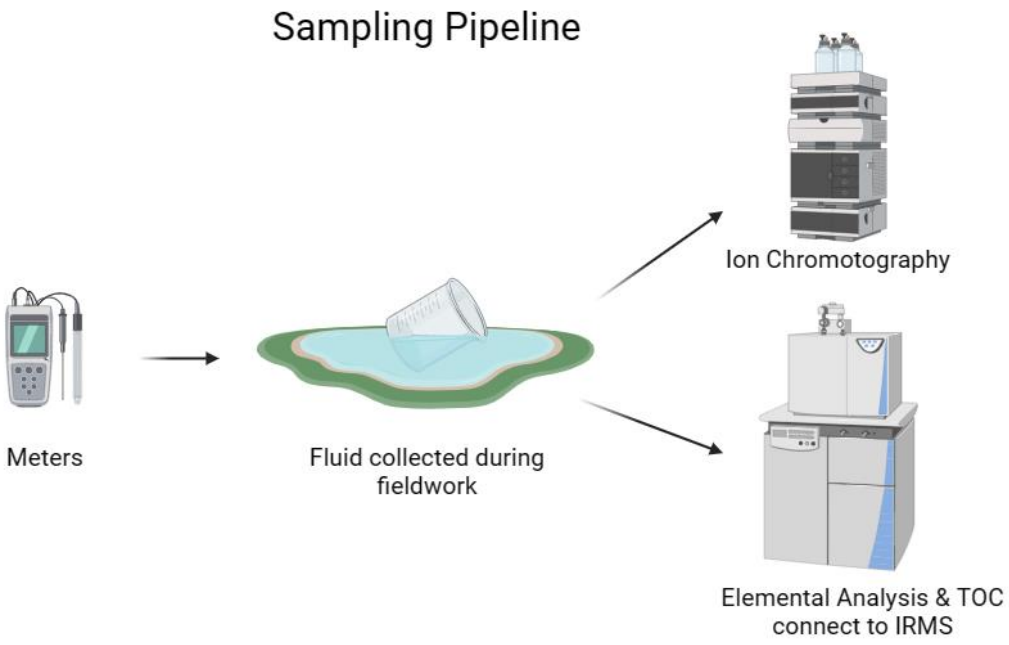

Figure 2.1: This schematic shows the sampling pipeline for fluid characterization used in this thesis. Meters are used to collect temperature, pH and conductivity data before fluid collection. Water samples filtered in the field, stored in vials appropriate for the types of data to be collected are transported to the laboratory for analysis.

REFERENCES

Harris, D., Horwath, W.R., and van Kessel, C., 2001. Acid fumigation of soils to remove carbonates prior to total organic carbon or carbon-13 isotopic analysis. Soil Science Society of America Journal 65: 1853-1856.

CHAPTER 3

CASE STUDIES

Introduction

Hot springs within Yellowstone National Park explored in this study range in pH from 1.2 to 9.5 at temperatures up to 95.3 °C as summarized in Fig. 3.1. This wide range of pH spans nearly 9 units and reflects large-scale variations due to complex mixing of sources and processes. These complexities make it difficult to interpret fluid composition and history for individual springs or thermal regions. The goal of this chapter is to take 15 years of data and determine locations that can test the conceptual model to unravel fluid history presented in Chapter 1 (Figure 1.5-1.8).

After examination of 707 samples and 10 different regions, Rabbit Creek South, Sentinel Meadows, GOPA, and Geyser Creek were chosen to investigate fluid history. Rabbit Creek South was chosen as the meteoric dominant fluid endmember due to low chloride and sulfate concentrations in most springs. On the other hand, Sentinel Meadows was chosen as the deeply sourced hydrothermal endmember fluid due to the elevated chloride signature and the local topography of raised sinter cones with little to no local meteoric infiltration. GOPA was chosen to represent a combination of the previous processes where meteoric water mixes with hydrothermal fluid and there is a substantial amount of phase separation detected. Lastly, Geyser Creek was chosen to test this model on a complex meteoric and deep hydrothermal mixing with large gas additions over diverse topography in a valley.

There are several orders of magnitude differences in sulfate and chloride for these various regions as well, as shown in Fig. 3.2. These areas display trends with dissolved carbon, and, by taking a process-driven approach, fluid paths in complex systems can be better understood after starting with endmember systems. This chapter focuses on four different case studies showing how adding concentrations of DIC and DOC, together with their corresponding isotopic compositions, helps unravel fluid histories. Appendix A includes discussions of additional regions and possible processes occurring within the hydrothermal system in each. Hot springs are referred to in this thesis with unofficial names that are given inside quotation marks.

DIC and DOC (Rabbit Creek South, Sentinel Meadows, GOPA, and Geyser Creek)

Carbon Abundance

The concentration of DIC reaches a park high of 10,609 µM at "Foam Pool" in the GOPA region and ranges between 4000-5000 µM in Sentinel Meadows, which hosts boiling neutral-chloride hot springs. In contrast, DIC is typically lower in the sulfate-dominant acidic hot springs at pH 1-5 (Fig. 3.3-3.5). The average DIC of all data points within Yellowstone National Park in this study is 2,241.5 µM. Concentrations of DOC range up to 1,275 µM at "Special Dark" in Sentinel Meadows (Fig. 3.6-3.7). Sulfate-dominant acidic hot springs tend to have higher DOC concentrations compared to neutral-chloride hot springs. High abundances of DOC in hot springs are rare and limited to specific hot springs. The average DOC of all regions in this study is only 191.7 µM. Typically, DOC abundance is lower than DIC abundance in each hot spring. However, there are hot springs where DOC abundance is higher than DIC and this typically occurs

in meteoric gas dominant hot springs. Such differences in carbon substrate abundances could be explored in future work to determine if the microbial community is actively increasing DOC in these specific hot springs.

Isotope Results

DIC $\delta^{13}C$ values typically range from -4‰ to +5‰ at pH 5-9 and from -7‰ to +3‰ at pH <5 with several springs more depleted in ^{13}C than -10‰ (Fig. 3.8-3.9). This range is indicative of a geogenic source (−12‰ to +5‰) (Campeau, 2017). Springs with DIC more depleted in ^{13}C than -10‰ have low concentrations of DIC but are within the calibration range for the isotope-ratio mass spectrometer (IRMS). Nevertheless, these low values could be artifacts due to being close to the lower end of the calibration range of 16 µM, or this could be a signal resulting from heterotrophy being a biogenic source of DIC (−26 to −18‰) (Campeau, 2017). Another way DIC can reach these values (-22‰ to -26‰) mentioned in Chapter 1 are a few signatures of C depleted in ^{13}C observed in mantle xenoliths (Deines, 2002), which has not been documented to be relevant to Yellowstone.

DOC $\delta^{13}C$ values parkwide range from -10‰ to -30‰ (Fig. 3.10-3.11). Within this range, springs in neutral-chloride regions in the Lower Geyser Basin are isotopically heavier than those in sulfate-dominant acidic regions. In hot springs with elevated levels of DOC, the range of $\delta^{13}C$ varies only between -20‰ and -26‰, which is likely to be caused by local exogenous organic matter runoff but may be caused by active microbial communities (Simkus, 2016).

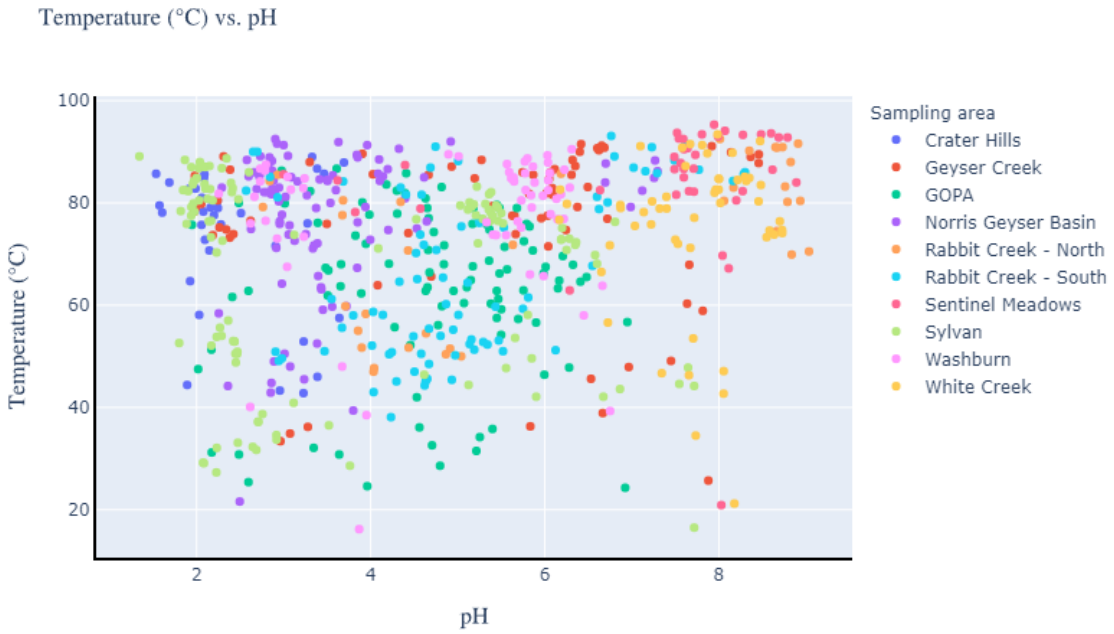

Figure 3.1: Temperature (°C) vs. pH for all 10 regions in this study.

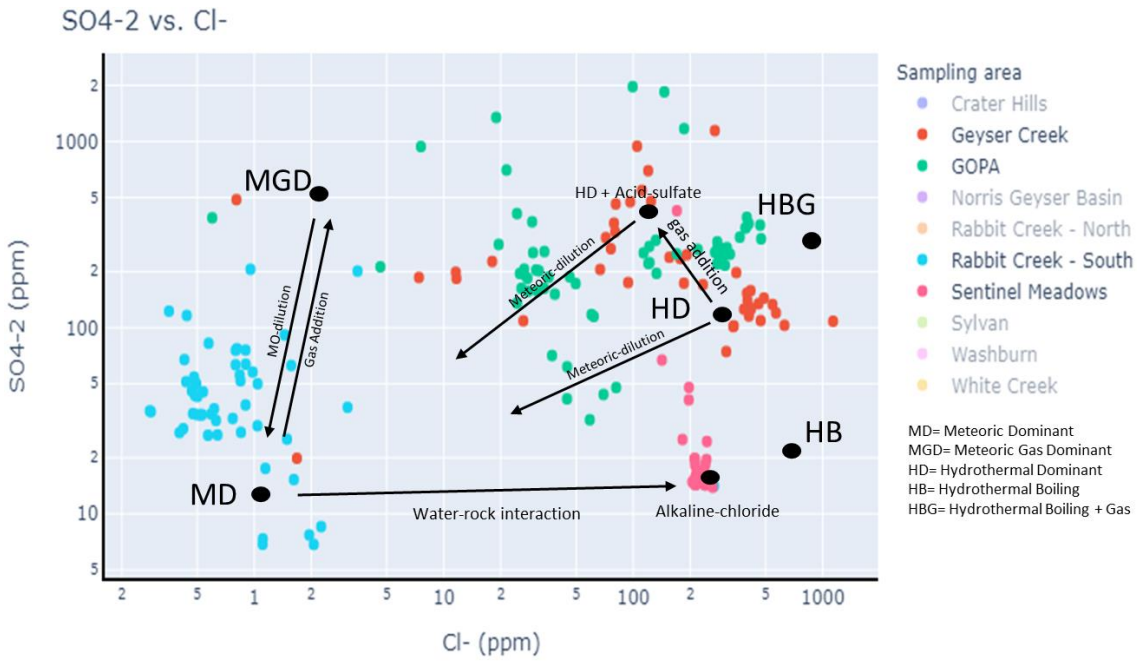

Figure 3.2: This figure is an adaptation from (Nordstrom et al., 2009 and Nye, 2020) displaying SO_4^{-2} (ppm) vs. Cl^- (ppm) for Geyser Creek, GOPA, Rabbit Creek – South,

and Sentinel Meadows from 2005-2019. Arrows show the compositional consequences of various processes affecting hot springs and leading to their distinct signatures.

Figure 3.3: DIC concentration vs. pH for Geyser Creek, GOPA, Rabbit Creek – South, and Sentinel Meadows from 2005-2019.

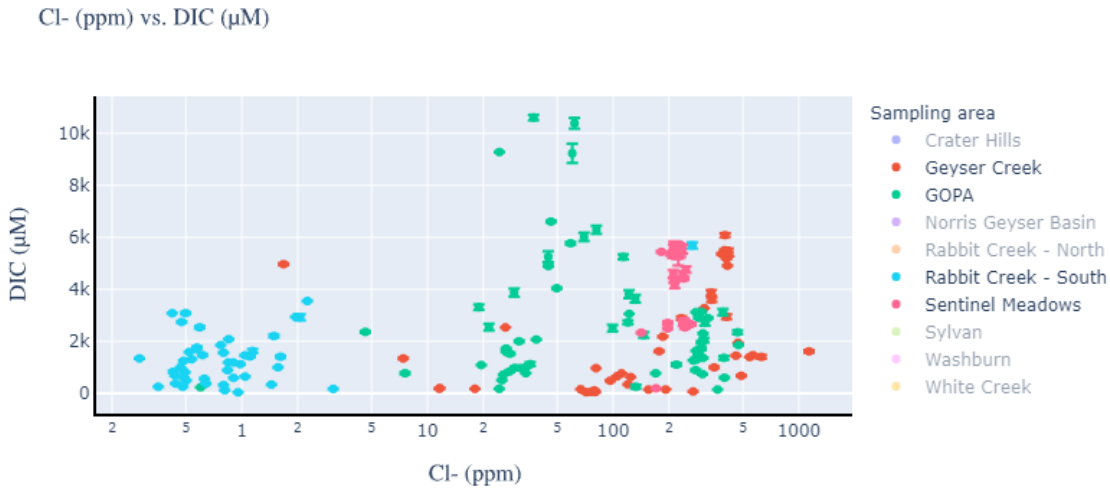

Figure 3.4: DIC concentration vs. Cl^- (ppm) for Geyser Creek, GOPA, Rabbit Creek – South, and Sentinel Meadows.

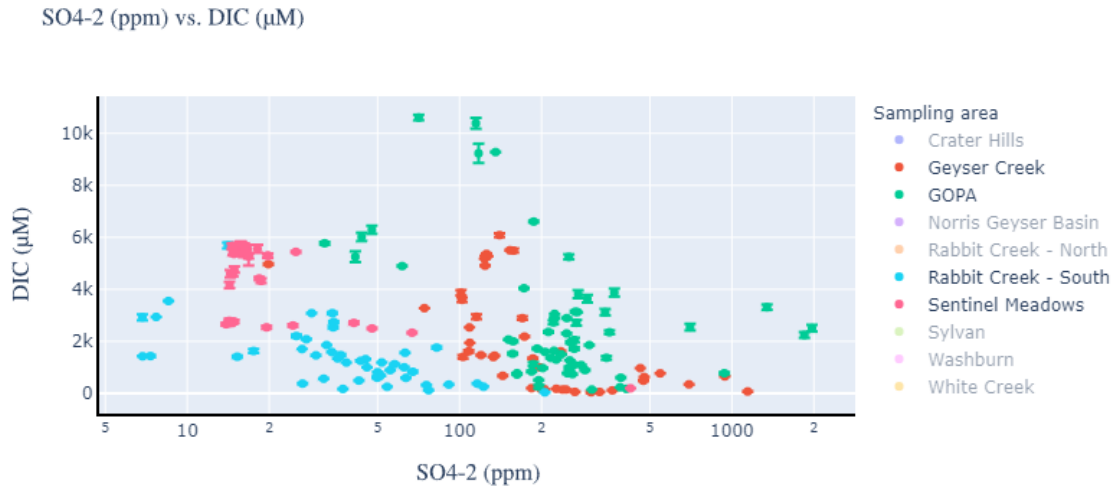

Figure 3.5: DIC concentration vs. SO_4^{-2} (ppm) for Geyser Creek, GOPA, Rabbit Creek – South, and Sentinel Meadows.

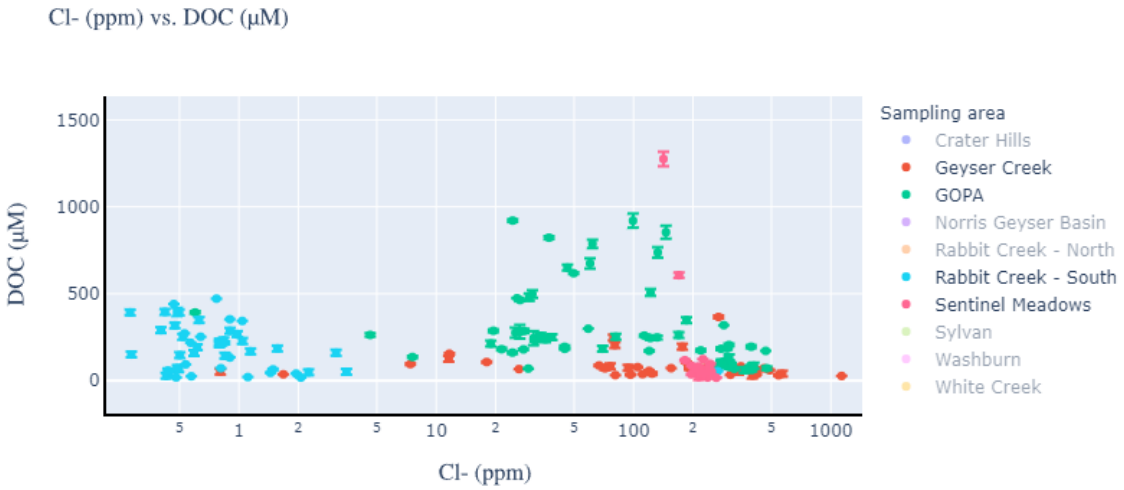

Figure 3.6: DOC concentration vs. Cl^- (ppm) for Geyser Creek, GOPA, Rabbit Creek – South, and Sentinel Meadows.

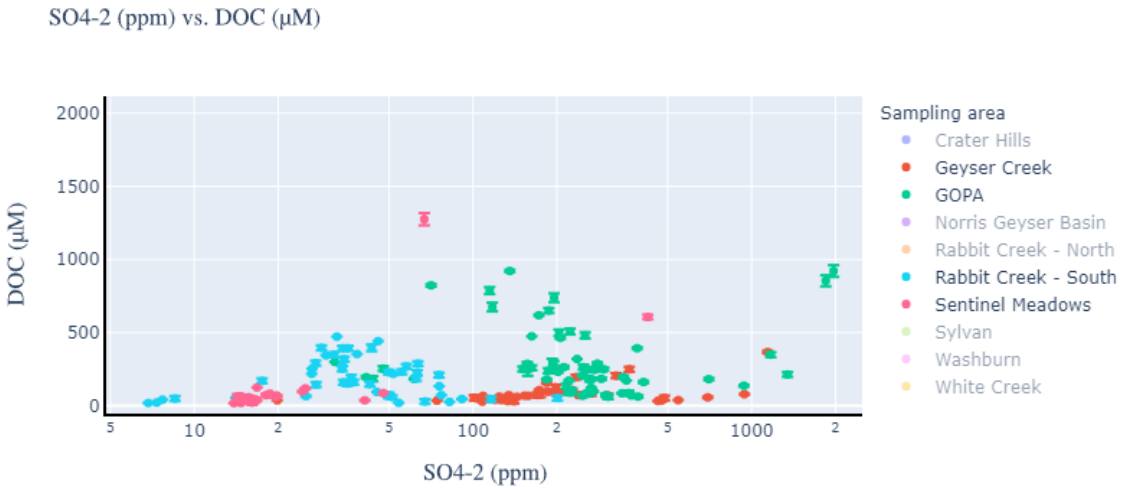

Figure 3.7: DOC concentration vs. SO_4^{-2} (ppm) for Geyser Creek, GOPA, Rabbit Creek – South, and Sentinel Meadows.

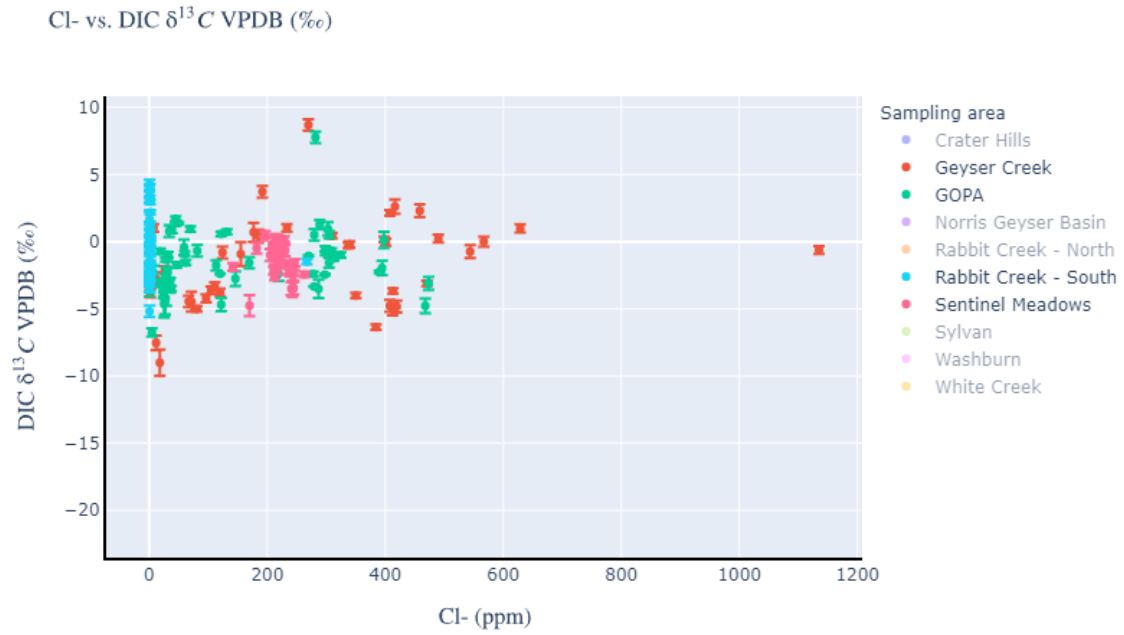

Figure 3.8: DIC $\delta^{13}C$ vs. Cl^- (ppm) for Geyser Creek, GOPA, Rabbit Creek – South, and Sentinel Meadows.

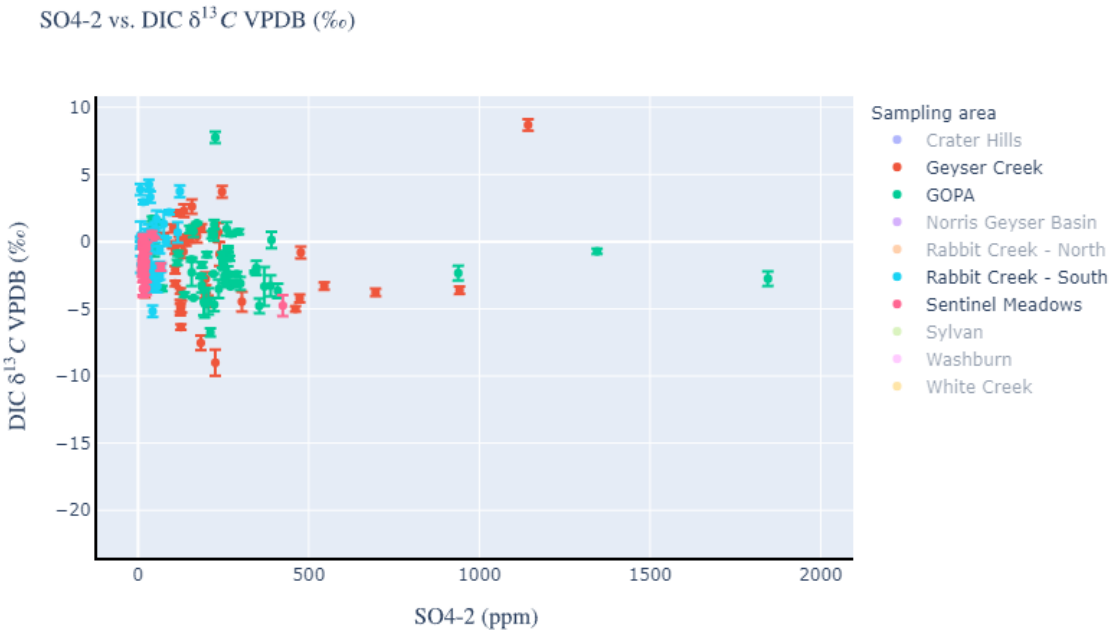

Figure 3.9: DIC $\delta^{13}C$ vs. SO_4^{-2} (ppm) for Geyser Creek, GOPA, Rabbit Creek – South, and Sentinel Meadows.

Figure 3.10: DOC $\delta^{13}C$ vs. Cl^- (ppm) for Geyser Creek, GOPA, Rabbit Creek – South, and Sentinel Meadows.

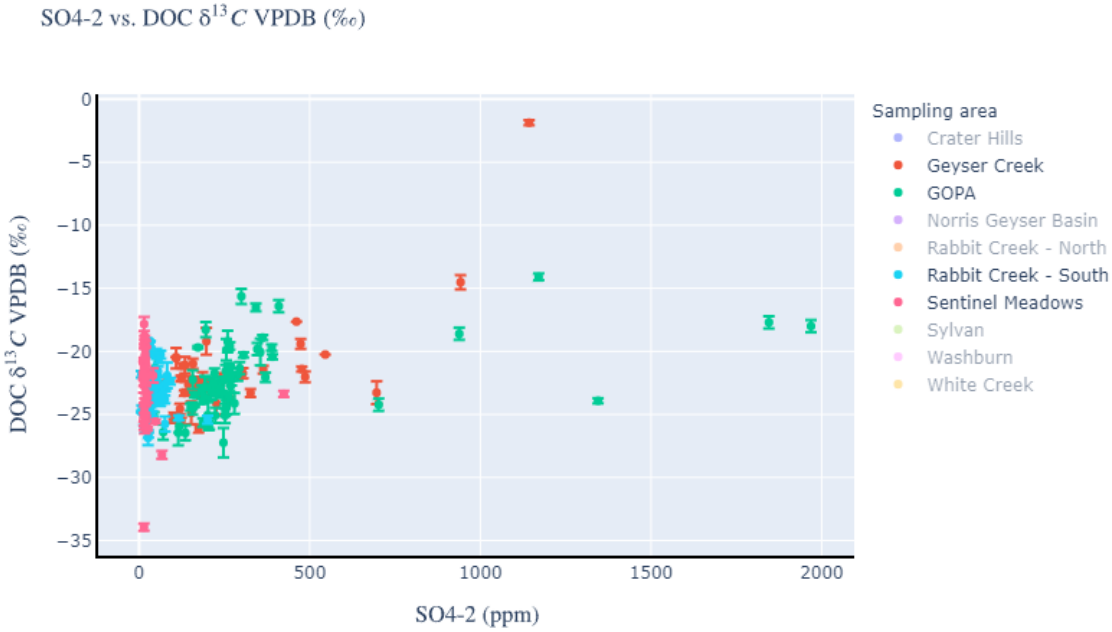

Figure 3.11: DIC $\delta^{13}C$ vs. SO_4^{-2} (ppm) for Geyser Creek, GOPA, Rabbit Creek – South, and Sentinel Meadows.

Rabbit Creek South (Meteoric)

Rabbit Creek is in the Midway Geyser Basin near the Firehole River. Hot spring locations are geologically controlled along faults, hillside, and other structures, and the hot springs themselves are mostly pools and some are outflowing. Many of the springs in this region are surrounded by lodgepole pine, and the springs vary in color from crystal blue to very murky or even “tomato soup” springs. The largest feature in this region is Rabbit Creek Source itself which is located in Rabbit Creek North. It is a very large bright blue hot spring that outflows to form Rabbit Creek. This impressive feature

provides a steady stream of outflowing thermal water. In some cases, there are complicated interconnections among springs through surface flow, but many springs in this area are not connected to each other via outflows and are standalone sources. Therefore, hot springs in this area tend to be different from each other even when neighboring hot springs are just a few meters apart. This area is thought to be largely influenced by meteoric water due to the very low and highly variable chloride levels. Rabbit North and South are separated by lodgepole pine. Rabbit Creek South could be influenced by meteoric water running down the surrounding steep hillsides as these springs tend to be located at the base of the surrounding hills. However, without investigating chloride values, this region would look very similar to other neutral-chloride hot springs.

Rabbit Creek South SO_4^{-2} vs. Cl^-

Rabbit Creek South is an example of primarily meteoric dominant water that has been heated. Sulfate (6 - 210 ppm) and chloride (0.28 - 4 ppm - outlier at 267 ppm) concentrations for this area are low and represent meteoric water that has undergone heating from the volcanic system below with very little water-rock reaction (Fig. 3.12). For the purpose of testing the conceptual models described in Chapter 1, Rabbit Creek South is an endmember within the dataset that is most like a typical pond or lake in a normal hydrological system that is influenced by volcanic gas and heat from below.

Rabbit Creek South DIC

Typical concentrations of DIC in a freshwater system vary between 20 – 5000 µM depending on the pH (Cole, 2014). Figure 3.13 shows that Rabbit Creek has hot springs along this entire range, and they are behaving nearly identically to how a lake and pond would without hydrothermal input. As shown in Fig 3.14, as sulfate concentrations increase there is a decrease in DIC concentration, which is expected in the conceptual model shown in Figure 1.5 in which acidic springs are not influenced by increases in DIC. Acidic springs have higher concentrations of sulfate. There is no correlation between chloride and DIC concentration, which is not surprising due to the very low concentration of chloride (Fig. 3.15). DIC $\delta^{13}C$ values are all geogenically sourced with a strong mantle or atmospheric signature. Some of these values are slightly enriched, which may be a product of evaporation at this location (Fig. 3.8 & 3.9). Overall, DIC $\delta^{13}C$ values are not very helpful at separting fluid types and history at Rabbit Creek South.

Rabbit Creek South DOC

DOC concentration is less than 500 µM for Rabbit Creek South which is low, and comparable to average meteoric water at 475.8 µM, which is the median concentration for 7514 lakes studied on six continents (Sobek, 2007). Due to the classification of the hot springs at Rabbit South as meteoric dominant, $\delta^{13}C$ values between -23‰ and -28‰ derived from photosynthetic exogenous material entering through the groundwater would be expected. The green box in Figure 3.16 indicates this prediction. However, there are numerous samples that are more enriched in ^{13}C as shown in Fig 3.16. This enrichment could be influenced by small additions of gas, which would also explain the variable concentrations of SO_4^{-2}, but the correlation is not strong as shown in Fig. 3.17. However,

an alternative that may be more likely is that meteoric water containing dissolved oxygen is reacting with trace H_2S gas from the volcanic system to create low levels of SO_4^{-2}, and decreasing the overall pH (Fournier, 1989; Gardner et al., 2010; Hurwitz and Lowenstern, 2014; Sims et al., 2023). As a result, conditions exist for chemical or biological DOC transformations that result in the enriched isotopic values. As shown in Fig 3.17, there is a weak trend of enrichment as sulfate increases. In summary, the DOC in the meteoric dominant fluids at Rabbit South shows effects of heat addition and acid alteration of the photosynthetic DOC in the meteoric dominant fluid. It is possible that DOC altered by heat and acid will provide an array of sulfur induced compounds as detected by Gonsior (2018). Altered photosynthetic dominant DOC in the shallow subsurface may provide a major source of energy and nutrients for microorganisms in these hot springs.

Rabbit Creek South Overview

A proposed schematic for how DOC is traveling along the fluid path in Rabbit Creek South is shown in Fig 3.18. Initially DOC is composed of photosynthetic material that infiltrates from the surface, and it is heated along the flow path and transported to the various hot springs. Ultimately Rabbit Creek South represents an endmember for meteoric dominant hydrothermal fluid. The concentrations of sulfate vs. chloride provide evidence that this area is heavily influenced by meteoric water and mixing with negligible input form deeply circulating fluids that have undergone substantial water-rock reaction. Using DIC and DOC as additional variables, together with their corresponding isotopic signatures introduces additional constraints on this model. Rabbit Creek South sets the foundation for distinguishing how concentrations of DIC and DOC and their

corresponding isotopic signatures will be impacted as the deeply circulating fluids of the hydrothermal system play more dominant roles in other regions.

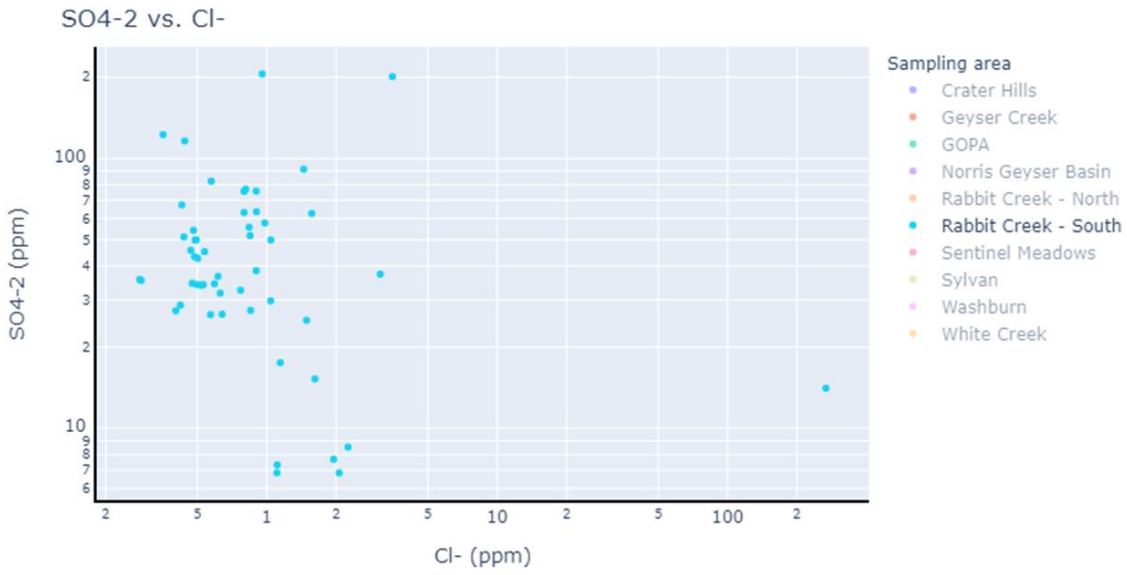

Figure 3.12: SO_4^{-2} (ppm) vs. Cl^- (ppm) for Rabbit Creek – South.

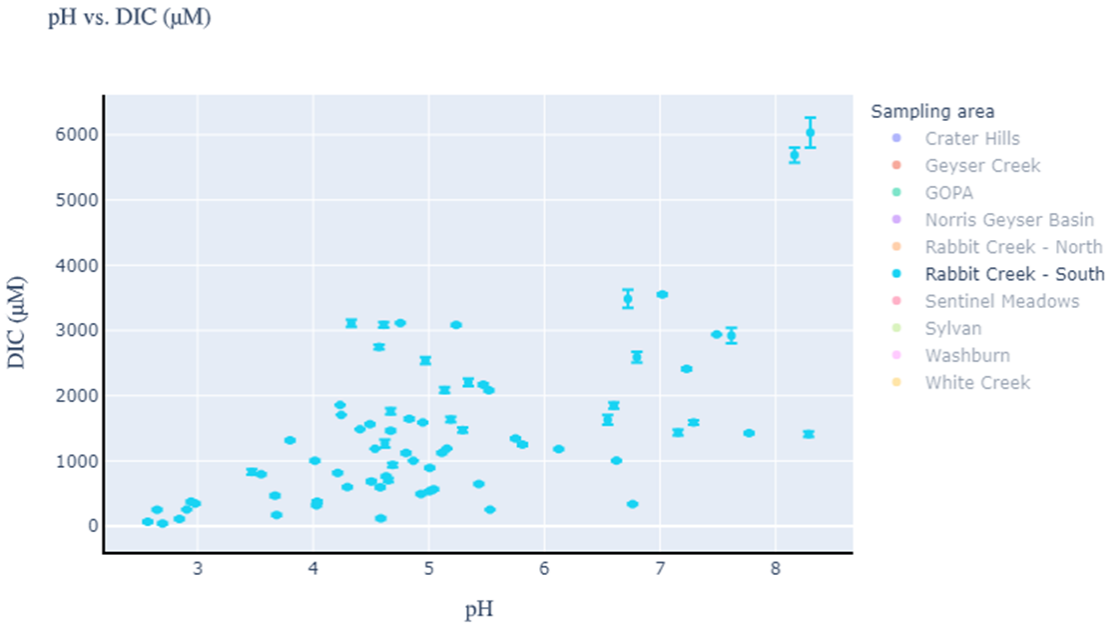

Figure 3.13: DIC concentration vs. pH for Rabbit Creek – South.

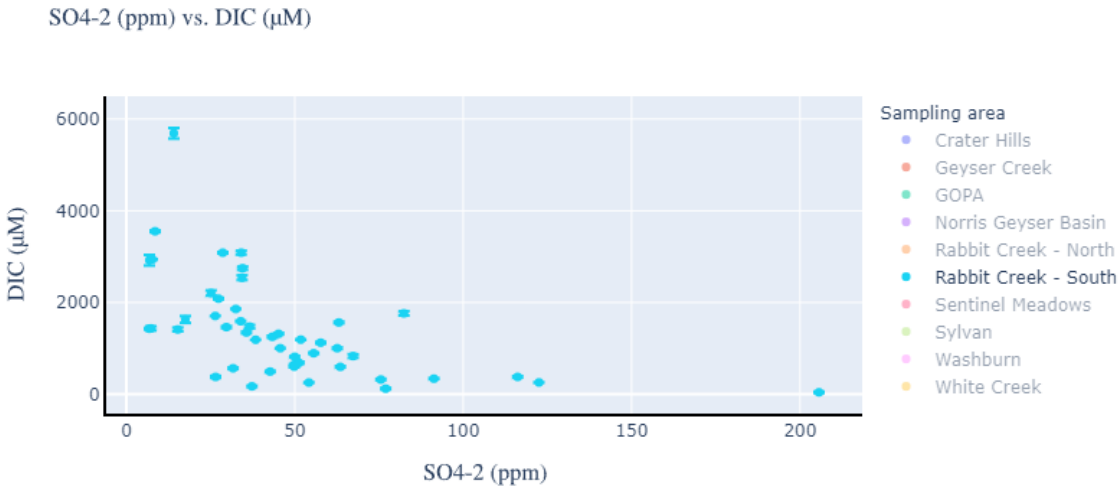

Figure 3.14: DIC concentration vs. SO_4^{-2} (ppm) for Rabbit Creek – South.

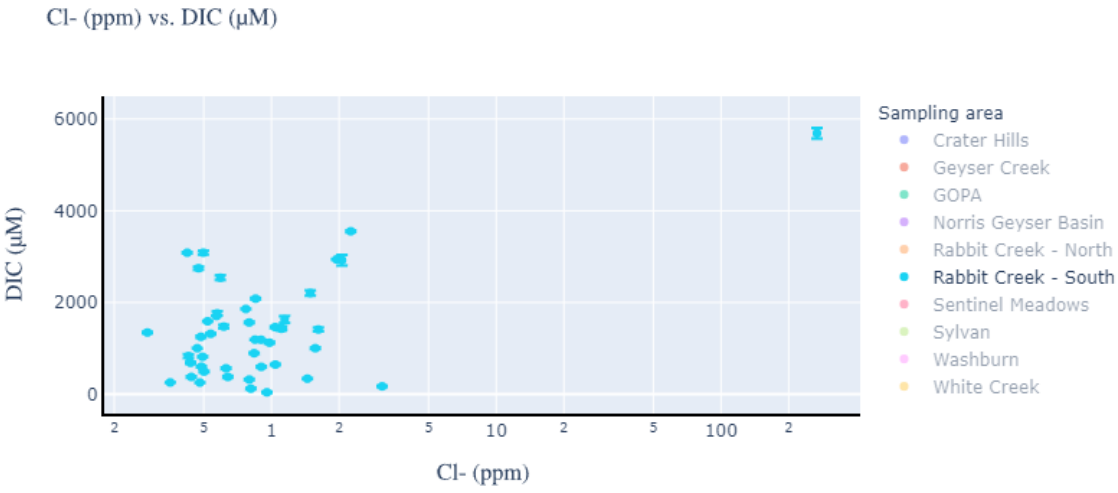

Figure 3.15: DIC concentration vs. Cl^- (ppm) for Rabbit Creek – South.

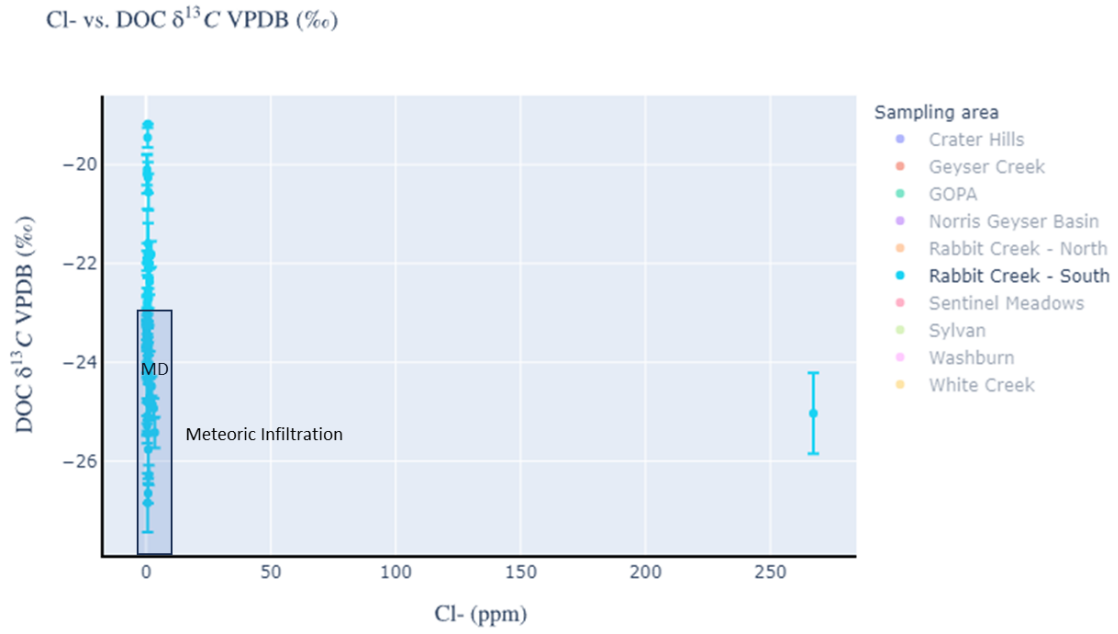

Figure 3.16: DOC $\delta^{13}C$ vs. Cl^- (ppm) for Rabbit Creek – South.

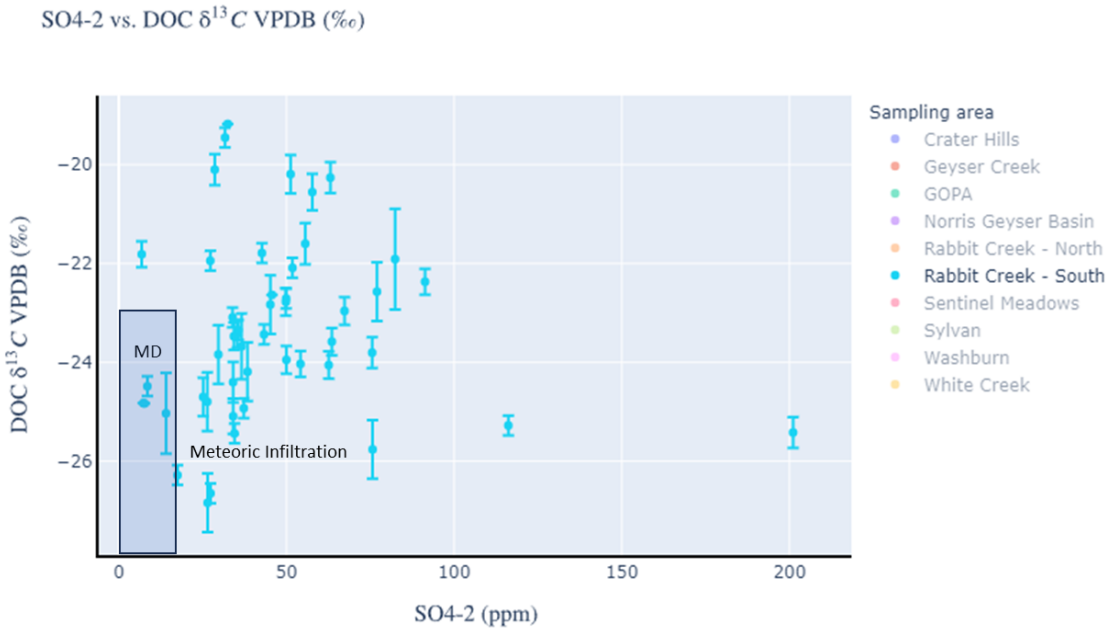

Figure 3.17: DOC $\delta^{13}C$ vs. SO_4^{-2} (ppm) for Rabbit Creek – South.

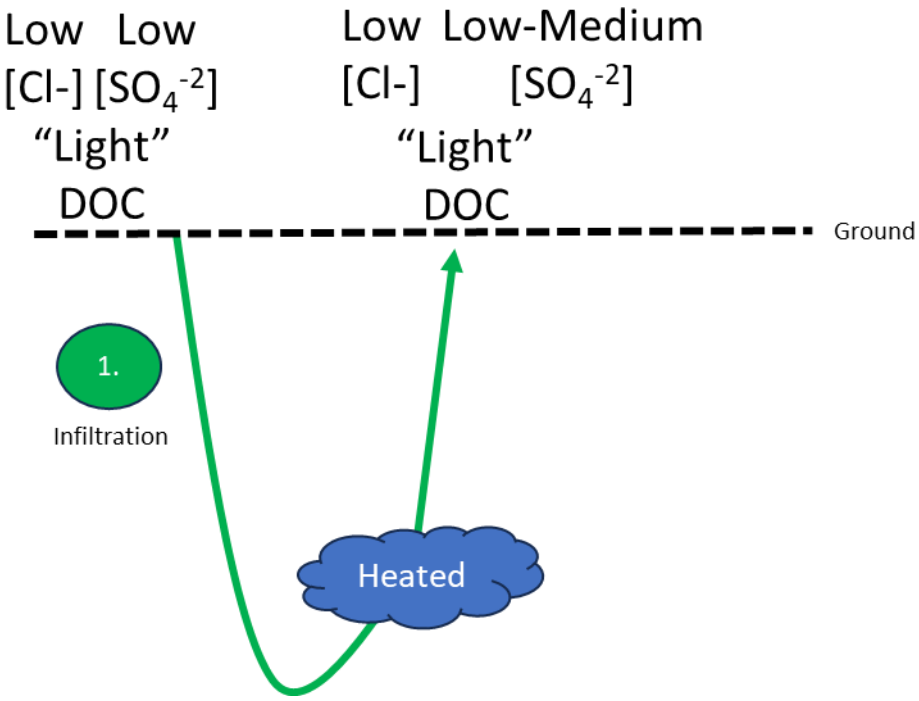

Figure 3.18: Schematic showing fluid path in Rabbit Creek South.

Sentinel Meadows (Deeply Sourced)

Sentinel Meadows lies in the Lower Geyser Basin (Fig. 1.11). The meadow is surrounded by grasses and Sentinel Creek runs through the middle of the meadow. Hot springs within this area are spread out and not localized to one specific area. Some hot springs have siliceous forming cones and mounds with "positive" topography whereas other springs are sitting at geographically "negative" points in the meadow (Fig. 1.8). Walking through the meadow it is apparent that there are remains of many inactive springs throughout the meadow. This is indicated by the silica sinter deposits. The active springs within this region have larger features with boiling clear blue water. Many

features are actively outflowing where bright yellow and orange biofilms are present as temperatures decrease down the outflow.

Sentinel Meadows SO_4^{-2} vs. Cl^-

Sentinel Meadows contains chloride rich fluid that is the deep hydrothermal end member. Chloride concentrations are typically between 200-260 ppm for alkaline-chloride hot springs with some concentrations that are lower than 200 ppm (Fig. 3.19). These springs that are below 200 are hypothesized to be hot springs that are dominated by phase separated fluid. Sulfate concentrations range from 10 to 66 ppm with an outlier at 424 ppm. Higher concentrations of sulfate are present in the phase separated and acidic hot springs. Low sulfate concentrations are characteristic of fluid that has interacted with high temperatures and boiling for longer amounts of time.

Sentinel Meadows DIC

DIC concentrations are higher in hot springs with more chloride versus hot springs with less chloride (Fig. 3.20). Chloride is increasing in these hot springs due to increased water-rock interaction, boiling, and evaporation of neutral-chloride hot springs (Fig. 1.5). The opposite is observed in the acidic hot springs where chloride is not present in phase separated fluid and DIC concentration is lower. [DIC] is higher (4000-6000 µM) in alkaline hot springs versus acidic hot springs (2500-3000 µM) in Sentinel Meadows where acidic hot springs tend to have more sulfate (Fig. 3.21). DIC $\delta^{13}C$ values all range in the geogenic classsifcation displaying a dominat source (Fig. 3.22). There is no correlation between

sulfate gas addtions and DIC $\delta^{13}C$ values which is expected due to overall low sulfate concentrations in these hot springs (Fig. 3.23).

Sentinel Meadows DOC

DOC in Sentinel Meadows is very low (<100 µM) for the alkaline-chloride springs. This is expected of deep fluid that has undergone extensive boiling and thermal alteration ultimately decreasing the concentration of DOC (Fig. 3.24). There is a higher [DOC] at acidic hot springs in Sentinel Meadows with low chloride and high sulfate (Fig. 3.25). These springs could have microorganisms that are very active oxidizing sulfate and producing DOC. These acidic springs may also have infiltration from groundwater since they are not silica precipitating therefore increasing the concentration of DOC. DOC $\delta^{13}C$ seems to indicate that metroric water may be infiltrating the acidic springs due to the DOC $\delta^{13}C$ signature in the range of C3 photosynthetic plant material. As alkaline-chloride fluids increase in chloride, there is a corresponding increase in ^{13}C enrichment (Fig. 3.26). This is expected as fluids have more water-rock interaction. There is no correlation between sulfate and DOC $\delta^{13}C$ which is also expected due to the lower levels of sulfate concentration in this region (Fig. 3.27). This therefore resmebles fluid that is deeply sourced that has undergone a large amount of boiling which reduces the level of sulfate in these fluids.

Sentinel Meadows Overview

Sentinel Meadows is characteristic of deeply sourced fluid and serves as the end member in this study for high water rock interactions with little gas influence. Many of

these springs are actively depositing sinter which acts as an “armored column” (Fig. 1.8) which therefore increases the topography of these features and limits groundwater infiltration. This therefore displays springs that are not influenced by their local environment compared to Rabbit Creek South which is directly connected to meteoric influences. Acidic hot springs are localized by “Bison Pool” and may be a product of the proposed leaky system (Smeltz, 2022) interacting with oxygenated groundwater. H_2S would then be oxidized creating an abundance of sulfate which would ultimaterly lower the pH resulting in acidic hot springs (Fig. 3.28). The higher concentration of DOC at these locations could be due to the shallow groundwater infiltration and also the abundance of bison excrement located around these hot springs. Bison in the winter use this area for warmth and plants due to the large heat influx around “Bison Pool”. These acidic features are also all bubbling, but they are not boiling like other alkaline-chloride hot springs. This bubbly could be due to CO_2 escaping in the gas form out of the leaky system of “Bison Pool” into the acidic hot springs and actively degassing Figure 3.28 summarizes how fluid path is primarily associated with Sentinel Meadows and that of deeply sourced alkaline-chloride rich features.

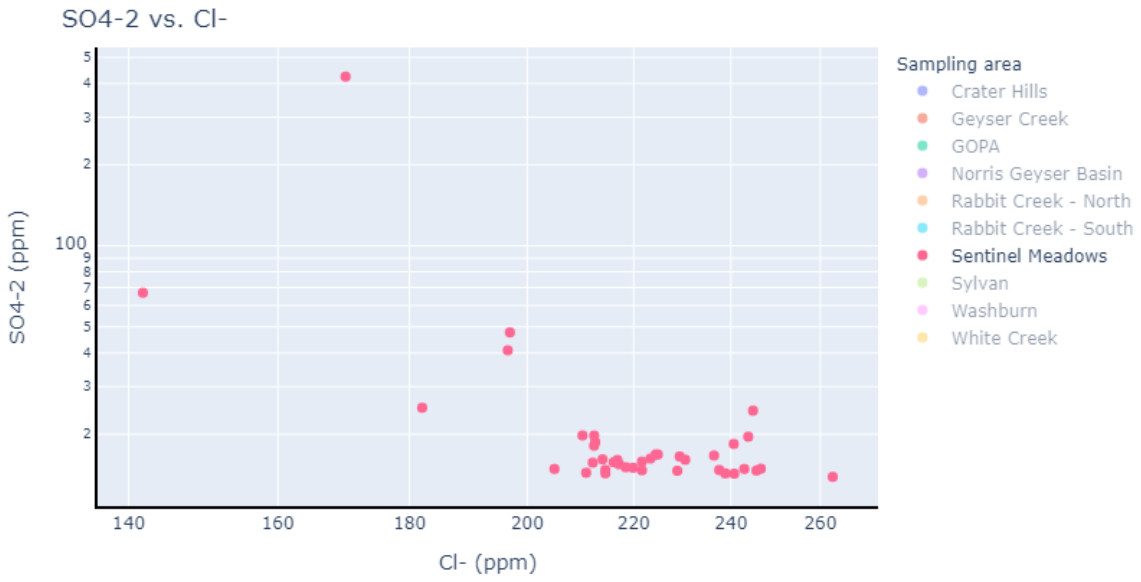

Figure 3.19: SO_4^{-2} (ppm) vs. Cl^- (ppm) for Sentinel Meadows.

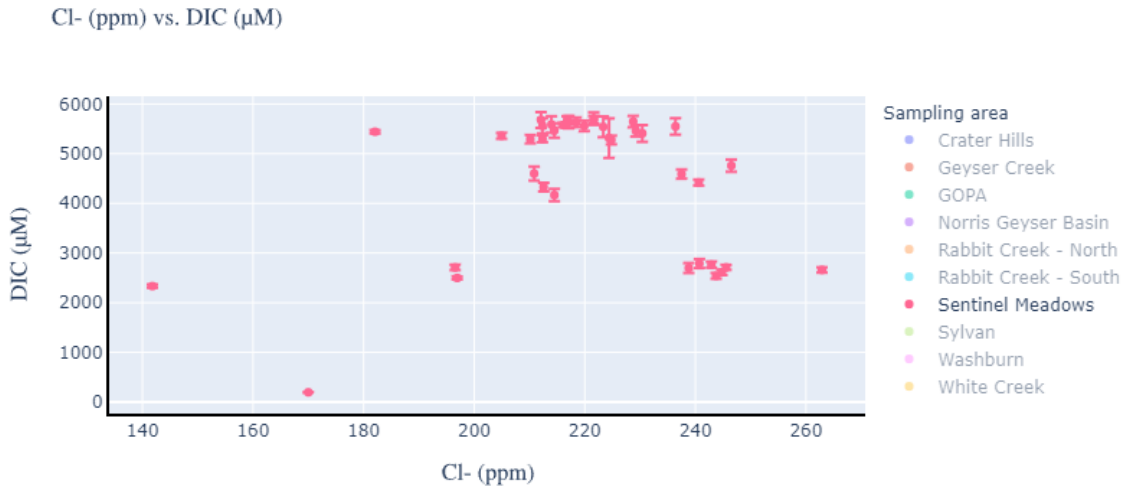

Figure 3.20: DIC concentration vs. Cl^- (ppm) for Sentinel Meadows.

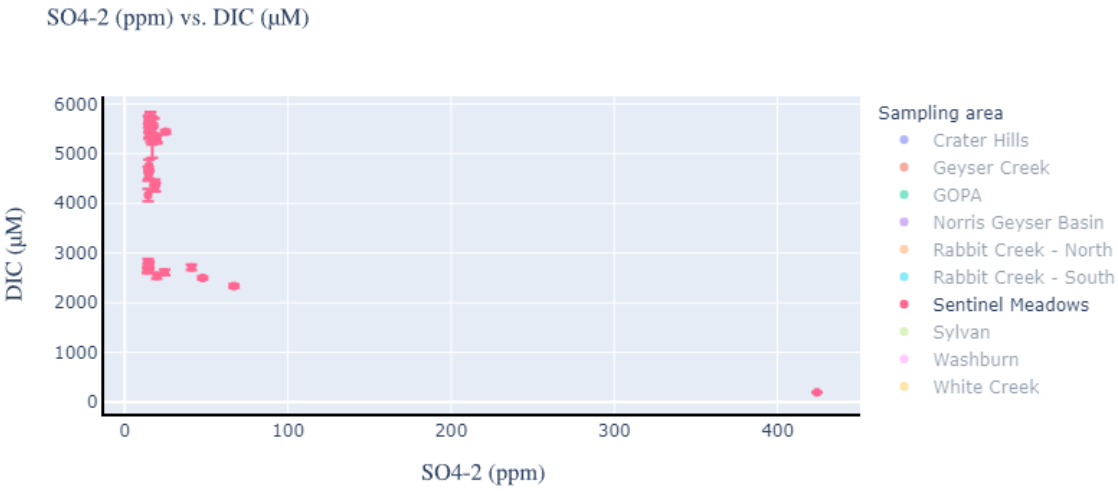

Figure 3.21: DIC concentration vs. SO_4^{-2} (ppm) for Sentinel Meadows.

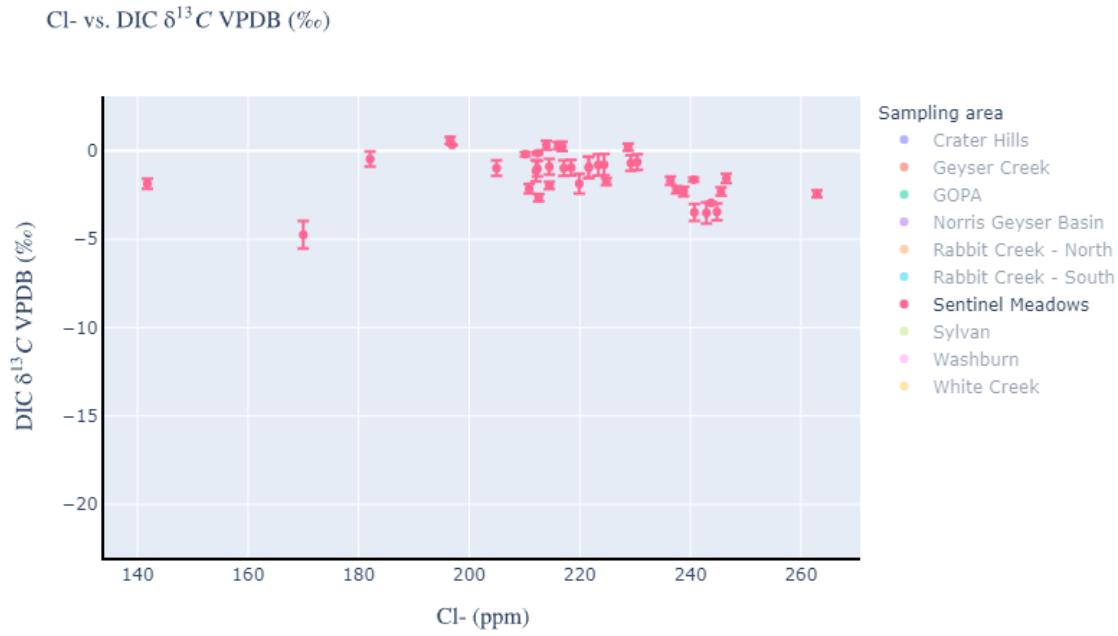

Figure 3.22: DIC $\delta^{13}C$ vs. Cl^- (ppm) for Sentinel Meadows.

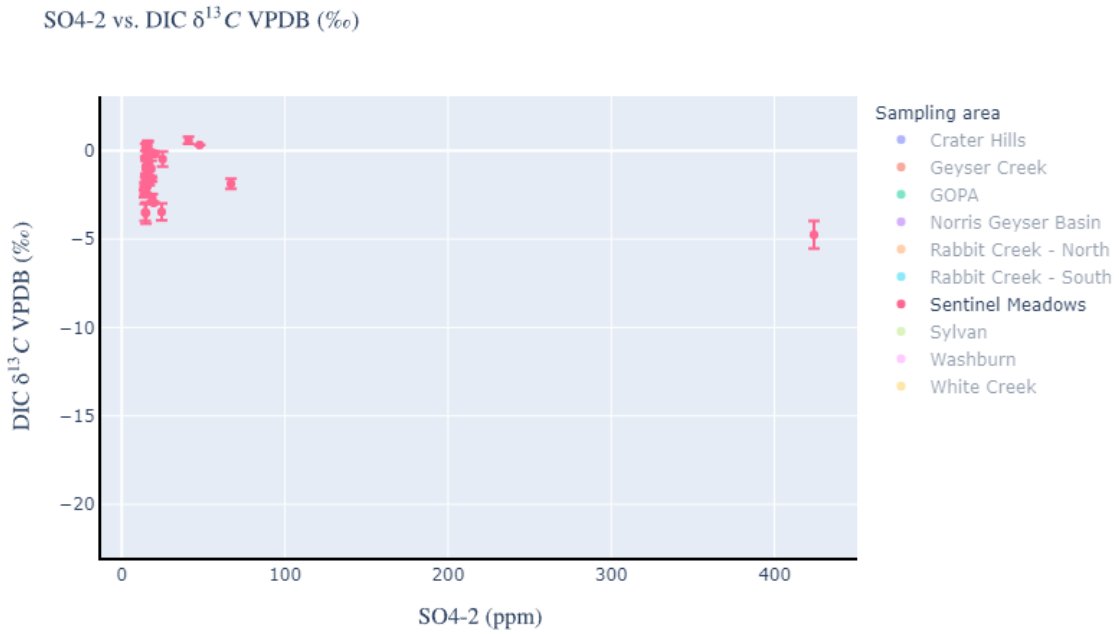

Figure 3.23: DIC $\delta^{13}C$ vs. SO_4^{-2} (ppm) for Sentinel Meadows.

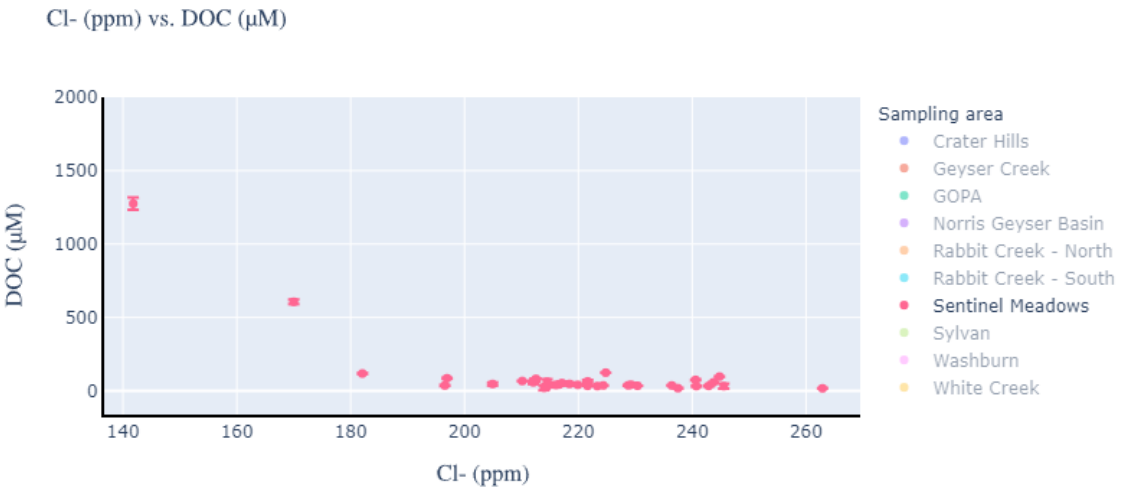

Figure 3.24: DOC concentration vs. Cl^- (ppm) for Sentinel Meadows.

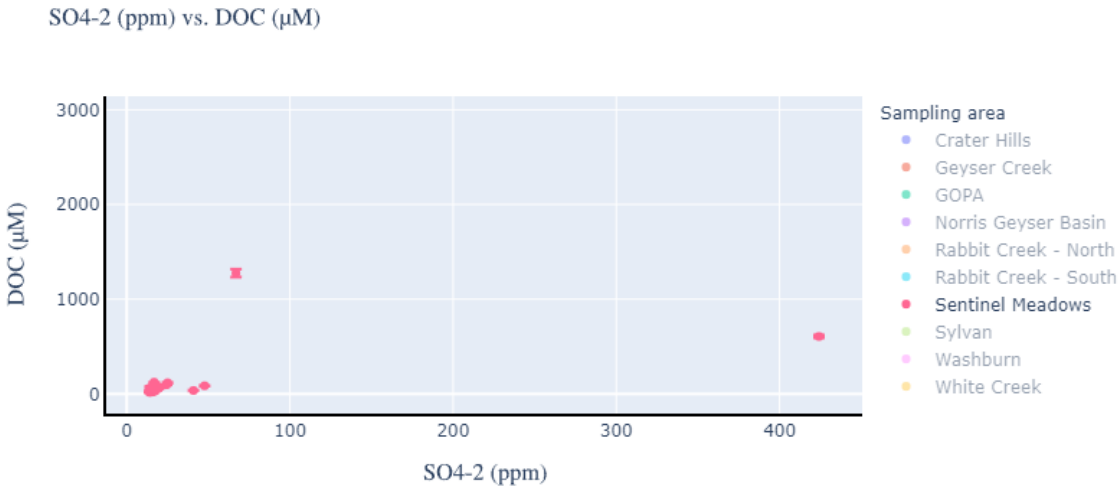

Figure 3.25: DOC concentration vs. SO_4^{-2} (ppm) for Sentinel Meadows.

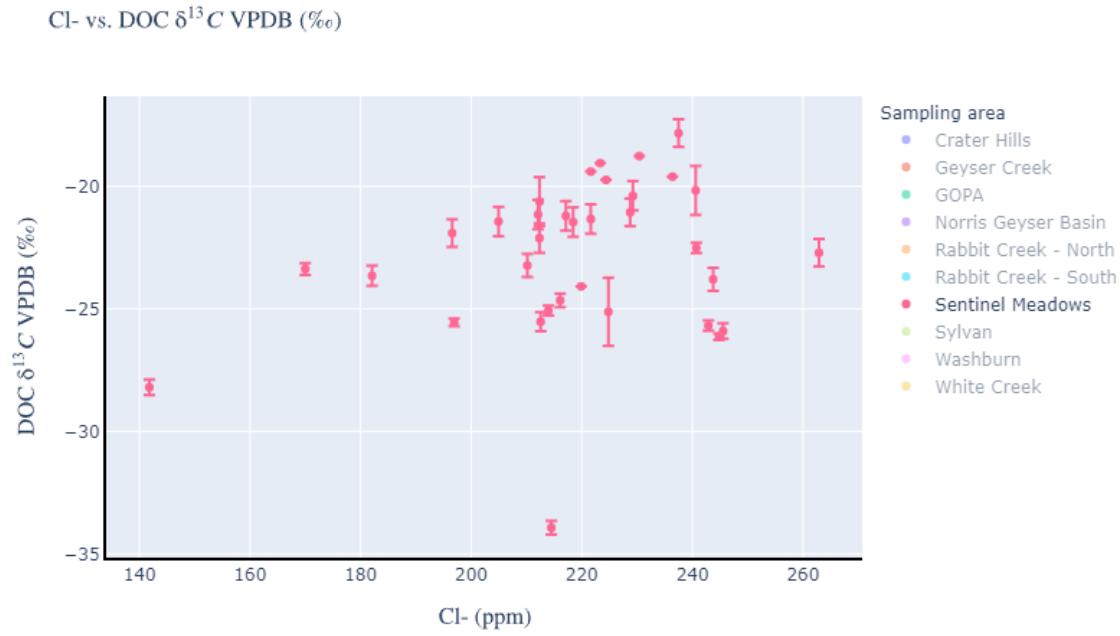

Figure 3.26: DOC $\delta^{13}C$ vs. Cl^- (ppm) for Sentinel Meadows.

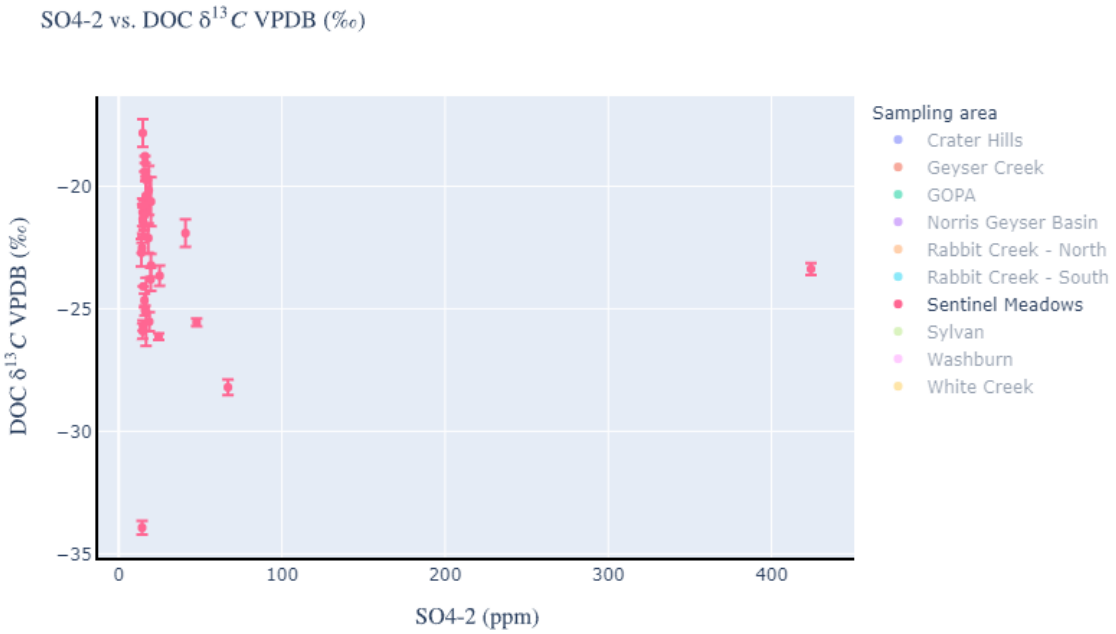

Figure 3.27: DOC $\delta^{13}C$ vs. SO_4^{-2} (ppm) for Sentinel Meadows.

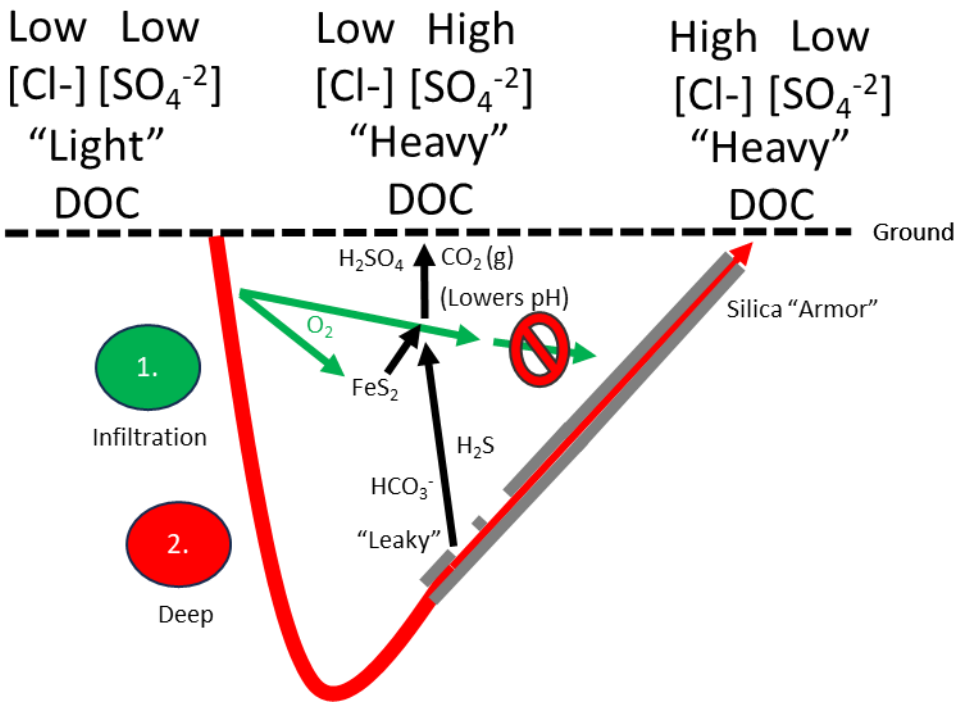

Figure 3.28: Schematic showing fluid path in Sentinel Meadows.

Greater Obsidian Pool Area (Meteoric and Deep Mixing with Phase Separation)

GOPA is located within the Hayden Valley and near an inferred boundary of previous calderas (Fig. 1.11). GOPA is classified by the USGS as glacial deposits with gravel. The meadow and hot springs drain into Goose Lake which is located topographically lower than the thermal features. The vegetation within this region is mostly grass and sage in the meadow. Higher up in the meadow, there are lodgepole pine that are topographically higher, but they are a great distance away from the hot spring features.

The hot springs in this region sit at topographic lows and the edges are not armored with silica. This therefore may allow access for exogenous material to be input into these springs. One-way organic carbon can be introduced to the hot springs when bison are present because they are actively churning up the soil around the hot springs. Storm surges could actively deposit this soil into the hot springs. Hot springs also melt the snow due to the heat which exposes vegetation allowing the bison to graze. Therefore, during winter months there may be a higher bison presence within the area compared to the summer.

GOPA SO_4^{-2} vs. Cl^-

GOPA is a variable region containing a range of hot springs from 30-2000 ppm SO_4^{-2} and 1-475 ppm Cl^- (Fig. 3.29). This range therefore has hot springs that are classified as Meteoric Dominant, Meteoric Gas Dominant, and Hydrothermal Boiling and

Gas. Primarily the signatures are hydrothermal boiling and gas with dilutions of meteoric water as points shift toward the MD region on Figure 3.29.

GOPA DIC

Comparing gas additions to SO_4^{-2} (Fig. 3.30) it can be determined that the expected trend from Figure 1.5 is not observed at these hot springs. SO_4^{-2} increases do not correspond with increases of DIC concentration. This could be happening due to there are acidic features where DIC is escaping through the vapor phase so therefore increases are not seen. The other explanation would be DIC concentration increasing through meteoric infiltration. The latter appears to be happening in this region due to the SO_4^{-2} vs. Cl^- concentrations plotting along the mixing line between "hydrothermal boiling and gas" and "meteoric dominant." Another line of evidence is that with increasing Cl^-, there is not a corresponding increase in DIC which would be expected for hot springs that have undergone more water rock interactions (Fig. 3.31). Therefore, concentrations of DIC indicate that meteoric water may be diluting and mixing within the system. DIC $\delta^{13}C$ values do not correlate with increasing sulfate or chlroide (Fig. 3.8 & 3.9). This is another line of evidence that mixing of metoeric water could be influencing this area because there are no expected isotopic trends observed (see Figure 1.6).

GOPA DOC

Investigating the concentrations and isotopic signature of DOC to determine if meteoric water is actively mixing in certain springs is a powerful tool to determine the fluid path for hot springs. Universally in GOPA there is a very low concentration of DOC

with most samples having under 500 µM DOC. There are samples between 500-1000 µM at lower concentrations which is expected with the arrival of meteoric groundwater replenishing DOC (Fig 3.32). The $\delta^{13}C$ signature of DOC vs. Cl^- is helpful to determine where photosynthetic material is in the system. The blue box at low concentrations of chloride represents the range of -23‰ to -28‰ for C3 photosynthetic carbon. As chloride is increased, the $\delta^{13}C$ become more enriched displaying the processing of organic carbon in the system. From these deeply processed and enriched fluids, a horizontal line can be drawn. Phase separation can occur ultimately separating the fluid into two components. One component has high chloride, and the other component has low chloride. The low chloride component explains the enriched signatures displayed in Figure 3.33. There is also a slight enrichment of $\delta^{13}C$ due to gas additions and heating (Fig. 3.34). This trend is not very strong and therefore it could be weaker due to meteoric infiltration occurring with oxygenated groundwater reacting with H_2S gas increasing the sulfate concentration.

GOPA Overview

Ultimately GOPA is a diverse region with many different hot springs. This area shows signs of meteoric infiltration colliding with deeply sourced thermally altered water. It is evident there are dilutions of SO_4^{-2} and Cl^-. Figure 3.35 depicts the proposed schematic for how fluid is traveling to these hot springs in GOPA. Due to the geographic location mentioned earlier, it is possible that springs in the meadow on the southwest side are acting as “shields” for other hot springs. This is due to the meteoric groundwater flowing from topographic highs to lows in the meadow infiltrating in the southwest. These hot springs tend to show more of a meteoric dominant $\delta^{13}C$ photosynthetic

signature compared to hot springs on the northeast. Therefore, it is possible that this infiltrating water is upwelling when it comes into contact and mixes at the hot springs on the southwest. This then creates a gradient where further away from this mixing point there is a dominant deeply sourced fluid that has not encountered the meteoric water infiltrating, and this is shown by higher concentrations of Cl^-. At these higher concentrations of Cl^-, the same enrichment is seen with low chloride so therefore this is the location of where a significant phase separation is happening in this region. More evidence for phase separation is the correlation between enriched DOC $\delta^{13}C$ and low concentrations of DOC which fits the schematic model and predictions in Figure 1.7.

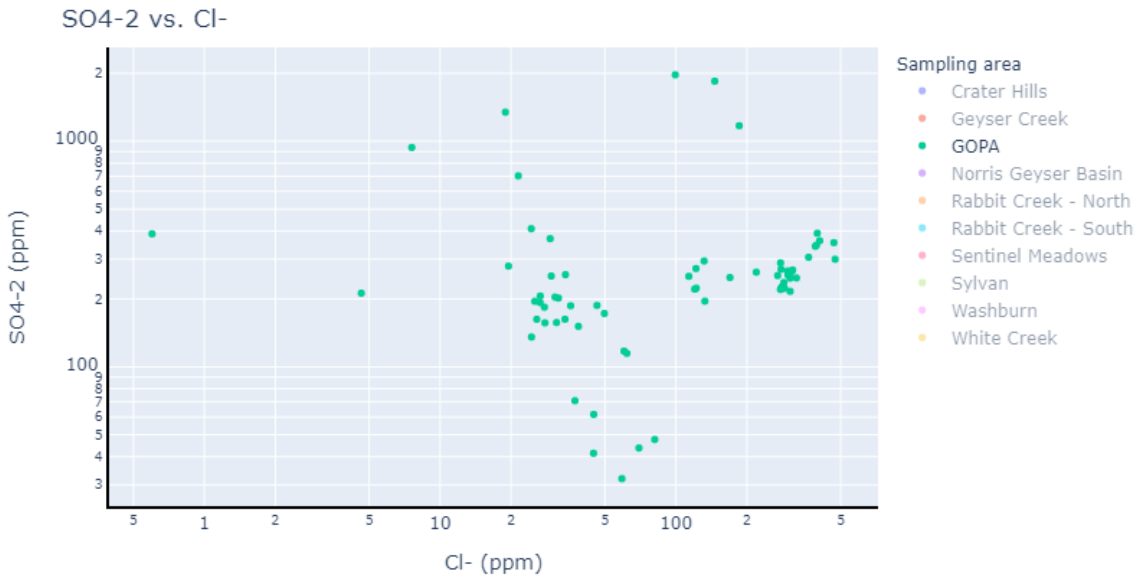

Figure 3.29: SO_4^{-2} (ppm) vs. Cl^- (ppm) for GOPA from 2005-2019.

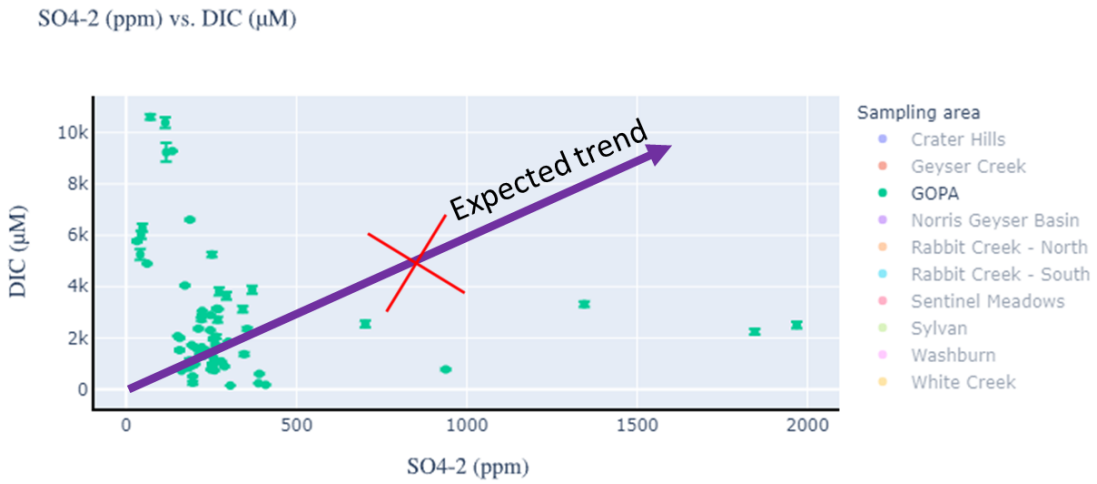

Figure 3.30: DIC concentration vs. SO_4^{-2} (ppm) for GOPA. The line with the predicted trend referring to Figure 1.5 is projected over the data.

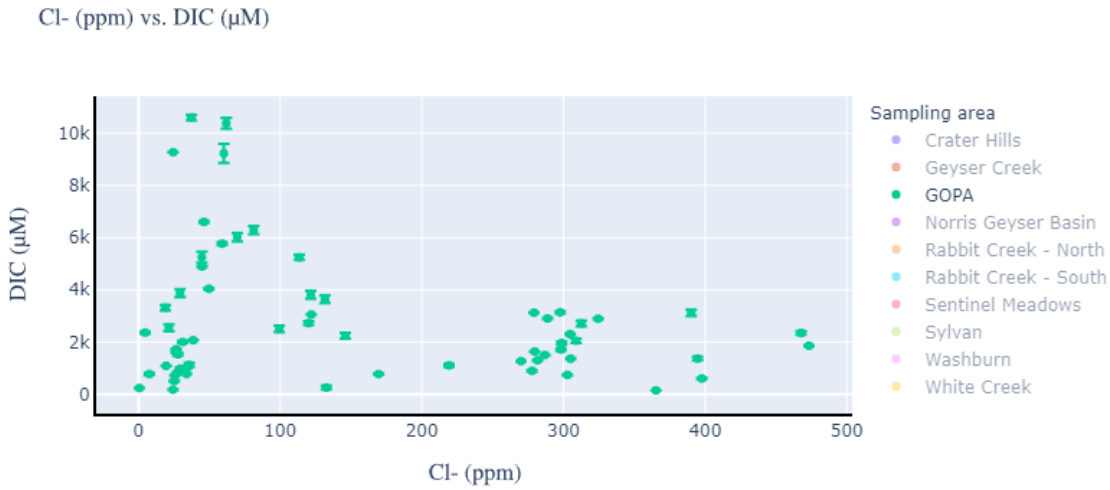

Figure 3.31: DIC concentration vs. Cl^- (ppm) for GOPA.

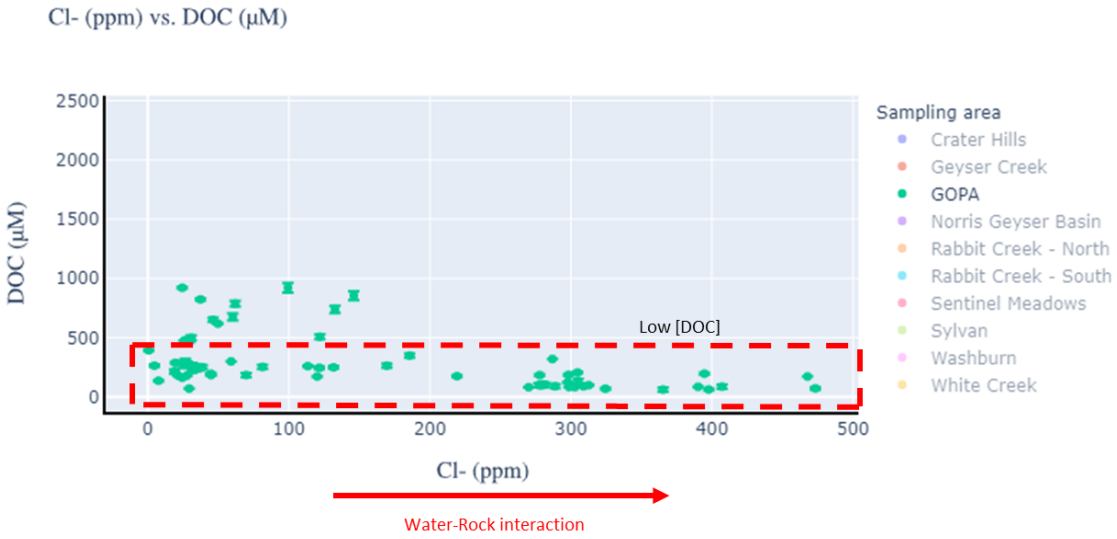

Figure 3.32: DOC concentration vs. Cl^- (ppm) for GOPA.

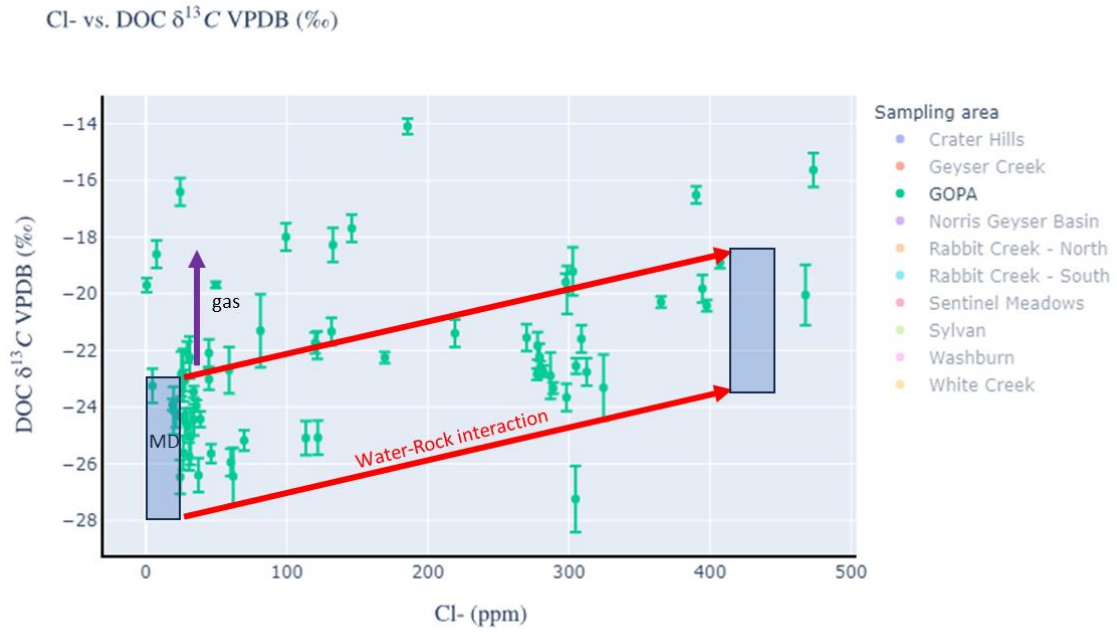

Figure 3.33: DOC $\delta^{13}C$ vs. Cl^- (ppm) for GOPA.

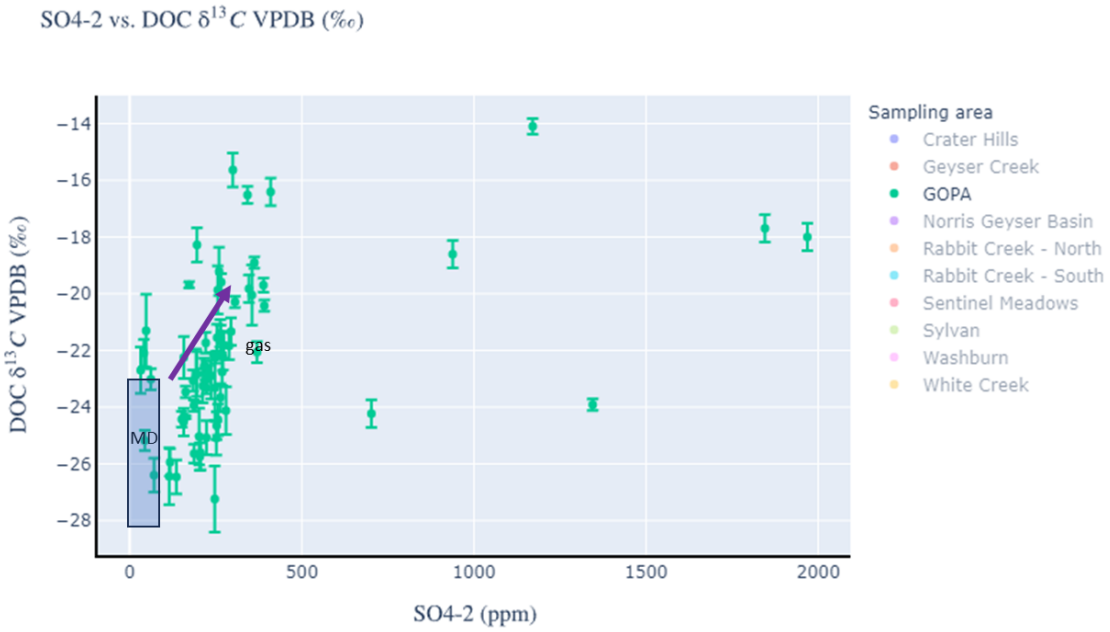

Figure 3.34: DOC $\delta^{13}C$ vs. SO_4^{-2} (ppm) for GOPA.

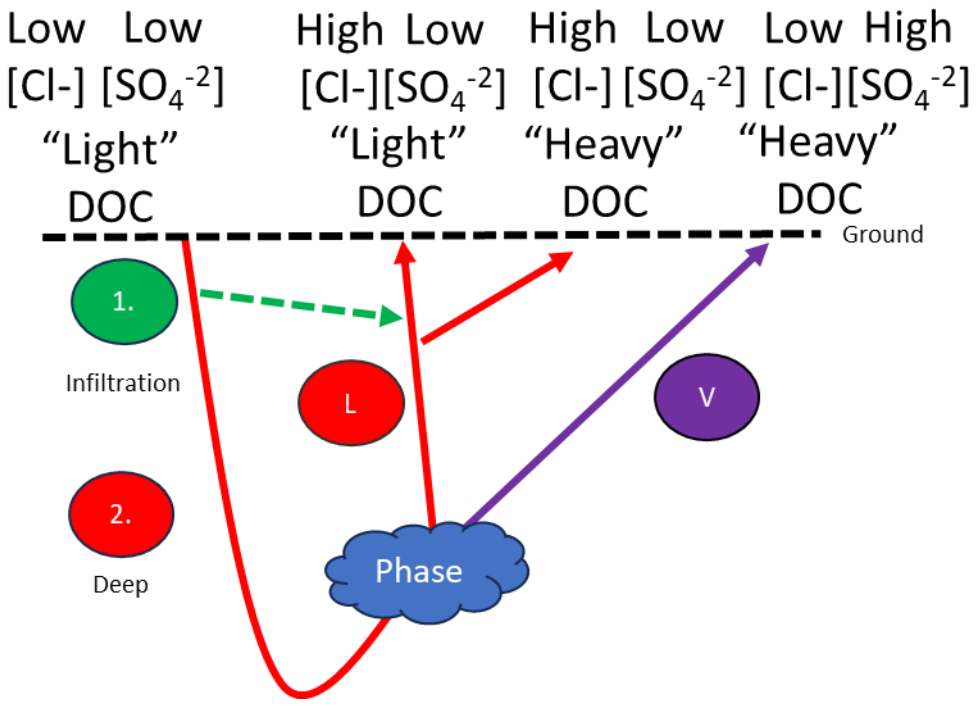

Figure 3.35: Schematic showing predicted fluid path for GOPA.

Geyser Creek (Complex Meteoric Mixing with Deep Gas Rich Fluid)

Geyser Creek is located north outside of the caldera (Fig. 1.11). Geyser Creek has two main hydrothermal areas where geyser creek runs through the middle of the hydrothermal area. Many of these springs are located downslope of the surrounding hills that are covered in lodgepole pine. The topography is diverse and each hot spring in this region is affected by topography differently which leads to complex mixing pathways. Hot springs are primarily located negatively compared to their surroundings and therefore are hypothesized to be greatly affected by the local environment. Many hot springs in this region are actively outflowing into Geyser Creek. There is a wide variety of hot springs (pH: 2-8.5) in this region (Fig. 3.1). Hot springs are unique in this area because many of the hot springs outflow or mix and some hot springs flow directly into other hot springs. There was no evidence of bison at this location as it is surrounded by a dense forest of lodgepole pine.

Geyser Creek SO_4^{-2} vs. Cl^-

Geyser Creek sulfate (20-1143 ppm) and chloride (1-1135 ppm) concentrations are a wide range that spans multiple orders of magnitude for both anions (Fig 3.36). This therefore means there are several different classifications for hot springs present in this location like GOPA, but more complex. Most of these signatures with lower chloride are neutral-chloride springs indicative of hydrothermal boiling. Acidic springs in this region have increased sulfate with lower chloride most likely caused by large, localized gas

additions which would lower the overall chloride and decrease pH values. Therefore, the fluid in this region is following a complex path that appears to be mixing of several different processes.

Geyser Creek DIC

[DIC] follows a similar distribution noticed in Rabbit Creek South across pH 2-8 with a range of 73 µM at pH 2 to 6000 µM at pH 8 (Fig 3.37). This is indicative of meteoric fluid impacting the system. Although at low pH there tends to generally be higher [DIC] in the system than expected for freshwater. [DIC] tends to decrease with additions of sulfate (Fig. 3.38). This is expected due to these hot springs being characteristically acidic and CO_2 is therefore escaping the fluid in the vapor phase. This therefore shows that hot springs exhibiting low [DIC] and high sulfate must be hydrothermal fluid entering the vapor phase for the fluid path. Concentration of DIC versus chloride also supports this hypothesis. As chloride is increased, there is a corresponding increase in [DIC] within the system (Fig. 3.39). This is caused by water rock interaction and supports the hypothesis that this fluid is resulting from deeply circulated fluid.

Geyser Creek DOC

DOC within Geyser Creek is very low which is comparable to both Rabbit Creek South and GOPA. The range of [DOC]is 27-366 µM in Geyser Creek. Figure 3.40 shows a slight decrease in [DOC] as chloride increases which is expected due to water rock interactions. There are several hot springs that do not follow this trend and have higher

[DOC] than others. These hot springs are very acidic around a pH of 2 and it is possible that this signature is due to a dominant and active microbiological community producing DOC. This will be further investigated in Chapter 6 of this thesis with "Jackhammer". Another line of evidence to support this hypothesis is that there is a weak trend of increasing [DOC] with increasing sulfate additions (Fig. 3.41). Gas and heat additions would be expected to decrease the [DOC] and that is not the case. Therefore, microbiology could be playing a major role at these hot springs. This is also possible due to the localization of these springs near vegetation at the base of the surrounding hills with a larger concentration of sulfate gas. Therefore, meteoric input could be increasing [DOC]. Throughout GOPA [DOC] is very low so that may allow this biogenic signature to be visible in the data.

The overall $\delta^{13}C$ for DOC versus chloride is relatively constant as chloride increases. Most of the samples fall in the photosynthetic region or slightly more enriched in ^{13}C (Fig. 3.42). This is evidence that there may be infiltration occurring in this area. Topographically this makes sense as many of these hot springs fall in a topographic low between the surrounding hillside and groundwater flow would go down the surrounding hillsides intercepting hot springs before making way into Geyser Creek itself. These slightly enriched samples at low chloride could be evidence of gas additions where deeply processed heated DOC is enriched with lower chloride. Several springs in Figure 3.42 display this as a potential pathway. To follow this idea further, with gas additions and heating, it would be expected to see a trend with sulfate and $\delta^{13}C$ of DOC. Figure 3.43 displays a strong trend showing photosynthetic organic carbon that has been

enriched due to heat and gas additions. This is noted by the purple arrows and appears to be shifted as more sulfate is added into the system. The highest concentrations of sulfate and most enriched samples have the lowest concentrations of chloride. This could be evidence of oxygenated groundwater could therefore be mixing with the localized large heat and gas additions from the deep surface resulting in enriched and thermally altered photosynthetic DOC.

Geyser Creek Overview

Overall, Geyser Creek has a diverse fluid path for hot springs which may be due to the geographic and topographic location between surrounding hillsides. By investigating [DIC] and [DOC] with their corresponding $\delta^{13}C$ signatures, it is hypothesized that this region is a mixture of intense volcanic gas and heat combining with meteoric infiltrating water throughout the system. Figure 3.44 displays a schematic of the proposed fluid path in this region for different hot springs. This location is unique to the previous location because it is not directly in a meadow where ground water is intercepted by the first few hot springs in the groundwater's path. Due to the hillsides groundwater most likely must take a haphazard approach resulting in complex mixing and a large range of distinct signals. This location is also affected by large gas additions and heating that is seen on a larger scale than the previously explored regions. These gas additions localized on the side of the hill lower the pH due to the addition of sulfuric acid. The high temperature acidic nature of these hot springs ultimately enriches fresh photosynthetic dissolved organic carbon that is being transported in from meteoric groundwater.

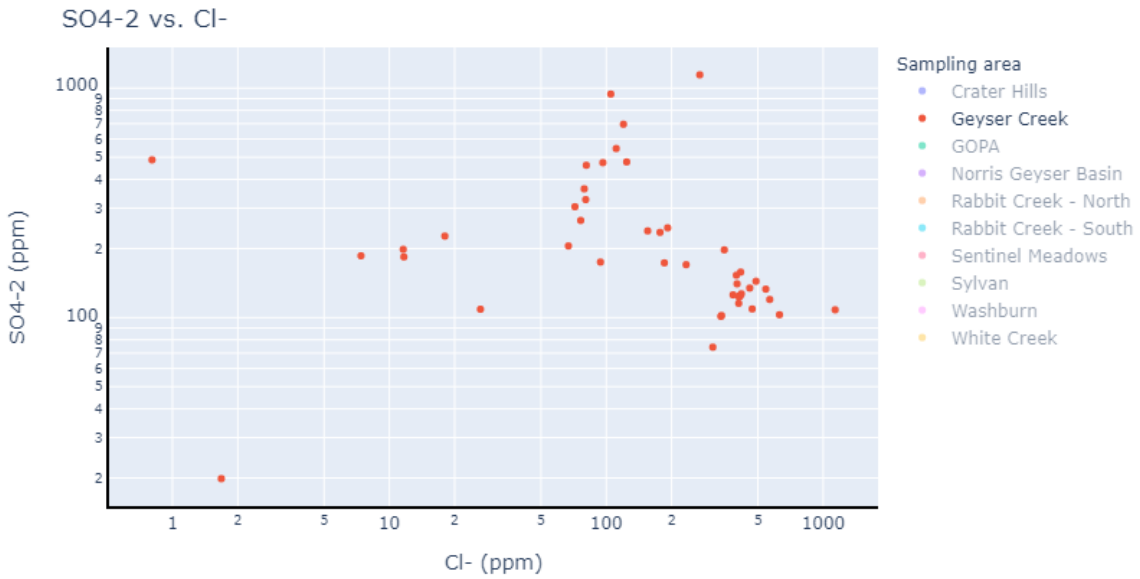

Figure 3.36: SO_4^{-2} (ppm) vs. Cl^- (ppm) for Geyser Creek.

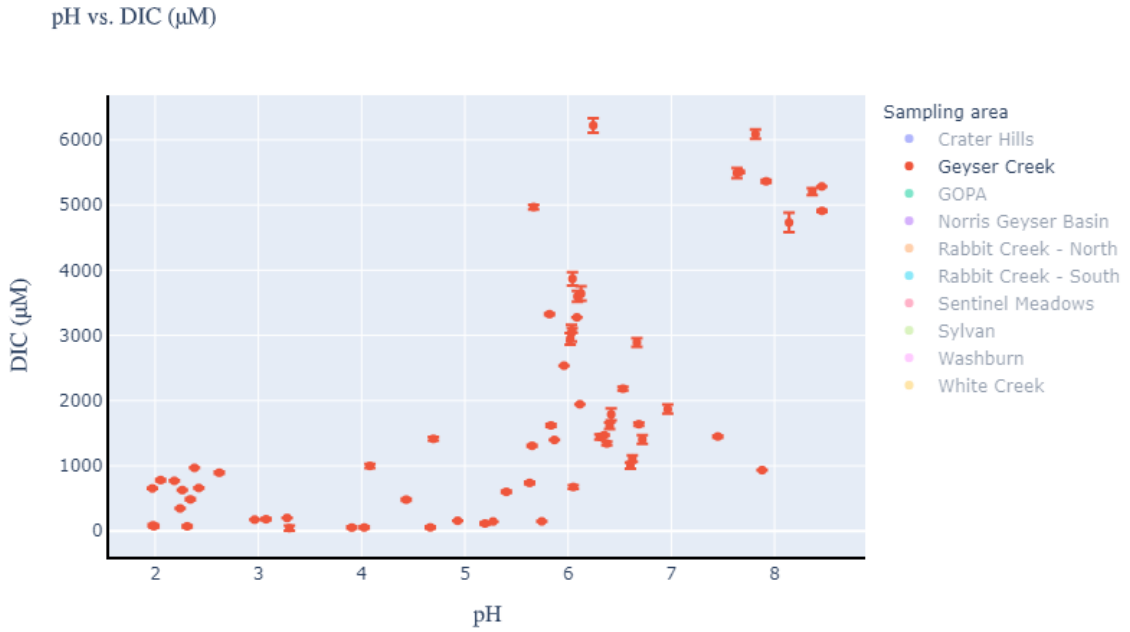

Figure 3.37: DIC concentration vs. pH for Geyser Creek.

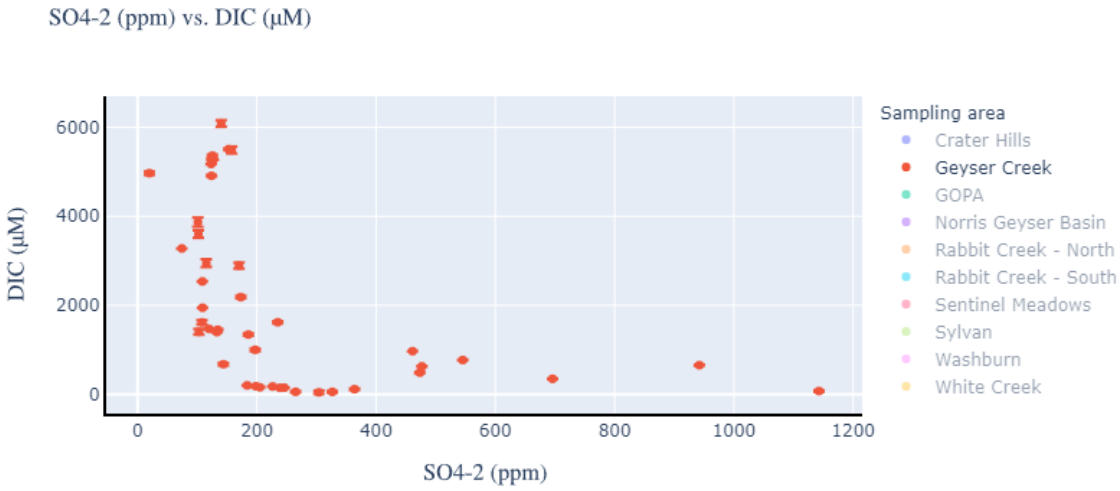

Figure 3.38: DIC concentration vs. SO_4^{-2} (ppm) for Geyser Creek.

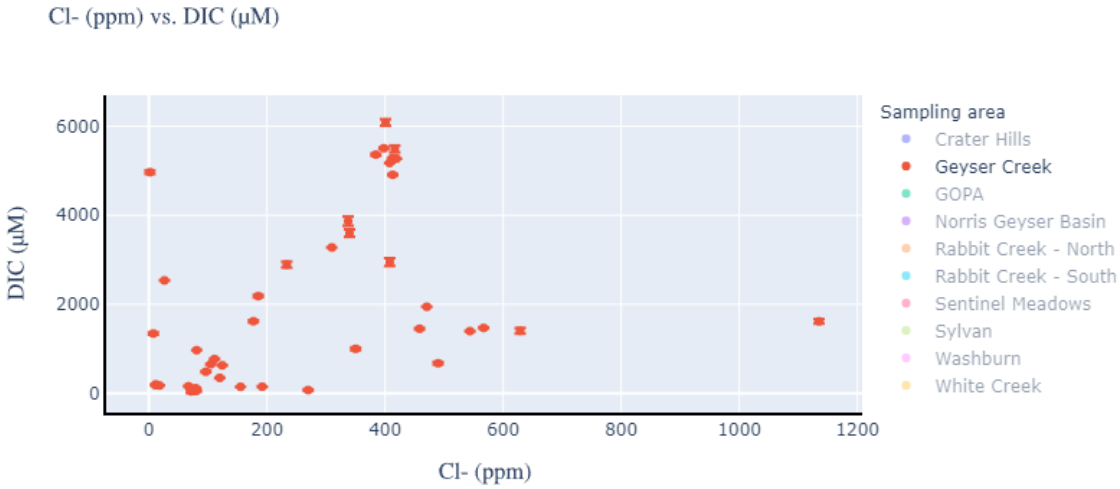

Figure 3.39: DIC concentration vs. Cl^- (ppm) for Geyser Creek.

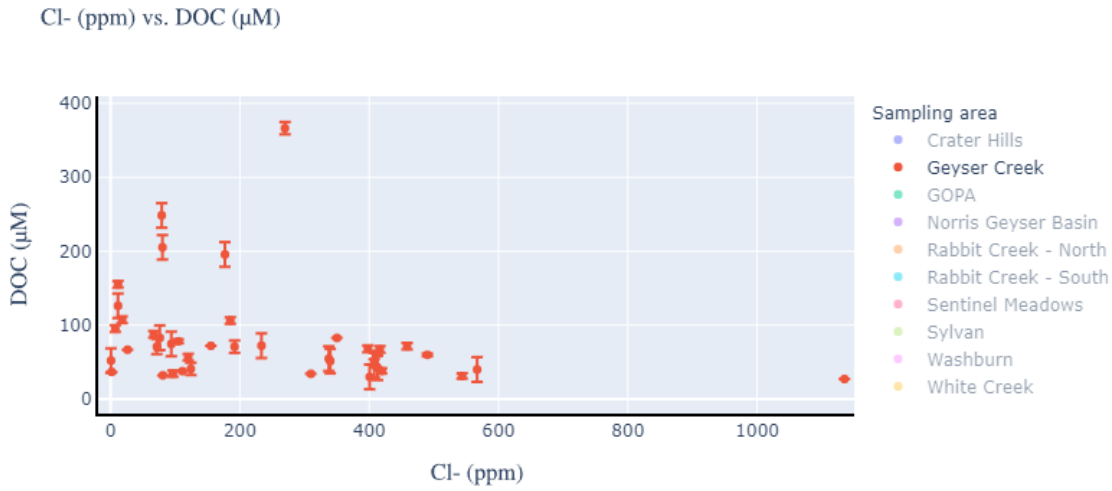

Figure 3.40: DOC concentration vs. Cl^- (ppm) for Geyser Creek.

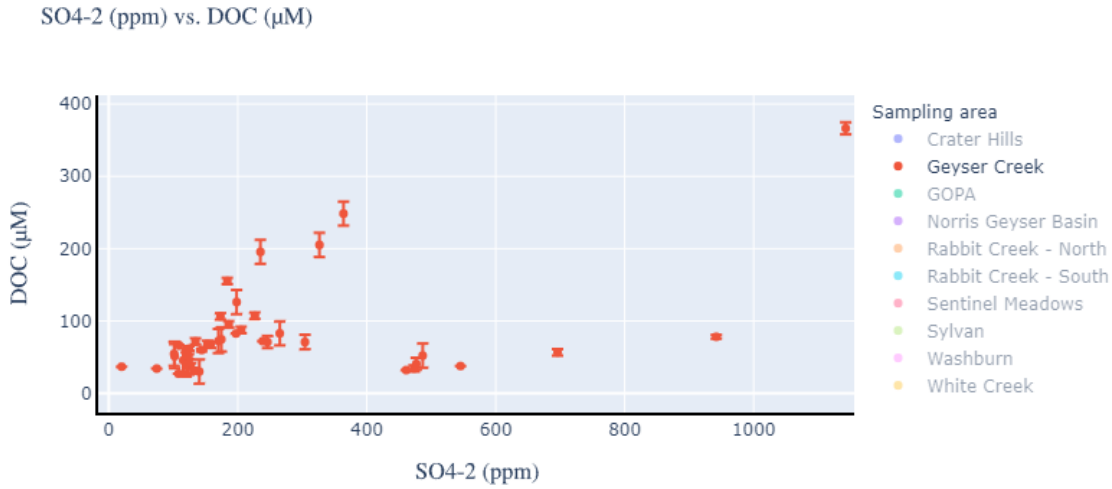

Figure 3.41: DOC concentration vs. SO_4^{-2} (ppm) for Geyser Creek.

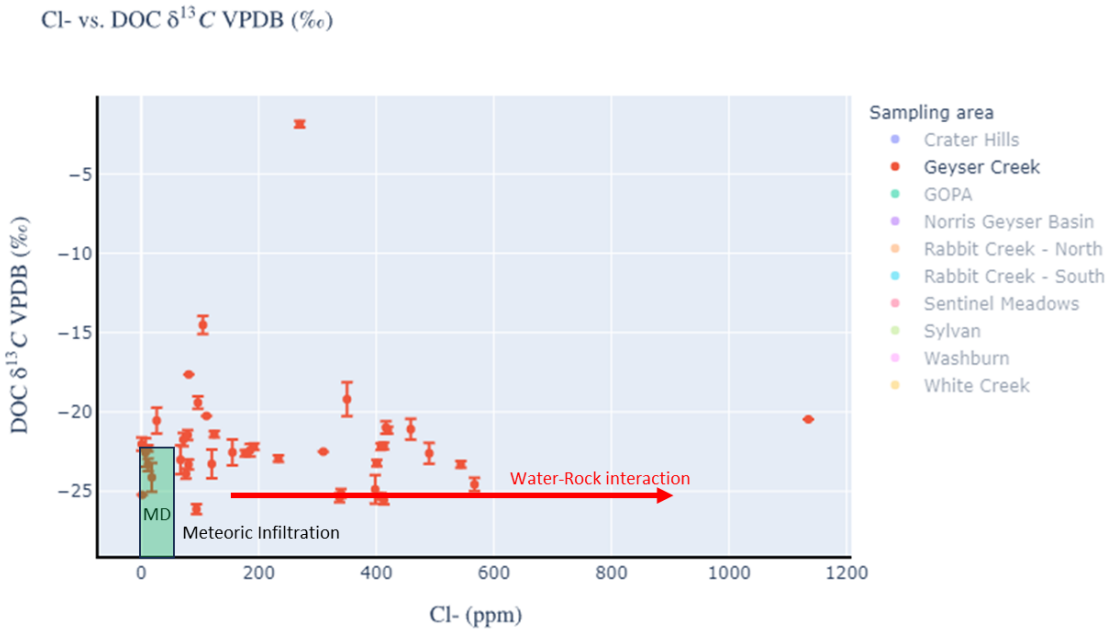

Figure 3.42: DOC $\delta^{13}C$ vs. Cl^- (ppm) for Geyser Creek.

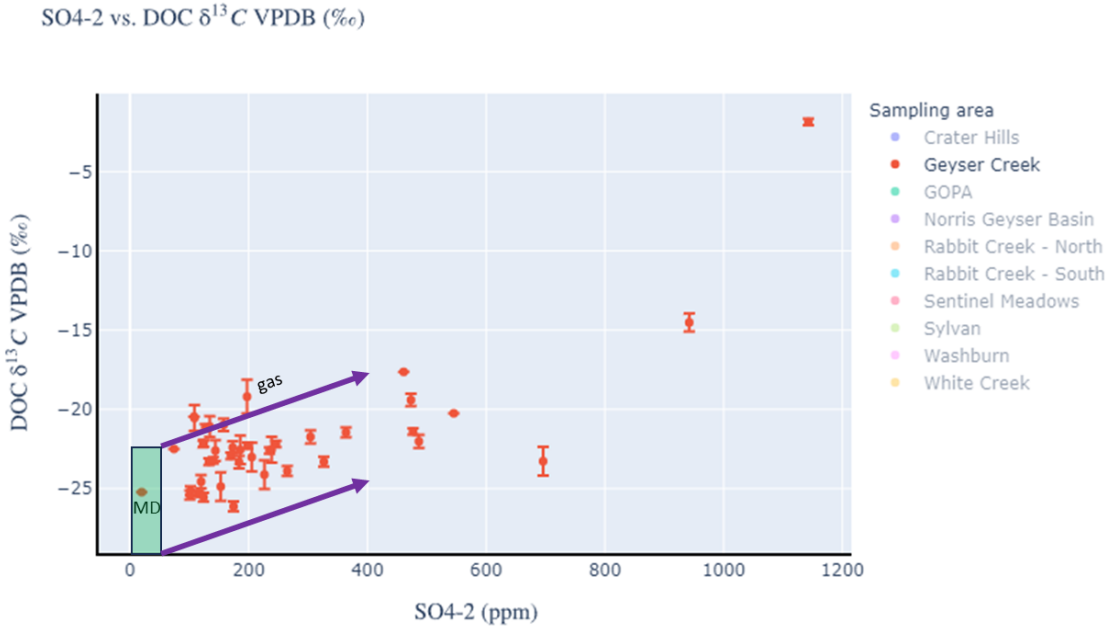

Figure 3.43: DOC $\delta^{13}C$ vs. SO_4^{-2} (ppm) for Geyser Creek.

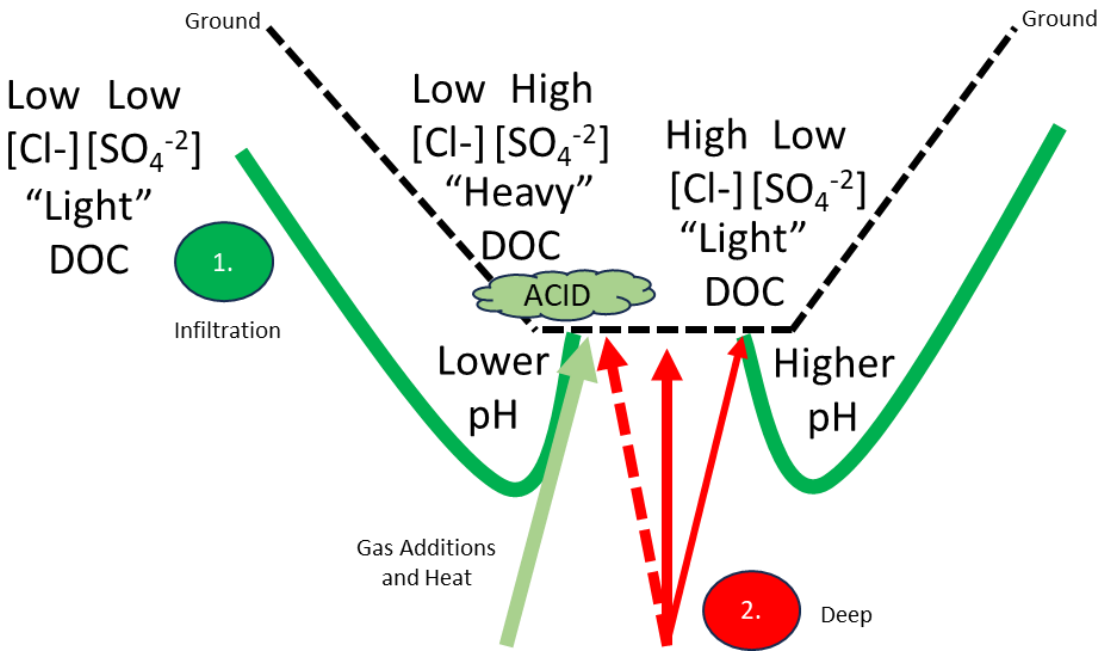

Figure 3.44: Schematic showing predicted fluid path for Geyser Creek.

REFERENCES

Cole, J. J., & Prairie, Y. T. (2014). Dissolved CO2 in freshwater systems.

Deines, P. (2002). The carbon isotope geochemistry of mantle xenoliths. *Earth-Science Reviews*, *58*(3-4), 247-278.

Fournier, R. O. (1989). Geochemistry and dynamics of the Yellowstone National Park hydrothermal system. *Annual review of earth and planetary sciences*, *17*(1), 13-53.

Gardner, W. P., Susong, D. D., Solomon, D. K., & Heasler, H. P. (2010). Using noble gases measured in spring discharge to trace hydrothermal processes in the Norris Geyser Basin, Yellowstone National Park, USA. *Journal of volcanology and geothermal research*, *198*(3-4), 394-404.

Hearn, E. H., Kennedy, B. M., & Truesdell, A. H. (1990). Coupled variations in helium isotopes and fluid chemistry: Shoshone Geyser Basin, Yellowstone National Park. *Geochimica et Cosmochimica Acta*, *54*(11), 3103-3113.

Hurwitz, S., & Lowenstern, J. B. (2014). Dynamics of the Yellowstone hydrothermal system. *Reviews of Geophysics*, *52*(3), 375-411.

Sobek, S., Tranvik, L. J., Prairie, Y. T., Kortelainen, P., & Cole, J. J. (2007). Patterns and regulation of dissolved organic carbon: An analysis of 7,500 widely distributed lakes. Limnology and oceanography, 52(3), 1208-1219.

Simkus, D. N., Slater, G. F., Lollar, B. S., Wilkie, K., Kieft, T. L., Magnabosco, C., ... & Onstott, T. C. (2016). Variations in microbial carbon sources and cycling in the deep continental subsurface. *Geochimica et Cosmochimica Acta*, *173*, 264-283.

Sims, K. W., Messa, C. M., Scott, S. R., Parsekian, A. D., Miller, A., Role, A. L., ... & Boyd, E. S. (2023). The Dynamic Influence of Subsurface Geological Processes on the Assembly and Diversification of Thermophilic Microbial Communities in Continental Hydrothermal Systems. *Geochimica et Cosmochimica Acta*.

Smeltz, N. Y., Sims, K. W., Carr, B. J., & Parsekian, A. D. (2022). Geologic controls on hydrothermal groundwater mixing in Yellowstone National Park. *Journal of Volcanology and Geothermal Research*, *431*, 107650.

CHAPTER 4

WEATHER EFFECTS ON DISSOLVED ORGANIC CARBON

Introduction

As described in preceding chapters, the abundance and isotopic composition of dissolved organic carbon (DOC) in hot spring fluids can be used to help identify fluid sources and pathways in the Yellowstone hydrothermal system. Assuming a surface-derived, exogenous source for DOC, it can be anticipated that its initial isotopic composition will reflect biological productivity from the surface ecosystems of Yellowstone (see Fig 1.7). That initial isotopic composition can be altered by deep circulation through the hydrothermal system, by acid-processing in hot springs, and by microbial production and consumption in hydrothermal ecosystems (see Chapters 1 and 3). It follows that hot springs that are primarily sourced by deeply circulating fluids or which contain high concentrations of acid will contain DOC with isotopic compositions that differ from that of DOC freshly produced from the surface ecosystem. Surface-derived isotopic composition of DOC can be preserved in hot springs that are dominated by input of surface-derived fluids. If so, then hot springs dominated by surface-derived fluids may have their DOC replenished during and after storm events that deliver pulses of surface-derived fluids. Likewise, the isotopic composition of that DOC should be reset toward the range of values derived from the surface ecosystem. If so, sampling DOC before and after storm events would allow tests of this hypothesis.

Luckily there are sets of samples taken over the course of certain field expeditions that correspond to unique weather events, with samples taken before and after

thunderstorms. The examples chosen for this chapter come from Geyser Creek and Crater Hills and allow tests of how the abundance and isotopic composition of DOC in hot springs can respond to large fluctuations in the direct delivery and shallow infiltration processes defined as paths A and B Fig. 1.7. In addition, a preliminary investigation of the effects of storm events on the organic carbon composition of hot spring sediments is included using data from samples taken in 2015 before and after a weather event affecting both the Norris and White Creek thermal areas. These data reflect preliminary samples from an individual weather event and suggest that comparisons from multiple rain events in various thermal areas would be beneficial to models of DOC and sediment transport in hot spring systems.

Crater Hills

GEOPIG researchers were in the field at Crater Hills in 2012 during an especially impressive storm event that dropped abundant rain and hail on the thermal area. Two hot springs, "Alice" and "Jabberwocky", were sampled before and after the storm and data from the DOC samples are the focus of this discussion. "Alice" was sampled before the storm and had a pH of 2.16 and contained 123.3 µM DOC. It was sampled again two days after the rainstorm and the pH was 2.06 and there was 3,097 µM DOC, which is more than a 25-fold increase. DOC $\delta^{13}C$ values at "Alice" change from -16.69‰ in the earlier sample to -23.86‰ in the later sample. "Jabberwocky" was sampled twice on the same day "Alice" was first sampled, once before and once after the storm. The first sample contained 88.3 µM DOC. In contrast, the later sample contained 1,673 µM DOC,

which is about a 19-fold increase. As in the case of "Alice" DOC $\delta^{13}C$ values at "Jabberwocky" became lighter changing from -11‰ to -24‰ as shown in Fig. 4.1.

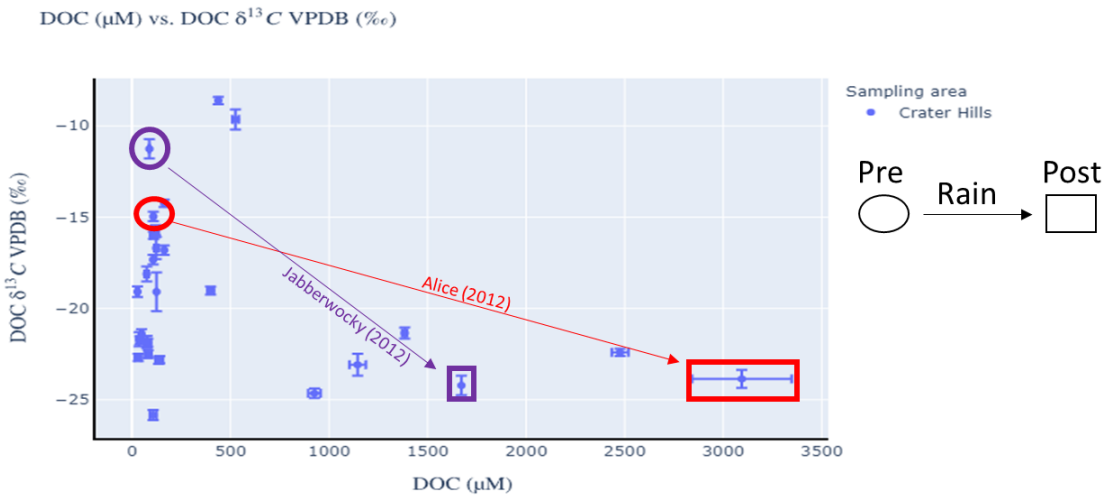

Figure 4.1: Comparison of concentrations and isotopic compositions of DOC from two hot springs, "Alice" and "Jabberwocky", within Crater Hills after the same weather event in 2012. Hot springs are identified by color and symbol shape corresponds to sampling time relative to the rain event as shown in the legend to the right of the figure. The concentration error bar is larger for Alice post-rain due to sample concentration higher than the range of the 10 mL loop leading to an increase in error when fitting to the calibration curve.

The changes in concentration and isotopic composition shown in Fig 4.1 demonstrate that these hot springs can be subject to large changes in exogenous carbon. Before the storm event, both springs exhibited low abundances of DOC that are similar to many other measurements from Crater Hills. The DOC in these two acidic springs also show heavy $\delta^{13}C$ values before the rain event, which are consistent with data from other acidic springs discussed in Chapter 3. The model for acidic hot springs developed in Chapter 1 and tested in Chapter 3 with data from Geyser Creek involves increasing $\delta^{13}C$ values of DOC as a consequence of acidic processing (whether chemical or biotic). It

appears that analogous processes are in effect in acidic springs at Crater Hills as well. The dramatic decreases in $\delta^{13}C$ in both springs after the storm event shown in Fig 4.1 point toward DOC derivation from the photosynthetically dominated surface ecosystem. Likewise, the sudden, radical increase in DOC concentrations suggest a readily available source that can be accessed by storm events, again suggestive of the surface. It should be noted that there are small channels leading to these springs in surrounding sediment that suggest runoff containing exogenous carbon can rapidly impact these systems. The data for "Alice" also hints at the duration of influence that large storm events can have on these systems as indicated by the elevated levels of DOC and its light isotopic composition two days later.

In the conceptual models outlined in Chapter 1, heavy isotopic values for DOC are expected in fluids that have deeply circulated through the hydrothermal system. The enriched DOC $\delta^{13}C$ values common to springs at Crater Hills are consistent with that hypothesis. However, the DOC concentrations are somewhat higher than observed at Sentinel Meadow where the effects of the deep circulation process can be identified (see Chapter 3). Notably, the springs at Crater Hills are acidic, which is not the case for fluids that correspond to "Deep Thermal Circulation" in Figure 1.7, such as those in Sentinel Meadow. Data from the storm event reveals that "Direct Delivery" also occurs at Crater Hills where local catchments funnel storm-derived fluids to the acidic springs. The persistence of elevated concentrations and isotopically light DOC at "Alice" suggests that "Infiltration" may also be an active process (see Fig 1.8).

The data summarized here show changes immediately after a storm event capable of introducing DOC to these springs. We assume that there are processes that drive such pulses of isotopically light DOC to the low concentration of heavy DOC observed before the storm, although we have no direct evidence of the rate of such processes. If heterotrophs use the new DOC as a nutrient, then they will over time deplete the organic carbon concentration back to the commonly observed values around 100-200 μM. We propose that the resulting heavier isotopic values would also reflect microbial consumption of DOC. These results provide a foundation for field experiments to test how mixing of hydrothermal fluid and young meteoric water rich in DOC could be the cause of the increased levels of DOC multiple days after the initial rainstorm. Related experiments could test the processes through which storm-driven perturbations return to the low concentrations of isotopically heavy DOC observed at Crater Hills and elsewhere. We expect variable results for hot springs depending on whether they are stagnant pools or actively outflowing. Catchment size, vegetation cover, local topography and hot spring surface area will also affect the extent to which local exogenous carbon can impact springs that are susceptible to runoff. In turn, characterizing the effects of such variables on the pathways that hydrothermal features are receiving organic carbon will provide a framework for explaining why microbial communities can differ among acidic springs receiving ample storm-derived DOC.

Geyser Creek

While large storm events, like that documented in Crater Hills, can have dramatic influences on the concentration and isotopic composition of DOC, smaller events can

also generate perturbations that reveal how hot spring systems work. Within the subset of samples from Geyser Creek, there are two sets of samples that were taken before and after rain events (Fig. 4.2). The rainstorms occurred in 2014 and 2015 and the hot spring locations affected are “Spitting Croissant” and “Complete Mix,” respectively. “Spitting Croissant” initially had 82.5 µM DOC and after the rain event it was resampled the same day with a new value of 205 µM DOC, which is about a 2.5-fold increase. Shortly after the second sample, there was a third sample collected yielding a value of 248.3 µM DOC, representing a factor of ~3 increase since before the event. The initial sample from “Complete Mix” contained 72.5 µM DOC. After the rain event a second sample showed there was 195.8 µM DOC, for a factor of ~2.7 increase. In two separate rain events, similar increases in DOC concentration occurred at these two hot spring locations. These preliminary results show that typical rain events can drive increases in DOC of several fold, and that these may be regular perturbations.

It should be noted that there is not much change in the isotopic composition of the DOC in the Geyser Creek examples as a result of these storm events despite the several-fold increase in concentration. This implies that the incoming DOC is similar in isotopic composition to the DOC in the springs, unlike the Crater Hill examples. In fact, the increase in DOC concentration at “Complete Mix” does not shift the isotopic composition to a discernable amount given the uncertainties in the measurements. All of the data shown for these springs, as well as the vast majority of other data from Geyser Creek shown in Fig 4.2 have $\delta^{13}C$ values consistent with derivation from the surrounding

surface environment. These preliminary results suggest that DOC is regularly supplied to these springs from the surface.

The abundance of hot spring DOC and especially its isotopic composition before and after these rain events imply that “Infiltration” with possible contributions from “Direct Delivery” are the processes in Fig 1.7 that explain the DOC in these hot springs. The differences in concentration with little change in isotopic composition suggest that the processes that consume DOC in these hot springs do not cause much measurable isotopic fractionation. If DOC is consumed by microbial life in these hot springs, the mild effects on isotopic composition suggest that DOC inputs of these magnitudes are regular events.

Hot springs are dynamic. The changes uncovered in this investigation could be tested with multiple samples during rain events, or experiments simulating rain events that can be used as proxies to determine the influence of local environments on individual hot springs.

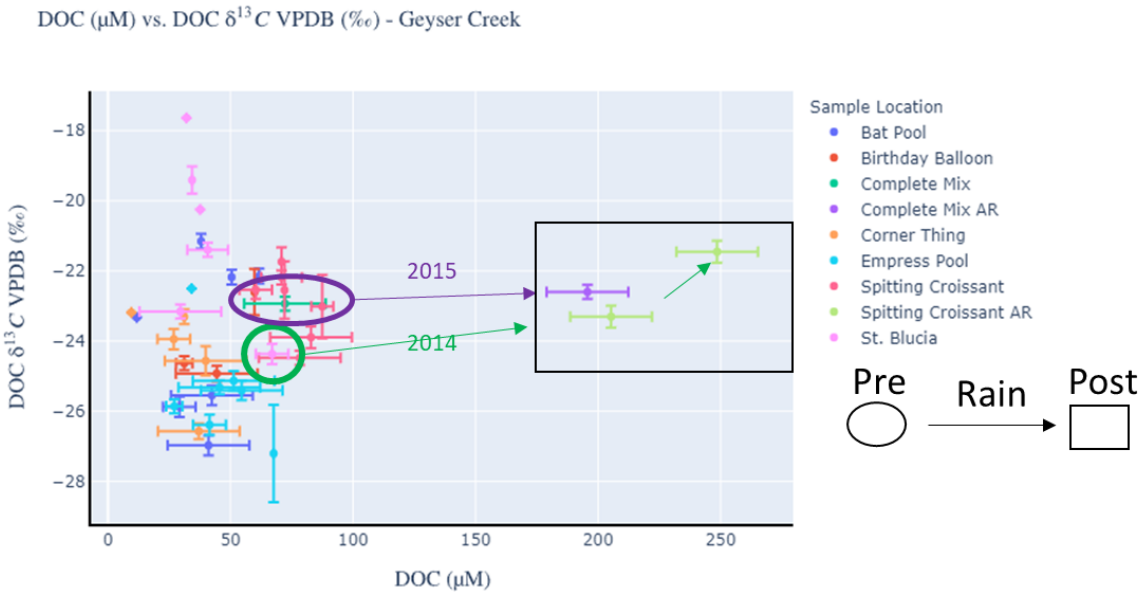

Figure 4.2: Comparison of responses of DOC to two rain events in Geyer Creek. The green circle shows the starting DOC concentration and isotopic composition at "Spitting Croissant" where two additional samples were taken after the rain event in 2014. The green arrows show the order in which the samples were taken. The purple oval corresponds to the initial DOC composition at "Complete Mix" in 2015, and the sample taken after the rain event is indicated as the purple point in the black box. Note that increases in DOC concentration are accompanied by little or no shift in isotopic composition.

2015 Organic Carbon in Sediments

Changes in DOC concentration and isotopic composition in response to rain events raise questions about the corresponding behavior of organic carbon in hot spring sediments. An exploratory study was conducted via elemental analysis and isotope-ratio mass spectrometry using samples from 2015 collected by D'Arcy Meyer-Dombard before and after a rainstorm. Sample locations are in both Norris Geyser Basin and White Creek (Table 4.1). Most of the samples were collected four days apart (24 and 28 July at Norris and 25 and 29 July at White Creek). One set of samples, from "The Gap" at Norris was

collected 11 days apart (17 and 28 July). The amount of organic carbon in the sediments is under 1.5 weight percent carbon (Fig. 4.3). Nevertheless, the changes are greater than the analytical uncertainties. These data are intriguing because they show trends of organic carbon both increasing and decreasing in these hot springs in response to the event. Concentration increases at “Woodchip Beach”, “Par 5”, “Spent Kleenex”, and “Eisentintenfisch”, and decreases at “The Gap”, “Log Stew”, “Log Jam”, and “Bug Cemetery”. These samples typically have < 80 µM DOC, which indicates organic-poor hot springs.

These data suggest that organic carbon can flux both into and out of hot spring sediments in response to weather events, and indicate that several processes may be involved. In three of the four hot springs samples showing weight percent carbon increases, ^{13}C is depleted. The fourth, “Eisentintenfisch” shows a tiny increase in abundance and a slightly heavier isotopic composition, just outside of analytical uncertainties. These changes would be expected if the sediment organic carbon behaves like changes observed in the DOC data. A possible explanation is provided by “fresh” photosynthesized-derived carbon washing into a hot spring due to a weather event and altering the existing signal. This process may provide a temporal increase in available organic carbon substrates for local heterotrophs in the hot spring.

The other response displayed in these data is a decrease in the weight percent of carbon paired with an enrichment of ^{13}C. Of the four springs with decreasing sediment organic C, only the samples from ‘The Gap” become isotopically lighter. A possible explanation for the more general phenomenon is that due to an initial increase in nutrients

there is increased primary productivity leading to already existing sediment organic carbon being rapidly consumed and lowering the amount of organic carbon in the sediment. In this scenario, microorganisms would prefer ^{12}C which could be released as $^{12}CO_2$ leaving behind organic carbon enriched in ^{13}C. This implies that little, in any, new organic carbon is added to the sediment during these events. It may be possible that organisms have consumed the most usable carbon from the material that washes in and what is then left is a less labile substrate.

One limitation of these preliminary sediment data involves the difficulty of taking samples that are as similar as possible from hot spring sediment. An expanded study could overcome this challenge by taking many samples at the same spring before and after storm events to understand the reproducibility of concentrations and isotopic composition of organic carbon in hot spring sediments. If the complexities of replicate sampling can be overcome, it may be possible to design live microcosm experiments in which either nutrients or sediment-destined organic carbon, or both, are added and subsampled over time to control the variable that may drive the observations obtained here.

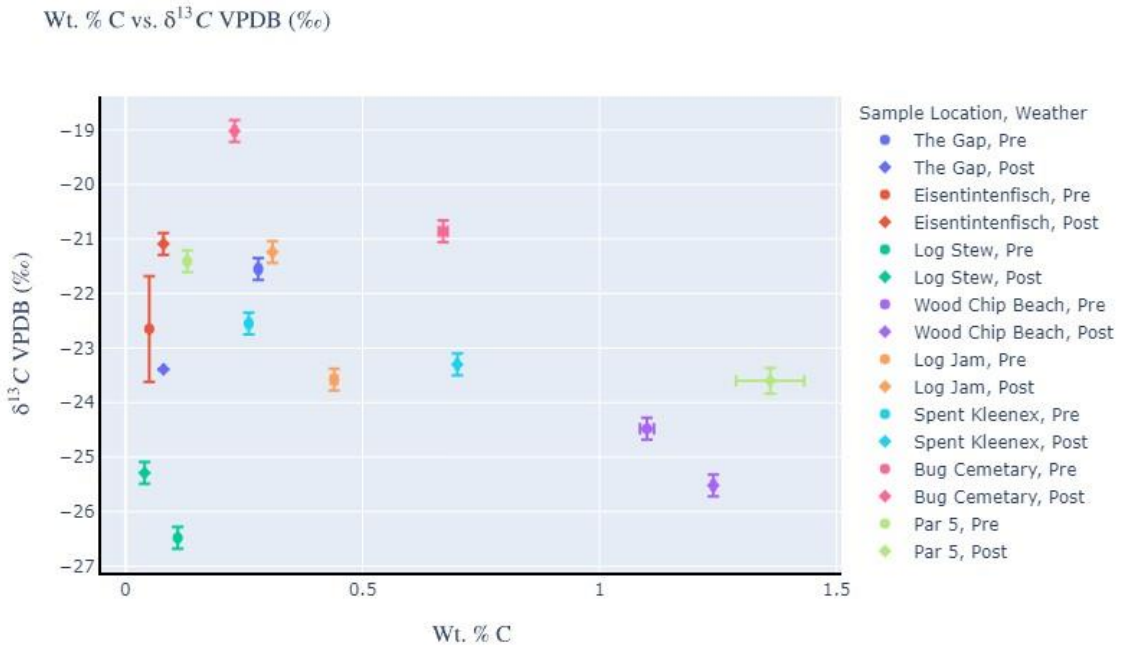

Figure 4.3: Wt. % C vs. δ^{13}C VPDB (‰) for samples corresponding to a weather event in 2015. Sample timing is either pre-rain or post-rain and this is indicated by the legend on the right of the figure. These samples are from White Creek ("Log Jam", "Spent Kleenex", "Bug Cemetery", and "Par 5") and Norris Geyser Basin ("The Gap", "Eisentintenfisch", "Log Stew", and "Wood Chip Beach.")

Table 4.1: Elemental Analysis of Hot Spring Sediments

Identifier 1	Sample Location	Wt. % C	Wt. % C stdev	δ^{13}C VPDB (‰)	δ^{13}C VPDB (‰) stdev
150717FB	The Gap	0.28	0.0038	-21.55	0.2
150724FM	Eisentintenfisch	0.05	0.00054	-22.65	0.97
150724FO	Log Stew	0.11	0.0015	-26.48	0.2
150724FP	Wood Chip Beach	1.1	0.015	-24.48	0.2
150725WB	Log Jam	0.44	0.0060	-23.58	0.2
150725WC	Spent Kleenex	0.26	0.00354	-22.55	0.2
150725WD	Bug Cemetery	0.67	0.0091	-20.86	0.2
150725WE	Par 5	0.13	0.0018	-21.41	0.2
150728C	Eisentintenfisch	0.08	0.00024	-21.09	0.2
150728I	Wood Chip Beach	1.24	0.0037	-25.52	0.2
150728Y	The Gap	0.08	0.00023	-23.39	0.0060
150728YA	Log Stew	0.04	0.00012	-25.29	0.2

Identifier 1	Sample Location	Wt. % C	Wt. % C stdev	δ^{13}C VPDB (‰)	δ^{13}C VPDB (‰) stdev
150729WF	Spent Kleenex	0.7	0.0021	-23.3	0.2
150729WG	Log Jam	0.31	0.00093	-21.24	0.2
150729WH	Par 5	1.36	0.072	-23.6	0.24
150729WI	Bug Cemetery	0.23	0.0031	-19.02	0.2

CHAPTER 5

SPECIFIC EXAMPLES OF DOMINANT DOC SOURCES

Introduction

In this short chapter I illustrate how combining fluorescence measurements with DIC/DOC measurements can reveal potential targets for further research. The primary goal of this approach is to determine which pathways are dominant fluid suppliers to an individual hot spring. Resulting hypotheses can be tested through additional analyses at this location including targeted geochemical and microbial experiments or sequencing. A secondary goal is to generalize this approach so that it can be applied to other hot springs in future work throughout Yellowstone.

Investigating an Autotrophic Dominant Hot Spring

Located within Geyser Creek is a hot spring unofficially named “Jackhammer”, which has a distinct $\delta^{13}C$ signature compared to the rest of Geyser Creek and other hot springs sampled in this study. Jackhammer typically has a temperature of 89°C and a pH of 1.99 (Fig. 3.1). It is intensely degassing, and the appearance of “Jackhammer” is very cloudy water with a surrounding structure that looks like an explosion has occurred leaving behind jumbled sinter blocks (see Figure 5.1). As shown in Fig. 5.2, “Jackhammer” has significantly higher conductivity than other hot springs within Geyser Creek, suggesting that factors of fluid delivery and thermal alteration are unique to “Jackhammer” within Geyser Creek. In addition, the enriched ^{13}C signature of the DOC shown in Fig 5.2 separates “Jackhammer” from the rest of the springs sampled at Geyser Creek. Such isotopically heavy DOC in 2019 rivals the DIC $\delta^{13}C$ present at this spring -

2.57‰ & -6.17‰, respectively. This is unique for the isotopic signature of DOC to be more enriched compared to the DIC $\delta^{13}C$ signature. It is important to emphasize that heavy DOC and high conductivity values are reported at this hot spring in both 2017 and 2019.

Concentrations of DOC for Geyser Creek are shown in Fig 5.3, and the values for "Jackhammer", 333 and 417 µM, are higher than the park average (192 µM C). Elevated concentrations of DOC correlate with Total Fluorescence reported by Nye (2020) for the same sample from 2017, as shown in Fig. 5.4. Pearson's correlation analysis between Total Fluorescence and DOC µM resulted in a value of 0.773, indicating a strong positive correlation. Fluorescence and concentration measurements combined confirm that there is dissolved organic carbon within this hot spring showing this elevated signal.

"Jackhammer" is one of the most acidic hot springs in Geyser Creek with a pH of 1.99. According to Nye (2020) there is a novel component present in acidic samples, making "Jackhammer" a possible place for further research into this component. In order to investigate this novel component further, isotopic values can be combined with fluorescent indices.

The isotopic values from the present study can be compared with fluorescence peak values from Nye (2020) for all samples that are common to both studies. As shown in Fig. 5.5, when isotopic data from DOC are plotted against the ratio of beta and alpha fluorescence peaks, β/α, "Jackhammer" differs considerably from the rest of the dataset. According to Nye (2020), higher β/α values indicate that the DOC is microbially derived in contrast to lower values that are terrestrially sourced. At "Jackhammer" this ratio is the

largest of any hot spring within this study, which suggests the presence of organic material in this hot spring generated by an autotrophic microbial community. If the elevated concentrations of DOC are being generated autotrophically, then the isotopically enriched values mean small extents of fractionation from DIC (which is -6.17‰) at "Jackhammer") . Small isotopic fractionations of carbon isotopes accompany carbon fixation by two major pathways at high temperatures. The "Jackhammer" microbial community is potentially using either the reverse tricarboxylic acid cycle (TCA) or the 3-hydroxypropionate pathway (3HP) based on data reviewed by Havig et al. (2011).

Combing fluorescence indices and $\delta^{13}C$ measurements on DOC and DIC makes it possible to make predictions about specific carbon fixing pathways in an autotrophic microbial community in this spring. It also leads to the prediction that DOC in "Jackhammer" was *not* being derived from the surrounding surface ecosystem at the times of sampling in 2017 and 2019. Therefore, the benefits of this combined approach include evidence about the sources of DOC and what they reveal about how a hydrothermal feature is linked to its local environment. This approach can be taken toward individual hot springs for future work to unravel more about fluid history in locations that are unique compared to surrounding hot springs.

Figure 5.1: This is a photo of “Jackhammer” located in Geyser Creek. In the middle of the hot spring there is intense degassing occurring. On the left side of the hot spring in this photo sinter blocks are jumbled around which looks like an explosion occurred. This photo was taken under Permit YELL-SCI-5434.

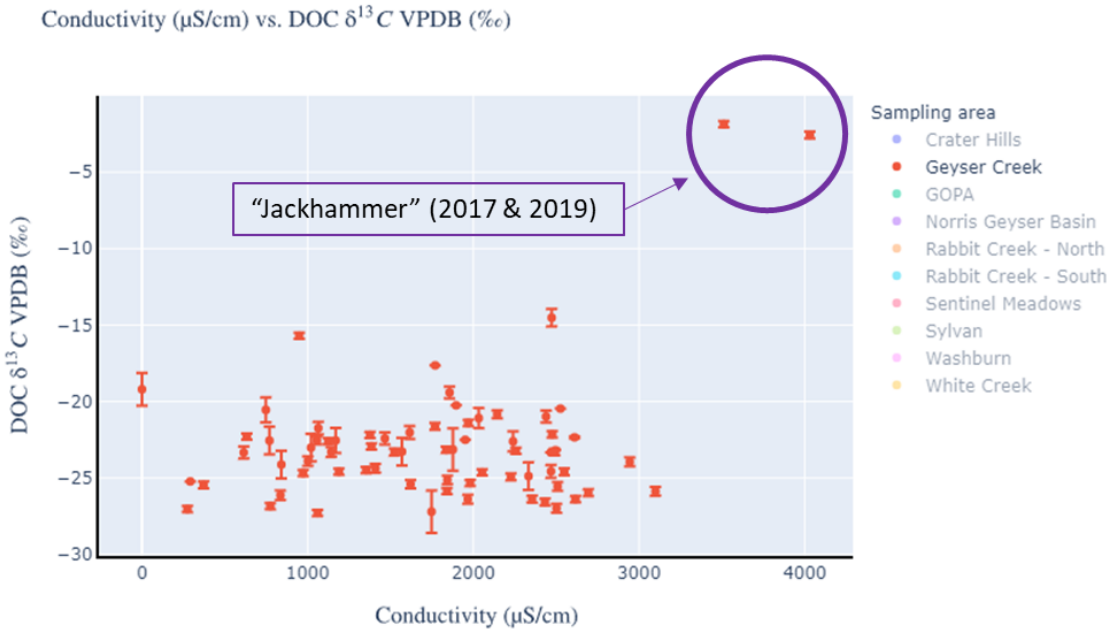

Figure 5.2: DOC $\delta^{13}C$ vs conductivity from hot springs sampled at Geyser Creek. The purple circle indicates two measurements of "Jackhammer", which is an acidic hot spring that differs considerably from other springs at Geyser Creek.

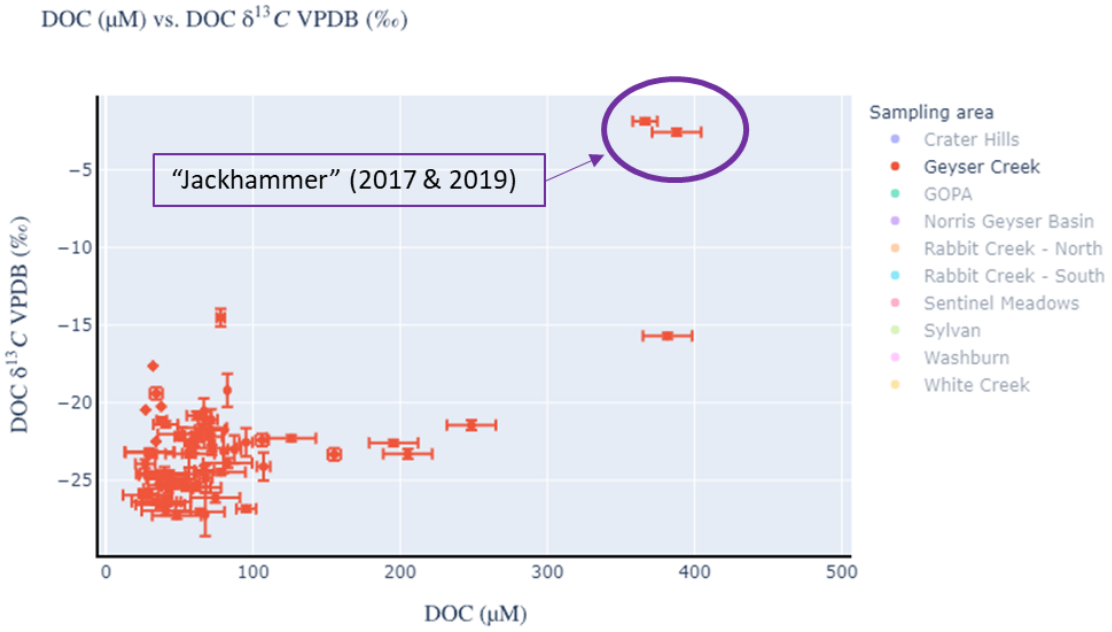

Figure 5.3: DOC $\delta^{13}C$ vs concentration of DOC for hot spring samples from Geyser Creek. The purple circle indicates two measurements of "Jackhammer" showing elevated concentrations and anomalously heavy isotopic data.

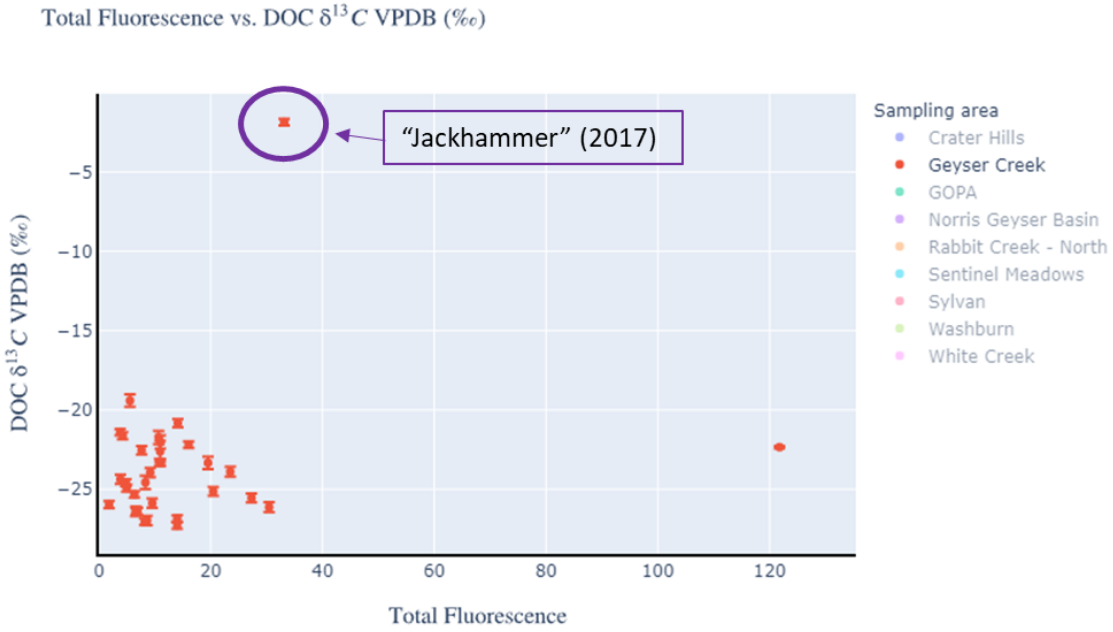

Figure 5.4: DOC $\delta^{13}C$ from this study vs. Total Fluorescence from Nye (2020) on paired samples from Geyser Creek. The purple circle indicates one set of measurements for "Jackhammer".

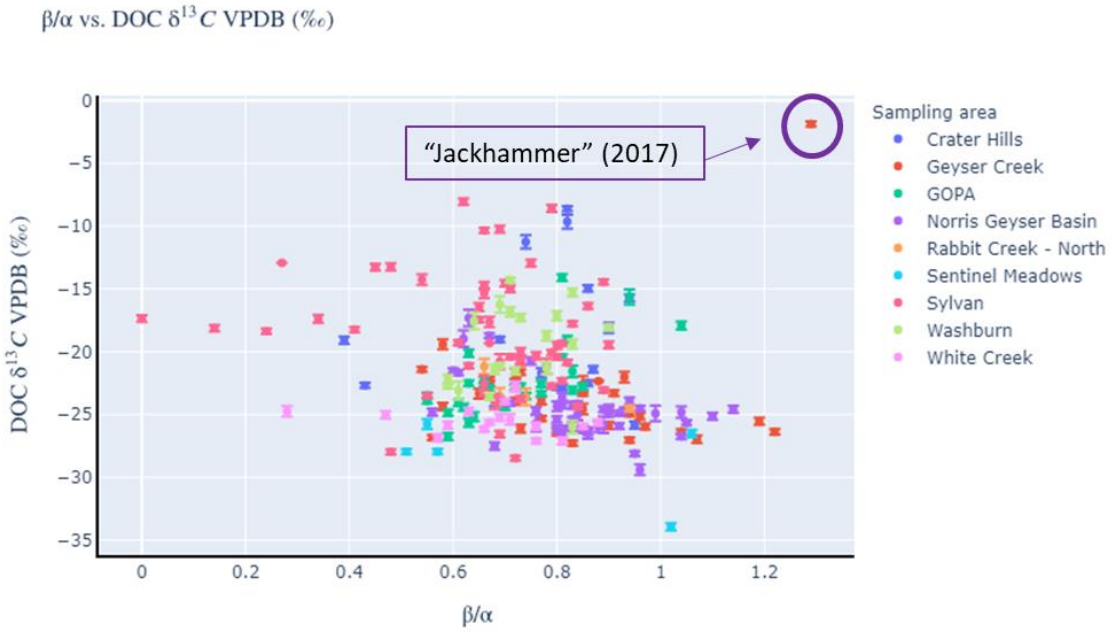

Figure 5.5: DOC $\delta^{13}C$ from this study plotted against the β/α peak ratios in the fluorescence data reported by Nye (2020) for all paired samples from across Yellowstone. The purple circle indicates one pair of measurements for "Jackhammer". Elevated β/α fluorescence peak ratios are interpreted to mean that the DOC is microbially derived rather than terrestrially sourced (Nye, 2020).

REFERENCES

Allen, E. T. and Day, A. L. (1935); Hot springs of the Yellowstone National Park. Carnegie Institution of Washington Publication 466, Carnegie Institute, Washington D. C., USA.

Bergfeld, D., Lowenstern, J. B., Hunt, A. G., Shanks, W. C. P., and Evans, W. C. (2014); Gas and isotope chemistry of thermal features in Yellowstone National Park, Wyoming. Scientific Investigations Report 2011-5012, United States Geological Survey, doi:10.3133/sir20115012.

Boyer, G., Robare, J., Ely, T., & Shock, E. (2021). AqEquil: Python package for aqueous geochemical speciation (0.13.4). Zenodo. https://doi.org/10.5281/zenodo.5768107

Campeau, A., Wallin, M. B., Giesler, R., Löfgren, S., Mörth, C. M., Schiff, S., ... & Bishop, K. (2017). Multiple sources and sinks of dissolved inorganic carbon across Swedish streams, refocusing the lens of stable C isotopes. *Scientific Reports*, *7*(1), 9158.

Christiansen, R. L. (2001), The Quarternary and Pliocene Yellowstone Plateau volcanic field of Wyoming, Idaho, and Montana, U.S. Geol. Surv. Prof. Pap. 729-G, Menlo Park, Calif.

Clifton, C., Walters, C., and Simoneit, B. (1990); Hydrothermal petroleums from Yellowstone National Park, Wyoming, U.S.A. Applied Geochemistry 5(1-2), pp. 169–191, doi:10.1016/0883-2927(90)90047-9.

Deines, P. (2002). The carbon isotope geochemistry of mantle xenoliths. *Earth-Science Reviews*, *58*(3-4), 247-278.

Feranec, R. S. (2007). Stable carbon isotope values reveal evidence of resource partitioning among ungulates from modern C3-dominated ecosystems in North America. *Palaeogeography, Palaeoclimatology, Palaeoecology*, *252*(3-4), 575-585.

Fournier, R. (1977); Chemical geothermometers and mixing models for geothermal systems. Geothermics 5(1-4), pp. 41–50, doi:10.1016/0375-6505(77)90007-4.

Fournier, R. O. (1989); Geochemistry and dynamics of the Yellowstone National Park hydrothermal system. Annual Review of Earth and Planetary Sciences 17(1), pp. 13–53, doi:10.1146/annurev.ea.17.050189.000305.

Gonsior, M., Hertkorn, N., Hinman, N., Dvorski, S. E.-M., Harir, M., Cooper, W. J., and Schmitt-Kopplin, P. (2018); Yellowstone hot springs are organic chemodiversity hot spots. Scientific Reports 8(1), p. 14155, doi:10.1038/s41598-018-32593-x

Gardner, W. P., Susong, D. D., Solomon, D. K., & Heasler, H. P. (2010). Using noble gases measured in spring discharge to trace hydrothermal processes in the Norris Geyser Basin, Yellowstone National Park, USA. *Journal of volcanology and geothermal research*, *198*(3-4), 394-404.

Gardner, W. P., Susong, D. D., Solomon, D. K., and Heasler, H. P. (2011); A multitracer approach for characterizing interactions between shallow groundwater and the hydrothermal system in the Norris Geyser Basin area, Yellowstone National Park. Geochemistry, Geophysics, Geosystems 12(8), doi:10.1029/2010GC003353.

Hawkes, J. A., Rossel, P. E., Stubbins, A., Butterfield, D., Connelly, D. P., Achterberg, E. P., Koschinsky, A., Chavagnac, V., Hansen, C. T., Bach, W., and Dittmar, T. (2015); Efficient removal of recalcitrant deep-ocean dissolved organic matter during hydrothermal circulation. Nature Geoscience 8, pp. 856–860, doi: 10.1038/ngeo2543.

Havig, J. R., Raymond, J., Meyer-Dombard, D. A. R., Zolotova, N., & Shock, E. L. (2011). Merging isotopes and community genomics in a siliceous sinter-depositing hot spring. *Journal of Geophysical Research: Biogeosciences*, *116*(G1).

Harris, D., Horwath, W.R., and van Kessel, C., 2001. Acid fumigation of soils to remove carbonates prior to total organic carbon or carbon-13 isotopic analysis. Soil Science Society of America Journal 65: 1853-1856.

Hamilton, T.L., Boyd, E.S., Peters, J.W. (2011), Environmental constraints underpin the distribution and phylogenetic diversity of nifH in the Yellowstone geothermal complex. Microbial Ecology 61, 860–870.

Hearn, E. H., Kennedy, B. M., & Truesdell, A. H. (1990). Coupled variations in helium isotopes and fluid chemistry: Shoshone Geyser Basin, Yellowstone National Park. *Geochimica et Cosmochimica Acta*, *54*(11), 3103-3113.

Holloway, J. M., Nordstrom, D. K., Böhlke, J., McCleskey, R. B., and Ball, J. W. (2011); Ammonium in thermal waters of Yellowstone National Park: Processes affecting speciation and isotope fractionation. Geochimica et Cosmochimica Acta 75(16), pp. 4611–4636, doi:10.1016/j.gca.2011.05.036.

Hurwitz, S. and Lowenstern, J. B. (2014); Dynamics of the Yellowstone hydrothermal system. Reviews of Geophysics 52(3), pp. 375–411, doi:10.1002/2014RG000452.

Jahnke, L. L., W. Eder, R. Huber, J. M. Hope, K. Hinrichs, J. M. Hayes, D. J. des Marais, S. L. Cady, and R. E. Summons (2001), Signature lipids and stable carbon isotope analysis of Octopus Spring hyperthermophilic communities compared with those

of Aquificales representatives, Appl. Environ. Microbiol., 67, 5179–5189, doi:10.1128/AEM.67.11.5179– 5189.2001.

Kirkels, F. M., De Boer, H. J., Concha Hernández, P., Martes, C. R., Van Der Meer, M. T., Basu, S., ... & Peterse, F. (2022). Carbon isotopic ratios of modern C 3 and C 4 vegetation on the Indian peninsula and changes along the plant–soil–river continuum–implications for vegetation reconstructions. *Biogeosciences*, *19*(17), 4107-4127.

Love, J. D. and Good, J. M. (1970); Hydrocarbons in thermal areas, northwestern Wyoming. Professional Paper 644-B, United States Geological Survey, doi:10.313 3/pp644b.

Lowenstern, J. B., Bergfeld, D., Evans, W. C., & Hunt, A. G. (2015). Origins of geothermal gases at Yellowstone. *Journal of Volcanology and Geothermal Research*, *302*, 87-101.

Lowenstern, J. B., & Hurwitz, S. (2008). Monitoring a supervolcano in repose: Heat and volatile flux at the Yellowstone Caldera. *Elements*, *4*(1), 35-40.

McCollom, T., Seewald, J., and Simoneit, B. (2001); Reactivity of monocyclic aromatic compounds under hydrothermal conditions. Geochimica et Cosmochimica Acta 65(3), pp. 455–468, doi:10.1016/S0016-7037(00)00533-0.

McCollom, T. M., Ritter, G., and Simoneit, B. R. T. (1999); Lipid synthesis under hydrothermal conditions by Fischer-Tropsch-type reactions. Origins of Life and Evolution of the Biosphere 29(2), pp. 153–166, doi:10.1023/A:1006592502746.

Meyer-Dombard, D. R., Swingley, W., Raymond, J., Havig, J., Shock, E. L., and Summons, R. E. (2011). Hydrothermal ecotones and streamer biofilm communities in the Lower Geyser Basin, Yellowstone National Park. Environ. Microbiol. 13, 2216–2231. doi: 10.1111/j.1462-2920.2011. 02476.x

NOAA Terrestrial Climate Data Records was accessed on 5/15/2023 from https://registry.opendata.aws/noaa-cdr-terrestrial.

Nordstrom, D. K., McCleskey, R. B., & Ball, J. W. (2009). Sulfur geochemistry of hydrothermal waters in Yellowstone National Park: IV Acid–sulfate waters. *Applied Geochemistry*, *24*(2), 191-207.

Nye, J. (2020). *Fluorescent Dissolved Organic Matter in Yellowstone National Park Hot Springs* (Doctoral dissertation, Arizona State University).

Pierce, K. L. & Morgan, L. A. Is the track of the Yellowstone hotspot driven by a deep mantle plume? — Review of volcanism, faulting, and uplift in light of new data.

Journal of Volcanology and Geothermal Research 188, 1–25, https://doi.org/10.1016/j. jvolgeores.2009.07.009 (2009).

Schubotz, F., Hays, L. E., Meyer-Dombard, D. A. R., Gillespie, A., Shock, E. L., & Summons, R. E. (2015). Stable isotope labeling confirms mixotrophic nature of streamer biofilm communities at alkaline hot springs. *Frontiers in microbiology*, *6*, 42.

Schubotz, F., Meyer-Dombard, D. R., Bradley, A. S., Fredricks, H. F., Hinrichs, K.- U., Shock, E. L., et al. (2013). Spatial and temporal variability of biomarkers and microbial diversity reveal metabolic and community flexibility in Streamer Biofilm Communities in the Lower Geyser Basin, Yellowstone National Park. Geobiology 11, 549–569. doi: 10.1111/gbi.12051

Seewald, J. S. (2003); Organic-inorganic interactions in petroleum-producing sedimentary basins. Nature 426(6964), pp. 327–333, doi:10.1038/nature02132

Stelten, M. E., Thomas, N., Pivarunas, A., & Champion, D. (2023). Spatio-temporal clustering of post-caldera eruptions at Yellowstone caldera: implications for volcanic hazards and pre-eruptive magma reservoir configuration. *Bulletin of Volcanology*, *85*(10), 1-17.

Simkus, D. N., Slater, G. F., Lollar, B. S., Wilkie, K., Kieft, T. L., Magnabosco, C., ... & Onstott, T. C. (2016). Variations in microbial carbon sources and cycling in the deep continental subsurface. *Geochimica et Cosmochimica Acta*, *173*, 264-283.

Sims, K. W., Messa, C. M., Scott, S. R., Parsekian, A. D., Miller, A., Role, A. L., ... & Boyd, E. S. (2023). The Dynamic Influence of Subsurface Geological Processes on the Assembly and Diversification of Thermophilic Microbial Communities in Continental Hydrothermal Systems. *Geochimica et Cosmochimica Acta*.

Smeltz, N. Y., Sims, K. W., Carr, B. J., & Parsekian, A. D. (2022). Geologic controls on hydrothermal groundwater mixing in Yellowstone National Park. *Journal of Volcanology and Geothermal Research*, *431*, 107650.

Sobek, S., Tranvik, L. J., Prairie, Y. T., Kortelainen, P., & Cole, J. J. (2007). Patterns and regulation of dissolved organic carbon: An analysis of 7,500 widely distributed lakes. Limnology and oceanography, 52(3), 1208-1219.

Swingley, W. D., Meyer-Dombard, D. R., Shock, E. L., Alsop, E. B., Falenski, H. D., Havig, J. R., et al. (2012). Coordinating environmental genomics and geochemistry reveals metabolic transitions in a hot spring ecosystem. PLoS ONE 7:e38108. doi: 10.1371/journal.pone.0038108

van der Meer, M. T. J., S. Schouten, J. W. de Leeuw, and D. W. Ward (2000a), Autotrophy of green nonsulfur bacteria in hot spring microbial mats: Biological

explanations for isotopically heavy organic carbon in the geological record, Environ. Microbiol., 2, 428–435.

van der Meer, M. T. J., S. Schouten, J. S. S. Damste, J. W. de Leeuw, and D. W. Ward (2003), Compound-specific isotopic fractionation patterns suggest different carbon metabolisms among chloroflexus-like bacteria in hot-spring microbial mats, Appl. Environ. Microbiol., 69, 6000– 6006, doi:10.1128/AEM.69.10.6000–6006.2003.

van der Meer, M. T. J., S. Schouten, M. M. Bateson, U. Nubel, A. Wieland, M. Kuhl, J. W. de Leeuw, J. S. S. Damste, and D. M. Ward (2005), Diel variations in carbon metabolism by green nonsulfur-like bacteria in alkaline siliceous hot spring microbial mats from Yellowstone National Park, Appl. Environ. Microbiol., 7 1, 3978 –3986, doi:10.1128/ AEM.71.7.3978–3986.2005.

van der Meer, M. T. J., S. Schouten, J. S. S. Damste, and D. M. Ward (2007), Impact of carbon metabolism on 13C signatures of cyanobacteria and green non-sulfur-like bacteria inhabiting a microbial mat from an alkaline siliceous hot spring in Yellowstone National Park (USA), Environ. Microbiol., 9, 482–491, doi:10.111/j.1462–2920.2006.01165.x.

Vaughan, R. (2014). Provisional Maps of Thermal Areas in Yellowstone National Park, based on Satellite Thermal Infrared Imaging and Field Observations. U.S. Geological Survey Scientific Investigations Report. 2014–5137. 22 p. 10.3133/sir20145137.

Zhang, C. L., B. W. Fouke, G. T. Bonheyo, A. D. Peacock, D. C. White, Y. Huang, and C. S. Romanek (2004), Lipid biomarkers and carbon- isotopes of modern travertine deposits (Yellowstone National Park, USA): Implications for biogeochemical dynamics in hot-spring systems, Geochim. Cosmochim. Acta, 68, 3157–3169, doi:10.1016/j.gca. 2004.03.005.

APPENDIX A

SITE DESCRIPTION AND ANALYSIS

Hydrothermal Areas in Yellowstone National Park

This section describes the different regions where hot springs were sampled (see Fig. 1.11). It is critical to note that regions have many different types of hot springs. Therefore, it is important to not only classify hot springs by their "man-made" geographical notation and to consider the type of fluid(s) that is present in the spring. However, the different regions do have significant trends within them, and they will be discussed below.

The chapter describes the different field sampling sites around Yellowstone National Park that are used for this thesis. Ten unique regions of Yellowstone National Park make up the data within this thesis: Crater Hills, Geyser Creek, Greater Obsidian Pool Area (GOPA), Norris Geyser Basin, Rabbit Creek North, Rabbit Creek South, Sentinel Meadows, Sylvan, Washburn, and White Creek. This chapter will include additional data and figures for regions discussed in Chapter 3 and the overviews of the topography in those locations can be found within Chapter 3.

Crater Hills

Crater Hills is located near the inner ring fracture zone within the caldera (Fig. 1.11). This area is near the Sour Creek resurgent dome. Crater Hills is topographically higher with lodgepole pine located in the middle of the hydrothermal area. This area is like GOPA where it is more open, yet Crater Hills is intensely acidic and sulfur rich. Evaporation is very prominent throughout this region which drives increased values of conductivity. The North Side has hills creating a strong topographic influence due to

weather events. This will be investigated later in this thesis, but organic carbon is greatly influenced in limited samples due to weather events. Over the years due to erosion, several springs have been buried by sinter. This is also apparent because many trees have fallen over facing in the same direction. Natural physical disruption is present in this region. There are also signs of a large bison presence in the region constantly disrupting the area.

Norris Geyser Basin

Norris Geyser Basin is located north of the caldera boundary and falls outside of the caldera (Fig. 1.11). Norris contains mostly high-chloride and deeply sourced springs. Norris is a large hydrothermal area surrounded by lodgepole pine as the dominant vegetation. There are also hills creating topographic lows and highs. Hot springs in this region switch between neutral-chloride to acid-sulfate distinctions based upon a shifting water table due to seasonal transitions (Gardner et al., 2011). The samples in this thesis are all completed in the summer season and therefore the effects of this transition in composition should be minimal. Several different areas of the larger Norris area have been investigated in this thesis. Samples mainly consist of the southwestern portion of Norris and the northern portion of the Norris region.

Sylvan

Sylvan is located outside the 0.6 Ma Yellowstone eruption caldera (Fig. 1.11). The hot springs in Sylvan are located topographically higher than the surrounding Gibbon Meadow and vary in shape and size. Some hot springs in this area are very large pools

with a high input of volcanic gas. Some other springs are very small and vary geochemically year to year such as “the Dryer” hot spring. At the top of the surrounding hills there are lodgepole pines that with a storm surge event, organic material would flow down into the hot springs. Hot springs are also dominant in two categories in this region. They either have a more neutral 5-6 pH and are predominantly Na^+ and Cl^- or they are very acidic with a pH of around 2 with a high input of sulfate. When it rained at this location, the outflows of several hot springs looked vibrant with life and some of the usual slow outflowing hot springs increased their outflow. The surrounding geology in this region is glacial deposits and gravel that have been hydrothermally altered.

Washburn

Washburn is inside 0.6 Ma Yellowstone eruption caldera, but the only region outside of the inner ring fracture (Fig. 1.11). The hydrothermal area is just from the peak of Mt. Washburn and the hydrothermal is separated into two areas (Upper and Lower). The Washburn Hydrothermal area is located on the side of a hilltop where “Upper Washburn” is located higher on the hill while “Lower Washburn” is located at the base of the hill. There is no apparent runoff and mixing from “Upper Washburn” to “Lower Washburn”. The local geology is glacial deposits consisting of sand and gravel that have been hydrothermally altered. These hot springs are classified as mud pots due to their muddy appearance. Due to Washburn being located on a hill, there will be input from precipitation impacting the springs as organic material and soil is deposited into the hot springs. There are no silica barriers to stop runoff at these hot springs. The entire area is also surrounded by lodgepole pine and therefore that will have an organic carbon impact

on these hot springs. Hot spring waters in this location have an acidic pH between 3-6.5 and there is also higher ammonium in this region potentially leading to a home for ammonia oxidizing bacteria (Holloway et al., 2011; Bergfeld et al., 2014). Sulfate and volcanic gas are high in this region compared to other regions. It has also been hypothesized that sedimentary rocks lie underneath this hydrothermal area leading to an increase in organic carbon by providing a source of ancient organic materials (Allen and Day, 1935; Love and Good, 1970; Fournier, 1989; Hurwitz and Lowenstern, 2014).

White Creek

White Creek is in the southeastern part of the Lower Geyser Basin (Fig. 1.11). Throughout the hydrothermal area White Creek flows rapidly down the hill slope. White Creek typically has a temperature of 50 to 60 degrees Celsius where hill slope be seen rising from the water. The hot springs within this region lie on either side of the creek and they discharge their outflow into the creek which is one reason the temperature of the creek is elevated. The vegetation is variable within the narrow valley. Near the creek are thick grasses, but on either side of the valley, the area is dominated by lodgepole pine. The slope of the valley is steep and therefore storm surges would cause vegetation to actively flow down slope into the hot springs at the bottom of the valley. This was observed as many of the hot springs within white creek have local vegetation or insects floating in the water or traveling down the hot spring outflow. Therefore, this region is not only influenced by the hot spring fluid, but also the surrounding environment. In Chapter 4 storm surge events and White Creek will be discussed to infer how the local environment, weather, and topography play a role within White Creek.

Carbon Abundance

DIC ranges up to a park high of 14,365 µM at "Foam Pool" in the GOPA region. DIC is over 4,166 ppm µM in Sentinel Meadows and White Creek which are boiling neutral-chloride hot springs. However, DIC is typically lower in the sulfate-dominant acidic hot springs at pH 1-5. The average DIC of all GEOPIG samples within Yellowstone National Park is 2,241 µM C (Fig. A.1). DOC ranges up to 4,825 µM C at "Mr. Clean" in Washburn. Sulfate-dominant acidic hot springs tend to have increased DOC compared to neutral-chloride hot springs. High abundances of DOC in hot springs are rare and is limited to specific hot springs. This will be discussed further into the chapter. The average DOC of all GEOPIG samples in this study is 192 µM C (Fig. A.2). Typically, DOC abundance is lower than DIC abundance in each hot spring. However, there are hot springs where DOC abundance is higher than DIC and this typically occurs in meteoric gas dominant hot springs. This change in carbon substrate abundance needs to be further explored to determine if the microbial community is different in these hot springs due to increased DOC.

Isotope Results

DIC $\delta^{13}C$ values typically range from -4‰ to +5‰ at pH 5-9 and from -7‰ to +3‰ at pH <5 with several springs more depleted in ^{13}C than -10‰ (Fig. A.3). This range is indicative of a geogenic source (−12‰ to 5‰) (Campeau, 2017). Springs more depleted in ^{13}C than -10‰ have low concentrations of DIC but are within the calibration range for the IRMS. These low values could be due to being close to the calibration range of 14 µM or this could be a signal resulting from autotrophy and biogenic source (−26 to

−18‰) (Campeau, 2017). Another way DIC can also reach these values (-22‰ to -26‰) that was mentioned previously and is inferred to be a minor signature of C depleted in ^{13}C that has been observed in mantle xenoliths (Deines, 2002).

DOC $\delta^{13}C$ values parkwide range from -10‰ to -30‰ (Fig. A.4). Within this range, neutral-chloride regions in the Lower Geyser Basin have ^{13}C depleted isotopes than sulfate-dominant acidic regions. In hot springs with elevated levels of DOC, the range only varies between -20‰ and -26‰ which may be caused by local exogenous organic matter runoff.

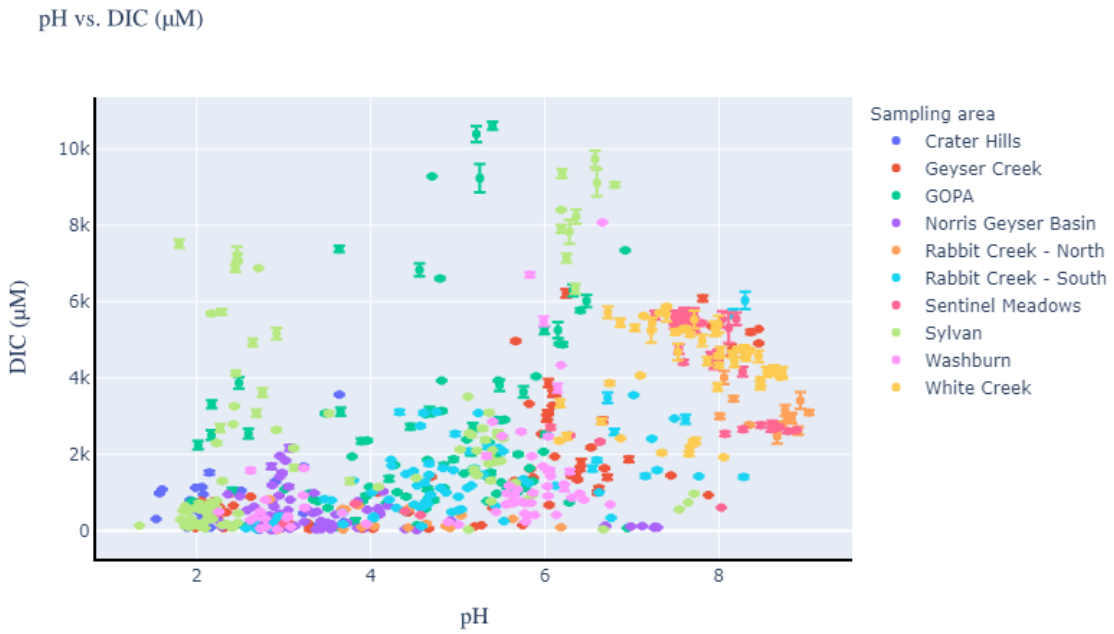

Figure A.1: pH vs. DIC µM across 10 regions from 2005-2019.

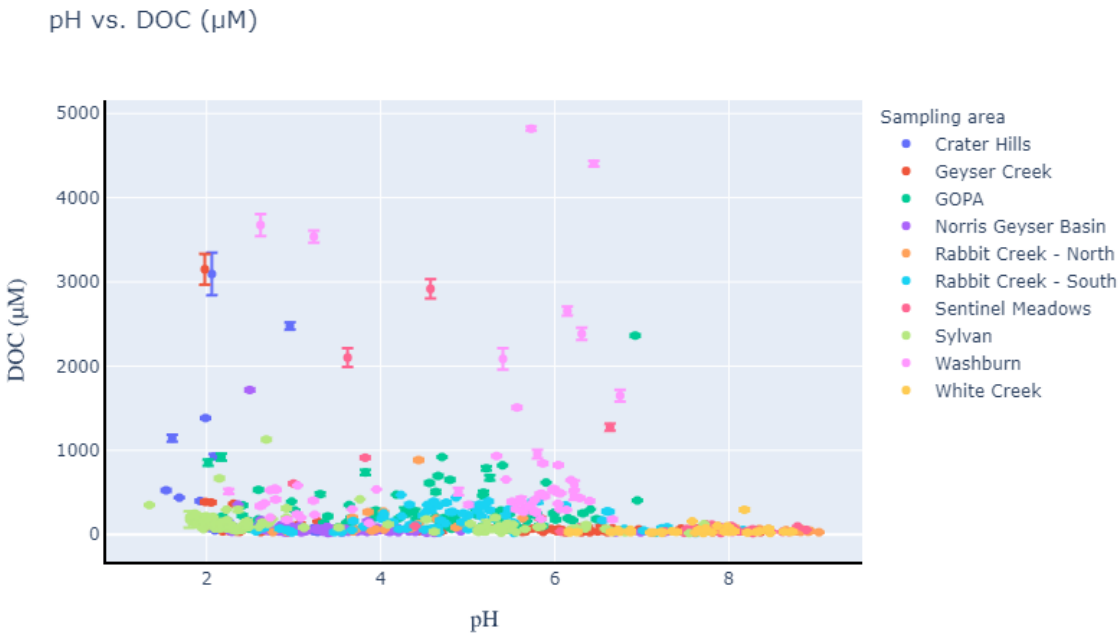

Figure A.2: pH vs. DOC µM across 10 regions from 2005-2019.

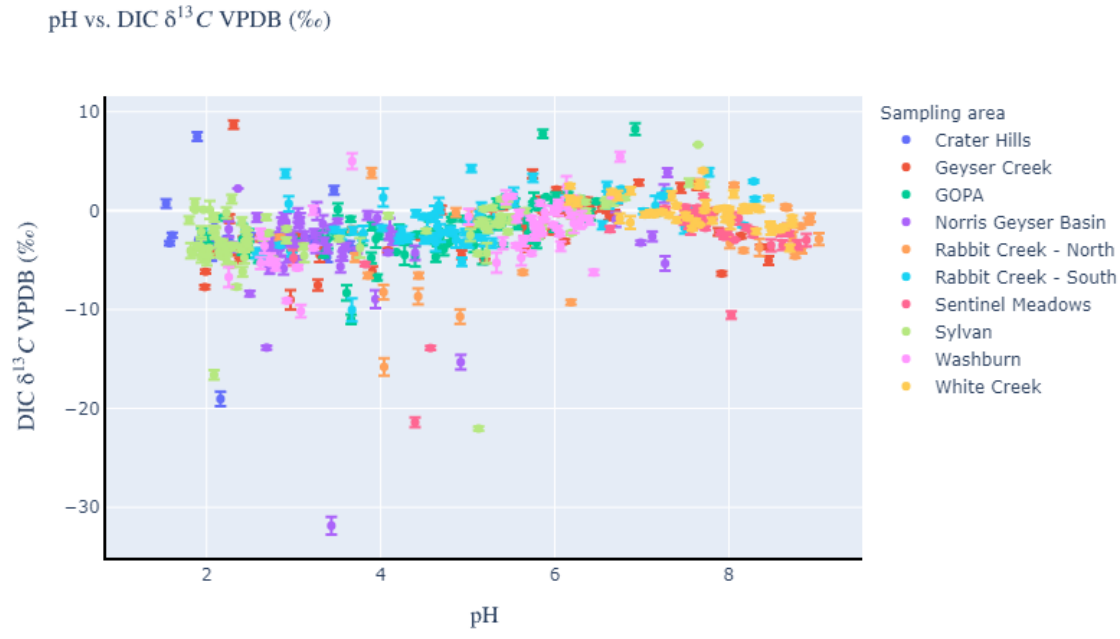

Figure A.3: pH vs. DIC δ^{13}C VPDB (‰) across 10 regions from 2005-2019.

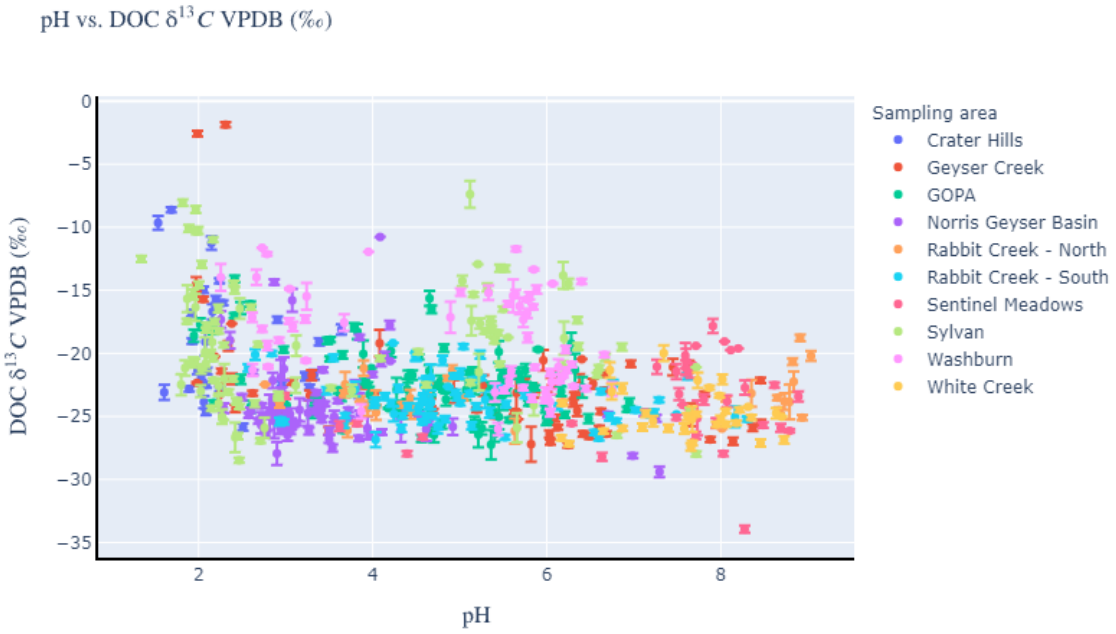

Figure A.4: pH vs. DOC δ^{13}C VPDB (‰) across 10 regions from 2005-2019.

Crater Hills

Crater Hills hydrothermal features have a pH range of 1.54 to 3.69. The highest value of DIC is 3,569 µM C located at "Rabbit Hole". The majority of hot springs in this region have DIC values under 833.3 µM C (Fig. A.5). The highest value of DOC in Crater Hills is 37.17 ppm C located at "Alice". Most hydrothermal features have under 166.65 µM DOC (Fig. A.6).

The DOC δ^{13}C at both "Alice" and "Jabberwocky" become ^{13}C depleted due to elevated levels of fresh photosynthesis derived DOC in the system due to a weather event. This analysis is expanded further in "Chapter 4: Weather Effects on DOC".

DIC $\delta^{13}C$ values are between -5‰ and +5‰ with increased levels of DIC ppm around -3‰ to -4‰ (Fig. A.7). There are two outlier values more $\delta^{13}C$ depleted than -15‰. Both values are either 83.33 µM C or below (Fig. A.9). These concentrations are toward the lower limit of detection and therefore this is possibly why their signature is ^{13}C depleted.

DOC $\delta^{13}C$ values within Crater Hills range -8.61‰ to -29.43‰ (Fig. A.8 & A.10) which is a large range compared to other regions in the park. Most of the hydrothermal DOC $\delta^{13}C$ values are between -15‰ and -25‰ and hydrothermal features with increased amounts of DOC tend to be around -24‰. Contextual samples around this value would give better context for what type of DOC is influencing hot springs in Crater Hills.

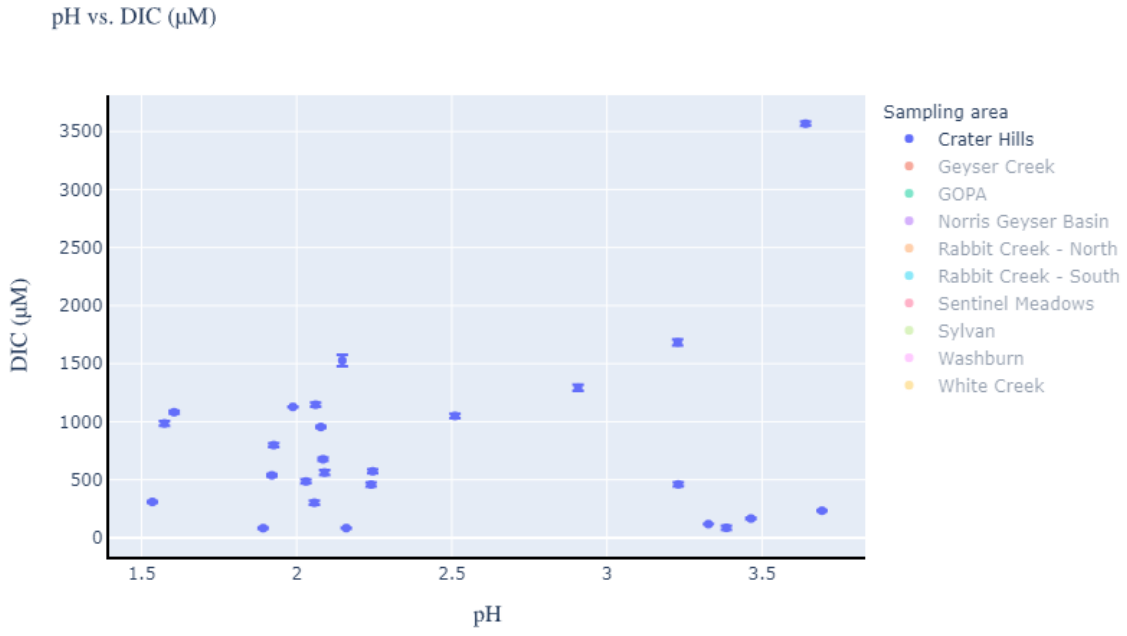

Figure A.5: pH vs. DIC µM for Crater Hills

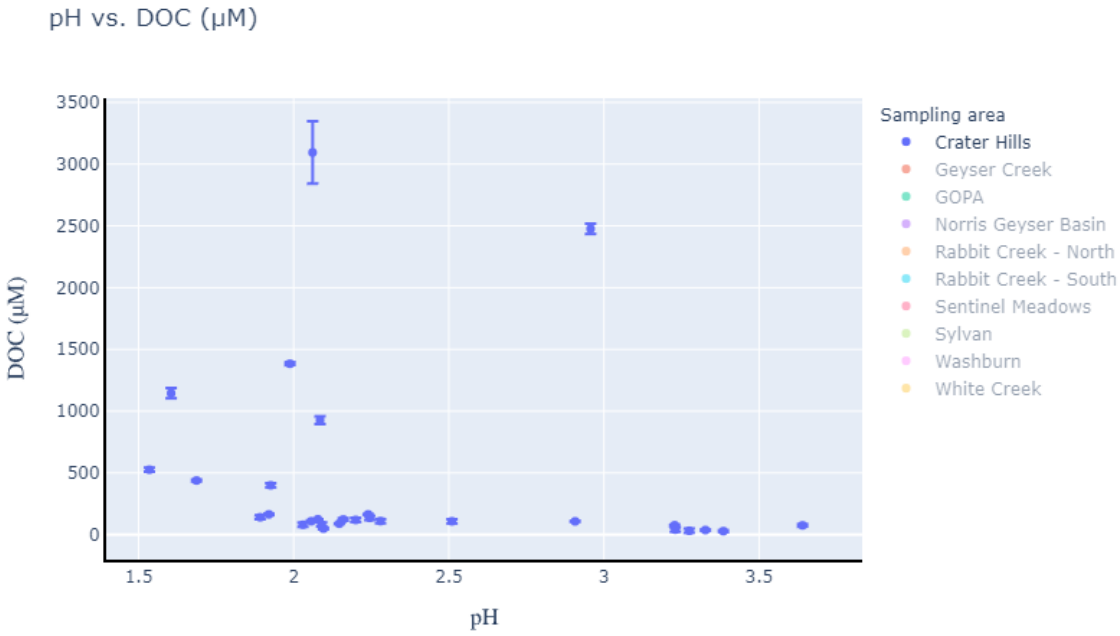

Figure A.6: pH vs. DOC µM for Crater Hills

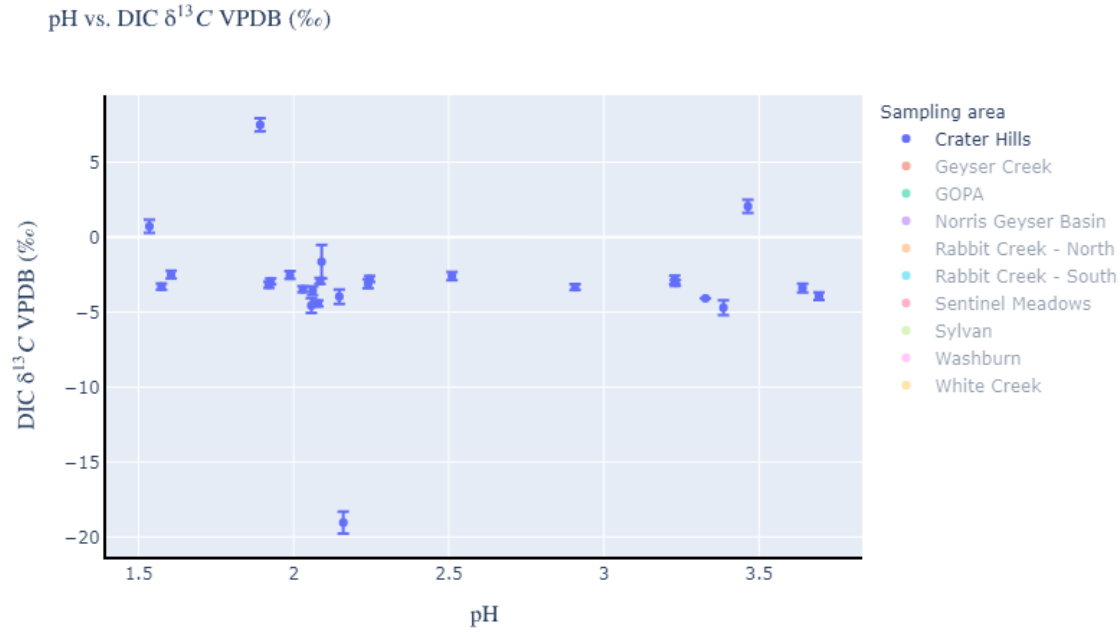

Figure A.7: pH vs. DIC δ^{13}C VPDB (‰) for Crater Hills

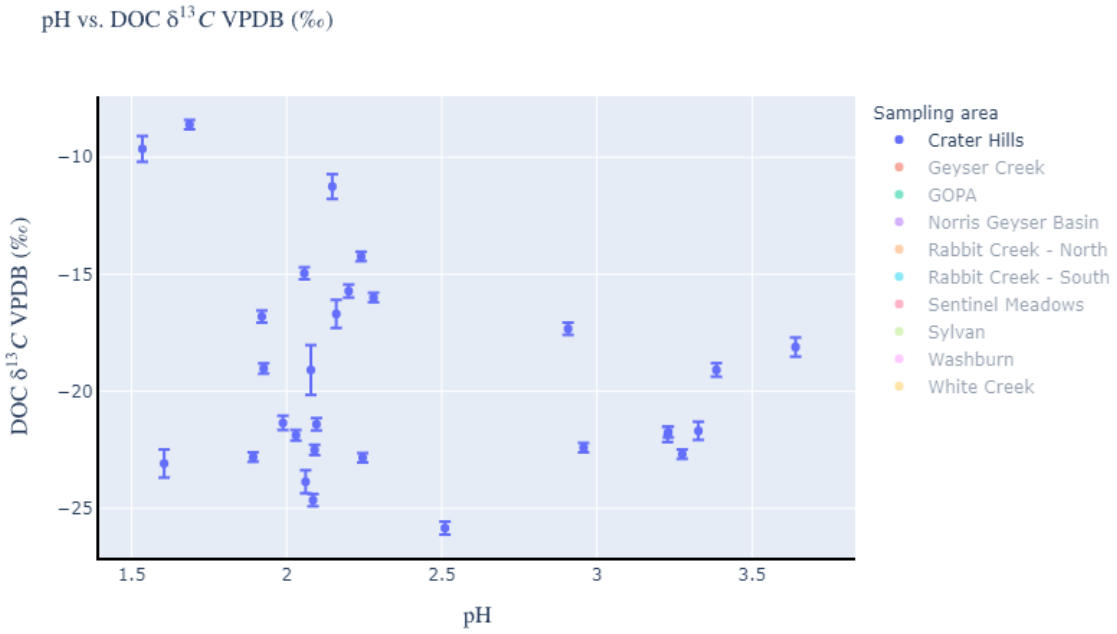

Figure A.8: pH vs. DOC δ^{13}C VPDB (‰) for Crater Hills

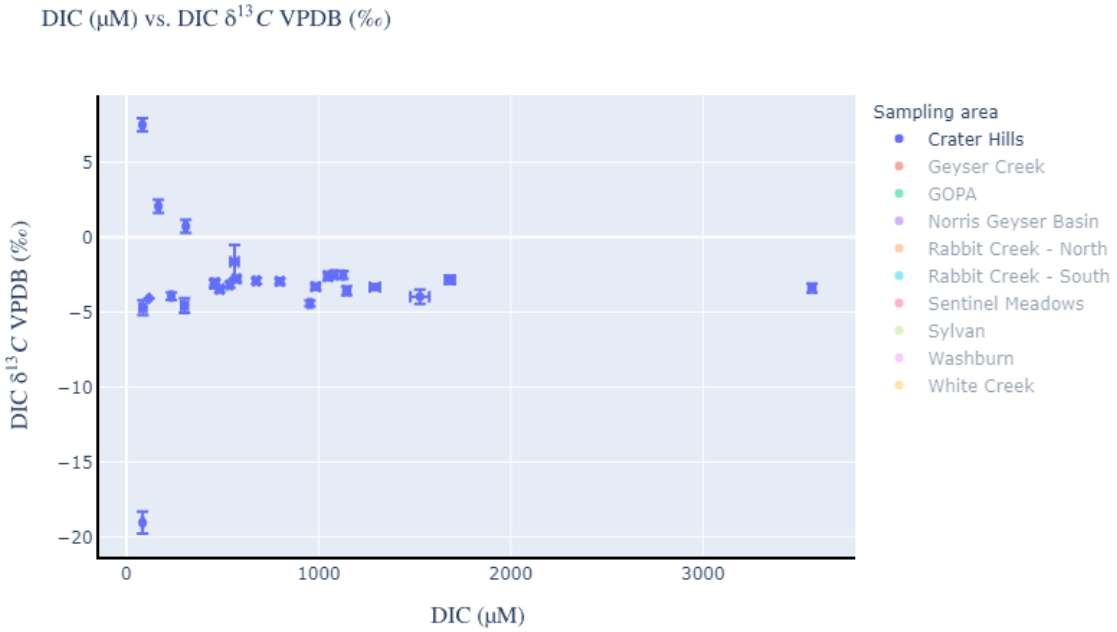

Figure A.9: DIC µM vs. DIC δ^{13}C VPDB (‰) for Crater Hills

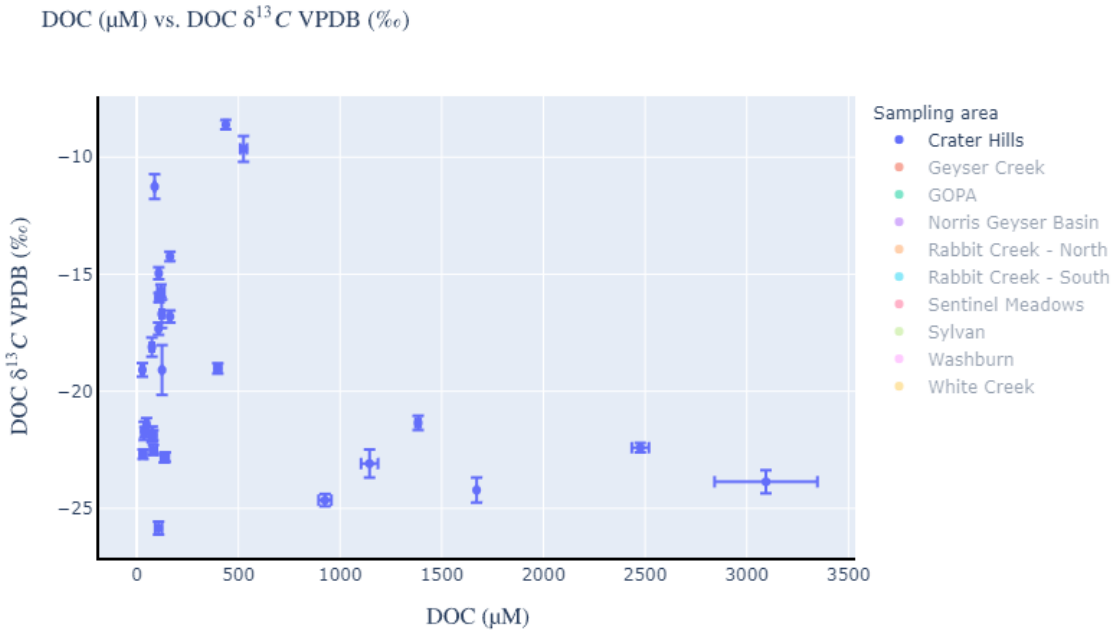

Figure A.10: DOC µM vs. DOC δ^{13}C VPDB (‰) for Crater Hills

Geyser Creek

The hydrothermal features in Geyser Creek range from pH values 1.97 to 8.55. DIC ppm range up to 6,224 µM C at "Man-O-War". Features between pH 1.97 to 5.40 all have under 1666.5 µM DIC. Above pH 5.40 there are elevated levels of DIC in the region (Fig. A.11). In Geyser Creek there are both sulfur-acidic dominant hot springs and neutral-chloride hot springs. DOC is relatively low throughout Geyser Creek compared to other regions within Yellowstone. Almost all features are below 83 µM DOC regardless of pH (Fig. A.12). The hot springs with higher than the average DOC are "Jackhammer", "Boiling Sombrero", and "The Monster". "The Monster" has a value of 3,152 µM DOC and this hot spring acidic with a pH of 1.98. This is a true outlier when compared to the rest of the samples and therefore it is possible it is connected to a different fluid source

than the rest of this region or has input from a local exogenous carbon source. The latter is more likely due to the $\delta^{13}C$ signature of -22.34‰ indicating that surrounding vegetation could be in the hot spring (Fig. A.14). This spring therefore falls in the category that is most likely dominated by process A: "Direct Delivery". There are two examples of weather sampling within Geyser Creek and these examples are further explained in Chapter 4 within this thesis.

The DIC $\delta^{13}C$ range from -9.01‰ to 8.69‰ (Fig. A.13). "Empress" has $\delta^{13}C$ enriched DIC values ranging 0‰ to 5‰. "Bat Pool" has a distinct cluster of samples ranging from -6.68‰ to -2.57‰ with elevated DIC at 4750 µM C (Fig. A.15). Other than "Bat Pool", there appears to be a link between increased µM DIC and ^{13}C enriched isotopic composition. This could potentially be a result of increased water rock interaction leading to more ^{13}C enriched carbon isotopes. "Bat Pool" does not fit in with that trend and appears to have an alternate source of DIC that is different from the rest of the region. Some scenarios that could lead to this difference would be dilution and mixing from multiple sources. There is a distinct difference in pH where "Bat Pool" is more alkaline vs. other springs in Geyser Creek that are more acidic with less concentration of DIC. "Bat Pool" also has higher signature of chloride compared to the more acidic springs within Geyser Creek and therefore it may be tapped into a deeply sourced fluid that has undergone increased amounts of boiling compared to other springs. These possible examples are why "Bat Pool" may have increased concentrations of DIC.

The DOC $\delta^{13}C$ values majority range from -14.52‰ to -27.85‰ (Fig. A.14). However, "Jackhammer" is an outlier with two samples taken in 2017 and 2019 with

DOC $\delta^{13}C$ values of -1.87‰ and -2.57‰ with concentrations of DOC of 366 and 383 µM respectively (Fig. A.16). These isotope values are significantly more ^{13}C enriched than the rest of the region. This suggests that "Jackhammer" is not receiving any meteoric water and that the hydrothermal fluid must be older than surrounding hot springs. The enriched ^{13}C value indicates that there is no additional DOC being added and it is possible the low amount of DOC in "Jackhammer" is being caused by organisms making organic carbon. This scenario could leave an enriched isotopic signature within the hot spring. If "Jackhammer" does not receive exogenous carbon runoff, then this would indicate that the hydrothermal fluid flows through an "armored" tube to the surface. An "armored" tube would be coated in silica and minerals, not allowing groundwater infiltration, or mixing (see Figure 1.9). More analysis needs to be conducted at "Jackhammer" to see what organisms are living there and if autotrophy dominates heterotrophs within this hot spring. The heterotrophic organisms in this hot spring would have to use heavier DOC to survive than other hot springs within Geyser Creek so it is possible there are distinctly different organisms living here. "Jackhammer" will be further investigated in Chapter 5 within this thesis.

"The Monster" has the highest concentration of DOC and therefore would be an interesting location to gather more samples in the future. The DOC $\delta^{13}C$ value is -22.34‰ which could be a direct result of exogenous carbon runoff. With only one sample it is uncertain whether this is the typical DOC signal for this hot spring. Geyser Creek has lighter isotopes than the rest of the park. Geyser Creek therefore presents itself as a unique region with hot springs such as "Jackhammer", "Bat Pool", and "The Monster"

that should be studied further to determine why these hot springs are outliers in this region.

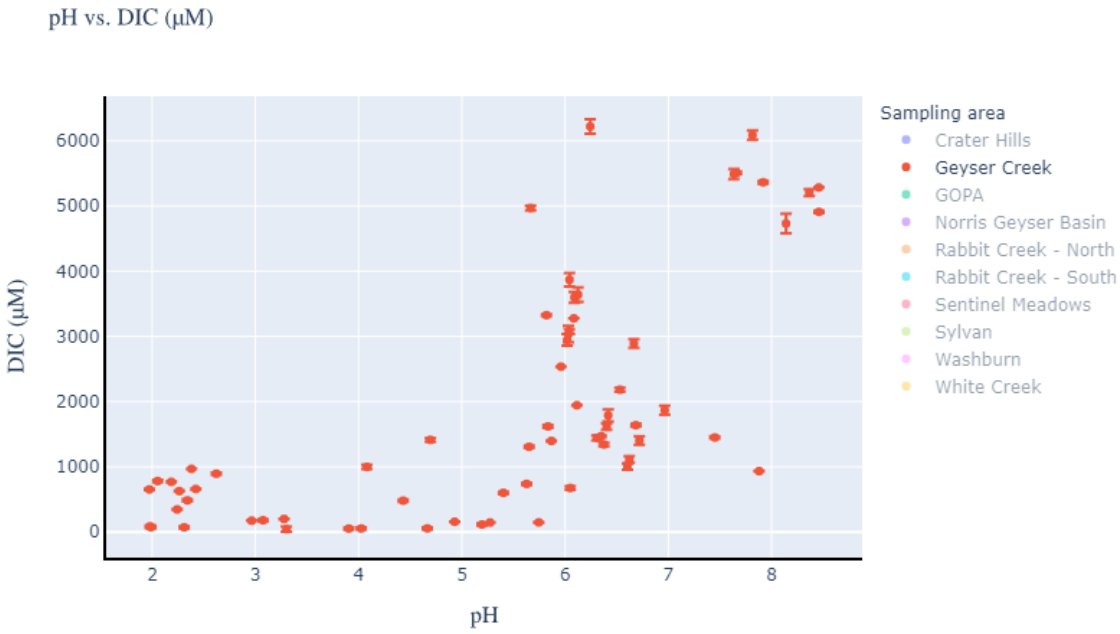

Figure A.11: pH vs. DIC µM for Geyser Creek

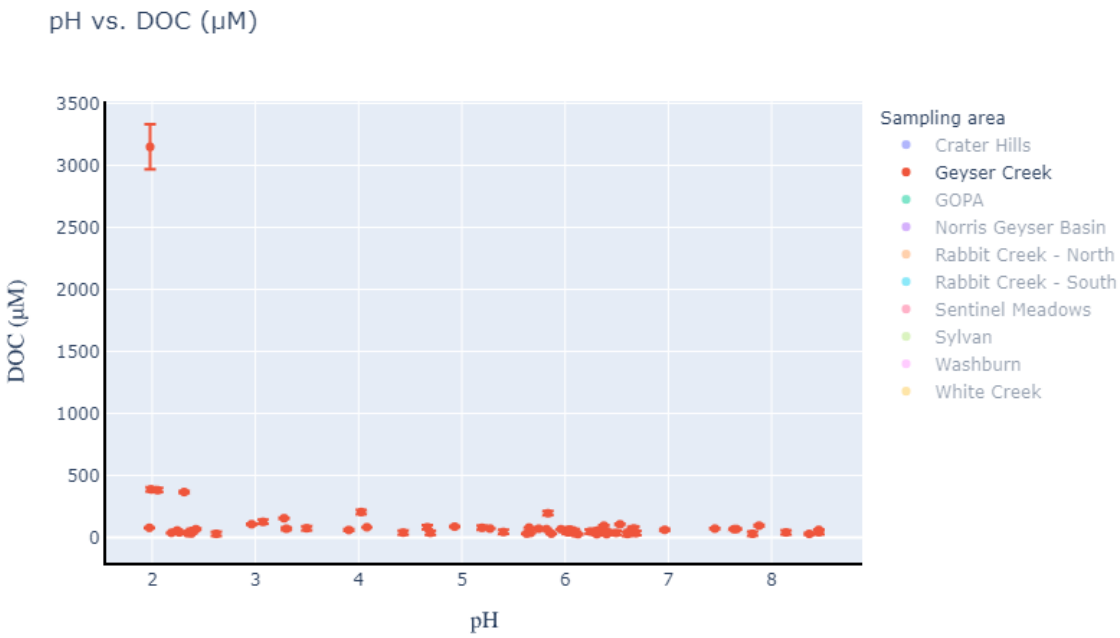

Figure A.12: pH vs. DOC µM for Geyser Creek

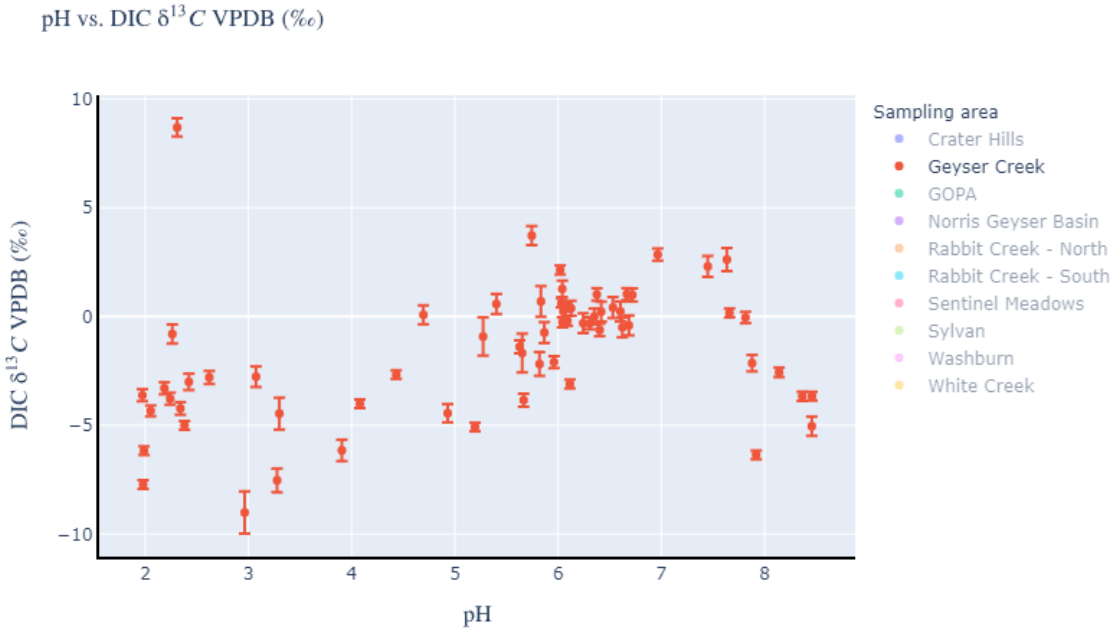

Figure A.13: pH vs. DIC δ^{13}C VPDB (‰) for Geyser Creek

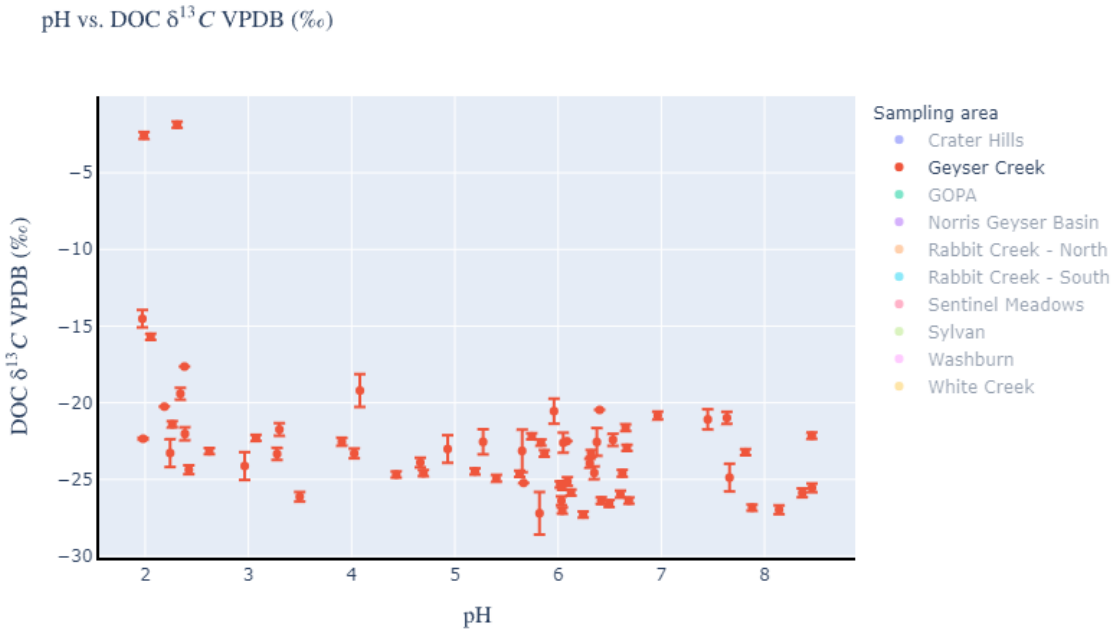

Figure A.14: pH vs. DOC δ^{13}C VPDB (‰) for Geyser Creek

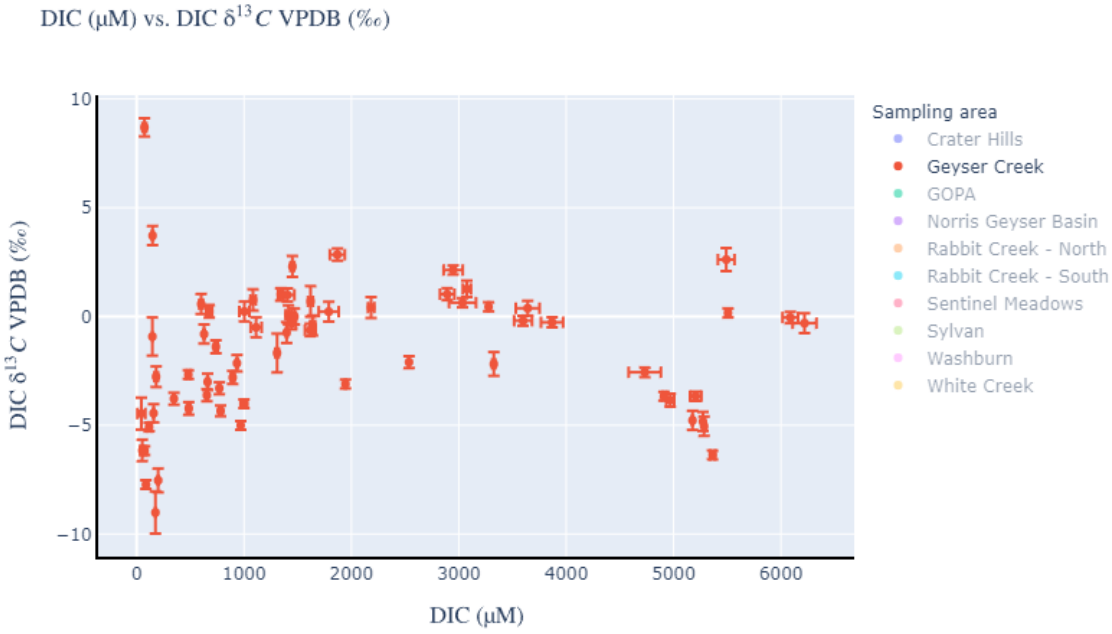

Figure A.15: DIC µM vs. DIC δ^{13}C VPDB (‰) for Geyser Creek

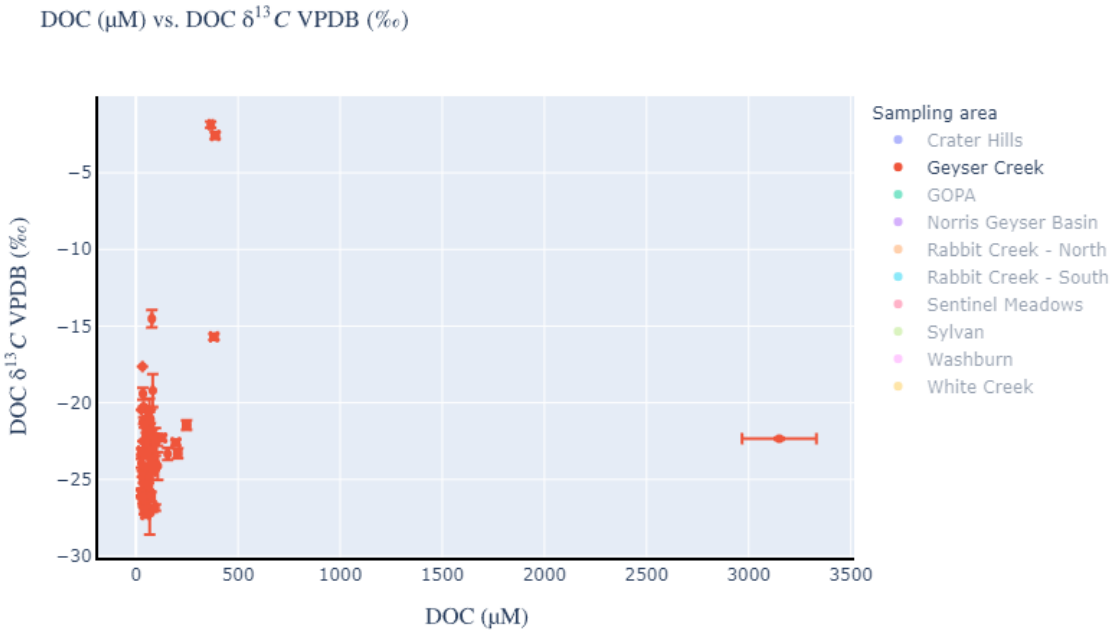

Figure A.16: DOC µM vs. DOC δ^{13}C VPDB (‰) for Geyser Creek

GOPA

The hydrothermal features in GOPA range pH 1.95 to 6.95 with DIC values up to 10,618 ppm which is the highest in the park (Fig. A.17). DIC values are much higher in GOPA and there are many samples that have over 4,166 µM DIC. However, DOC in this region is low with a range up to 921 µM DOC for hydrothermal features and Goose Lake has 2,365 µM DOC. Most samples in GOPA have below 417 µM DOC (Fig. A.18). As mentioned previously GOPA is a large meadow where trees and exogenous carbon runoff do not appear to occur overland. Topographically these springs sit in the middle of the meadow and are not lower compared to the surrounding environment. This location is very frequent for Bison to use the hot springs for warmth and for access to food in the Winter. They therefore could have an influence on the microbial community by transporting microbes from one area into GOPA.

There are currently no weather event contextual samples for GOPA yet, but it could be hypothesized that there would not be a large increase in DOC for these springs due to the local topography. “Spotted Grizzly” and “Witch’s Brew” have the largest values of DOC in the region averaging near 917 µM. “Foam Pool” has multiple samples with the highest DIC in the region and the park. Most samples with higher DIC have very low DOC values <83 µM. However, in “Foam Pool” this is not the case and there are DOC values 675 to 823 µM. This would provide energy for autotrophic and heterotrophic organisms, and it is therefore a candidate for further studies to look at the community composition due to this distinct signature. This would serve as an end member of the highest DIC for Yellowstone and sequencing efforts would help understand if high levels

of DIC impact community composition. There may be organisms taking advantage of the abundant DIC in the system and therefore producing large amounts of organic carbon. Another possibility could be that autotrophic organisms are inhibited from living in this environment and therefore DIC may not be consumed and is accumulating.

The DIC $\delta^{13}C$ values become heavier with increasing pH values (Fig A.19). Typically, the hydrothermal features of a DIC $\delta^{13}C$ between -5‰ and 0‰. Above pH 5.3, the isotopic values start to cross 0 and become enriched in ^{13}C with increasing pH. "Pedro's Tar Pit" is the most $\delta^{13}C$ depleted spring at -11‰. "Spotted Grizzly" and "Foam Pool" with abundant DIC have $\delta^{13}C$ signatures from -3.94‰ to -0.87‰ (Fig. A.21).

The DOC $\delta^{13}C$ values range from -27.24‰ to -12.94 ‰ (Fig. A.20). Most hot springs have DOC $\delta^{13}C$ values between -20‰ and -25‰ in GOPA. Hot springs with increased ppm DOC have isotopic values around -18‰ and -26‰ (Fig A.22). This suggests that there are different inputs of DOC into this region. Some input may be exogenous carbon runoff due to bison or the grassland in the meadow. Another source could be meteoric water influence in the meadow from multiple sources where this may be slightly altered due to increases in volcanic gas.

Therefore, GOPA is a region that has multiple signatures and possible hydrothermal fluid input. Some of the hydrothermal features seem to be influenced by deep hydrothermal fluids whereas other features seem to be influenced by younger meteoric water. This split within the same region leads to diverse geochemistry and

reinforces the hypothesis that young meteoric water is mixing with these hot springs in the meadow.

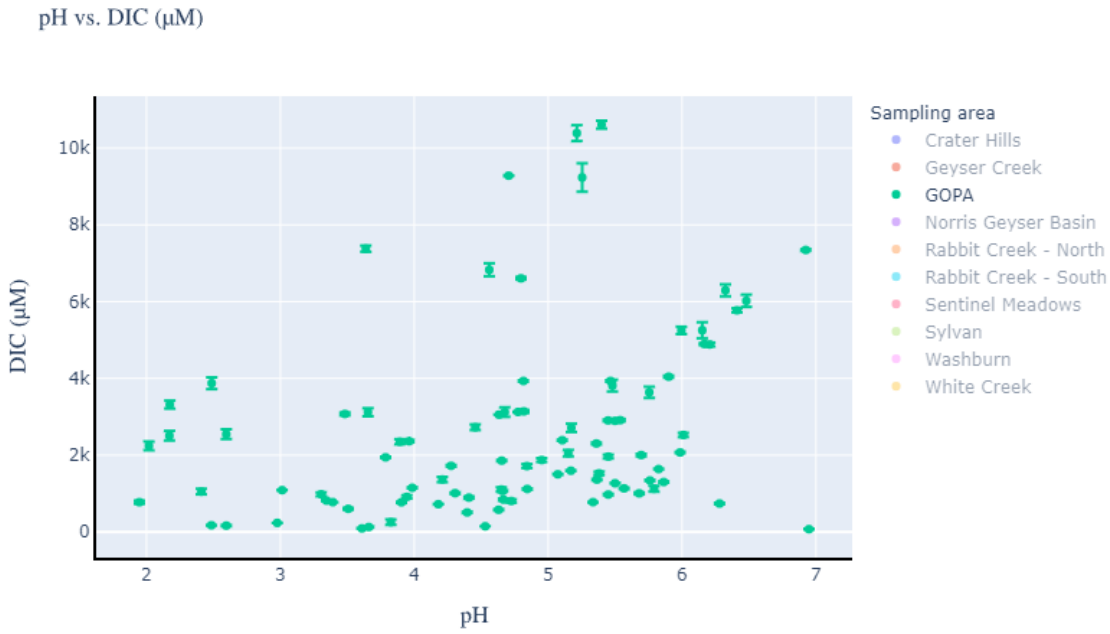

Figure A.17: pH vs. DIC µM for GOPA

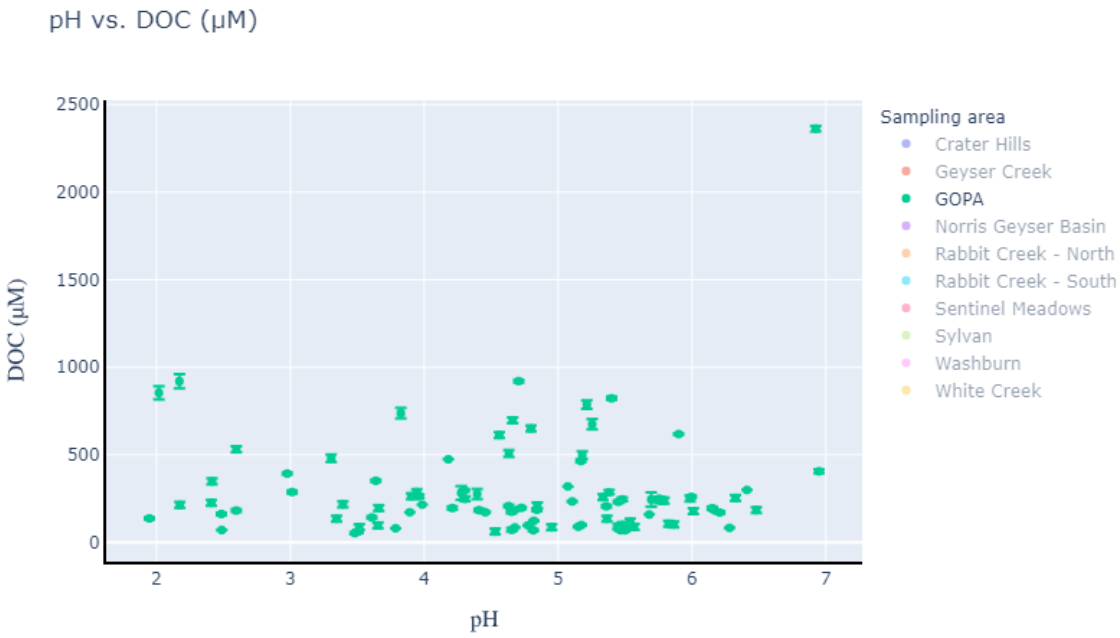

Figure A.18: pH vs. DOC µM for GOPA

Figure A.19: pH vs. DIC δ^{13}C VPDB (‰) for GOPA

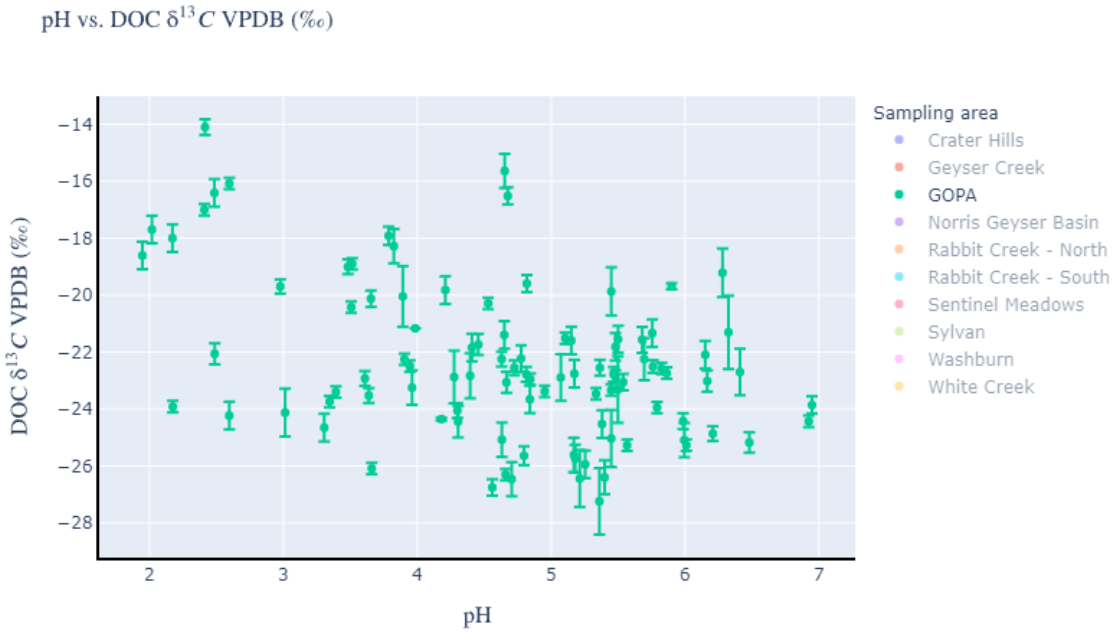

Figure A.20: pH vs. DOC δ^{13}C VPDB (‰) for GOPA

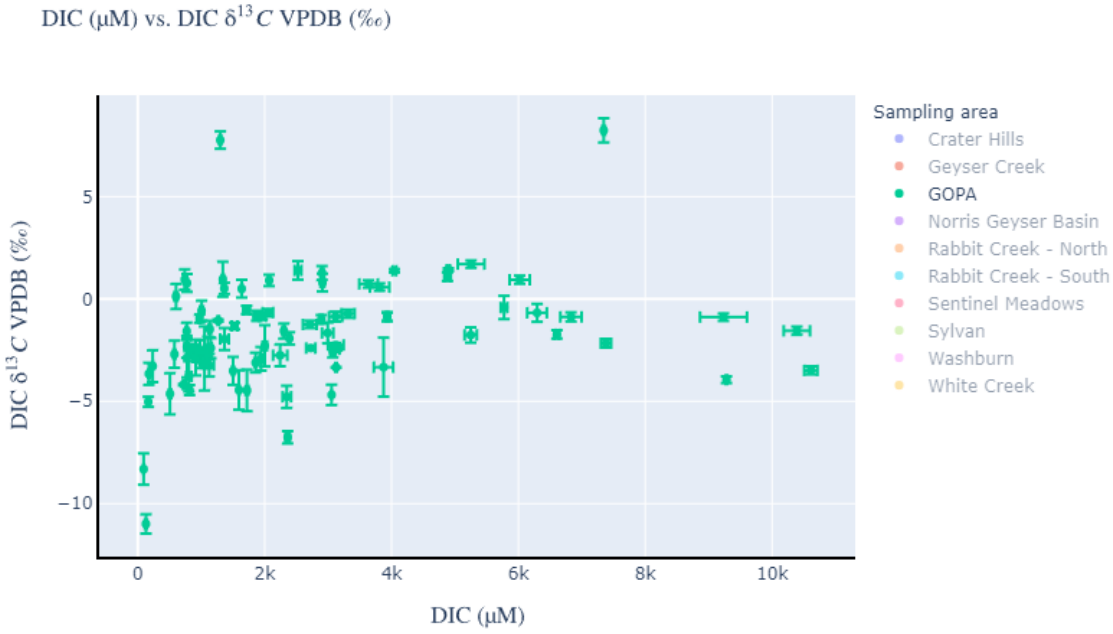

Figure A.21: DIC µM vs. DIC δ^{13}C VPDB (‰) for GOPA

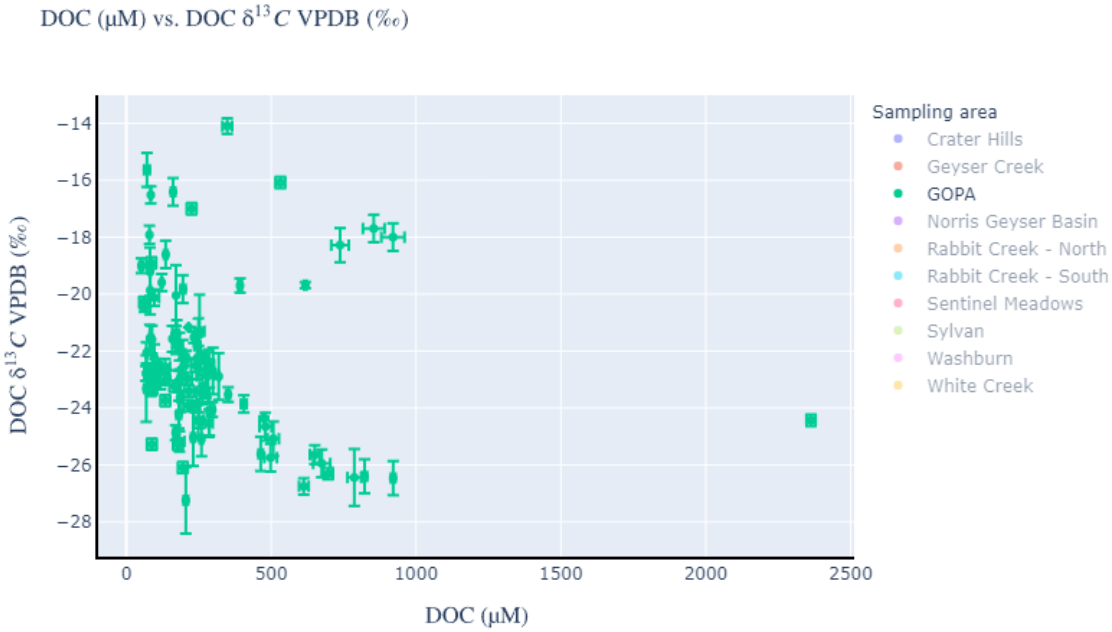

Figure A.22: DOC µM vs. DOC δ^{13}C VPDB (‰) for GOPA

Norris Geyser Basin

Hydrothermal features in Norris Geyser Basin range from pH 2.26 to 7.30 with DIC ranging up to 2,169 ppm (Fig. A.23). This particularly low DIC when compared to other regions. The acidic features have increased DIC which is unlike other regions. The neutral-chloride spring, "Perpetual Spouter", has around pH 7 and has 83 µM DIC. Typically, neutral springs parkwide tend to have more DIC than acidic areas. Most of the features in Norris are acidic with a pH < 4. DOC values range up to only 341 µM in Norris with one outlier at 1,718 µM named "Turnadeli". "Perpetual Spouter" in Norris also has under 42 µM DOC (Fig. A.24). Combining this with DIC these springs all have under 167 µM dissolved carbon. This value is very low compared to most springs in Yellowstone. These sites provide an excellent opportunity for further investigation through sequencing techniques to find out what organisms live in these hot springs with very low dissolved carbon values.

On the other hand, more investigation needs to be done at "Turnadeli" to figure out why the signature of DOC is much larger than the rest of the region. With only one sample it is tough to say whether this is caused by overland delivery or if this is the typical signal at this hot spring. Overall, Norris exhibits very low DIC and DOC values compared to every other region. This region serves as the end member for low dissolved carbon in this study.

The DIC $\delta^{13}C$ values mostly range from -5‰ to 0‰ as DIC ppm increases. There is no slope as DIC ppm increases for this region (Fig. A.25). There are several depleted signatures in $\delta^{13}C$ with low DIC µM. These samples need to be retaken at these regions

in a further study, and due to their low DIC µM they need to be run on a GasBench to make sure the isotope values are correct. These samples are very close to the lower limit of detection on the IRMS and therefore that could lead to the unusual light isotope signature. This is however not true for "Di Di Yu" with a DIC concentration of 277 µM and a $\delta^{13}C$ signature of -15.32‰ (Fig. A.27). This is well within the detection range, and it is unusually isotopically light compared to parkwide data. Therefore, this region provides an excellent opportunity for further research to examine low ppm carbon isotopes signatures. If these values were held up on an alternate instrument, these hydrothermal features in Norris would be different from the rest of the park. Norris Geyser Basin being dominated by higher levels of boiling could help explain this phenomenon.

The DOC $\delta^{13}C$ values range primarily from -20‰ to -29‰ (Fig. A.26). There are only a few samples less the -20‰ that range heavier to -10.77‰. "Turnadeli" with the highest value of DOC ppm has an isotopic signature of -23.46‰ (Fig. A.28). This is around the range of previous regions that had higher values of DOC. This is most likely due to exogenous organic carbon runoff into the hot spring from local topography. As previously mentioned, there are lodgepole pine in the area and many slopes within Norris.

Cinder pool has several samples that are heavier than the majority of the region. This hot spring provides an excellent opportunity to understand why Cinder Pool would be significantly isotopically heavier than other hot springs. Organisms seem to be fractionating carbon differently and the source of carbon appears to be different from the

rest of the regions in Norris. Similar springs that show this heavier signature are “Darko’s Vision” and “Dog Bone”. These springs do not have significant differences in chloride or sulfate concentration compared to the rest of Norris.

Ultimately, Norris Geyser Basin is a unique hydrothermal region outside of the caldera that provides multiple unanswered questions for further investigation. Lower values of DIC and DOC may provide limitations for local biology.

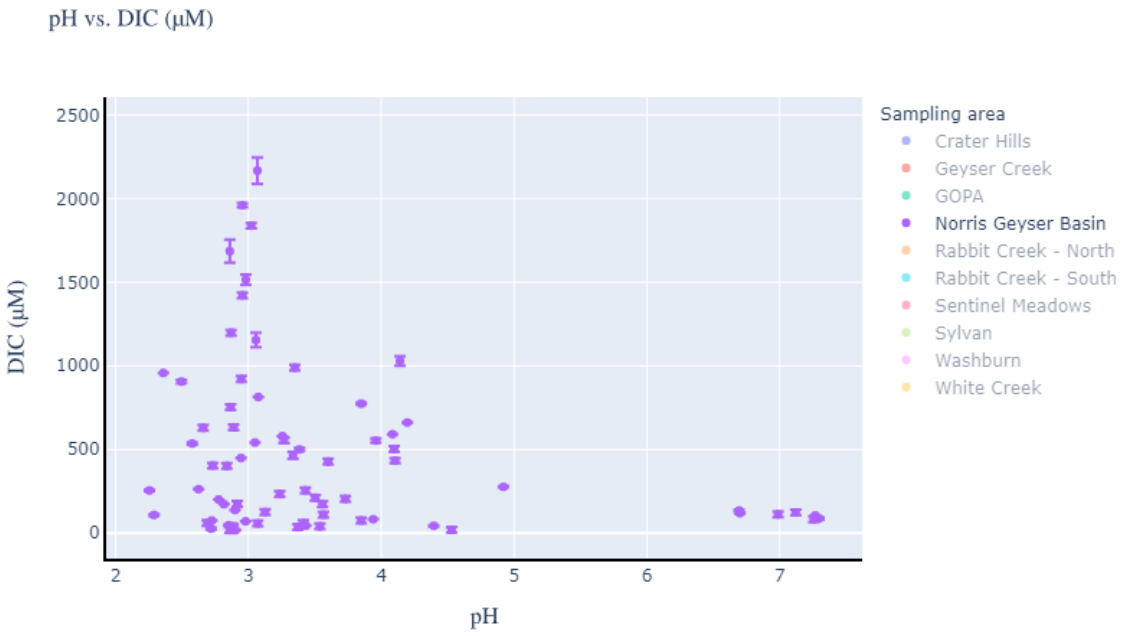

Figure A.23: pH vs. DIC µM for Norris Geyser Basin

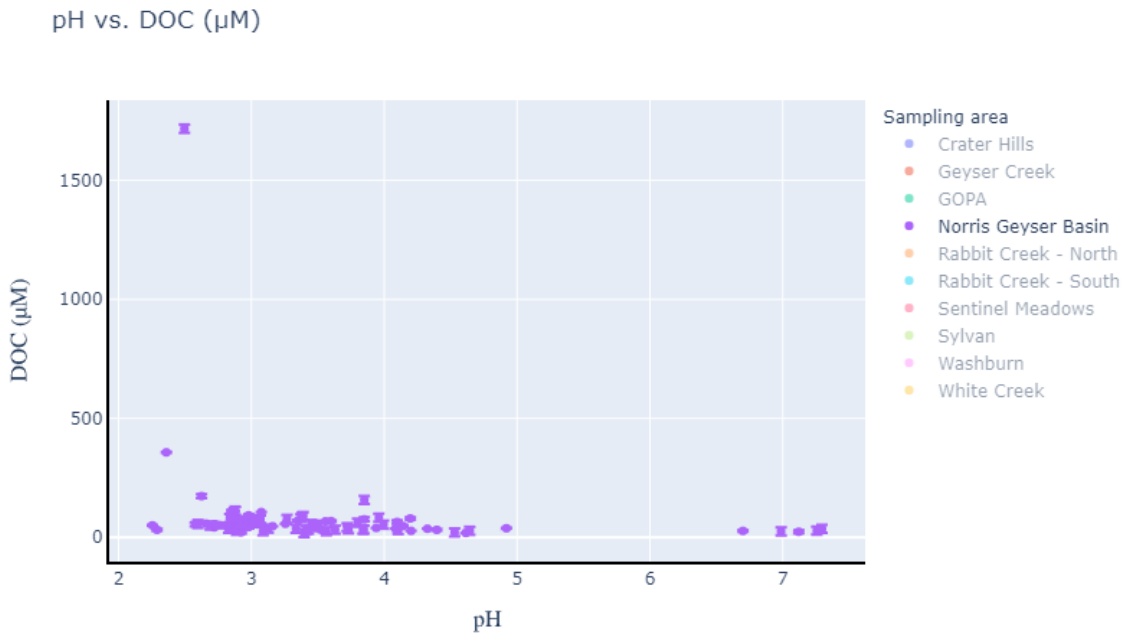

Figure A.24: pH vs. DOC µM for Norris Geyser Basin

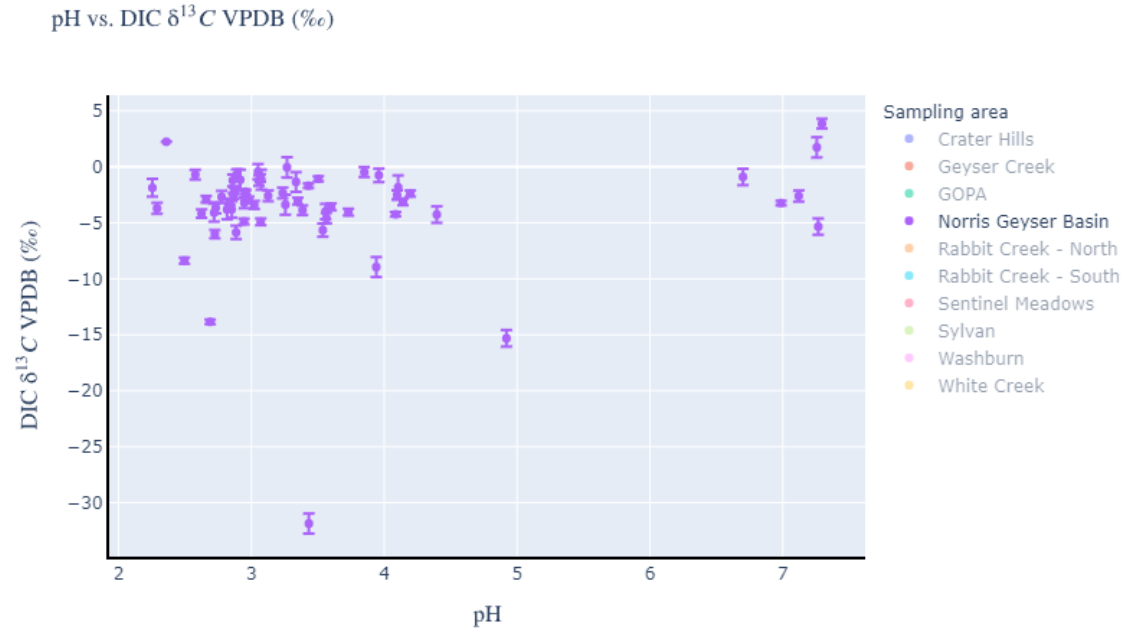

Figure A.25: pH vs. DIC δ^{13}C VPDB (‰) for Norris Geyser Basin

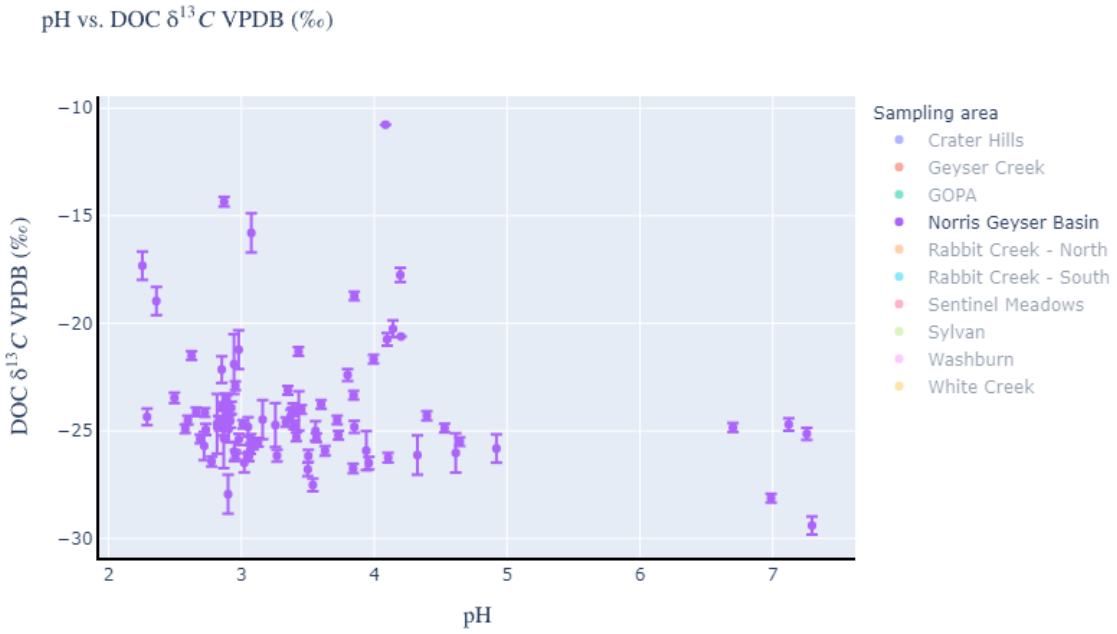

Figure A.26: pH vs. DOC δ^{13}C VPDB (‰) for Norris Geyser Basin

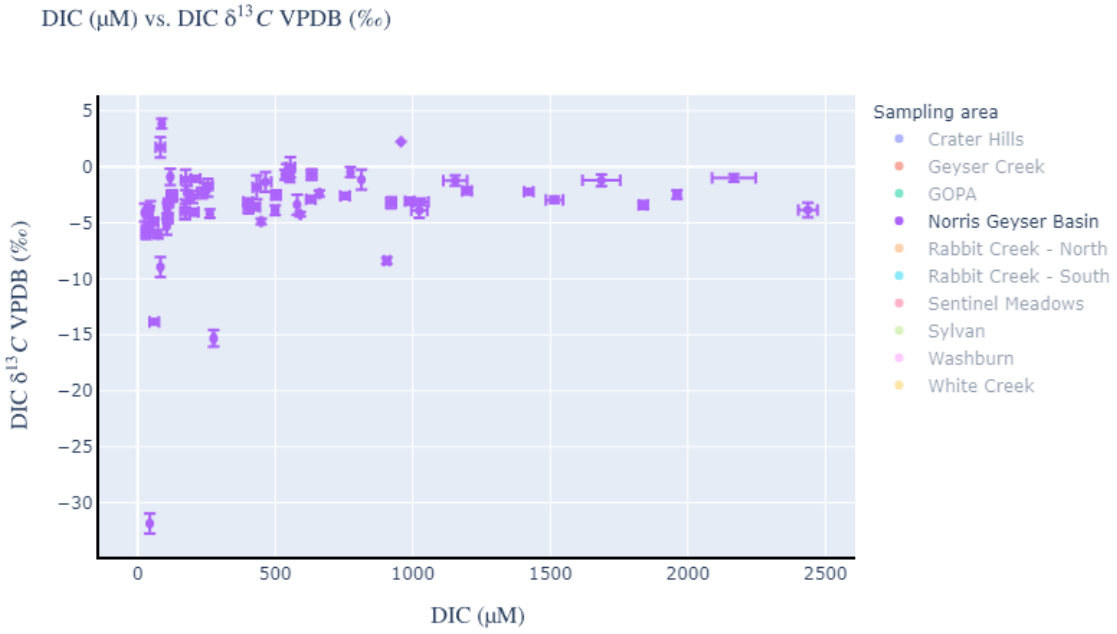

Figure A.27: DIC µM vs. DIC δ^{13}C VPDB (‰) for Norris Geyser Basin

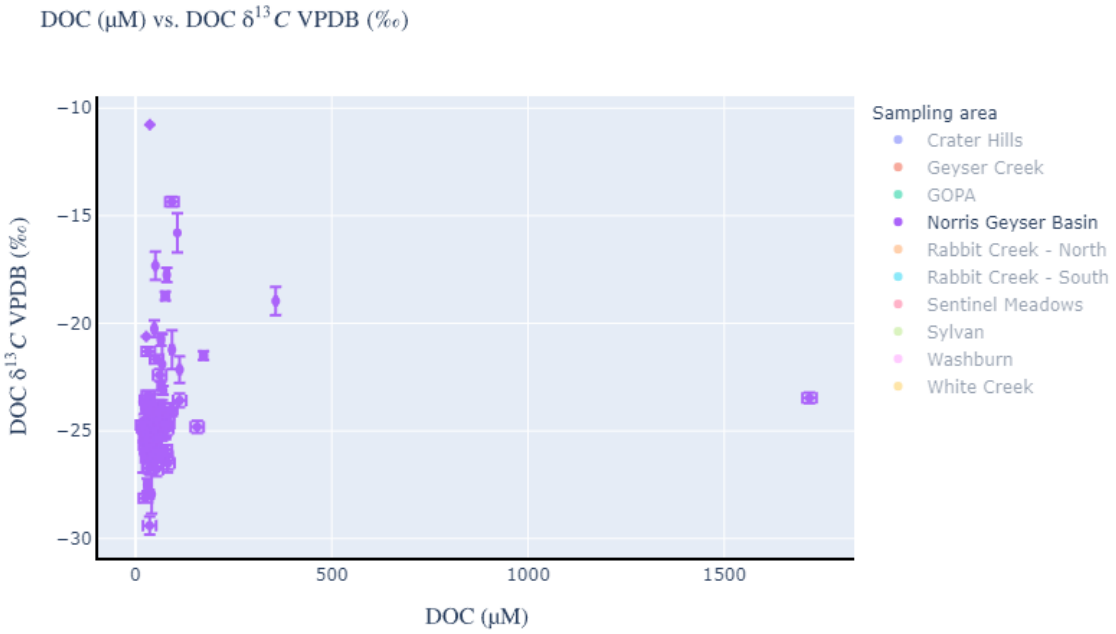

Figure A.28: DOC µM vs. DOC δ^{13}C VPDB (‰) for Norris Geyser Basin

Rabbit Creek North vs. South

Hydrothermal Features in Rabbit Creek North and South range from pH 2.76 to 9.28 and pH 2.57 to 8.3 respectively. DIC ranges up to 6,038 µM C at "Zen Garden" in Rabbit Creek South compared to a high of 4,016 µM C at "Shrimp" in Rabbit Creek North. DIC µM is typically higher in both regions of Rabbit Creek because there are only a handful of features lower than 417 µM C. Rabbit Creek North has a distinct difference in pH within the area. There are neutral springs above 8 pH and then a cluster of hot springs ranging from pH 2.7 to 6.2 (Fig A.29).

Both regions have very low levels of chloride, so Rabbit Creek is considered meteoric influenced instead of deep hydrothermally influenced. DOC, however, is

typically very low for both areas within Rabbit Creek. The data falls below 472 µM DOC other than one outlier at 886 µM DOC which is “Rum Runner” (Fig. A.30). “Rum Runner” is downhill from local vegetation and lodgepole pine. It is cut out in the side of the hill leaving easy access to exogenous carbon runoff from higher on the hill directly into the hot spring. This is not surprising to see an elevated signature of DOC at this location. It is unusual due to the meteoric classification for these springs to have low concentration of DOC. It would be hypothesized that due to younger water there would be increased levels of organic carbon being pumped into the system as these springs are inferred to be heated rainwater pools in some areas of Rabbit.

The DIC $\delta^{13}C$ values for Rabbit Creek North are in two distinct clusters. The first cluster with low DIC µM has a depleted $\delta^{13}C$ isotopic signature below -5‰. The second cluster of hot springs ranging from 2,417 to 3,583 µM DIC have an isotopic signature between -5‰ to 0‰ (Fig A.31). These hot spring fluids are most likely interacting with the same rocks on their way to the surface leading to very little differences in isotopic value. There is very little overlap between Rabbit Creek South data and the second cluster from Rabbit Creek North. Rabbit Creek South has nearly half of the data points more enriched in $\delta^{13}C$ then 0‰. There are also several data points with low DIC µM that cluster with similar points in Rabbit Creek North. The difference between the regions is that Rabbit Creek South dominates 833 µM to 1,667 µM DIC (Fig. A.33). Therefore, Rabbit Creek South still has a similar isotopic signature to data from Rabbit Creek North, but the DIC µM is different. Therefore, these two areas could be exhibiting different water resonance times and different hydrology between the two areas within Rabbit

Creek itself. Investigating this further, sulfate concentrations are similar between the two regions with the majority of samples < 100 ppm. Chloride concentrations are different with Rabbit North containing concentrations of chloride up to 355 ppm. Rabbit South only has a range up to 3.5 ppm chloride and therefore this difference shows these two areas within Rabbit Creek have different influences from the magmatic system below.

The DOC $\delta^{13}C$ values between Rabbit Creek North and South are very similar. The difference between the two areas is that Rabbit Creek South tends to have more DOC ppm than Rabbit Creek North. "Rum Runner" has the elevated signature of DOC ppm at a $\delta^{13}C$ of -24.61‰ (Fig. A.34). This is like other areas around similar vegetation. This therefore enforces the hypothesis that elevated levels of DOC are being caused by local exogenous carbon runoff into the hot spring. Rabbit Creek North has both the heaviest and lightest isotopic values and therefore has the larger range when compared to Rabbit Creek South. One thing to notice is that both areas have a range of most of their values between -19‰ to -27‰ (Fig. A.32). This is isotopically depleted in $\delta^{13}C$ than other areas within Yellowstone and there are no isotopically enriched signatures in Rabbit Creek. Other areas tend to have lighter isotopes ranging from -25‰ to -30‰, but that is not the case here. This observation aligns with the classification of these springs as meteoric dominant hot springs, and they are represented as the endmember of meteoric water influenced hot springs.

Ultimately, Rabbit Creek Area is dominated by meteoric water and therefore this plays a large impact on DOC within the area. More investigation into time series and weather would help explain differences in dissolved organic carbon within the region.

Sequencing efforts comparing Rabbit Creek North vs. South would be helpful to determine if biology is controlling the difference in DOC µM between the areas or if it is dominated by shallow subsurface input from local vegetation.

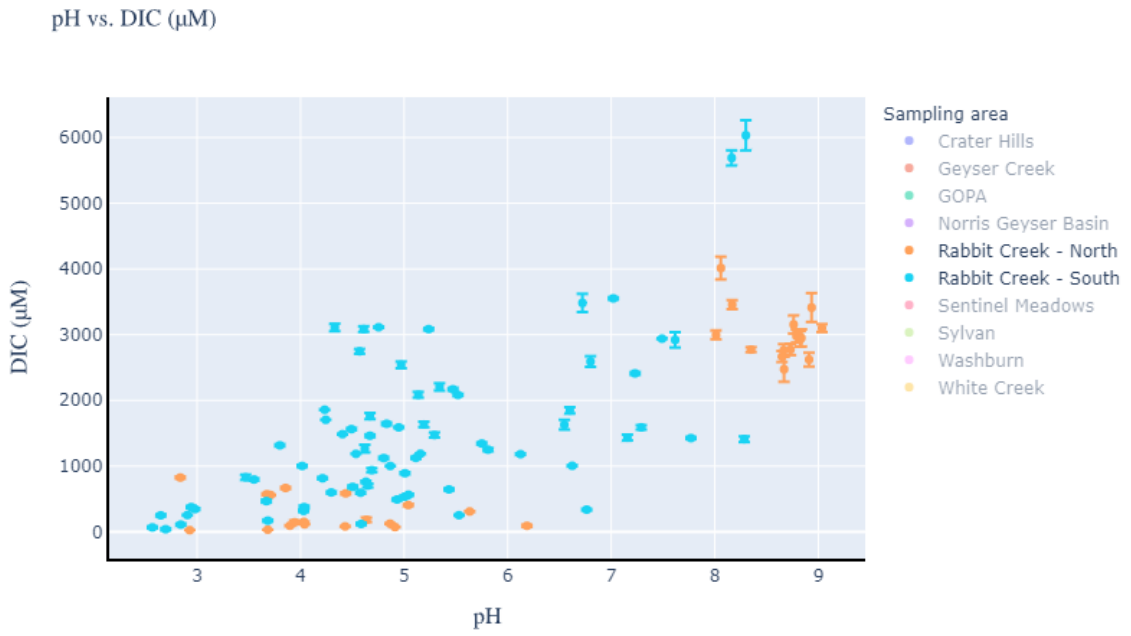

Figure A.29: pH vs. DIC µM for Rabbit Creek North & South

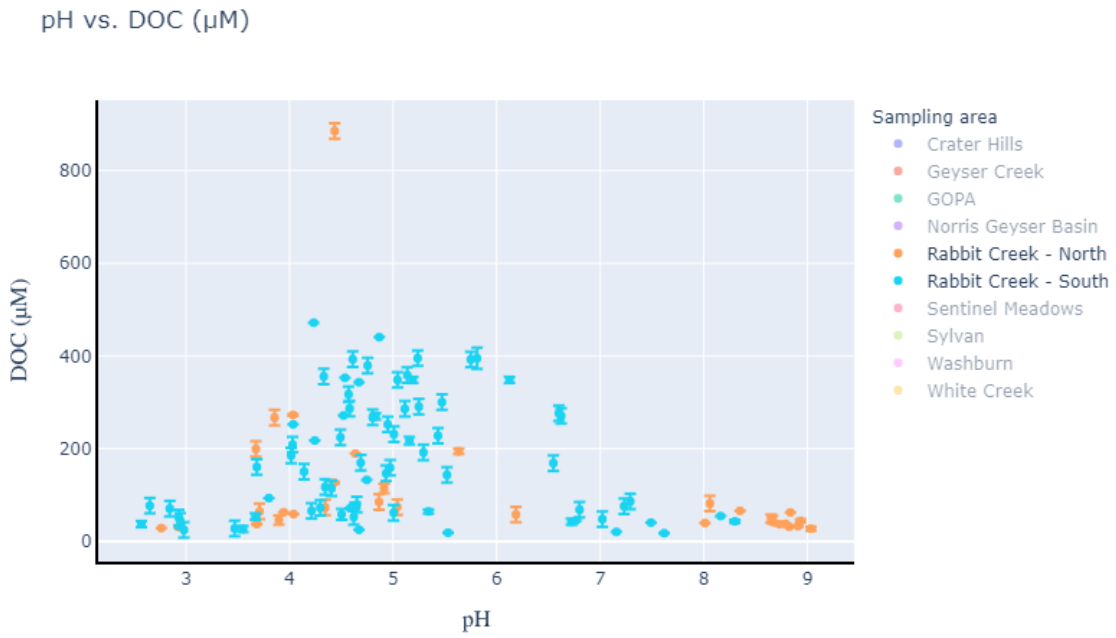

Figure A.30: pH vs. DOC µM for Rabbit Creek North & South

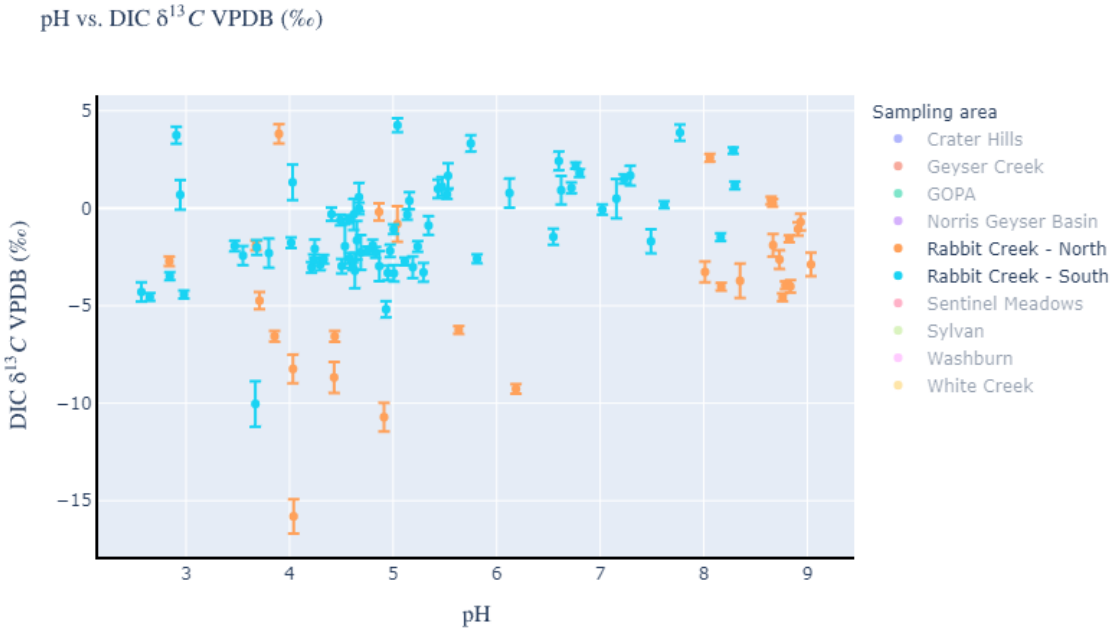

Figure A.31: pH vs. DIC δ^{13}C VPDB (‰) for Rabbit Creek North & South

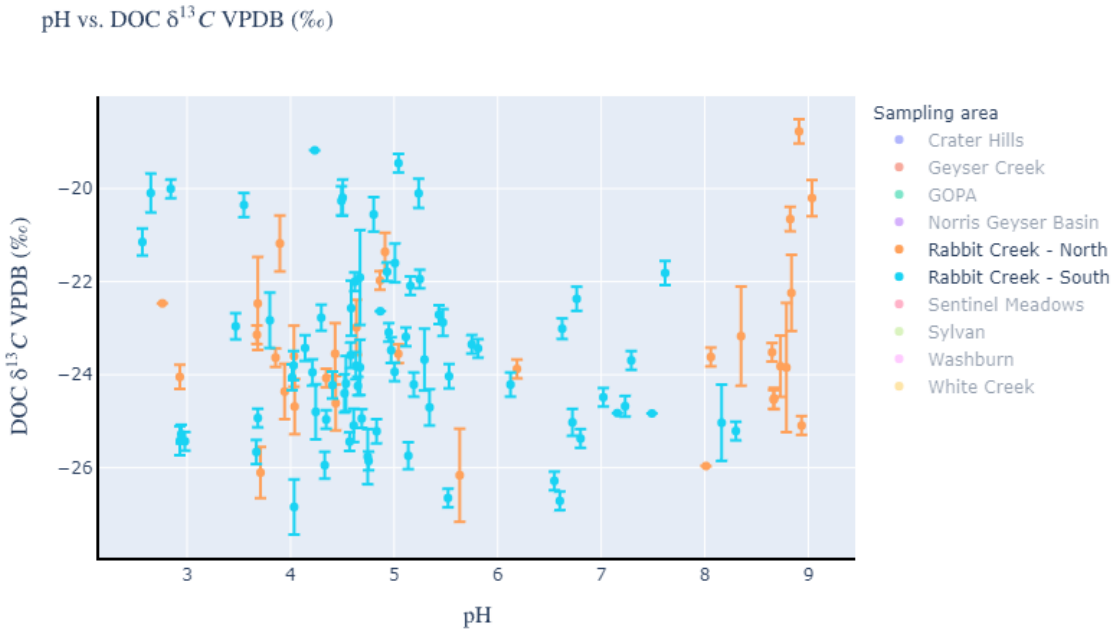

Figure A.32: pH vs. DOC δ^{13}C VPDB (‰) for Rabbit Creek North & South

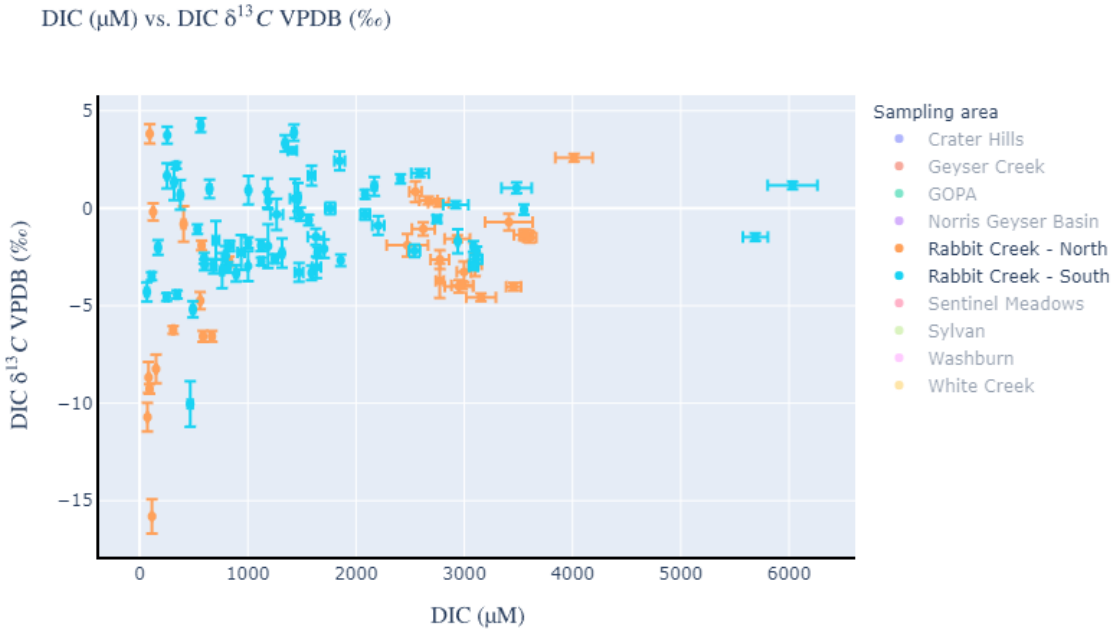

Figure A.33: DIC µM vs. DIC δ^{13}C VPDB (‰) for Rabbit Creek North & South

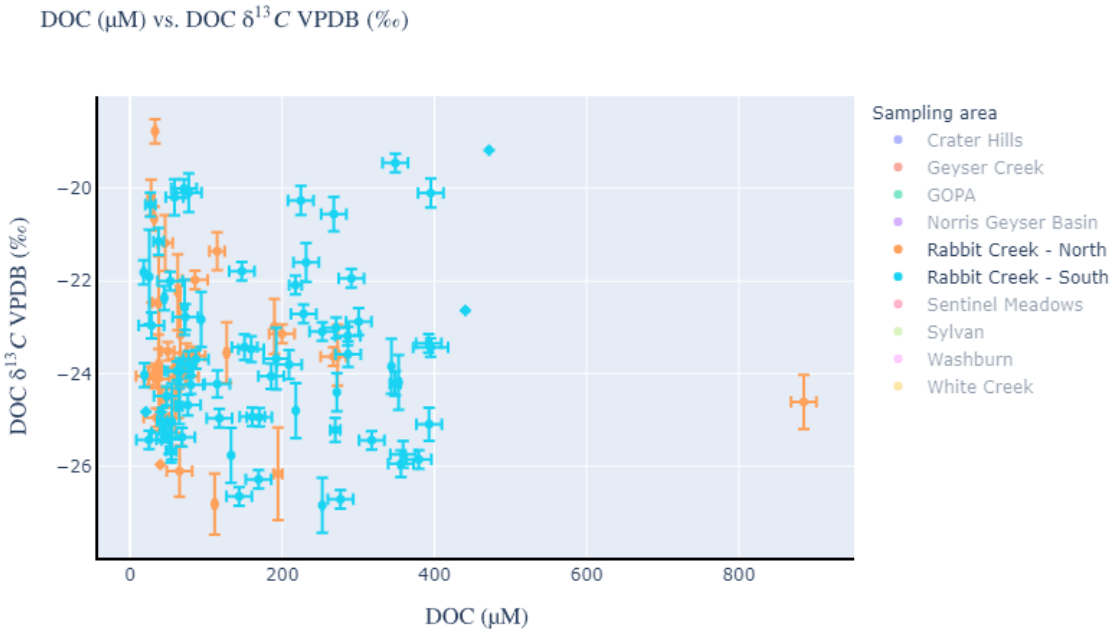

Figure A.34: DOC µM vs. DOC δ^{13}C VPDB (‰) for Rabbit Creek North & South

Sentinel Meadows

Sentinel Meadows along with areas in White Creek illustrate the "deep hydrothermal" endmember for hydrothermal features in Yellowstone. Samples within these two areas contain large amounts of chloride in hydrothermal fluid. The hydrothermal features in Sentinel Meadows in this study range from pH 2.99 to 9.55 with DIC concentrations up to 6,830 µM C. As mentioned previously, the hydrothermal features in this region are spread out and have different topographic locations. Many of these features have been sampled repeatedly throughout this study.

Each hydrothermal feature also has a distinct amount of DIC ppm that does not fluctuate with small perturbations of pH between the years. "Bison Pool" has the highest amount of DIC averaging 5,500 µM C. "Mound Spring" located topographically high has very little fluctuation in DIC over the course of the study. This hydrothermal feature is between 2,500 to 2,641 µM DIC over a pH range from 8.07 to 8.89 (Fig. A.35). At the other end of the pH scale, "Milk Chocolate", "Special Dark", and "Cole's Coffee" are low in DIC concentration compared to the other features in the region. These features are small springs located next to "Bison Pool". These acidic features have a DIC concentration of 711 µM C and below. "Iron Pots" in this region has a pH range 6.07 to 6.80 which is directly between the acidic features and the neutral chloride features in this region. What is also unique at "Iron Pots" is that there is DIC µM ranging from 2,712 at pH 6.07 to 2,180 at pH 6.80. As pH becomes more acidic at these hot springs in Sentinel Meadows, DIC µM decreases.

DOC µM of Sentinel Meadows is a contrast of DIC µM because features with high DIC, will have low DOC and vice versa. “Milk Chocolate”, “Special Dark” have the highest DOC µM out of the features in Sentinel Meadows. “Special Dark” has a high of 2,920 µM C and “Milk Chocolate” has a high of 914 µM C. However, “Cole’s Coffee” stays low with a DOC concentration of 102.5 µM (Fig. A.36). It is hypothesized that these springs may have elevated concentrations of DOC due to the fact they are topographically lower in the meadow and that bison frequently are around them. There are large amounts of bison feces around these springs and the weather could wash this fresh organic carbon into these hot springs. However, the big features in this region have very little DOC. This is because features such as “Mound Spring” and “Flat Cone” are topographically high and surrounded by sinter. These springs have topographically positive classification (Fig. 1.9). Therefore, exogenous carbon has no path to flow into these hot springs in a weather event. DOC concentrations for these features that are deep neutral chloride hot springs are typically less than 83 µM C. This is ultimately going to affect the organisms living in these hot springs and they could differ from previous regions in this study due to the extremely low DOC input. “Iron Pot” even though it has a more acidic pH than the other neutral chloride springs, it still shows a very low DOC concentration of around 83 µM.

The DIC $\delta^{13}C$ values within Sentinel Meadows range from -21.40‰ to 1.66‰ (Fig A.37). The isotopically depleted $\delta^{13}C$ signatures are shown in the acidic hot springs. “Cole’s Coffee” is interesting because this feature shows the most depleted $\delta^{13}C$ signature of DIC at -21.4‰. This feature was not high in DOC nor DIC µM and therefore

needs to be investigated further to understand why there is such a uniquely light signature for DIC. “Special Dark” fluctuates from a DIC $\delta^{13}C$ value of -8.54‰ to -13.90‰. “Milk Chocolate” fluctuates from -4.76‰ to -5.42‰. It is unknown what is causing these depleted $\delta^{13}C$ signatures of DIC in the region and this needs to be investigated further in these hot springs. “Mound Spring”, “Bison Pool”, and “Steep Cone” all have different clusters of the similar µM DIC and similar DIC $\delta^{13}C$ values. These clusters result in isotopically $\delta^{13}C$ enriched DIC as DIC concentration increases (Fig. A.39). The only spring that does not fit this trend are “Iron Pots” which display a very similar isotopic composition to “Bison Pool”.

The DOC $\delta^{13}C$ values have a wide range in Sentinel Meadows from -11.94‰ to -33.94‰ (Fig. A.38). The signatures are not distinct between the different hydrothermal features and these values for each hot spring fluctuate between samples. “Milk Chocolate” and “Special Dark” with high values of DOC µM have isotopic signatures ranging from -23.38‰ to -28.20‰. This range fits in with other regions that show high DOC concentrations. Elevated concentrations of DOC in Yellowstone seem to show a depleted $\delta^{13}C$ value in the mid-twenties (Fig. A.40). This elevated signature most likely is caused due to increased infiltration or response to storm events.

Ultimately, Sentinel Meadows has very distinct features from one another at different ends of the pH scale. This leads to differences in DIC and DOC characteristics in the region. Sentinel Meadows is a great location to study organisms that rely solely upon the DIC from the system due to the very low DOC concentrations and the topographic locations of these hot springs. They therefore will have a unique community

that will not be influenced by local topography, which is the case for hot springs in different regions. These elevated hot springs therefore may give an insight into ancient hot spring systems due to their locations and these are locations to isolate the pathway of thermal alteration.

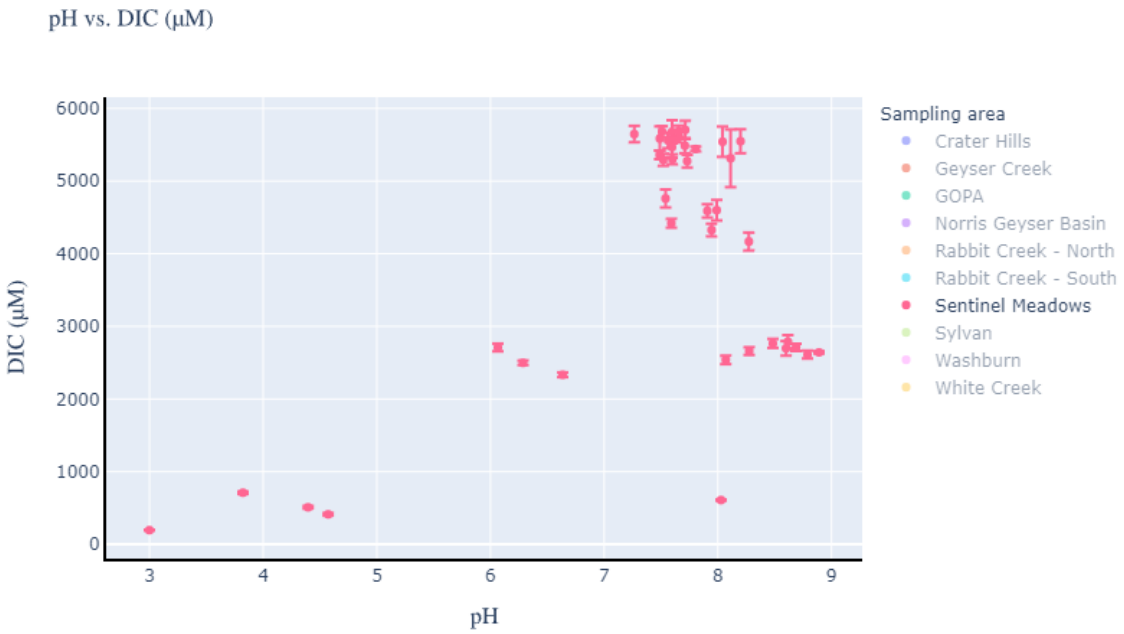

Figure A.35: pH vs. DIC µM for Sentinel Meadows

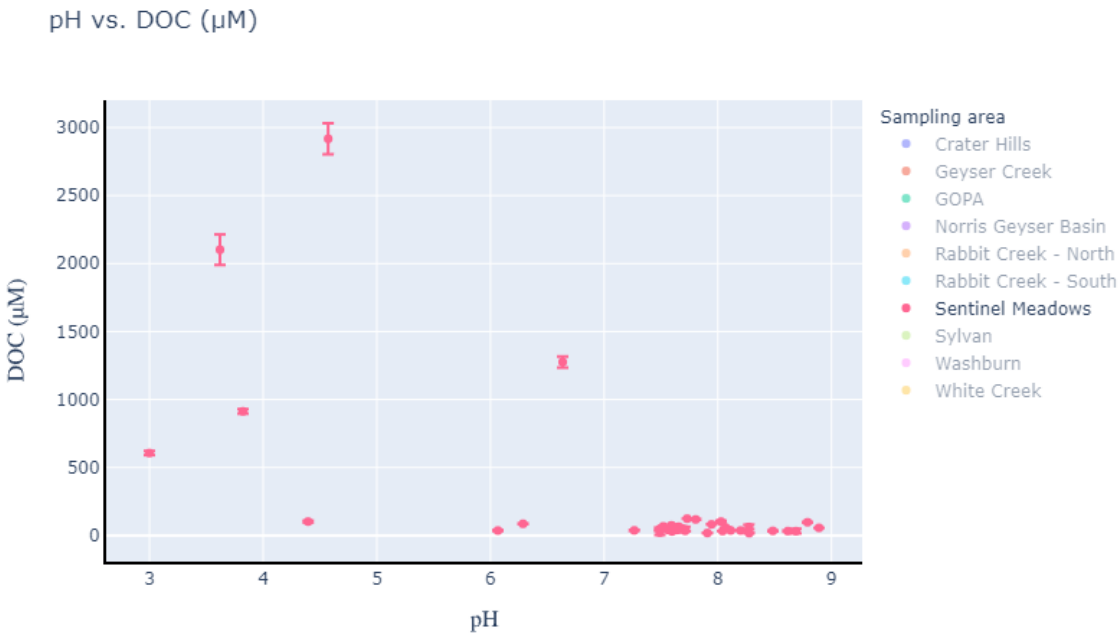

Figure A.36: pH vs. DOC µM for Sentinel Meadows

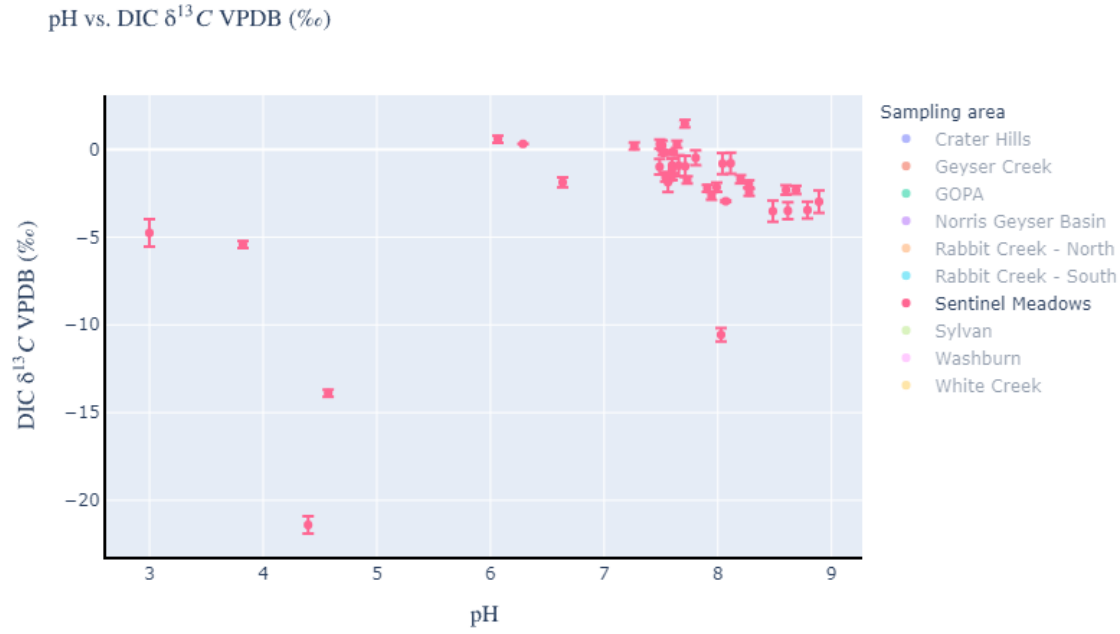

Figure A.37: pH vs. DIC δ^{13}C VPDB (‰) for Sentinel Meadows

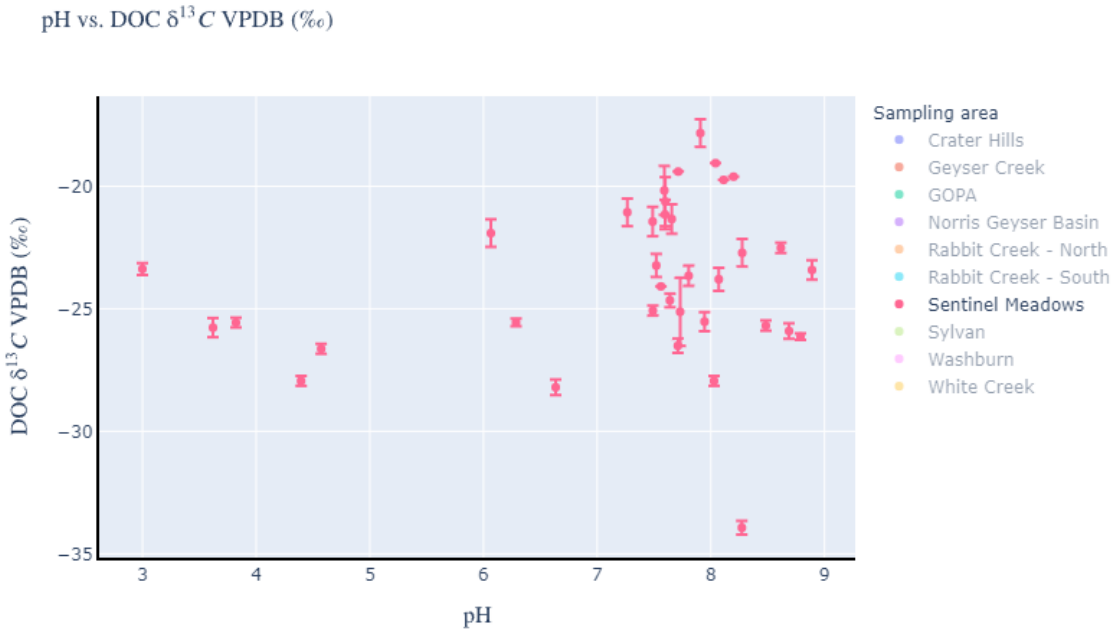

Figure A.38: pH vs. DOC δ^{13}C VPDB (‰) for Sentinel Meadows

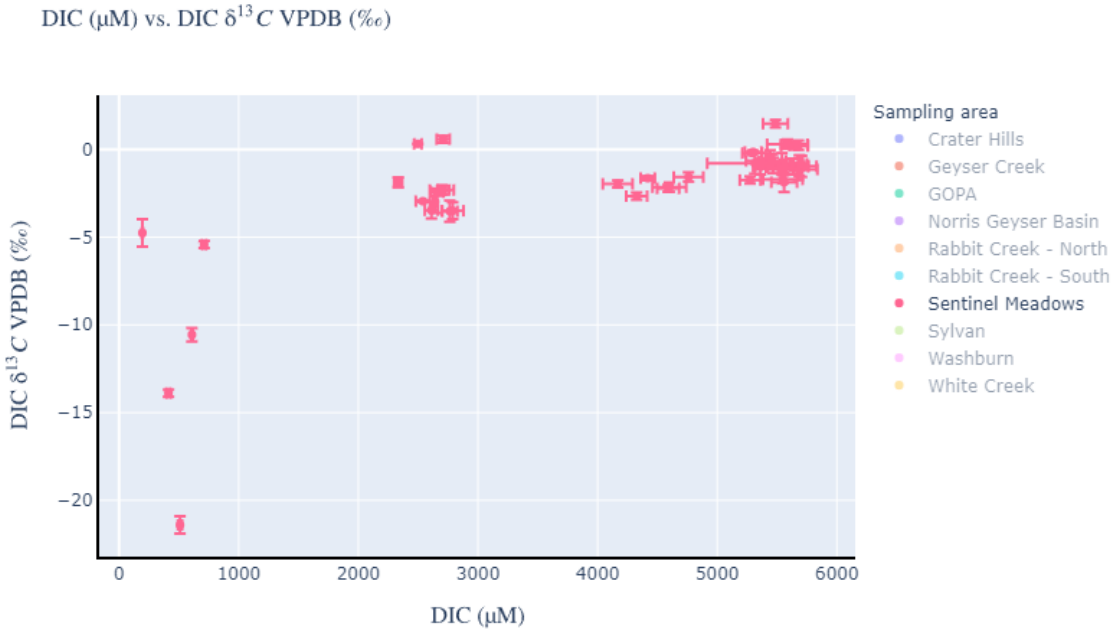

Figure A.39: DIC µM vs. DIC δ^{13}C VPDB (‰) for Sentinel Meadows

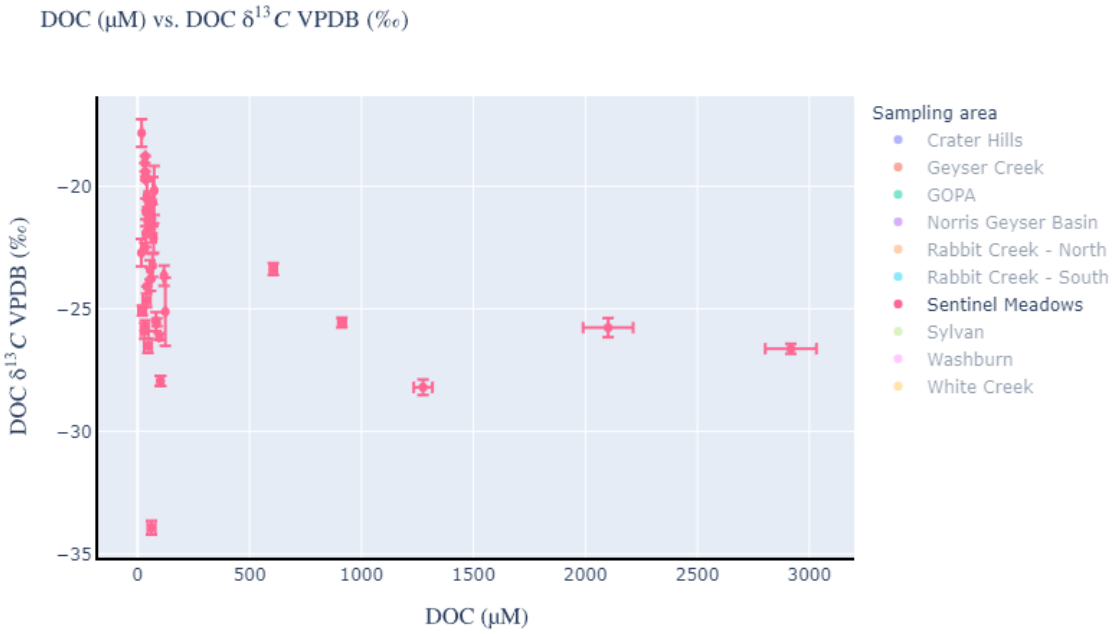

Figure A.40: DOC µM vs. DOC δ^{13}C VPDB (‰) for Sentinel Meadows

Sylvan

Sylvan is one of the most unique locations of hydrothermal features in Yellowstone. Hydrothermal features in Sylvan in this study range from a study low pH of 1.23 to 8.69. Sylvan has both acidic features with some hot springs that are neutral. DIC varies along the pH range with a region high of 14,729 µM at "Avocado". Both "Avocado" and "Goldilocks" have high concentrations of DIC compared to other features in Sylvan (Fig. A.41). DOC concentrations range up to 667.4 µM which is characteristically low for acidic features in Yellowstone. There is a slight correlation in decreasing DOC µM as pH increases (Fig. A.42). Ultimately, DOC is not very high and there are no outliers. The highest point of DOC is taken from a Zygo Mat at "Blondie". This sample could be demonstrating the DOC concentration the Zygo Mat is putting into the fluid.

The DIC $\delta^{13}C$ values have a range from -7.70‰ to 6.67‰ with an outlier at -16.61‰ at "Little Red Head", -22.04‰ at "The Dryer", and another outlier at -37.51‰ at the Dryer. Excluding the outliers, as pH increases, DIC $\delta^{13}C$ values become isotopically enriched (Fig. A.43). This could be due to increased water rock interaction resulting in enriched $\delta^{13}C$ values. This is also demonstrated because samples with high DIC µM have enriched $\delta^{13}C$ values (Fig. A.45). More rock-water interaction could be caused by an increase in time of contact for these hot springs. Therefore, this gives insight into the hydrology at these locations. Samples with $\delta^{13}C$ depleted signatures have very small amounts of DIC concentrations and therefore these samples should be double checked on

another instrument to verify these values are accurate even though they are within the detectable range.

The DOC $\delta^{13}C$ values range from -7.38‰ to -28.47‰ (Fig. A.44) and samples that have more DOC than the average display $\delta^{13}C$ values between -19‰ to -24.5‰ (Fig. A.46). This is slightly $\delta^{13}C$ depleted than other regions with elevated DOC, but DOC concentration still is considerably lower than other regions with elevated DOC. There is one outlier at "Evening Primrose" with an enriched $\delta^{13}C$ isotopic concentration of 7.21‰. This is interesting because "Evening Primrose" in other samples has an isotopic concentration of around -18‰. Therefore, this is most likely due to a sampling mistake or an issue with analyzing this sample.

"The Dryer" is the most unique feature within Sylvan as it frequently changes orders of magnitude in pH throughout this study. Hot springs in Yellowstone National Park vary and change, but no hot springs have varied like "The Dryer" does. "The Dryer is in the middle of Sylvan next to "The Washing Machine", but none of these features vary and change in pH like "The Dryer". Geochemistry changes, yet DIC and DOC do not change drastically at this location throughout the years. The pH at "The Dryer" fluctuates from 4.02 in 2005, to 7.72 in 2010, to 5.13 in 2018. DIC µM and DOC µM concentrations are (17.5, 42.5), (973, 38), and (30, 31.7) respectively (Fig. A.43 & A.44). There are increases in DIC concentration, but DOC throughout the different samples is relatively within error. The DIC $\delta^{13}C$ values change drastically but the DOC $\delta^{13}C$ values are relatively similar within 0.3‰. This therefore gives insight to see that the large differences in this hot spring are not being controlled by biology and that this spring is

being controlled by the deep subsurface. However, as mentioned previously, other features surrounding “The Dryer” do not show similar characteristics. This therefore needs further investigation on how a hot spring can be receiving different changing fluid frequently and other hot springs are not receiving similar changes. If this is being controlled by changes in heat from below in the subsurface, how are these changes not affecting local hot springs in a similar way. Hot springs have been shown to be in proximity with different fluid sources, but it has not been explained how one fluid can change by order of magnitude. This would be due to overall larger system perturbations, and it is interesting how these larger changes only impact one feature. Organisms seem to be able to adapt to these changes within this hot spring as there are not large differences in DOC concentration or $\delta^{13}C$ values of communities shifting to different carbon biogeochemical cycling processes.

Ultimately Sylvan has the most acidic hydrothermal features along with “The Dryer” which is the most pH variable hot spring in this study. Sylvan needs further investigation to understand how this acidic and sulfur dominated hot spring receives hydrothermal fluid from the subsurface. Further investigation with sequencing and transcriptomics is necessary to understand what biogeochemical processes are occurring in each hydrothermal feature. This region does not have many outliers with DIC and DOC concentrations and therefore these hot spring systems may have similar organisms to one another in this area.

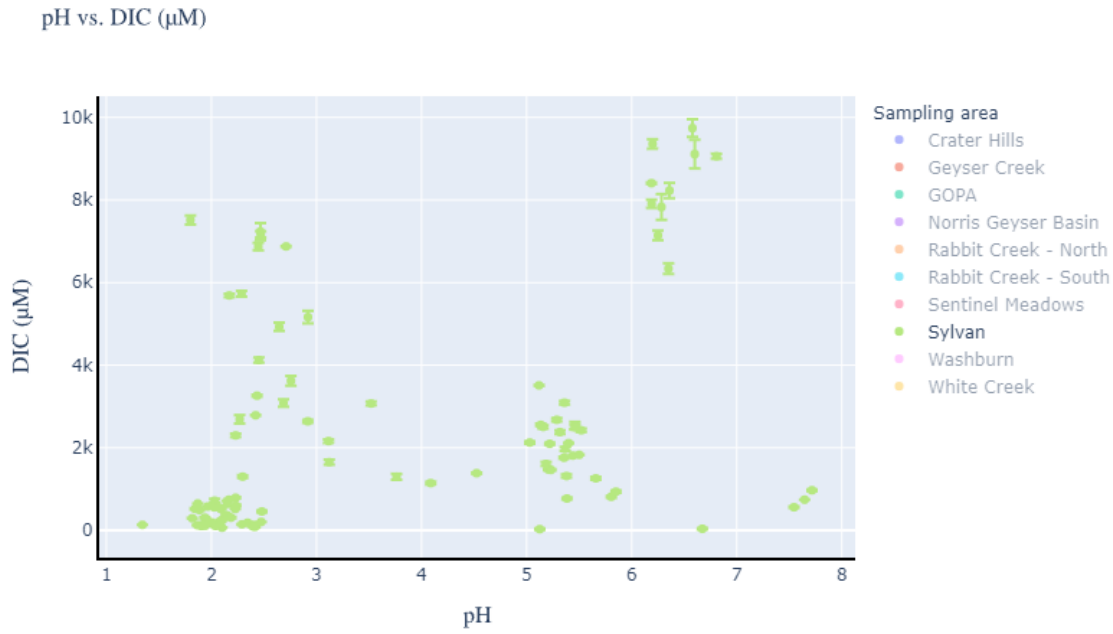

Figure A.41: pH vs. DIC µM for Sylvan

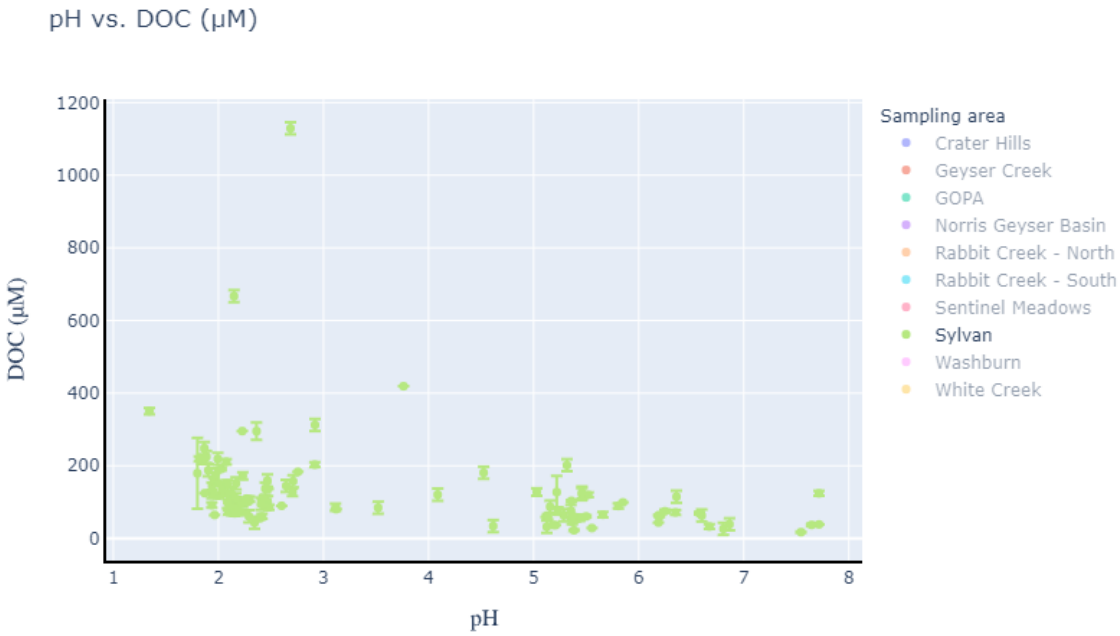

Figure A.42: pH vs. DOC µM for Sylvan

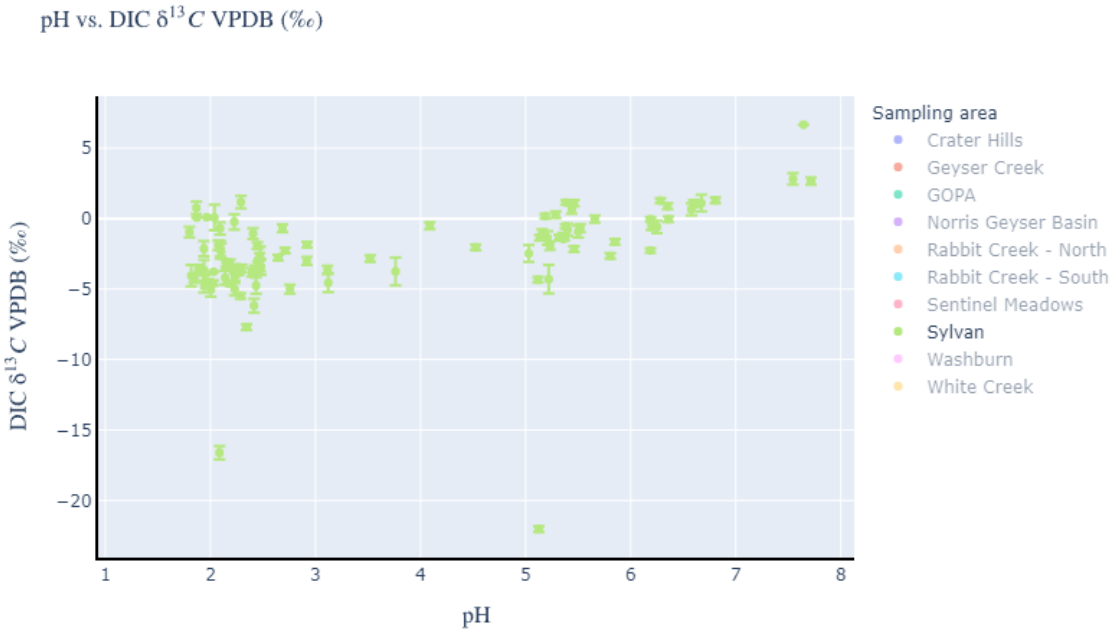

Figure A.43: pH vs. DIC δ^{13}C VPDB (‰) for Sylvan

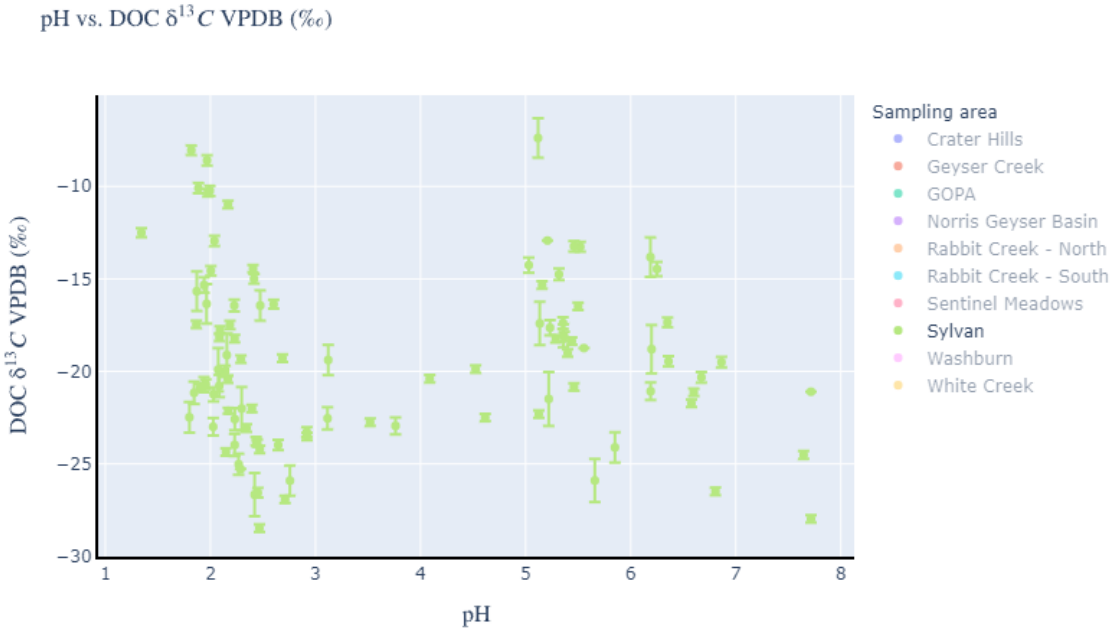

Figure A.44: pH vs. DOC δ^{13}C VPDB (‰) for Sylvan

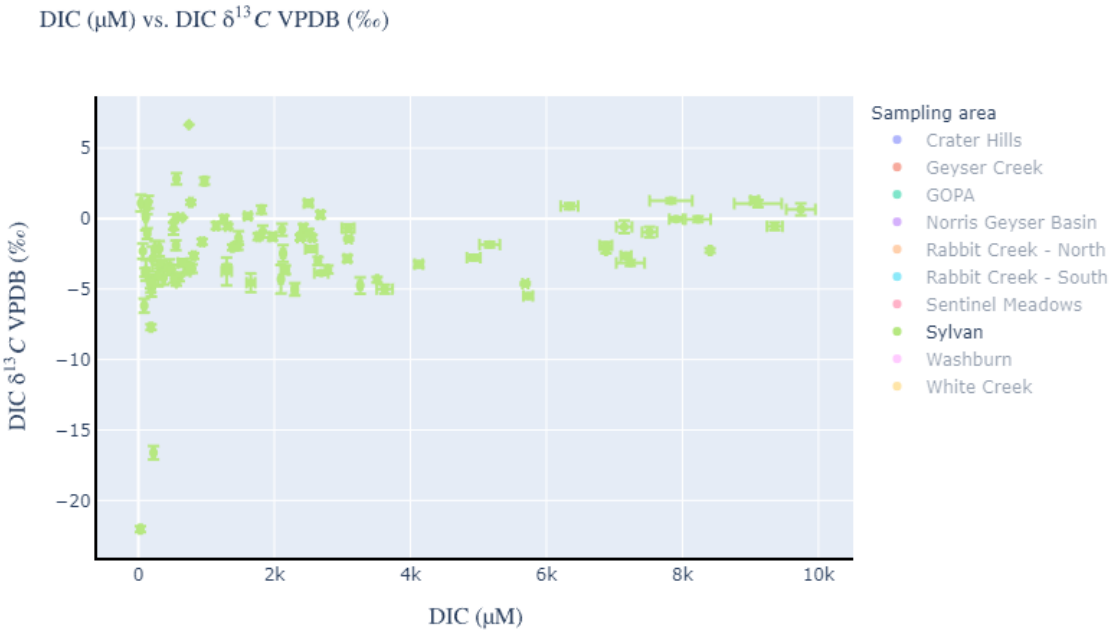

Figure A.45: DIC µM vs. DIC δ^{13}C VPDB (‰) for Sylvan

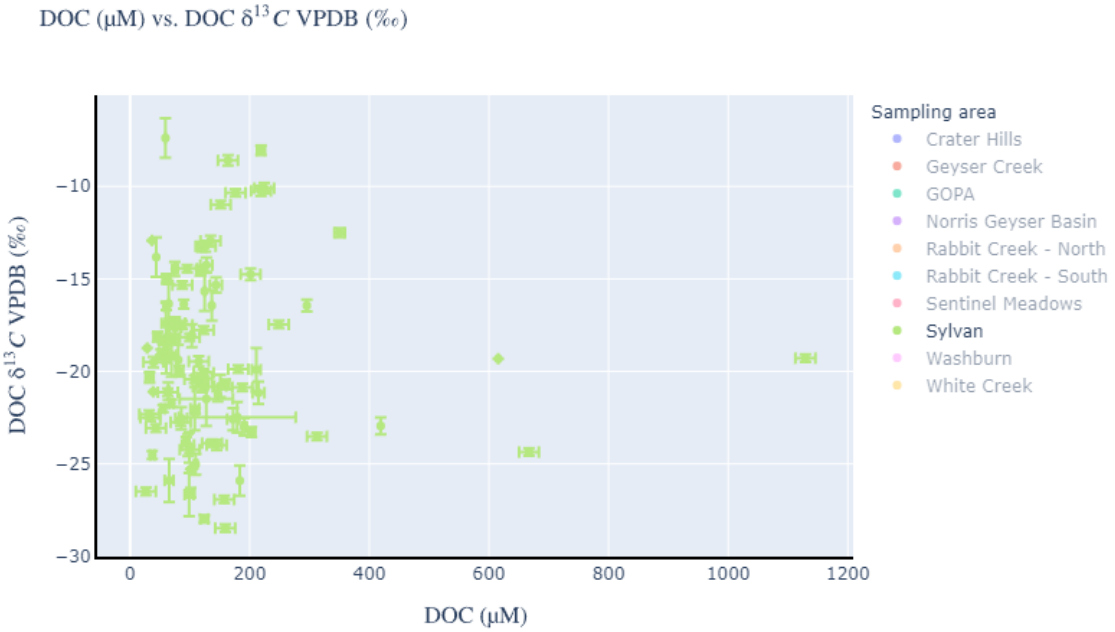

Figure A.46: DOC µM vs. DOC δ^{13}C VPDB (‰) for Sylvan

Washburn

Hydrothermal features in Washburn are unique compared to other regions in this study due to their being the highest concentration of DOC in several hot springs. The pH range in this study recorded at Washburn is 2.26 to 8.26. There is a divide of hot springs less than pH 4 and pH 5 and higher. Hot spring features that are less than pH 4 range up to 1,643 µM DIC whereas features pH 5 and higher range up to 8,083 µM (Fig. A.47). Several of these features are unique because they also have high concentrations of DOC along with DIC. "FLIP", "Mr. Clean", and "Jackson's Tub-O-Luv" all have DOC concentration highs of 3,954, 4,824, and 3,679 µM, respectively. Most samples taken have between 83 and 830 µM DOC (Fig. A.48). Previous regions in this study had many DOC samples below 167 µM, and this is not the case for Washburn. Therefore, a source of organic carbon must be present for these springs to be elevated in DOC. It has been hypothesized that there is ancient sedimentary rock underlying the Washburn hot springs and therefore as erosion occurs, ancient organic carbon would enter the hydrothermal fluid. This area is also classified as "meteoric gas dominant" due to the elevated amount of sulfate and very low chloride. Therefore, a ground water source carrying fresh organic carbon could be the reason these hot springs are displaying this signature.

As mentioned previously, Washburn hot springs are typically broken down into upper and lower regions. Topographically the upper region flows into the lower region. Both areas are on the side of a steep hill. The area is mostly sinter and at the very top of the hill there is a lodgepole pine that could have runoff into the springs. Exogenous carbon does not seem as though it is as much of a factor for these hot springs when

compared to other areas with large amounts of vegetation. Therefore, local exogenous runoff alone cannot be responsible for the elevated levels of DOC.

Hot springs that are steam driven and high in sulfate display this elevated signature of DOC along with a fractionation of boron from chloride. Boron and chloride are typically not fractionated relative to one another by boiling or other geochemical processes and a difference is typically when different fluids combine with one another (Hearn, 1990). Therefore, this is possible evidence that multiple fluids are mixing which then leads to increased levels of DOC.

Another possible explanation and the most likely is the eroding of DOC from sedimentary rock and the transport of DOC. As mentioned earlier, around the Washburn area it is hypothesized that there are ancient sedimentary rocks which would contain an abundance of organic carbon. This would directly increase the levels of organic carbon and impact local biology within the hot spring because overall these hot springs have an abundance of DOC compared to other locations where it may be limiting such as Lower Geyser Basin. This introduction sedimentary rock could be different between the hot springs leading to a mixing of fluid. This mixture of fluid could therefore be causing the fractionation of boron from chloride that is present within the data.

The DIC $\delta^{13}C$ values in Washburn range from -10.16‰ to 5.46‰ (Fig. A.49). There is an outlier at -42.61‰, but the DIC concentration is only 35.83 µM which is near the limit of detection range (Fig. A.51). “Rastaman” also typically has a signature of around -5‰ so this could be instrumental error due to low DIC. It is unclear what causes these depleted $\delta^{13}C$ values at lower detection limits. As samples increase in DIC

concentrations, there are enriched $\delta^{13}C$ values in the samples above 3,333 µM. Enriched $\delta^{13}C$ samples could be due to increased time for water rock reactions in the subsurface.

DOC $\delta^{13}C$ values in Washburn are typically enriched in $\delta^{13}C$ when compared with other regions. The samples range from -26.00‰ to -11.63‰ (Fig. A.50). A majority of this range of samples has $\delta^{13}C$ more enriched than -20‰. This is unique to Washburn and enriched values would display that organisms are not fractionating carbon as much as other areas. Hydrothermal features that have elevated DOC µM have a $\delta^{13}C$ of around -22‰ (Fig. A.52). This is also more enriched than other regions with elevated DOC ppm that typically had around -24‰ to -26‰. Context sampling will be helpful to understand what is causing these springs to have around -22‰ in "Flip", "Mr. Clean", "Jackson's Tub-O-Luv", and "Grayson's Ditch of Joy".

Ultimately, Washburn is a great place to study meteoric gas dominant hot springs that are acidic and sulfate dominant with high concentrations of both DIC and DOC. It is unclear how certain hot springs in this area receive high levels of DOC compared to neighboring hot springs. A handful of hot springs in this area stand out for further research and sequencing within this region would be beneficial to understand if biology plays a big role in the surface or if these signatures are due to ancient sedimentary organic matter. More geochemical interpretations are needed to understand how acidic-sulfate dominant hot springs potentially result in increased amounts of DOC.

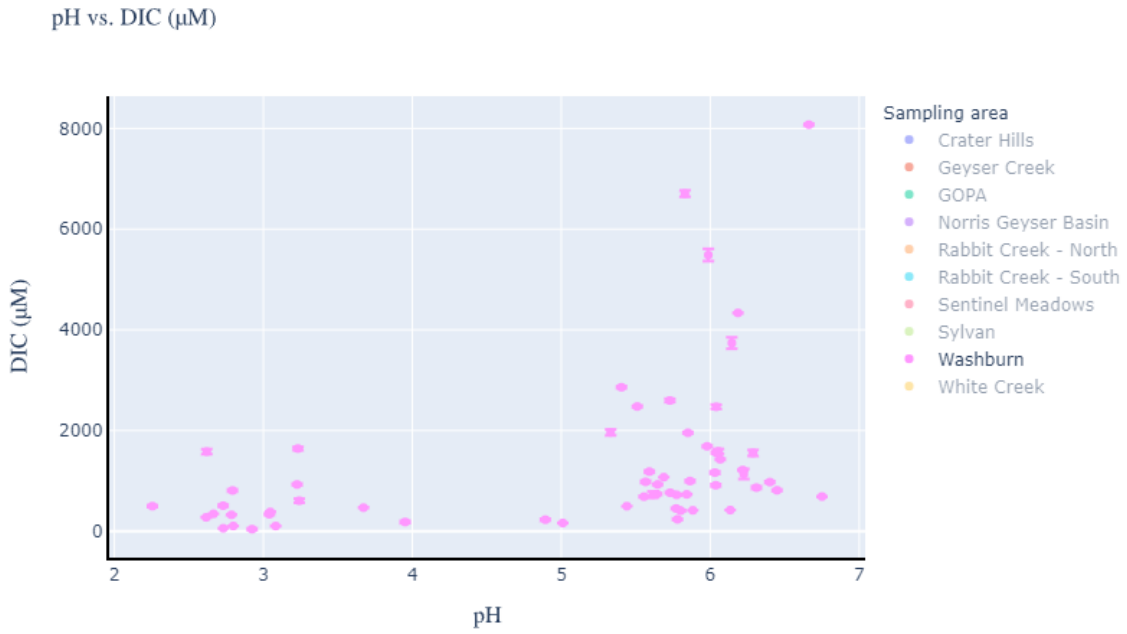

Figure A.47: pH vs. DIC µM for Washburn

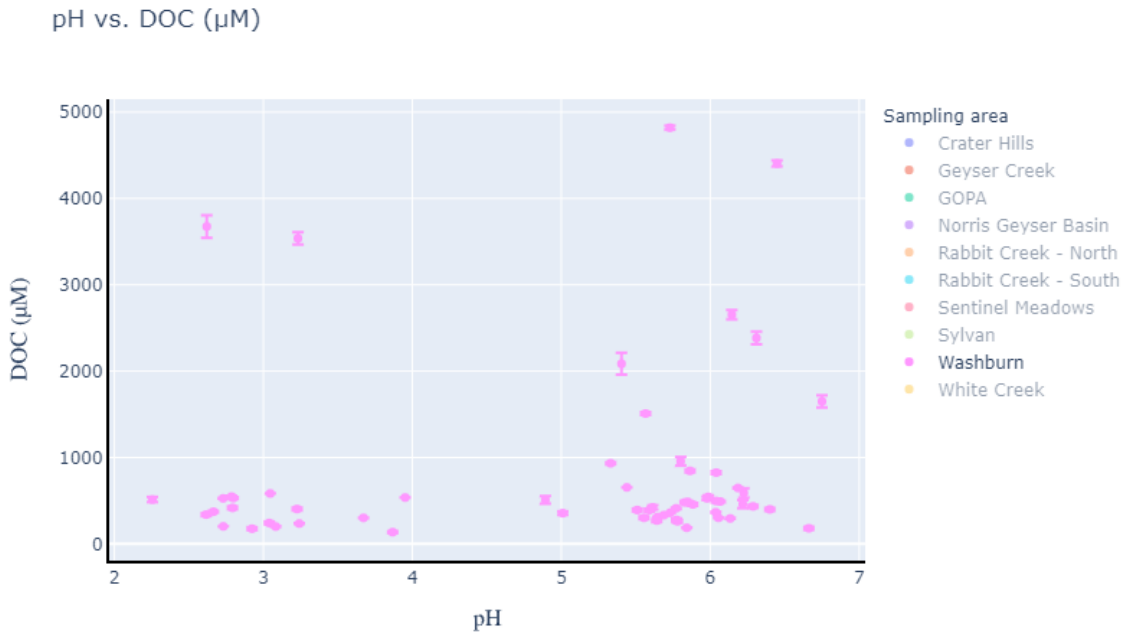

Figure A.48: pH vs. DOC µM for Washburn

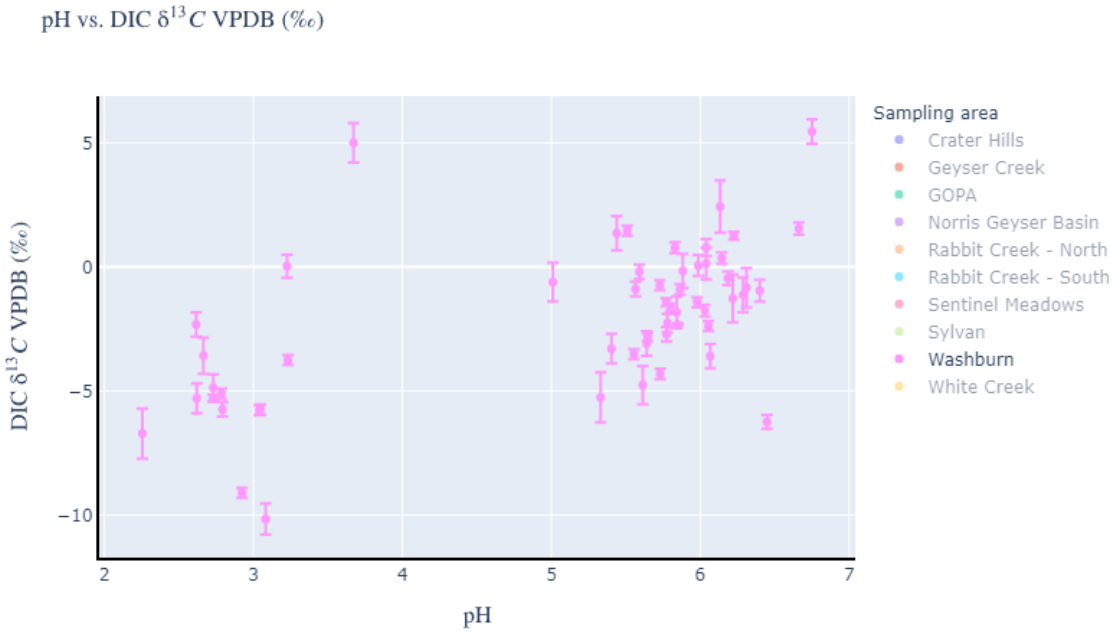

Figure A.49: pH vs. DIC δ^{13}C VPDB (‰) for Washburn

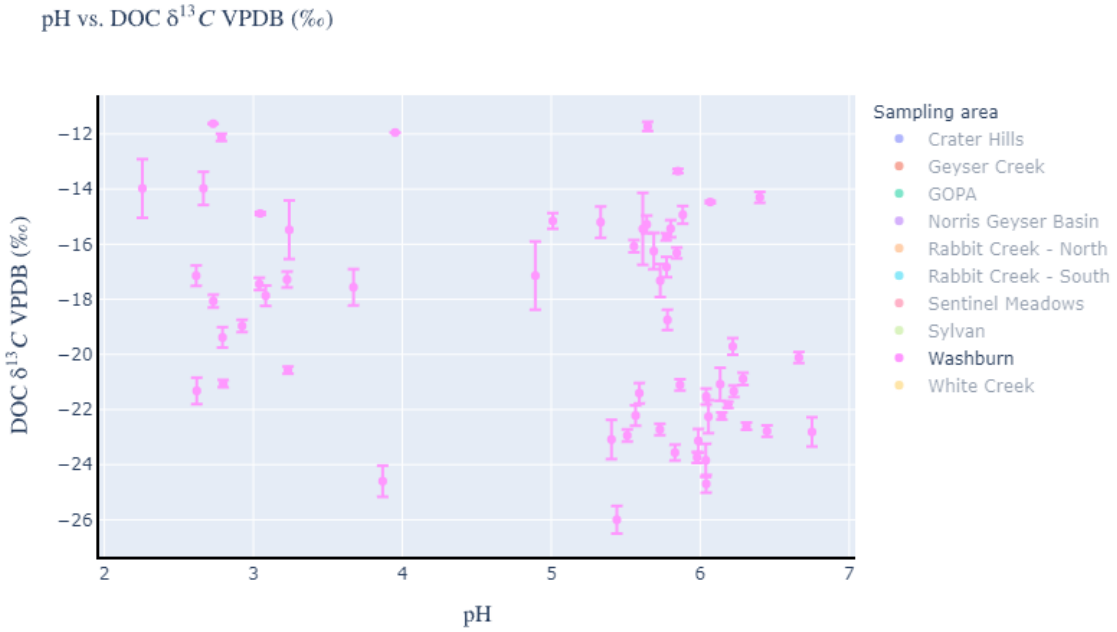

Figure A.50: pH vs. DOC δ^{13}C VPDB (‰) for Washburn

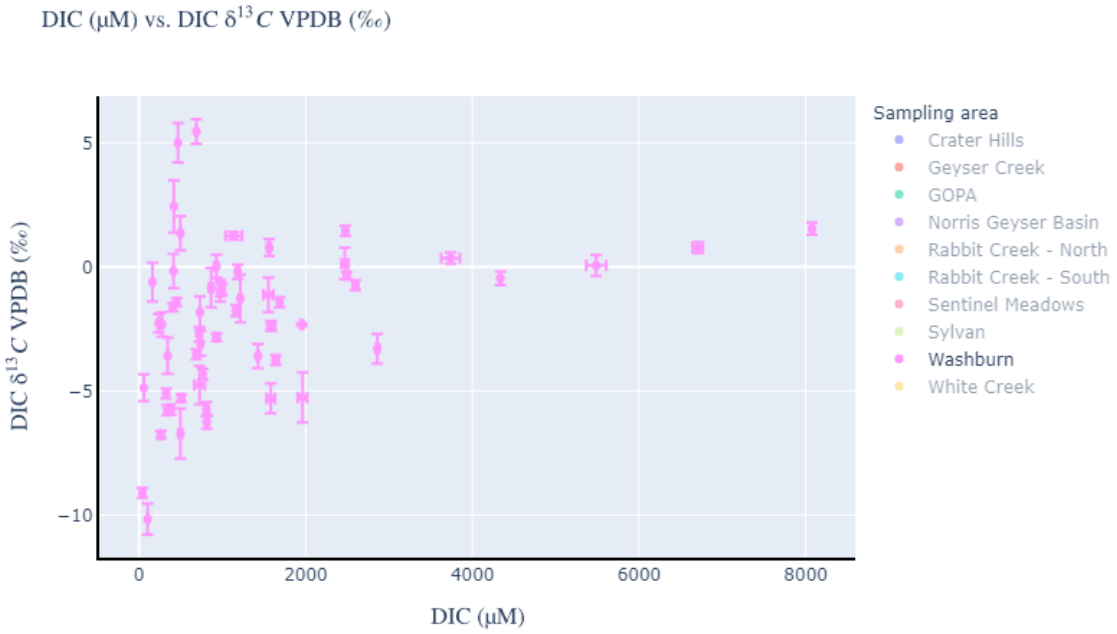

Figure A.51: DIC µM vs. DIC δ^{13}C VPDB (‰) for Washburn

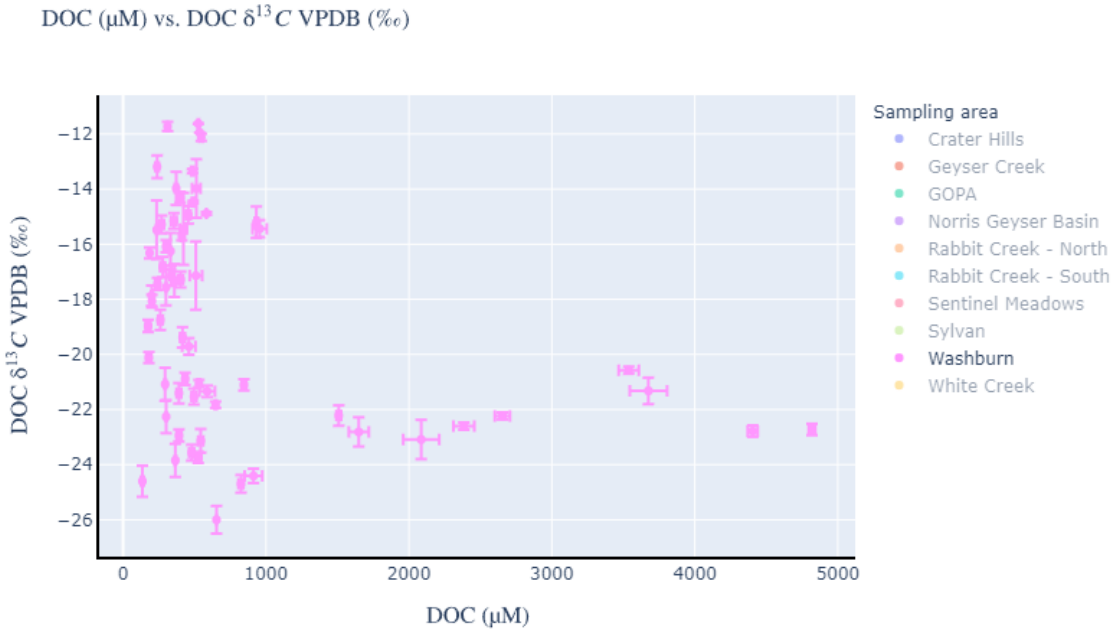

Figure A.52: DOC µM vs. DOC δ^{13}C VPDB (‰) for Washburn

White Creek

Hydrothermal features in White Creek range from pH 6.17 to 8.73 in this study with a range of DIC ppm up to 5,871 µM. White Creek is unique from previous regions because the lowest value of DIC is 1,882 µM (Fig. A.53). Therefore, there is a higher average of DIC in this region than other regions and no hot springs have low values of DIC. White Creek is also unique due to the very small pH range of just over two orders of magnitude. Other regions in this study had changes in magnitude that were greater than this region. The hot springs in White Creek are typically high in chloride and low in sulfate. These values are very similar to Sentinel Meadows which is in close proximity and these hot springs are identified as "deep hydrothermal features" according to the USGS. There is a correlation between increasing pH and lower concentrations of DIC in Figure A.53. These clusters of hot springs displaying this trend are all near the road at the bottom of the valley. The data points that are spread out and less than 4,166 µM in Figure A.53 are features near the top of the valley. This divide in location within White Creek does not seem to affect the pH differing between the top versus the bottom of the valley, but it seems to impact the overall concentration of DIC in these hot springs.

DOC ppm is very low throughout White Creek with a region high of 295 µM. These samples are typically under 83 µM with a few samples above 167 µM at "Octopus Spring". These values seem to have no correlation with pH (Fig. A.54). It is surprising to see low levels of DOC in this region because these hot springs are at the base of local topographic hills covered in vegetation. It is common to see logs and various vegetation floating in these hot springs when samples are taken. These hot springs seem like they

would be perfect candidates to observe weather effects, but the data displays it is not that simple due to these low values. There are very few weather samples taken, but the data displays small increases in DOC concentration. However, since the value is originally low, small increases create big percentage changes. Therefore, life in these springs may respond differently to large percentage changes if these organisms are specific. The organism, however, could not be affected by a change of 83 µM DOC and this needs to be further studied. Future work could consist of culturing microbes from various hot springs in White Creek and feeding them different amounts of DOC while observing growth. This is one to investigate how weather affects organisms in each region.

DIC $\delta^{13}C$ values range from -3.79‰ to 4.04‰ and there is a slight correlation with depleted $\delta^{13}C$ isotopic values as pH increases (Fig. A.55). The hot springs at the top of the valley all have $\delta^{13}C$ more enriched than 0‰, whereas the lower part of the valley near the road has $\delta^{13}C$ more depleted than 0‰. “Spent Kleenex” is right along the 0‰ mark (Fig. A.57). Hot springs with multiple samples taken across different years show very little variation in $\delta^{13}C$ values. Due to the deep hydrothermal signature these hot springs seem to be very consistent. This lines up with the theory that these hot springs are not receiving young meteoric water that is variable and are receiving very old water that has undergone boiling in the deep subsurface. Therefore, by investigating the changes in variance of DIC µM and $\delta^{13}C$ signature, processes the hydrothermal water has undergone can be predicted.

Similar findings occur with DOC $\delta^{13}C$ values. The range is -19.98‰ to -27.60‰. Most of the values tend to cluster around -24‰ to -27‰ (Fig. A.56). There is a very narrow range in White Creek of $\delta^{13}C$ values compared to other regions. These signatures overall are typically more depleted in $\delta^{13}C$ than other regions as well. There is little variance in $\delta^{13}C$ values which could be attributable to lower concentrations of DOC (Fig. A.58). The low value could be driven by biology within these hot springs and further context sampling needs to be done in this region to determine the source of DOC. More weather sampling in the future would be beneficial to determine if there are large fluctuations in DOC as predicted by local topography. DOC $\delta^{13}C$ in White Creek similar to most of the park are independent of pH values.

Ultimately, White Creek serves as an end member of hot springs influenced by deep hydrothermal fluids that have undergone boiling within the deep subsurface. These springs have increased amounts of DIC with low amounts of DOC. White Creek is very similar to Sentinel Meadows geochemically as well as DIC and DOC data, yet the local setting is very different between these two locations. Therefore, more investigation is needed on local topography influencing hot springs. Due to the very low variance within the hot springs in White Creek, it therefore shows that hot springs that display this low variance could be deeply sourced, and the hydrothermal fluid has undergone boiling or additional processes. White Creek shows a system that is combined with thermal alteration and overland delivery leading to a competition of autotrophy and heterotrophy in these hot springs.

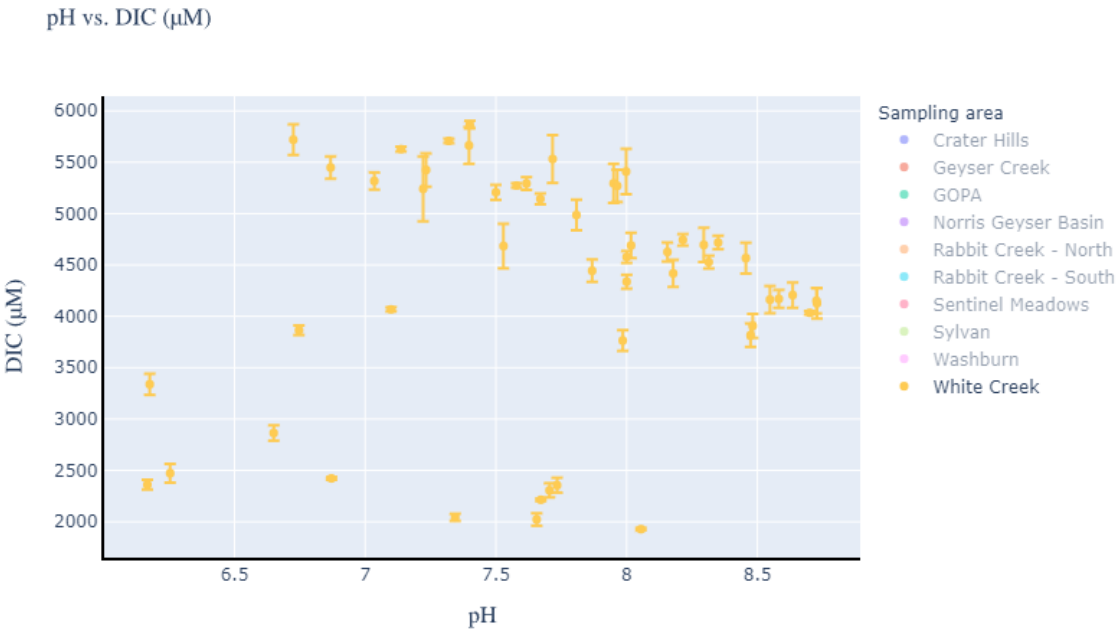

Figure A.53: pH vs. DIC µM for White Creek

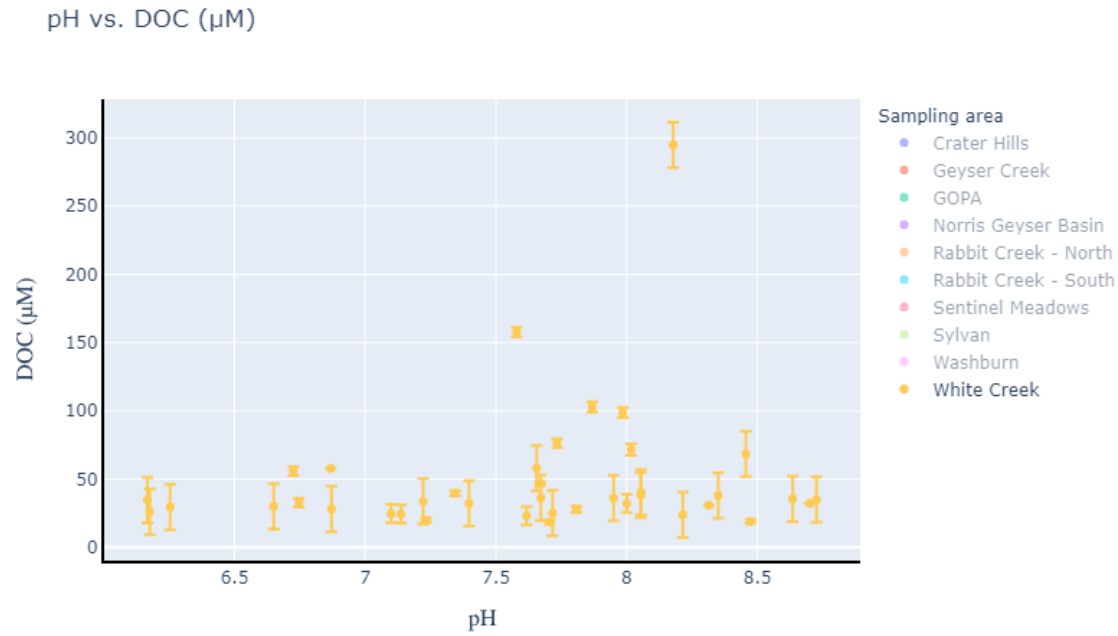

Figure A.54: pH vs. DOC µM for White Creek

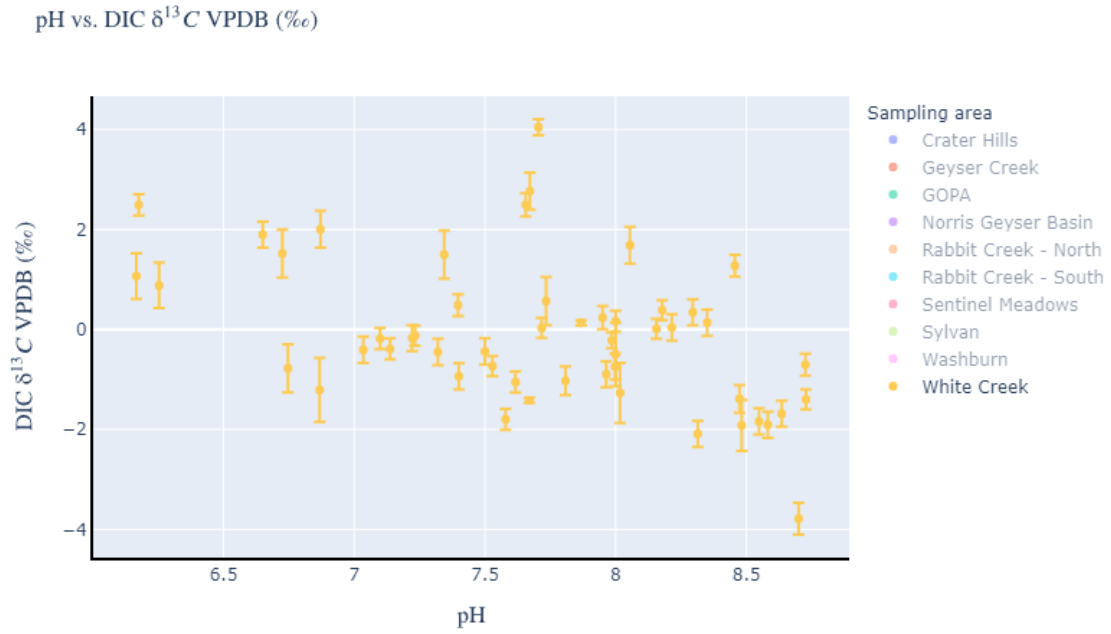

Figure A.55: pH vs. DIC δ^{13}C VPDB (‰) for White Creek

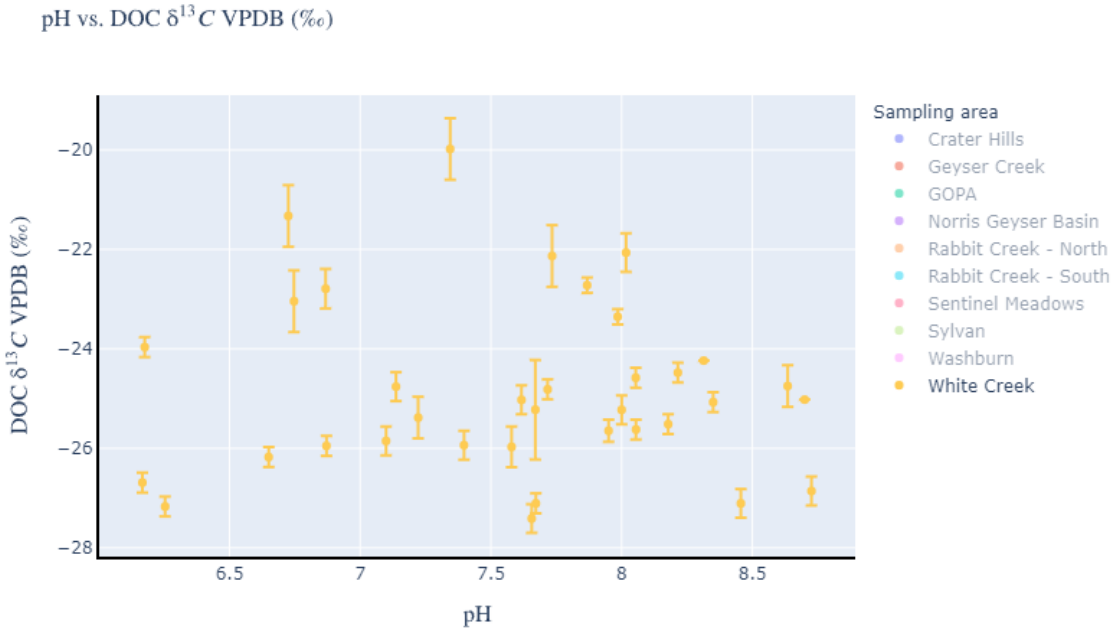

Figure A.56: pH vs. DOC δ^{13}C VPDB (‰) for White Creek

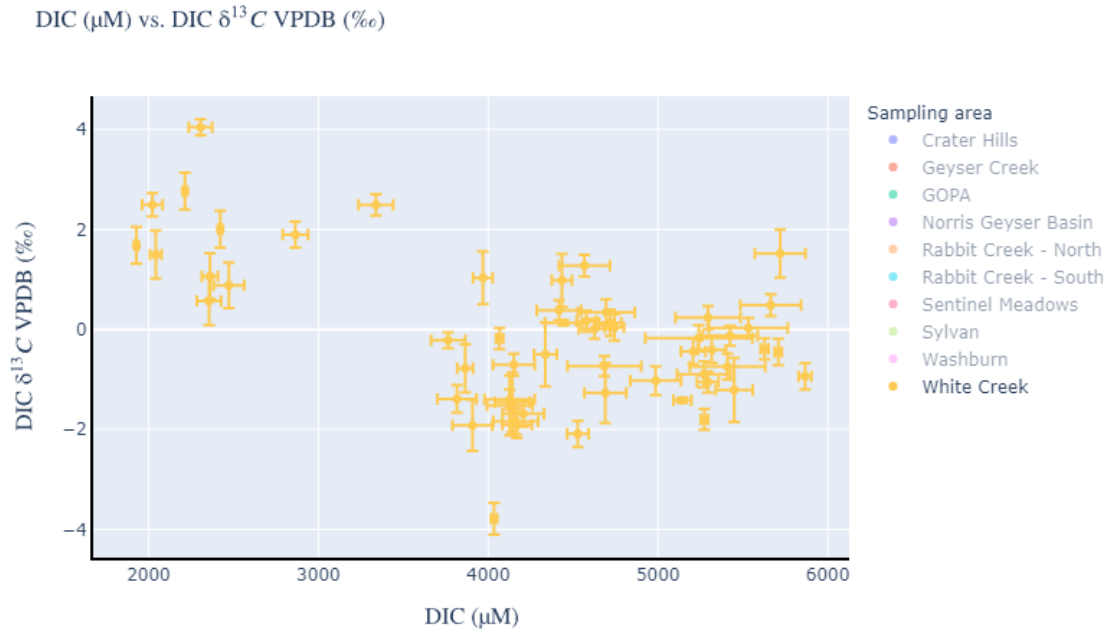

Figure A.57: DIC µM vs. DIC δ^{13}C VPDB (‰) for White Creek

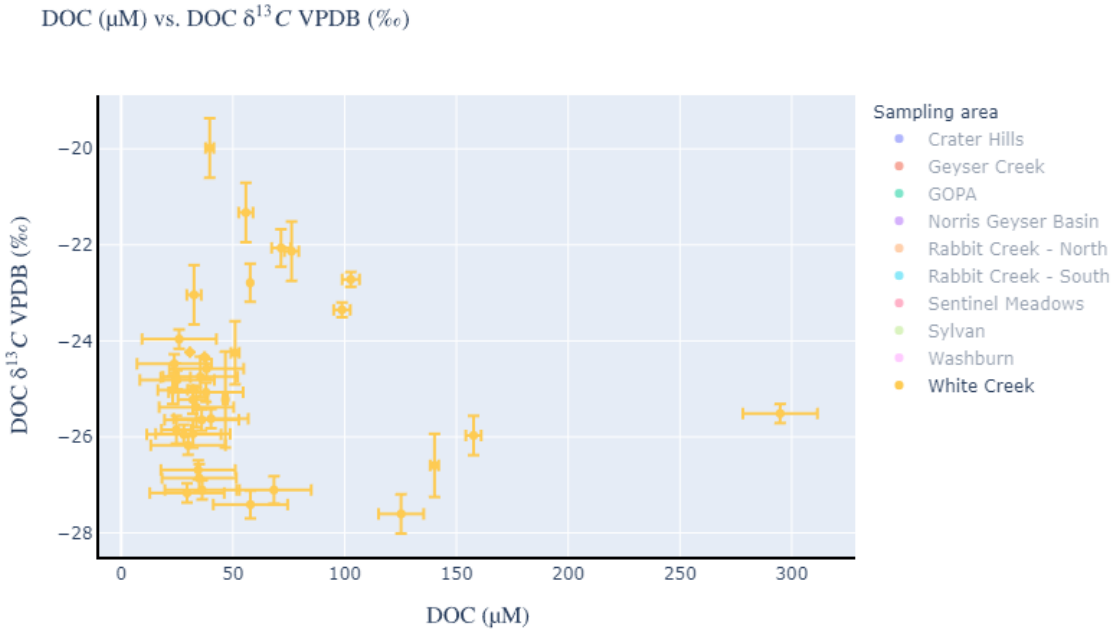

Figure A.58: DOC µM vs. DOC δ^{13}C VPDB (‰) for White Creek

REFERENCES

Allen, E. T. and Day, A. L. (1935); Hot springs of the Yellowstone National Park. Carnegie Institution of Washington Publication 466, Carnegie Institute, Washington D. C., USA.

Bergfeld, D., Lowenstern, J. B., Hunt, A. G., Shanks, W. C. P., and Evans, W. C. (2014); Gas and isotope chemistry of thermal features in Yellowstone National Park, Wyoming. Scientific Investigations Report 2011-5012, United States Geological Survey, doi:10.3133/sir20115012.

Fournier, R. O. (1989); Geochemistry and dynamics of the Yellowstone National Park hydrothermal system. Annual Review of Earth and Planetary Sciences 17(1), pp. 13–53, doi:10.1146/annurev.ea.17.050189.000305.

Gardner, W. P., Susong, D. D., Solomon, D. K., and Heasler, H. P. (2011); A multitracer approach for characterizing interactions between shallow groundwater and the hydrothermal system in the Norris Geyser Basin area, Yellowstone National Park. Geochemistry, Geophysics, Geosystems 12(8), doi:10.1029/2010GC003353.

Holloway, J. M., Nordstrom, D. K., Böhlke, J., McCleskey, R. B., and Ball, J. W. (2011); Ammonium in thermal waters of Yellowstone National Park: Processes affecting speciation and isotope fractionation. Geochimica et Cosmochimica Acta 75(16), pp. 4611–4636, doi:10.1016/j.gca.2011.05.036.

Hurwitz, S. and Lowenstern, J. B. (2014); Dynamics of the Yellowstone hydrothermal system. Reviews of Geophysics 52(3), pp. 375–411, doi:10.1002/2014RG000452.

Love, J. D. and Good, J. M. (1970); Hydrocarbons in thermal areas, northwestern Wyoming. Professional Paper 644-B, United States Geological Survey, doi:10.313 3/pp644b.

Vaughan, R. (2014). Provisional Maps of Thermal Areas in Yellowstone National Park, based on Satellite Thermal Infrared Imaging and Field Observations. U.S. Geological Survey Scientific Investigations Report. 2014–5137. 22 p. 10.3133/sir20145137.

APPENDIX B

HOT SPRING GEOCHEMISTRY

Sample ID	Sample Location	Year	Sampling area	pH	Temp °C	Sp. Cond. * (µS/cm)	Cl^- (ppm)	Cl^- %RSD	SO_4^{-2} (ppm)	SO_4^{-2} %RSD
160720J	Crater Hills Geyser	2016	Crater Hills	3.385	87.2	4723.7	-	-	-	-
180714SN	Crater Hills Geyser Pool	2018	Crater Hills	3.275	78.8	3853.6	-	-	-	-
120715TW	Crater Hills Geyser Source	2012	Crater Hills	3.327	89	5307.0	812.08	0.003	515.55	0.007
190719ZF	Crater Hills Geyser (Small pool for gas and bio)	2019	Crater Hills	3.23	52.5	4122.6	-	-	-	-
160720I	Jabberwocky	2016	Crater Hills	2.096	73.1	3470.9	-	-	-	-
120713SK	Rabbit Hole	2012	Crater Hills	3.64	61.2	4808.6	-	-	-	-
100801YA	Rabbit Hole	2010	Crater Hills	3.228	49	4006.8	977.00	0.000	600.40	0.000
190719ZH	Cynadium Falls	2019	Crater Hills	2.03	57.4	4551.0	-	-	-	-
180714SM	Delilah	2018	Crater Hills	2.09	87.6	4143.0	-	-	-	-
120713SJ	Jabberwocky	2012	Crater Hills	2.147	69.9	3967.3	2.03	0.262	1384.46	0.008
090728PA	Crumpet Spring	2009	Crater Hills	2.907	71.6	3970.0	764.10	0.000	670.42	0.001
140729SG	Jabberwocky	2014	Crater Hills	2.51	91.7	697.1	4.13	0.157	1154.60	0.543
160720H	Alice	2016	Crater Hills	2.057	76.1	3095.9	-	-	-	-
190719ZG	Alice	2019	Crater Hills	2.28	74.8	1530.6	-	-	-	-
140729SB	Alice	2014	Crater Hills	2.2	78.1	2696.4	1.31	0.194	976.19	0.020
120713SH	Alice	2012	Crater Hills	2.16	79.3	2785.2	1.28	0.446	998.99	0.109
110713D	Alice	2011	Crater Hills	2.078	79.5	2641.1	0.89	0.407	889.00	0.368
180714SL	Alice	2018	Crater Hills	2.245	81.3	2436.5	-	-	-	-
170724TD	Cyanidium Falls	2017	Crater Hills	1.892	44.5	5964.0	1.66	0.002	1686.08	0.106
190719ZI	Rabbit Hole	2019	Crater Hills	2.24	83.4	1909.6	-	-	-	-
090728QA	Caterpillar	2009	Crater Hills	1.92	82.4	3631.3	1.22	0.066	1151.12	0.014
180714SO	Frabjousday	2018	Crater Hills	1.926	64.5	5016.8	-	-	-	-
160720K	Rabbit Hole	2016	Crater Hills	1.687	84.2	5952.4	-	-	-	-
170724TA	Rabbit Hole	2017	Crater Hills	1.535	85.8	8799.6	1.86	0.061	2710.34	0.279
090728OA	Alice Spring	2009	Crater Hills	2.085	84.9	1947.2	1.20	0.095	1275.37	0.001
100810R1	Mock Turtle	2010	Crater Hills	1.605	78	10427.2	0.39	0.000	4240.00	0.000
100801AA	Alice	2010	Crater Hills	1.988	81	4292.5	2.93	0.002	2446.00	0.000

Sample ID	Sample Location	Year	Sampling area	pH	Temp °C	Sp. Cond. * (µS/cm)	Cl^- (ppm)	Cl^- %RSD	SO_4^{-2} (ppm)	SO_4^{-2} %RSD
120713SL	Jabberwocky After Rain/Hail	2012	Crater Hills	-	-	-	-	-	-	-
180714SP	White Rabbit	2018	Crater Hills	2.957	46.3	2103.8	-	-	-	-
120715TU	Alice	2012	Crater Hills	2.061	81.6	3710.1	0.94	3.405	1490.26	0.068
170724TE	Crater Hills Geyser Source	2017	Crater Hills	3.464	87.2	4122.1	802.89	0.041	518.37	0.048
090728NA	Crater Hills Geyser	2009	Crater Hills	3.693	90	4008.7	854.19	0.002	487.42	0.002
090728RA	Mockturtle	2009	Crater Hills	1.574	79.9	7488.1	0.37	0.372	3321.61	0.006
160723Z	Corner Thing	2016	Geyser Creek	6.307	85.9	2944.1	-	-	-	-
100804WA	Bull's Eye Pool	2010	Geyser Creek	6.402	91	2525.9	1135.00	0.000	108.10	0.001
190725ZI	Empress Source	2019	Geyser Creek	6.125	81.8	1841.3	-	-	-	-
180722TS	Big Bowl Geyser ("Gucci")	2018	Geyser Creek	6.603	92.3	2693.9	-	-	-	-
160723V	Bat Pool	2016	Geyser Creek	8.365	90.5	3099.6	-	-	-	-
190723VU	St. Blucia	2019	Geyser Creek	2.621	74.5	1836.2	-	-	-	-
150724MB	Alkaline Stream	2015	Geyser Creek	7.815	59.4	2257.1	400.78	0.024	140.27	0.139
120719SS	Corner Thing	2012	Geyser Creek	5.867	86.8	2491.1	543.69	0.221	133.01	0.091
190723VY	Birthday Balloon	2019	Geyser Creek	5.627	77.4	2053.2	-	-	-	-
110714Q	St. Blucia	2011	Geyser Creek	2.381	72.4	1770.0	80.90	0.500	461.17	0.009
100803IA	Empress Pool Source	2010	Geyser Creek	6.085	82.6	1951.2	309.80	0.000	74.30	0.000
120719SX	St. Blucia Source	2012	Geyser Creek	2.341	75.8	1856.6	96.47	0.069	473.34	0.119
180722TN	Bullseye	2018	Geyser Creek	6.685	91	2616.4	-	-	-	-
JRH110714O	Lemon Lick (Yellow Filament site emptying into Empress Pool)	2011	Geyser Creek	5.666	74.6	291.7	1.68	1.525	19.86	0.460
190723VW	Corner Thing	2019	Geyser Creek	6.494	85.8	2432.3	-	-	-	-
190725ZJ	Fallen Angel Hair	2019	Geyser Creek	4.695	66.6	1188.9	-	-	-	-
100804TA	St. Blucia	2010	Geyser Creek	2.186	73.6	1896.6	111.10	0.001	545.47	0.000
120719K2	Bat Pool	2012	Geyser Creek	-	-	-	419.47	0.220	126.90	0.053
190725ZH	Salami Source	2019	Geyser Creek	4.432	76.2	972.8	-	-	-	-
170719SF	Corner Thing	2017	Geyser Creek	6.35	87	2468.8	566.97	0.056	119.90	0.218

Sample ID	Sample Location	Year	Sampling area	pH	Temp °C	Sp. Cond. * (µS/cm)	Cl^- (ppm)	Cl^- %RSD	SO_4^{-2} (ppm)	SO_4^{-2} %RSD
170719SE	St. Blucia	2017	Geyser Creek	2.263	74.9	1969.5	124.18	0.023	476.86	0.021
180713SH	Bat Pool Source	2018	Geyser Creek	8.14	89.5	2502.2	-	-	-	-
180722TO	Boulder Burper	2018	Geyser Creek	6.417	91.8	2354.5	-	-	-	-
160723U	Empress Pool	2016	Geyser Creek	6.032	82.8	1966.6	-	-	-	-
140724SB	Bat Pool	2014	Geyser Creek	8.459	89.2	2508.8	412.92	0.101	124.01	0.729
180722TP	Hot Hot Hot!	2018	Geyser Creek	6.622	92.7	2548.9	-	-	-	-
180722TM	Birthday Balloon	2018	Geyser Creek	5.402	79.4	2226.5	-	-	-	-
170718TZ	Empress Source	2017	Geyser Creek	6.02	81	1980.7	407.94	0.042	115.36	0.025
180713SJ	Man-O-War	2018	Geyser Creek	6.243	74.9	1060.1	-	-	-	-
120719K1	Bat Pool	2012	Geyser Creek	-	-	-	407.76	0.023	123.53	0.122
140729TZ	Empress Source	2014	Geyser Creek	6.09	78.3	1843.2	339.77	0.217	102.08	0.304
170719SH	Left Ventricle	2017	Geyser Creek	2.385	86.7	1615.9	0.81	0.313	486.70	0.127
140724SF	Empress Source	2014	Geyser Creek	6.042	80.2	1621.2	337.47	0.012	101.20	0.021
100804VA	Pig Nose Dipped in Custard	2010	Geyser Creek	2.242	85	1569.5	120.00	0.004	695.90	0.000
180722TQ	Left Ventricle	2018	Geyser Creek	6.319	86.1	1523.9	-	-	-	-
120719SY	Birthday Balloon	2012	Geyser Creek	6.05	85.5	2239.8	489.98	0.017	144.01	0.433
160723X	Spitting Croissant	2016	Geyser Creek	3.905	90	1055.7	-	-	-	-
120719K5	Bat Pool	2012	Geyser Creek	8.457	89.1	2475.9	412.49	0.135	124.18	0.277
180722TT	Compression Slam	2018	Geyser Creek	-	89.4	371.9	-	-	-	-
160723A	Dirty Doughnut	2016	Geyser Creek	6.965	47.2	2144.0	-	-	-	-
180713SF	Lemon Lick	2018	Geyser Creek	6.04	72.6	274.1	-	-	-	-
180722TR	Possible Tourette's	2018	Geyser Creek	6.654	90.9	1768.8	-	-	-	-
110714G	Hot Ice Hole	2011	Geyser Creek	5.96	76.3	747.8	26.30	1.062	108.72	0.045
160723Y	St Blucia	2016	Geyser Creek	2.423	74	1409.1	-	-	-	-
120724SB	Running Paint	2012	Geyser Creek	7.635	60.7	2438.7	416.47	0.195	157.86	0.296
110714E	Empress Pool Source	2011	Geyser Creek	5.82	82	1747.7	-	-	-	-
100804NA	Geyser Creek, alkaline inflow channel	2010	Geyser Creek	7.66	68	2333.3	398.00	0.001	153.00	0.002

Sample ID	Sample Location	Year	Sampling area	pH	Temp °C	Sp. Cond. * (µS/cm)	Cl^- (ppm)	Cl^- %RSD	SO_4^{-2} (ppm)	SO_4^{-2} %RSD
170719SG	Spitting Croissant	2017	Geyser Creek	5.745	86.7	1376.5	191.84	0.132	246.07	0.078
120724SY	Spitting Croissant	2012	Geyser Creek	3.3	88.3	1064.4	71.69	0.068	304.17	0.056
120719ST	Snake City	2012	Geyser Creek	7.45	48.8	2032.5	458.57	0.057	134.45	0.049
110714H	Spitting Croissant	2011	Geyser Creek	5.273	86.2	1169.1	155.20	0.076	238.70	0.053
150723MC	Complete Mix	2015	Geyser Creek	6.666	38.9	1385.0	233.43	0.012	170.05	0.071
140729TC	Salami Outflow	2014	Geyser Creek	3.497	76.1	835.8	94.01	0.033	174.54	0.072
100804ZA	Bubblin' Hat	2010	Geyser Creek	1.973	76.5	2472.9	104.90	0.001	942.00	0.000
190723VX	Spitting Croissant	2019	Geyser Creek	5.195	89.3	1353.9	-	-	-	-
110714I	Dirty Donut	2011	Geyser Creek	5.651	77.7	1876.8	-	-	-	-
110714J	Doily	2011	Geyser Creek	4.08	61.2	0.0	350.10	0.113	197.30	0.165
140729TY	Spitting Croissant	2014	Geyser Creek	4.665	85.6	1001.4	76.22	0.034	265.10	0.005
100804UA	Spitting Croisant	2010	Geyser Creek	4.93	88.2	1020.3	66.90	0.001	205.20	0.001
100804RA	Hot Icehole	2010	Geyser Creek	6.375	78.7	769.5	7.40	0.043	185.90	0.000
160723JN7	Geyser Creek	2016	Geyser Creek	7.879	26.1	775.0	-	-	-	-
120724SZ	Wild Paint Mix	2012	Geyser Creek	6.531	45.6	1466.0	185.25	0.040	173.13	0.050
100804MA	Geyser Creek, above alkaline inflow	2010	Geyser Creek	2.964	33	841.4	18.02	0.001	226.50	0.001
150724MA	Acidic Stream	2015	Geyser Creek	3.074	34.7	632.3	11.58	0.205	198.30	0.014
120724SA	Mr. Toad's Wild Ride	2012	Geyser Creek	3.278	35.9	614.1	11.66	0.049	183.79	0.057
150723MCAR	Complete Mix After Rain	2015	Geyser Creek	5.834	35.7	1124.4	176.93	0.117	235.15	0.025
140729TD	Spitting Croissant AR (after rain)	2014	Geyser Creek	4.025	84.5	1142.5	80.37	0.019	326.66	0.006
140729TE	Spitting Croissant AR2	2014	Geyser Creek	-	-	-	79.15	0.313	363.90	0.001
170719SI	Jackhammer	2017	Geyser Creek	2.31	89.6	3512.2	269.73	0.061	1142.71	0.176
190723VZ	Boiling Sombrero	2019	Geyser Creek	2.053	80.2	949.1	-	-	-	-
190723VV	Jackhammer	2019	Geyser Creek	1.988	88	4031.0	-	-	-	-
180713SI	The Monster	2018	Geyser Creek	1.98	89.9	2611.0	-	-	-	-
170718TA	Bone Pool	2017	Geyser Creek	6.719	76.8	2696.5	628.73	0.036	102.89	0.078

Sample ID	Sample Location	Year	Sampling area	pH	Temp °C	Sp. Cond. * (µS/cm)	Cl^- (ppm)	Cl^- %RSD	SO_4^{-2} (ppm)	SO_4^{-2} %RSD
110714P	Corner Thing	2011	Geyser Creek	6.114	85.6	2495.5	470.70	0.141	109.02	0.078
110714F	Bat Pool Source	2011	Geyser Creek	7.918	91.1	2467.7	384.20	0.050	125.60	0.302
160724C	Figure 8	2016	GOPA	3.482	67.4	2388.0	-	-	-	-
150727U	Happy Harfter + Fig 8 Mix	2015	GOPA	4.53	42	1899.3	365.29	0.070	305.94	0.058
170713TB	Figure 8 Source	2017	GOPA	3.507	61.7	2432.5	397.69	0.073	390.93	0.072
160724E	Happy Harfer	2016	GOPA	5.466	61.3	1688.9	-	-	-	-
160724F	Phantom Pants	2016	GOPA	4.815	84	577.5	-	-	-	-
100807ZA	Happy Harfer	2010	GOPA	5.499	54.7	1750.9	324.50	0.001	247.75	0.000
050718R	Spotted Grizzly Pool	2005	GOPA	2.487	31.1	1277.2	29.29	0.056	370.01	0.041
120712TA	Figure 8 Source	2012	GOPA	4.653	64.3	2316.9	473.37	0.218	299.76	0.239
130716DC	Figure 8 Source	2013	GOPA	3.786	62	2448.3	-	-	-	-
060810 XIII	Happy Harfer Pool, East Side	2006	GOPA	5.5	59.9	1375.1	270.07	0.027	253.90	0.201
050718W	HH Runoff Orange Mat	2005	GOPA	6.28	48.3	1605.0	302.78	0.062	259.69	0.091
050718V	HH East Pool Edge	2005	GOPA	5.449	57.7	1495.2	298.72	0.165	255.78	0.210
050717E	Figure 8 Source	2005	GOPA	4.676	66.6	2031.7	390.22	0.033	342.34	0.038
190728ZT	Happy Harfer	2019	GOPA	4.952	63.5	1711.9	-	-	-	-
150720I	Figure 8	2015	GOPA	3.514	67	2369.6	407.19	0.004	362.07	0.053
190724ZE	OB1 Heim	2019	GOPA	5.567	76.4	1729.3	-	-	-	-
090802U1	Happy Harfer Source	2009	GOPA	5.15	65.8	1393.2	308.86	0.002	264.09	0.002
170713TC	Happy Harfer	2017	GOPA	5.448	62.4	1799.2	288.77	0.044	223.02	0.213
180719SI	Figure 8 Source	2018	GOPA	3.654	66.8	2282.1	-	-	-	-
060804D	Skippy's Bathtub Source	2006	GOPA	4.775	56.7	1707.5	279.22	0.056	270.79	0.056
170713TD	OB1-Heim	2017	GOPA	5.48	78.9	1751.7	277.42	0.134	220.20	0.075
090725ZA	Happy Harfer Source	2009	GOPA	5.173	67.9	1770.7	312.60	0.001	268.51	0.011
170714SJ	Skippy's Bathtub Source	2017	GOPA	5.863	70.9	1780.5	281.72	0.019	226.49	0.045
170714SK	Fudge Factory	2017	GOPA	5.825	74.6	1787.1	279.73	0.007	222.05	0.142
180719SM	Happy Harfer	2018	GOPA	5.538	71.2	1694.4	-	-	-	-

Sample ID	Sample Location	Year	Sampling area	pH	Temp °C	Sp. Cond. * (µS/cm)	Cl^- (ppm)	Cl^- %RSD	SO_4^{-2} (ppm)	SO_4^{-2} %RSD
050717D	Skippy's Bathtub Source	2005	GOPA	4.818	58.9	1621.6	297.74	0.094	265.94	0.092
140725TI	Fudge Factory	2014	GOPA	5.364	74	1227.3	305.04	0.056	216.23	0.003
190728ZQ	Spotted Grizzly	2019	GOPA	3.345	32.6	709.2	-	-	-	-
090723D	Dreamcicle	2009	GOPA	1.947	74.5	2708.5	7.58	0.039	938.16	0.003
160714E	Phantom Pants	2016	GOPA	3.609	89.9	274.2	-	-	-	-
130716SG	Fudge Factory	2013	GOPA	5.68	78.9	1799.8	-	-	-	-
090802B1	Orpheus-in-a-bucket	2009	GOPA	2.485	76.7	744.8	24.35	0.008	409.47	0.002
150720K	Cuppa Muck	2015	GOPA	-	-	-	-	-	-	-
160724G	Green Cheese	2016	GOPA	6.207	69.5	654.5	-	-	-	-
050718U	OP Black Mat	2005	GOPA	4.456	55.9	698.4	120.10	0.109	221.08	0.003
110713S	Figure 8 Source	2011	GOPA	3.892	63	2301.1	467.80	0.068	355.20	0.224
090802V1	Fudge Factory	2009	GOPA	4.65	79	1121.6	219.23	0.002	262.88	0.001
190728ZR	Green Cheese	2019	GOPA	6.01	68.8	425.4	-	-	-	-
050718S	Obsidian Pool	2005	GOPA	4.666	76.4	510.8	27.68	0.266	183.89	0.026
090723E	Spear's Latrine	2009	GOPA	2.596	25.5	2007.9	21.45	0.004	702.15	0.001
050718T	Green Cheese	2005	GOPA	6.166	64.5	380.4	44.80	0.098	61.55	1.104
090725CA	Fudge Factory	2009	GOPA	4.408	84.1	1378.1	277.84	0.001	288.87	0.004
140726SN	Green Cheese	2014	GOPA	6.48	65.9	698.0	69.70	0.103	43.70	0.098
090723C	Skippy's Bathtub Source	2009	GOPA	4.841	68.1	1560.2	298.30	0.001	263.74	0.004
090723J	Green Cheese	2009	GOPA	6.151	62.8	611.6	44.73	0.006	41.42	0.007
150727X	Pedro's Tarpit	2015	GOPA	3.66	64	616.9	-	-	-	-
090723F	Figure 8 Pool	2009	GOPA	4.21	68.3	2221.9	394.66	0.007	346.36	0.009
160714C	OB1-Heim	2016	GOPA	4.725	74.4	1519.6	-	-	-	-
100807SA	Skippy's Bathtub	2010	GOPA	5.36	72.6	1009.2	304.70	0.000	247.20	0.001
160714D	Fudge Factory	2016	GOPA	4.63	81	1015.1	-	-	-	-
190724ZD	Skippy's Bathtub	2019	GOPA	4.844	73.8	1661.4	-	-	-	-
170713TE	Spear's Latrine	2017	GOPA	2.174	30.4	3445.8	18.91	0.307	1344.90	0.117

Sample ID	Sample Location	Year	Sampling area	pH	Temp °C	Sp. Cond. * (µS/cm)	Cl^- (ppm)	Cl^- %RSD	SO_4^{-2} (ppm)	SO_4^{-2} %RSD
160714B	Skippy's Bathtub	2016	GOPA	3.985	77.1	1505.4	-	-	-	-
190728ZV	Phantom Pants	2019	GOPA	3.392	75.7	704.1	-	-	-	-
190728ZS	Muddy Pizza	2019	GOPA	2.41	62.9	1971.0	-	-	-	-
090725XA	South Obsidian Pool	2009	GOPA	5.449	79.6	315.0	31.75	0.001	201.88	0.001
190724ZB	Figure 8	2019	GOPA	5.105	65.6	2193.7	-	-	-	-
150720J	Obsidian Pool	2015	GOPA	5.791	78.9	670.8	35.77	0.251	186.54	0.030
180719SL	South Obsidian	2018	GOPA	5.76	72.6	541.0	-	-	-	-
070715T	Green Cheese 57	2007	GOPA	5.695	57.3	616.0	31.16	0.287	157.20	0.204
090802S1	Vomit Pool	2009	GOPA	5.48	65.9	1179.3	121.63	0.006	272.76	0.001
100807XA	Obsidian Pool	2010	GOPA	4.305	73.2	664.0	34.00	0.005	256.20	0.001
090725BA	Vomit Pool	2009	GOPA	5.755	60.5	1140.4	131.68	0.000	294.54	0.010
140725TK	Obsidian Pool	2014	GOPA	5.986	66.8	662.3	38.58	0.086	151.19	0.035
120712TD	Green Cheese	2012	GOPA	6.324	72.5	717.9	81.31	0.152	47.64	0.041
170714SI	Obsidian Pool	2017	GOPA	5.335	75.5	451.2	33.85	0.009	162.57	0.194
JRH110713N	Vomit Pool	2011	GOPA	5.995	50.2	1256.6	113.44	0.040	251.90	0.044
150727T	Fudge Factory (main source)	2015	GOPA	3.904	81.5	419.7	169.52	0.002	248.90	0.055
110713Z	Brittany's Feast	2011	GOPA	3.961	24.3	363.7	4.63	0.796	212.00	0.956
070715R	Obsidian Pool	2007	GOPA	4.395	84.8	252.7	25.20	0.506	195.26	0.928
070715U	Obsidian Pool Black Mat (BITNB)	2007	GOPA	4.275	54.8	411.7	26.53	0.705	192.66	0.455
090723K	Obsidian Pool Black Mat	2009	GOPA	5.38	57.6	563.0	27.83	0.006	156.65	0.002
190724ZA	South Obsidian	2019	GOPA	3.945	76	667.8	-	-	-	-
100807OA	Submarine	2010	GOPA	3.013	80.9	1004.2	19.50	0.003	279.60	0.001
160724D	Obsidian Pool	2016	GOPA	4.3	85.4	398.6	-	-	-	-
110713A	Green Cheese	2011	GOPA	6.41	69.5	648.1	59.00	0.735	31.96	0.137
JRH110713M	Skippy's Bathtub	2011	GOPA	5.072	60.9	1397.0	286.90	0.088	236.50	0.216
140726SS	OB1-Heim	2014	GOPA	2.415	80.2	3208.2	185.60	0.055	1170.79	0.102
160724H	Spotted Grizzly	2016	GOPA	3.638	30.7	646.3	-	-	-	-

Sample ID	Sample Location	Year	Sampling area	pH	Temp °C	Sp. Cond. * (µS/cm)	Cl^- (ppm)	Cl^- %RSD	SO_4^{-2} (ppm)	SO_4^{-2} %RSD
100807WA	Hot Shit Hill	2010	GOPA	2.977	-	-	0.60	0.014	388.50	0.000
100808GCL	Green Cheese	2010	GOPA	6.948	57	41.2	-	-	-	-
110713U	Obsidian Pool	2011	GOPA	5.17	76.4	598.1	26.59	0.135	205.96	0.038
060804E	Obsidian	2006	GOPA	4.18	85.3	-	25.68	0.072	162.52	0.110
090723I	Phantom Pants	2009	GOPA	3.305	82	387.4	29.60	0.011	252.61	0.003
090723G	Obsidian Pool	2009	GOPA	5.18	79.1	474.5	30.71	0.001	203.84	0.009
110713Y	Obsidian Pool Black Mat	2011	GOPA	4.632	61.3	989.6	122.01	0.048	223.20	0.412
190728ZU	Dreamsicle	2019	GOPA	2.596	64.4	1451.9	-	-	-	-
180719SN	Spotted Grizzly	2018	GOPA	4.56	35.8	515.6	-	-	-	-
060804B	Green Cheese	2006	GOPA	5.9	54.9	866.7	49.72	3.103	172.42	0.090
140725TH	Spotted Grizzly	2014	GOPA	4.797	28.2	669.2	46.27	0.074	187.19	0.021
090725AA	Foam Pool	2009	GOPA	5.254	34.4	635.5	60.23	0.002	117.43	0.002
180719SO	Phantom Pants	2018	GOPA	4.66	70.6	502.1	-	-	-	-
JRH110713L	Owl	2011	GOPA	3.825	73.6	380.3	132.68	0.033	195.50	0.333
090802T1	Foam Pool	2009	GOPA	5.214	30.9	630.6	61.94	0.001	114.79	0.000
110713V	Foam Pool	2011	GOPA	5.399	35.5	489.3	37.30	2.413	70.80	0.656
090802Q1	Witch's Brew	2009	GOPA	2.018	47.7	4786.8	146.05	0.001	1845.47	0.000
090725YA	Witch's Brew	2009	GOPA	2.171	51.7	4824.0	99.37	0.003	1968.66	0.001
110713T	Spotted Grizzly	2011	GOPA	4.705	31.4	465.4	24.40	2.666	135.60	0.613
160724JN8	GOPA Pond North	2016	GOPA	6.924	24.1	637.5	-	-	-	-
150717FB	The Gap	2015	Norris Geyser Basin	3.397	68.9	1767.8	-	-	-	-
110910G	Breathe Deep	2011	Norris Geyser Basin	4.614	85.3	2289.2	613.73	0.004	34.70	1.381
150728A	Log Stew	2015	Norris Geyser Basin	4.53	75.3	2340.5	668.53	0.105	27.12	0.832
160719E	Red Bubbler	2016	Norris Geyser Basin	2.924	92.5	1543.8	-	-	-	-
160719D	Perpetual Spouter	2016	Norris Geyser Basin	7.12	82.3	2781.9	-	-	-	-

Sample ID	Sample Location	Year	Sampling area	pH	Temp °C	Sp. Cond. * (µS/cm)	Cl^- (ppm)	Cl^- %RSD	SO_4^{-2} (ppm)	SO_4^{-2} %RSD
180721SV	Perpetual Spouter	2018	Norris Geyser Basin	6.987	82.6	2513.9	-	-	-	-
180721SU	Red Bubbler	2018	Norris Geyser Basin	3.088	92	1627.8	-	-	-	-
150720FH	The Gap	2015	Norris Geyser Basin	3.565	85.5	1674.2	424.56	0.234	79.29	0.063
120718SO	Perpetual Spouter Source	2012	Norris Geyser Basin	6.7	87.9	2745.8	734.86	0.031	44.16	0.187
110719A	Mickey Face	2011	Norris Geyser Basin	4.202	74.1	1968.7	440.20	0.111	169.00	0.368
150724FN	Beowulf	2015	Norris Geyser Basin	2.889	50.3	1457.5	433.72	0.017	133.54	0.039
150724FO	Log Stew	2015	Norris Geyser Basin	4.644	76.6	250.5	-	-	-	-
140804SR	Perpetual Spouter Source	2014	Norris Geyser Basin	7.256	85.8	2761.7	726.89	0.016	44.32	0.008
160719F	The Gap	2016	Norris Geyser Basin	3.538	79.6	1760.0	-	-	-	-
180721SS	Hoku	2018	Norris Geyser Basin	4.105	88	1991.2	-	-	-	-
150728Y	The Gap	2015	Norris Geyser Basin	3.414	84.6	1703.9	-	-	-	-
120714TR	Mickey Face Source	2012	Norris Geyser Basin	4.396	81	2400.9	404.31	0.133	167.99	0.025
120718SQ	Don't Tell Scottie (Scottie Doesn't Know)	2012	Norris Geyser Basin	2.29	83.5	322.6	323.77	0.055	182.93	0.253
150728B	Dragonmail	2015	Norris Geyser Basin	3.845	67.3	1806.6	431.04	0.022	135.38	0.069
180721SR	Grendal	2018	Norris Geyser Basin	3.63	91.9	2061.6	-	-	-	-
150720FI	Ferric Tenticles	2015	Norris Geyser Basin	3.43	66	1082.4	432.40	0.023	92.27	0.012
110910C	Dermatitis	2011	Norris Geyser Basin	3.433	62.9	833.3	149.60	0.141	82.40	0.124
190730VH	The Gap	2019	Norris Geyser Basin	3.73	83.5	1588.9	-	-	-	-
180718SG	Arrow	2018	Norris Geyser Basin	3.841	89.1	2152.1	-	-	-	-
140725FB	Red Bubbler (source)	2014	Norris Geyser Basin	2.83	87	1817.0	318.50	0.017	209.39	0.079
120714TO	Red Bubbler Source	2012	Norris Geyser Basin	2.904	91.7	2459.3	299.12	0.043	214.09	0.052

Sample ID	Sample Location	Year	Sampling area	pH	Temp °C	Sp. Cond. * (µS/cm)	Cl^- (ppm)	Cl^- %RSD	SO_4^{-2} (ppm)	SO_4^{-2} %RSD
170725TN	Perpetual Spouter	2017	Norris Geyser Basin	7.295	85.1	2765.7	666.55	0.055	38.83	0.052
180718SH	Banana Flex	2018	Norris Geyser Basin	3.336	71.5	2007.3	-	-	-	-
110910B	Cream of Wheat	2011	Norris Geyser Basin	4.325	91	1012.9	271.09	0.015	72.93	0.036
110719P	Cinder Pool	2011	Norris Geyser Basin	4.085	84.6	2340.3	585.00	0.334	72.22	0.017
150722FK	Coral Snake	2015	Norris Geyser Basin	3.126	-	5740.0	335.58	0.054	135.34	0.007
120718SP	Di Di Yu	2012	Norris Geyser Basin	4.92	91.8	2461.5	628.32	0.054	47.38	0.013
110910A	Ginger Kid	2011	Norris Geyser Basin	3.94	77.5	958.0	260.69	0.012	69.67	0.044
180721ST	Middle Realgar Spring	2018	Norris Geyser Basin	2.86	45	1689.3	-	-	-	-
100804 E1	Don't Tell Scottie	2010	Norris Geyser Basin	2.9	82.3	1738.1	326.00	0.002	192.00	0.002
120718SK	The Gap Source	2012	Norris Geyser Basin	2.72	85.9	1748.9	400.89	0.237	90.91	0.024
150724FP	Woodchip Beach	2015	Norris Geyser Basin	3.721	60.8	1930.7	590.62	0.245	72.69	0.169
140803FN	The Gap	2014	Norris Geyser Basin	3.504	83.8	1681.5	375.47	0.080	92.72	0.009
160719B	Dragon Spring	2016	Norris Geyser Basin	2.981	77.9	2006.8	-	-	-	-
110719X	Don't Tell Scottie	2011	Norris Geyser Basin	2.817	81.1	1632.4	287.30	0.051	189.30	0.293
150724FM	Eisentintenfisch	2015	Norris Geyser Basin	-	-	-	369.65	0.068	163.60	0.018
110910H	Something Lame	2011	Norris Geyser Basin	3.16	84.9	1421.3	290.50	0.072	178.40	0.236
120718DK	Cinder Pool	2012	Norris Geyser Basin	4.141	85.6	2323.7	641.91	0.418	70.16	0.086
110719W	Red Bubbler	2011	Norris Geyser Basin	2.868	85.5	1675.1	-	-	-	-
150728C	Eisentintenfisch	2015	Norris Geyser Basin	2.86	80.3	1870.8	379.06	0.053	168.35	0.177
160719C	HFS	2016	Norris Geyser Basin	2.732	88.8	1835.7	-	-	-	-
160719A	Eisen Tintinfisch	2016	Norris Geyser Basin	2.885	84.7	2016.4	-	-	-	-

Sample ID	Sample Location	Year	Sampling area	pH	Temp °C	Sp. Cond. * (µS/cm)	Cl^- (ppm)	Cl^- %RSD	SO_4^{-2} (ppm)	SO_4^{-2} %RSD
180721SQ	Eisentintenfisch	2018	Norris Geyser Basin	2.69	83	1879.6	-	-	-	-
130712TM	Don't Tell Scottie	2013	Norris Geyser Basin	2.776	82.2	1609.1	-	-	-	-
120718SM	Darko's Vision	2012	Norris Geyser Basin	2.255	57.2	1412.4	339.36	0.103	193.02	0.198
180718SD	Beowulf	2018	Norris Geyser Basin	2.956	76.2	1977.8	-	-	-	-
130723SY	Beowulf east source	2013	Norris Geyser Basin	2.947	84	2064.7	-	-	-	-
140803FM	Brain	2014	Norris Geyser Basin	3.5	82.2	875.9	433.49	0.041	89.79	0.095
170725TI	Jack Sparrow	2017	Norris Geyser Basin	3.995	72.8	2561.3	670.04	0.035	50.95	0.176
170715SN	HFS	2017	Norris Geyser Basin	2.578	88.6	1188.4	265.58	0.028	233.52	0.010
190730VG	Eisentintenfisch	2019	Norris Geyser Basin	3.07	85.1	1823.3	-	-	-	-
170715SO	Eisen Tintenfisch	2017	Norris Geyser Basin	2.725	86.1	1941.0	360.09	0.019	181.16	0.095
180721SP	HFS	2018	Norris Geyser Basin	2.598	87.4	1653.9	-	-	-	-
150728Z	Woodchip Beach	2015	Norris Geyser Basin	3.451	59	2215.5	588.91	0.130	88.31	0.010
110910E	Coke Fiend	2011	Norris Geyser Basin	3.256	73.4	1343.5	279.99	0.020	110.99	0.030
190730VD	HFS	2019	Norris Geyser Basin	2.66	86.7	1666.1	-	-	-	-
180718SE	Full Cup	2018	Norris Geyser Basin	3.057	73.6	1959.9	-	-	-	-
140803FL	Soggy Crik	2014	Norris Geyser Basin	3.8	38.6	1735.8	442.55	0.028	73.50	0.060
130719DJ	Beowulf East	2013	Norris Geyser Basin	-	-	-	-	-	-	-
130723SX	HFS	2013	Norris Geyser Basin	3.05	89.4	1837.0	-	-	-	-
160719Z	Cinder Pool	2016	Norris Geyser Basin	4.097	88.5	2092.5	-	-	-	-
170715SP	Dragon Spring	2017	Norris Geyser Basin	2.955	76.1	1988.1	401.12	0.023	133.57	0.137
130723SW	Merica	2013	Norris Geyser Basin	3.558	61.4	2117.5	-	-	-	-

Sample ID	Sample Location	Year	Sampling area	pH	Temp °C	Sp. Cond. * (µS/cm)	Cl^- (ppm)	Cl^- %RSD	SO_4^{-2} (ppm)	SO_4^{-2} %RSD
110719Q	Little Cinder Pool	2011	Norris Geyser Basin	2.945	83.2	1698.2	-	-	-	-
190730VE	Something Good	2019	Norris Geyser Basin	3.6	82.6	1757.9	-	-	-	-
190730VF	Comet	2019	Norris Geyser Basin	3.35	71.8	1935.4	-	-	-	-
140727FD	Beowulf E Iron Mat	2014	Norris Geyser Basin	2.916	71.3	2000.5	412.28	0.030	147.40	0.052
170725TJ	Dragon East OF	2017	Norris Geyser Basin	3.011	49.8	2099.6	420.92	0.116	140.55	0.021
170725TK	Dragon East Source	2017	Norris Geyser Basin	3.068	75.1	1963.0	405.73	0.185	134.65	0.327
170715SM	Cinder Pool	2017	Norris Geyser Basin	3.85	89	1886.0	555.77	0.050	97.66	0.033
130719DK	Dragon Tail Red	2013	Norris Geyser Basin	-	-	0.0	-	-	-	-
140727FE	Flamethrower	2014	Norris Geyser Basin	3.268	81.6	863.0	356.19	0.083	141.32	0.032
130719DL	Dragon tail yellow surface	2013	Norris Geyser Basin	-	-	-	-	-	-	-
100803O1	Cinder Pool	2010	Norris Geyser Basin	4.196	88.4	2495.6	786.18	0.000	80.80	0.001
140803FO	HFS after rain	2014	Norris Geyser Basin	2.866	88.5	1683.3	426.63	0.096	341.89	0.057
140803FK	Comet	2014	Norris Geyser Basin	3.373	79.6	1914.4	414.25	0.157	121.36	0.006
130719DI	Dragon Mouth source	2013	Norris Geyser Basin	-	-	-	-	-	-	-
130723SZ	Dragon Spring source	2013	Norris Geyser Basin	3.022	81.7	1940.0	-	-	-	-
140803FI	HFS	2014	Norris Geyser Basin	2.838	89.3	1771.7	279.23	0.196	229.49	0.025
180718SF	Cinder Pool	2018	Norris Geyser Basin	3.96	91.8	2251.7	-	-	-	-
170725TH	Tribble	2017	Norris Geyser Basin	3.385	54.3	1708.7	353.31	0.003	135.26	0.045
140803FJ	Something good	2014	Norris Geyser Basin	3.389	76.8	1227.4	432.34	0.075	120.85	0.031
190730VC	Cinder Pool	2019	Norris Geyser Basin	2.87	83.3	2650.0	-	-	-	-
100804X1	Chili Blow Out	2010	Norris Geyser Basin	2.98	66.8	696.6	230.60	0.001	90.75	0.000

Sample ID	Sample Location	Year	Sampling area	pH	Temp °C	Sp. Cond. * (µS/cm)	Cl^- (ppm)	Cl^- %RSD	SO_4^{-2} (ppm)	SO_4^{-2} %RSD
110910F	Dog Bone	2011	Norris Geyser Basin	3.075	47.1	1366.9	300.96	0.015	144.80	0.088
120714TQ	Tantalus Creek	2012	Norris Geyser Basin	2.852	43.9	2839.6	331.64	0.074	212.31	0.133
140727FF	Eisen Tintenfisch	2014	Norris Geyser Basin	2.88	82.2	2048.5	375.45	0.040	189.01	0.011
140804SV	Mutant Minnie Source	2014	Norris Geyser Basin	3.85	77.5	2112.7	661.56	0.043	84.68	0.131
170725TL	Mickey Face	2017	Norris Geyser Basin	2.625	74.3	1520.1	163.12	0.024	236.60	0.128
120718SL	Dirty Dishwater	2012	Norris Geyser Basin	2.36	43.2	3173.0	618.97	0.197	237.87	0.179
100803U1	Turnadeli (Turnada Alley)	2010	Norris Geyser Basin	2.496	-	-	586.00	0.002	462.00	0.002
110719Y	Perpetual Spouter	2011	Norris Geyser Basin	7.267	87	2825.9	679.00	0.298	38.50	0.297
110719Z	Di Di Yu	2011	Norris Geyser Basin	6.694	84.3	2662.4	613.00	0.479	37.00	0.310
150720FJ	Honey Glazed	2015	Norris Geyser Basin	3.236	45.3	1806.5	454.16	0.046	93.70	0.183
150723M	OG Mat	2015	Rabbit Creek - North	-	-	-	305.72	0.024	18.60	0.063
120718TO	Peekaboo	2012	Rabbit Creek - North	9.035	70.7	2073.1	270.54	0.239	23.67	0.180
JRH110708B	Painful Past (Now with heartbeat action!)	2011	Rabbit Creek - North	2.762	77.1	377.6	20.00	0.000	91.80	0.954
090726R1	Painful Past	2009	Rabbit Creek - North	2.93	85.5	448.4	31.76	0.001	59.09	0.004
090726M1	Old Blue Eyes Left Eye	2009	Rabbit Creek - North	8.825	83.5	1552.1	342.68	0.000	22.32	0.002
090726P1	Hammer Source	2009	Rabbit Creek - North	8.91	91.3	1978.9	355.07	0.000	15.97	0.008
150723L	Rabbit Creek Pink Mat	2015	Rabbit Creek - North	-	-	-	292.89	0.020	18.05	0.117
150723N	Green Filaments	2015	Rabbit Creek - North	-	-	-	299.01	0.027	19.33	0.423
120718TM	Tarantula Surface	2012	Rabbit Creek - North	8.731	91.7	2215.1	265.32	0.064	20.97	0.265
090726S1	Nefarious Now	2009	Rabbit Creek - North	3.683	80.3	286.3	62.28	0.000	53.06	0.000
BSC110720C	Old Blue Eyes (Right Eye)	2011	Rabbit Creek - North	8.788	85.6	1623.0	-	-	-	-

Sample ID	Sample Location	Year	Sampling area	pH	Temp °C	Sp. Cond. * (µS/cm)	Cl^- (ppm)	Cl^- %RSD	SO_4^{-2} (ppm)	SO_4^{-2} %RSD
JRH110708A	Rose Terrace Pool	2011	Rabbit Creek - North	8.012	93.1	1486.0	-	-	-	-
130713TO	Tarantula	2013	Rabbit Creek - North	8.669	91	1778.0	-	-	-	-
190727ZL	Rabbit Source	2019	Rabbit Creek - North	8.935	85	1977.3	-	-	-	-
120718TK	Rum Runner	2012	Rabbit Creek - North	3.897	53.3	180.8	0.38	0.682	38.48	0.262
170713SC	Peekaboo Source	2017	Rabbit Creek - North	8.665	74.7	1628.4	255.07	0.009	25.41	0.056
170713SF	The Hammer (Head)	2017	Rabbit Creek - North	8.65	91.2	2022.4	310.23	0.132	13.72	0.074
190727ZN	Chocolate Chip Cookie	2019	Rabbit Creek - North	6.186	86.7	232.8	-	-	-	-
110708B	Nefarious Now	2011	Rabbit Creek - North	4.039	57.4	416.3	47.00	0.820	109.00	1.100
BSC110720B	Old Blue Eyes (Left Eye)	2011	Rabbit Creek - North	8.836	65.4	1224.0	231.10	0.077	23.97	0.364
110708C	Sex on the Beach	2011	Rabbit Creek - North	3.943	57.4	68.1	0.53	0.658	18.70	1.500
170713SD	Rum Runner	2017	Rabbit Creek - North	3.71	59.6	109.5	0.64	0.227	32.32	0.234
110708A	Hammer Source	2011	Rabbit Creek - North	8.35	87.5	1888.9	313.00	0.442	13.20	1.992
140805SY	No Filter	2014	Rabbit Creek - North	4.344	81.7	249.3	35.49	0.007	37.75	0.052
140802SE	Sex on the Beach	2014	Rabbit Creek - North	5.04	50.7	63.7	0.47	0.364	18.34	0.017
190727ZO	Shrimp	2019	Rabbit Creek - North	8.059	82.7	1475.4	-	-	-	-
170713SE	Sex on the Beach	2017	Rabbit Creek - North	4.864	50.4	62.2	0.41	0.258	17.75	0.040
120718TN	Tanantula Deep	2012	Rabbit Creek - North	-	-	10340.0	266.33	0.181	17.81	0.046
120718TJ	Sex on the Beach	2012	Rabbit Creek - North	4.912	51.6	95.0	0.54	0.430	18.94	0.216
120718TL	Tiny Danza's Meat Flute	2012	Rabbit Creek - North	4.43	68.1	342.6	24.27	0.050	61.34	0.047
110708D	The Rum Runner	2011	Rabbit Creek - North	4.636	55.5	58.0	0.49	2.156	26.56	0.047
090726T1	Frightening Future	2009	Rabbit Creek - North	5.633	70.8	330.9	251.15	0.001	24.27	0.006

Sample ID	Sample Location	Year	Sampling area	pH	Temp °C	Sp. Cond. * (µS/cm)	Cl^- (ppm)	Cl^- %RSD	SO_4^{-2} (ppm)	SO_4^{-2} %RSD
190727ZK	Gravy Boat	2019	Rabbit Creek - North	3.675	81.4	187.8	-	-	-	-
140802SD	Rum Runner	2014	Rabbit Creek - North	3.855	54.9	189.6	0.60	0.236	68.68	0.121
120718TI	Dew U	2012	Rabbit Creek - North	4.033	45.7	1531.8	163.25	0.033	194.86	0.012
140805SX	Rum Runner	2014	Rabbit Creek - North	4.436	52.2	276.5	1.26	0.059	107.50	0.057
190727ZR	Whole Milk	2019	Rabbit Creek - North	2.839	84.5	729.7	-	-	-	-
BSC110720A	Rabbit's Nest	2011	Rabbit Creek - North	8.761	79.9	1873.2	252.33	0.035	20.49	0.133
JRH110708C	Rabbit Creek Source	2011	Rabbit Creek - North	8.168	83	1868.1	282.00	0.343	18.69	0.021
090803YA	Hissing Cliff	2009	Rabbit Creek - South	7.617	87.5	381.3	2.06	0.015	6.84	0.027
090803VA	Time Bomb	2009	Rabbit Creek - South	5.53	75.2	163.9	0.48	0.021	54.19	0.001
JRH110710E	Spitting Cobra	2011	Rabbit Creek - South	7.156	88.8	256.6	1.11	0.983	7.33	0.450
180718TZ	Big Filter	2018	Rabbit Creek - South	2.98	49.6	431.0	-	-	-	-
110720H1	Harp	2011	Rabbit Creek - South	4.67	47.3	186.9	0.57	0.616	82.40	0.504
160725P	Shipyard	2016	Rabbit Creek - South	3.55	61	324.4	-	-	-	-
140724TE	Rogue Dead Guy	2014	Rabbit Creek - South	3.47	49.9	185.9	0.43	0.076	67.32	0.033
160725M	Iron Fist	2016	Rabbit Creek - South	2.569	92.8	880.7	-	-	-	-
110710A	Hissing Cliff	2011	Rabbit Creek - South	7.49	88.9	392.0	1.95	0.533	7.69	0.285
160725O	Hissing Cliff	2016	Rabbit Creek - South	6.722	80.5	408.1	-	-	-	-
190718VB	Zen Garden Source	2019	Rabbit Creek - South	8.3	86.5	1741.7	-	-	-	-
140805TM	Big Filter	2014	Rabbit Creek - South	2.944	49.7	571.0	0.44	0.344	116.16	0.070
090803ZA	Pau Pau Long	2009	Rabbit Creek - South	6.763	92.6	329.1	1.45	0.001	91.33	0.002
150719D	Hissing Cliff	2015	Rabbit Creek - South	7.02	87.1	419.7	2.25	0.381	8.53	0.956

Sample ID	Sample Location	Year	Sampling area	pH	Temp °C	Sp. Cond. * (µS/cm)	Cl^- (ppm)	Cl^- %RSD	SO_4^{-2} (ppm)	SO_4^{-2} %RSD
140730TK	Iron Fist	2014	Rabbit Creek - South	2.931	80.3	672.8	3.51	0.150	201.08	0.038
180718TE	Aqua Marine	2018	Rabbit Creek - South	4.62	44.7	151.1	-	-	-	-
160725Q	Allagash	2016	Rabbit Creek - South	3.67	54	288.0	-	-	-	-
110710V	Zen Garden	2011	Rabbit Creek - South	8.163	85.8	564.1	267.20	0.309	14.09	0.275
120713TL	Aqua Marine (aka PNAS Pool)	2012	Rabbit Creek - South	4.503	49.3	165.7	0.44	0.243	51.24	0.089
190718VD	Leinenkugels	2019	Rabbit Creek - South	5.005	90	113.0	-	-	-	-
120713TH	Harp	2012	Rabbit Creek - South	5.342	52.1	254.1	1.49	0.152	25.16	0.263
140724TC	Aqua Marine (aka PNAS Pool)	2014	Rabbit Creek - South	4.212	50.4	152.1	0.49	0.014	49.99	0.009
190718VC	Epiphany	2019	Rabbit Creek - South	6.8	88.7	344.8	-	-	-	-
190727VL	Iron Fist	2019	Rabbit Creek - South	2.843	91.1	824.7	-	-	-	-
110710W	Hell's Gate	2011	Rabbit Creek - South	4.585	82.5	203.3	0.81	2.875	77.00	1.365
140805TL	Aqua Marine (aka PNAS Pool)	2014	Rabbit Creek - South	4.296	45.7	161.6	0.49	0.012	49.83	0.004
180718TA	Epiphany	2018	Rabbit Creek - South	7.23	90.4	319.3	-	-	-	-
160725L	Aquamarine	2016	Rabbit Creek - South	4.631	44.3	146.2	-	-	-	-
KF180718E	Iron Fist	2018	Rabbit Creek - South	2.65	91.8	791.1	-	-	-	-
190727VR	Aquamarine	2019	Rabbit Creek - South	4.65	44.1	159.6	-	-	-	-
KF180718F	Heady Topper	2018	Rabbit Creek - South	7.29	87.2	215.6	-	-	-	-
110720F1	SHIfT Hole	2011	Rabbit Creek - South	3.8	56.8	163.1	0.54	0.566	45.20	0.751
180718TD	Monk's CafÃ©	2018	Rabbit Creek - South	4.405	83.4	165.3	-	-	-	-
190727VQ	Whistilng Marmot	2019	Rabbit Creek - South	4.344	81.7	116.8	-	-	-	-
110710X	Dragon's Belly	2011	Rabbit Creek - South	4.745	91	238.8	0.90	1.563	75.70	1.220

Sample ID	Sample Location	Year	Sampling area	pH	Temp °C	Sp. Cond. * (µS/cm)	Cl^- (ppm)	Cl^- %RSD	SO_4^{-2} (ppm)	SO_4^{-2} %RSD
140805TO	Harp	2014	Rabbit Creek - South	5.52	51.5	168.8	0.85	0.199	27.37	0.004
170723TR	Aqua Marine	2017	Rabbit Creek - South	4.932	45.2	151.4	0.50	0.025	42.69	0.078
140805TK	Bozone	2014	Rabbit Creek - South	4.14	57.8	123.1	0.28	0.184	35.35	0.107
140730TH	Kiltlifter	2014	Rabbit Creek - South	4.971	50.4	139.5	0.59	0.234	34.34	0.346
140730TI	Old Chub	2014	Rabbit Creek - South	3.684	85.8	120.0	3.11	0.086	37.29	0.039
170723TW	Vince's Man Cave	2017	Rabbit Creek - South	6.547	68.5	238.1	1.14	0.012	17.52	0.060
190727VN	Monk's Cafe	2019	Rabbit Creek - South	4.687	88.1	159.0	-	-	-	-
140805TJ	Allagash	2014	Rabbit Creek - South	4.015	52.9	200.0	1.57	0.041	62.61	0.085
120713TK	Kiltlifter	2012	Rabbit Creek - South	5.293	52.2	176.4	0.61	0.035	36.60	0.094
140805TN	Shipyard	2014	Rabbit Creek - South	4.029	58.8	215.1	0.80	0.008	75.56	0.053
170723TU	Allagash	2017	Rabbit Creek - South	5.157	52.9	187.7	0.85	0.116	51.79	0.076
110710D	Kiltlifter	2011	Rabbit Creek - South	4.243	51	114.5	0.57	4.781	26.40	0.486
140730TJ	Allagash	2014	Rabbit Creek - South	4.491	54.1	205.8	0.80	0.090	63.09	0.168
150719FG	Shipyard	2015	Rabbit Creek - South	5.433	57.4	148.8	1.04	0.022	49.91	0.049
170723TT	Shipyard	2017	Rabbit Creek - South	5.008	59	182.2	0.84	0.047	55.61	0.199
170723TV	Kiltlifter	2017	Rabbit Creek - South	4.948	54.8	132.5	0.52	0.242	33.96	0.180
110720G1	Aqua Marine	2011	Rabbit Creek - South	4.034	42	154.8	0.64	1.536	26.50	0.687
120713TI	Allagash	2012	Rabbit Creek - South	4.803	54	260.6	0.98	0.778	57.71	0.043
160725N	Shift Hole	2016	Rabbit Creek - South	4.831	77.6	137.8	-	-	-	-
190727VP	Elmo's Screech	2019	Rabbit Creek - South	6.623	79.4	159.6	-	-	-	-
120713TJ	SHIfT Hole	2012	Rabbit Creek - South	4.521	70.3	219.8	0.53	0.027	34.07	0.040

Sample ID	Sample Location	Year	Sampling area	pH	Temp °C	Sp. Cond. * (µS/cm)	Cl^- (ppm)	Cl^- %RSD	SO_4^{-2} (ppm)	SO_4^{-2} %RSD
KF180718G	Focal Banger	2018	Rabbit Creek - South	6.6	81.3	307.1	-	-	-	-
190727VM	Shipyard	2019	Rabbit Creek - South	5.113	64.4	170.9	-	-	-	-
140805TP	Allagash (after rain)	2014	Rabbit Creek - South	4.58	50.5	202.3	0.90	0.002	63.53	0.001
170723TS	Monk's CafÃ©	2017	Rabbit Creek - South	5.248	75.9	157.1	0.40	0.098	27.29	0.109
180718TY	Allagash	2018	Rabbit Creek - South	5.471	52.7	169.6	-	-	-	-
170723TY	SHIfT Hole	2017	Rabbit Creek - South	4.57	73.3	134.5	0.47	0.242	34.50	0.199
110710B	Allagash	2011	Rabbit Creek - South	4.67	54.6	166.7	1.04	4.168	29.70	0.558
160725K	Moose Drool	2016	Rabbit Creek - South	6.124	53.3	161.2	-	-	-	-
160725J	Kiltlifter	2016	Rabbit Creek - South	5.19	51.6	98.3	-	-	-	-
140724TF	Monk's CafÃ©	2014	Rabbit Creek - South	5.042	75.2	159.9	0.63	0.023	31.70	0.030
110710C	Shipyard	2011	Rabbit Creek - South	4.535	64.2	153.2	0.90	3.274	38.40	0.386
180718TB	SHIfT Hole	2018	Rabbit Creek - South	4.33	64.2	123.0	-	-	-	-
180718TC	Kiltlifter	2018	Rabbit Creek - South	5.137	52.4	134.6	-	-	-	-
190727VO	Shift Hole	2019	Rabbit Creek - South	4.754	71.8	141.7	-	-	-	-
170723TZ	Moose Drool	2017	Rabbit Creek - South	5.75	58.5	183.3	0.28	1.435	35.66	0.037
140724TB	SHIfT Hole	2014	Rabbit Creek - South	4.61	71.8	140.8	0.50	0.092	34.11	0.001
140724TD	Moose Drool	2014	Rabbit Creek - South	5.81	61.8	146.0	0.49	0.249	43.32	0.076
140730TG	Monk's CafÃ©	2014	Rabbit Creek - South	5.237	77	157.5	0.42	0.179	28.62	0.010
110710Y	Moose Drool Pool	2011	Rabbit Creek - South	4.866	60.8	151.5	0.47	0.544	45.70	0.933
110720D1	Mr. Toad	2011	Rabbit Creek - South	4.233	36.9	214.0	0.77	3.626	32.50	2.825
170723TX	Big Filter	2017	Rabbit Creek - South	2.907	50.2	616.4	0.35	0.261	122.51	0.122

Sample ID	Sample Location	Year	Sampling area	pH	Temp °C	Sp. Cond. * (µS/cm)	Cl^- (ppm)	Cl^- %RSD	SO_4^{-2} (ppm)	SO_4^{-2} %RSD
090803UA	Spitting Cobra	2009	Rabbit Creek - South	8.285	87.5	264.0	1.62	0.417	15.26	0.723
150719F	Spitting Cobra	2015	Rabbit Creek - South	7.77	86.7	250.7	1.11	0.046	6.85	0.051
150719E	Ironfist	2015	Rabbit Creek - South	2.697	92.2	611.3	0.96	0.041	205.64	0.087
090724PA	Mound Spring Source	2009	Sentinel Meadows	8.276	93.9	1589.6	262.90	0.000	13.88	0.002
090724T1	Flat Cone Spring Source	2009	Sentinel Meadows	7.908	93.8	1481.1	237.50	0.000	14.72	0.001
150729H	Bison Mouth Waterfall	2015	Sentinel Meadows	7.49	89.9	1523.1	213.96	0.177	16.12	0.670
120716DD	Bison Pool	2012	Sentinel Meadows	7.597	-	6700.0	214.49	0.008	14.72	0.003
140725SH	Mound Source	2014	Sentinel Meadows	8.688	93.6	1566.6	245.55	0.002	14.65	0.057
120717DX	Mound Spring	2012	Sentinel Meadows	8.616	86.8	1534.9	240.72	0.183	14.26	0.336
120720DC	Bison Pool	2012	Sentinel Meadows	8.042	69.2	1501.6	223.33	0.230	16.23	0.059
120712SB	Mound Source	2012	Sentinel Meadows	8.484	93.5	1621.5	242.89	0.054	14.85	0.048
120720DD	Bison Pool	2012	Sentinel Meadows	7.713	82.7	1512.1	221.63	0.275	15.81	1.355
120714DC2	Bison Pool	2012	Sentinel Meadows	-	89	1550.4	230.39	0.152	16.07	0.039
090724TA	Iron Pot	2009	Sentinel Meadows	6.065	86.4	1224.0	196.55	0.000	40.92	0.003
110716E	Bison Pool Source corresponds to 110712E, 110713E	2011	Sentinel Meadows	8.2	89.5	-	236.40	0.283	16.66	0.039
120720DB	Bison Pool	2012	Sentinel Meadows	8.113	67.3	1509.8	224.38	0.013	16.81	0.011
090724M1	Bison Source	2009	Sentinel Meadows	7.265	93.4	1517.7	228.75	0.005	14.62	0.003
140730SL	Bison Source	2014	Sentinel Meadows	7.64	92.2	1495.7	216.09	0.038	15.73	0.173
JRH110720H	Bison Pool Source	2011	Sentinel Meadows	7.561	88.9	1514.5	219.90	0.382	15.00	0.892
120714DC1	Bison Pool	2012	Sentinel Meadows	-	89	1550.4	229.24	0.200	16.53	0.228

Sample ID	Sample Location	Year	Sampling area	pH	Temp °C	Sp. Cond. * (µS/cm)	Cl^- (ppm)	Cl^- %RSD	SO_4^{-2} (ppm)	SO_4^{-2} %RSD
120716DE	Bison Pool	2012	Sentinel Meadows	7.488	-	6980.0	204.94	0.033	14.85	0.021
180712SD	Bison Source	2018	Sentinel Meadows	7.71	87.8	1518.2	-	-	-	-
120714DE2	Bison Pool	2012	Sentinel Meadows	-	62.7	1732.6	218.44	0.008	15.06	1.032
120714DE1	Bison Pool	2012	Sentinel Meadows	-	62.7	1732.6	217.12	0.262	15.46	0.173
130718DE	Mound Spring Source	2013	Sentinel Meadows	8.89	87.5	1546.7	-	-	-	-
120720DE	Bison Pool	2012	Sentinel Meadows	7.597	88.2	1504.9	212.09	0.180	15.67	0.062
060807E	Mound Source	2006	Sentinel Meadows	8.07	93.8	1549.7	243.75	0.087	19.56	0.054
140730SM	Flat Cone	2014	Sentinel Meadows	8.273	83	1490.3	214.50	0.019	14.31	0.092
120717DD	Bison Pool	2012	Sentinel Meadows	7.656	84	1511.0	221.64	0.005	14.68	1.103
060807B	Bison Source	2006	Sentinel Meadows	7.52	93.2	1489.0	210.15	0.096	19.77	0.089
060812B	Bison Source, Shallow	2006	Sentinel Meadows	7.6	89.5	1493.4	212.35	0.060	19.75	0.812
120716DE2	Bison Pool	2012	Sentinel Meadows	-	-	6980.0	212.34	0.373	18.12	0.061
060812A	Steep Cone Source	2006	Sentinel Meadows	7.591	92.7	1552.3	240.60	0.003	18.38	0.764
060807C	Flatcone Source	2006	Sentinel Meadows	7.945	94.3	1449.7	212.56	0.040	18.69	0.187
060812C	Iron Pot	2006	Sentinel Meadows	6.286	62.8	1189.1	196.92	0.246	47.69	0.773
070711B	Mound Cone Source	2007	Sentinel Meadows	8.789	93.7	1618.8	244.80	0.144	24.44	0.051
160715K	Cole's Coffee	2016	Sentinel Meadows	4.395	87.7	377.1	-	-	-	-
160715JN4	Sentinal Spring 3	2016	Sentinel Meadows	8.028	20.8	121.3	-	-	-	-
070710I	Bison Source	2007	Sentinel Meadows	7.805	93.6	1517.7	182.06	0.113	25.05	4.870
110712E	Bison Pool at edge of Source	2011	Sentinel Meadows	7.73	90	1458.7	224.80	0.222	16.80	0.972
100808HA	Milk Chocolate	2010	Sentinel Meadows	2.999	84.7	1606.7	170.00	0.000	424.20	0.000

Sample ID	Sample Location	Year	Sampling area	pH	Temp °C	Sp. Cond. * (µS/cm)	Cl^- (ppm)	Cl^- %RSD	SO_4^{-2} (ppm)	SO_4^{-2} %RSD
190718ZB	Milk Chocolate	2019	Sentinel Meadows	3.822	84.8	623.9	-	-	-	-
100808IA	Special Dark	2010	Sentinel Meadows	6.635	82	776.2	141.80	0.000	66.91	0.000
160715G	Special Dark	2016	Sentinel Meadows	3.62	84.4	1181.4	-	-	-	-
190718ZD	Special Dark	2019	Sentinel Meadows	4.572	81.5	1286.4	-	-	-	-
150729D	Mound Spring	2015	Sentinel Meadows	8.6	94.2	1552.0	238.80	0.001	14.29	0.051
150729F	Flat Cone	2015	Sentinel Meadows	7.99	93.6	1500.8	210.84	0.075	14.38	0.030
150729E	Steep Cone	2015	Sentinel Meadows	7.54	93.6	1602.0	246.51	0.249	14.88	0.161
150717A	Colony Flats	2015	Sentinel Meadows	7.51	83.3	1426.6	216.81	0.012	16.03	0.006
090730ZA	The Dryer	2009	Sylvan	7.545	44.5	2441.7	601.26	0.001	176.28	0.002
090730WA	Evening Primrose	2009	Sylvan	5.384	81.8	2453.2	555.59	0.002	141.76	0.001
190729ZB	Tidepool	2019	Sylvan	6.807	80.1	1196.5	-	-	-	-
110715S	The Dryer	2011	Sylvan	5.555	47.7	2199.4	496.40	0.118	202.24	0.039
180723TZ	The Dryer	2018	Sylvan	5.125	45.1	2229.0	-	-	-	-
160721Q	The Dryer	2016	Sylvan	6.673	42.4	2193.6	-	-	-	-
190729ZA	The Dryer	2019	Sylvan	4.615	45.5	2312.8	-	-	-	-
120721TB	Evening Primrose	2012	Sylvan	5.208	77.5	3468.3	530.13	0.098	133.49	0.287
090730YA	Sylvan Spring	2009	Sylvan	5.185	79.5	2540.7	574.18	0.001	196.32	0.005
120722SN	The Dryer	2012	Sylvan	7.646	48.2	2359.3	524.86	0.402	162.61	0.020
100730GA	The Dryer	2010	Sylvan	7.716	44	2484.8	603.80	0.000	155.10	0.001
140731SV	The Dryer	2014	Sylvan	6.864	43.5	2279.6	501.71	0.019	195.01	0.052
180723TX	Burning Eye	2018	Sylvan	2.344	88	1811.5	-	-	-	-
110715L	Avocado Source	2011	Sylvan	6.188	73.1	2024.5	256.30	0.066	182.81	0.047
160717U	Evening Primrose	2016	Sylvan	5.367	77.4	2558.6	-	-	-	-
190720ZL	Sylvan Spring	2019	Sylvan	5.4	79.2	2423.2	-	-	-	-
190720ZK	Burning Eye	2019	Sylvan	2.395	88.2	1852.9	-	-	-	-

Sample ID	Sample Location	Year	Sampling area	pH	Temp °C	Sp. Cond. * (µS/cm)	Cl^- (ppm)	Cl^- %RSD	SO_4^{-2} (ppm)	SO_4^{-2} %RSD
170720SK	Evening Primrose	2017	Sylvan	5.44	80	2461.9	516.95	0.140	149.54	0.224
110715U	Sylvan Spring	2011	Sylvan	5.118	79.4	2351.1	455.00	0.524	146.80	0.164
100730FA	Sylvan Spring	2010	Sylvan	5.135	80.3	2568.9	570.20	0.000	205.00	0.001
050721P	Avocado Pool	2005	Sylvan	6.199	75	1966.5	306.76	0.030	211.46	0.005
190720ZO	Evening Primrose	2019	Sylvan	5.5	77.7	2283.3	-	-	-	-
090730W1	Gunter's Fancy	2009	Sylvan	5.38	74.5	1364.8	318.78	0.025	94.37	0.027
170720SO	Burning Eye	2017	Sylvan	2.29	86.4	1820.9	0.33	0.888	598.43	0.034
160721P	Little Red Head	2016	Sylvan	2.415	80.8	874.3	-	-	-	-
170716TR	Avocado	2017	Sylvan	6.6	68.3	2079.3	236.61	0.087	176.24	0.182
170720SM	Sylvan Spring	2017	Sylvan	5.287	76.8	2627.7	533.96	0.031	197.77	0.233
060805L	Avocado Source	2006	Sylvan	6.19	73	2076.5	289.81	0.024	181.44	0.226
110715Q	Roman Bath	2011	Sylvan	1.964	79.7	2299.4	1.66	0.708	718.80	0.118
100730HA	Go Bears!	2010	Sylvan	5.659	53.3	714.6	111.90	0.001	200.40	0.001
100730KA	Roman Bath	2010	Sylvan	2.156	82.7	1439.2	1.59	0.006	755.57	0.000
190729ZW	Avocado	2019	Sylvan	6.578	72.4	2079.1	-	-	-	-
190720ZN	Roman Bath	2019	Sylvan	2.23	71.4	2541.5	-	-	-	-
090730XA	Lobster Claw	2009	Sylvan	2.095	87.7	2990.2	4.08	0.017	1179.60	0.002
160721N	Avocado	2016	Sylvan	6.35	71.6	2061.1	-	-	-	-
120722SO	Avocado	2012	Sylvan	6.25	71.8	2073.9	277.57	0.084	250.26	0.036
120721TA	Gunter's Fancy	2012	Sylvan	5.232	73.2	2238.3	287.51	0.107	109.73	0.103
140802TW	Evening Primrose	2014	Sylvan	5.356	78.7	2292.7	479.76	0.152	135.76	0.011
110715N	Danny Boy	2011	Sylvan	3.121	73.8	411.4	0.64	1.066	134.00	0.854
160717X	Roman Bath	2016	Sylvan	2.14	76.5	2916.3	-	-	-	-
140731ST	Go Bears!	2014	Sylvan	3.52	38.5	1059.8	109.83	0.047	268.62	0.196
090730X1	Barfing Boulder	2009	Sylvan	2.48	81.3	1526.3	0.92	0.125	541.09	0.000
120721TC	Go Bears!	2012	Sylvan	3.115	42.9	1631.1	102.63	0.019	277.75	0.034
150718FE	Sylvan Spring	2015	Sylvan	5.157	79.3	2293.4	521.08	0.021	177.86	0.029

Sample ID	Sample Location	Year	Sampling area	pH	Temp °C	Sp. Cond. * (µS/cm)	Cl^- (ppm)	Cl^- %RSD	SO_4^{-2} (ppm)	SO_4^{-2} %RSD
190720ZM	Lobster Claw	2019	Sylvan	2.185	88.5	2572.7	-	-	-	-
090730VA	Go Bears!	2009	Sylvan	5.805	58.7	827.4	84.36	0.001	181.56	0.007
130721SF	Rice Milk (Little Read Head)	2013	Sylvan	2.602	87.9	1271.9	-	-	-	-
090730UA	Lil' Hottie	2009	Sylvan	2.101	83.9	2984.4	97.34	0.000	993.27	0.001
090730TA	Acid Pants	2009	Sylvan	1.938	78.1	2953.4	0.47	0.330	1018.44	0.003
130714TU	Goldilocks Source	2013	Sylvan	2.434	52.8	1606.7	-	-	-	-
140802TT	Lil' Red Head	2014	Sylvan	2.406	86	927.0	7.81	0.034	404.22	0.008
120721TW	Goldilocks Source	2012	Sylvan	2.231	53.5	3859.9	133.00	0.726	530.50	0.075
100805GA	Goldilocks Source	2010	Sylvan	2.421	53	2206.4	153.20	0.001	522.00	0.001
110715T	Go Bears!	2011	Sylvan	5.85	48.4	755.4	67.48	0.104	201.83	0.016
150718FC	Little Red Head	2015	Sylvan	2.086	88.6	1113.6	12.21	0.105	336.68	0.065
190729ZY	Goldielocks	2019	Sylvan	2.469	46	2352.1	-	-	-	-
RH110715Y	Goldilocks Source	2011	Sylvan	2.287	53.8	1764.0	121.00	0.122	591.47	0.009
160721R	Goldilocks	2016	Sylvan	2.451	49.3	-	-	-	-	-
050721K	Sylvan Spring	2005	Sylvan	5.36	81.6	2315.2	554.20	0.086	171.75	0.015
180723TU	Roman Bath	2018	Sylvan	2.166	73.4	2652.4	-	-	-	-
100809I1	Danny Boy	2010	Sylvan	2.297	72.6	2699.8	0.61	0.012	780.00	0.000
090730U1	Goldilocks Source	2009	Sylvan	2.436	52.9	1527.6	104.54	0.004	419.89	0.001
060805K	Goldilocks Source	2006	Sylvan	2.17	-	0.0	134.26	0.135	515.80	0.076
050721M	Goldielocks Source	2005	Sylvan	2.269	55.8	987.0	139.22	0.137	531.28	0.012
140731SU	Avocado	2014	Sylvan	6.36	72.5	2085.1	248.98	0.072	252.52	0.019
160721O	Little Hottie	2016	Sylvan	2.004	84.5	3086.8	-	-	-	-
160717V	Sylvan Spring	2016	Sylvan	5.52	76	2846.5	-	-	-	-
170716TS	Gunter's Fancy	2017	Sylvan	4.087	71.6	1464.8	286.63	0.033	184.75	0.040
120722SM	Roman Bath	2012	Sylvan	1.94	81.1	2521.2	3.05	0.341	900.64	0.122
140731SW	Gunter's Fancy	2014	Sylvan	5.46	77.4	1503.9	306.37	0.022	107.04	0.030
180723TW	Lobster Claw	2018	Sylvan	2.125	80.6	2987.7	-	-	-	-

Sample ID	Sample Location	Year	Sampling area	pH	Temp °C	Sp. Cond. * (µS/cm)	Cl^- (ppm)	Cl^- %RSD	SO_4^{-2} (ppm)	SO_4^{-2} %RSD
170720SN	Lobster Claw	2017	Sylvan	2.091	83.6	3029.5	3.50	0.066	1090.09	0.094
160721JN5	Sylvan Stream	2016	Sylvan	7.716	16.7	263.9	-	-	-	-
110715K	Lobster Claw	2011	Sylvan	1.87	85.3	2570.3	2.74	0.263	1139.00	0.193
180723TY	Sylvan Spring	2018	Sylvan	5.46	79.3	2545.5	-	-	-	-
090730C1	Blondie Source	2009	Sylvan	2.705	36.9	1684.2	76.34	0.005	433.01	0.003
070714D	Evening Primrose	2007	Sylvan	5.22	83.7	2511.5	559.00	0.167	185.61	0.333
120722SP	Sylvan Spring	2012	Sylvan	5.03	80.6	2556.8	496.09	0.143	200.06	0.033
140802TR	Little Hottie	2014	Sylvan	2.038	89.9	1218.5	114.86	0.081	972.65	0.079
110715W	Little Hottie	2011	Sylvan	2.474	32.7	1559.8	129.90	0.427	879.00	0.000
170716TT	Goldilocks Source	2017	Sylvan	2.446	50.6	2206.3	123.75	0.063	532.44	0.109
120722SK	Little Hottie	2012	Sylvan	1.94	87.7	2972.5	128.19	0.120	933.88	0.056
140731SX	Blondie Fringe	2014	Sylvan	2.645	33.1	1885.5	82.63	0.047	505.70	0.123
050721N	Burning Eye	2005	Sylvan	2.03	82.9	1214.1	0.54	0.552	622.47	0.144
120721TY	River Styx	2012	Sylvan	2.084	29.1	4685.8	111.88	0.100	652.26	0.144
190720ZJ	Acid Pants	2019	Sylvan	2.167	82.9	1005.6	-	-	-	-
190729ZX	Blondie	2019	Sylvan	2.711	34.2	1609.8	-	-	-	-
140802TX	Goldilocks	2014	Sylvan	2.466	50.8	2180.1	153.56	0.038	519.94	0.197
160717T	Lobster Claw	2016	Sylvan	1.957	83.6	3683.2	-	-	-	-
140802TS	Acid Pants	2014	Sylvan	1.968	85.2	816.7	0.07	3.945	959.95	0.060
KF120721L	GoldiStyx Myx	2012	Sylvan	2.232	31.6	4779.2	129.43	0.143	635.69	0.074
180723TV	Acid Pants	2018	Sylvan	1.975	75.4	3645.4	-	-	-	-
070714C	Goldielocks Source	2007	Sylvan	1.8	52.9	2425.5	138.87	0.109	494.97	0.156
190729ZZ	Gunter's Fancy	2019	Sylvan	4.524	79.1	1165.2	-	-	-	-
110715O	Blondie	2011	Sylvan	2.757	38.4	787.9	65.40	0.200	411.35	0.000
150718FF	Lobster Claw	2015	Sylvan	1.904	81.2	3154.4	3.70	2.051	1514.61	0.034
060810T	Lobster Claw	2006	Sylvan	2.026	87.7	2999.1	4.65	3.939	1288.50	0.046
140802TV	Sylvan Spring	2014	Sylvan	5.317	80	2481.0	521.71	0.266	196.50	0.036

Sample ID	Sample Location	Year	Sampling area	pH	Temp °C	Sp. Cond. * (µS/cm)	Cl^- (ppm)	Cl^- %RSD	SO_4^{-2} (ppm)	SO_4^{-2} %RSD
160717W	Go Bears	2016	Sylvan	2.917	34.4	1641.4	-	-	-	-
100805CA	River Styx, before Goldistyx myx	2010	Sylvan	2.074	29.6	3742.7	110.00	0.002	707.00	0.001
120722SL	Lobster Claw	2012	Sylvan	1.845	82.6	3396.8	3.22	1.076	1373.01	0.078
140731SY	Biting Moth	2014	Sylvan	1.994	84.9	2807.1	0.53	1.330	1295.99	0.153
160721S	Acid Pants	2016	Sylvan	1.818	91.5	84.6	-	-	-	-
140731SS	Acid Pants	2014	Sylvan	1.886	75.7	934.0	0.21	0.034	1124.70	0.087
170716TU	Lil' Hottie	2017	Sylvan	1.866	89.1	2147.2	109.81	0.026	882.90	0.230
090730Y1	3 Bears - Water (pool 'B')	2009	Sylvan	2.363	56.3	2319.8	70.61	0.002	445.21	0.001
130714TY	River Styx	2013	Sylvan	2.227	27.7	2816.9	-	-	-	-
170720SP	Go Bears!	2017	Sylvan	2.919	34.9	1485.0	103.67	0.076	353.21	0.088
100805KA	Sulfur Island	2010	Sylvan	1.343	91	8732.8	3.05	0.001	8860.00	0.000
130714TZ	Nap Cap	2013	Sylvan	3.762	30	1117.3	-	-	-	-
120722SQ	Peaceful Pool	2012	Sylvan	-	32.2	3408.2	196.85	0.077	623.28	0.015
140802TU	Lobster Claw	2014	Sylvan	2.148	87.4	2895.9	3.37	0.601	1346.80	0.092
170716TQ	Blondie Zygo Mat	2017	Sylvan	2.686	31.4	1709.2	35.70	0.028	468.96	0.162
090730T1	Avocado Source	2009	Sylvan	6.283	73.1	2124.9	299.92	0.013	189.29	0.000
090801O1	Sulfur Creek	2009	Washburn	3.868	16.1	295.6	0.32	0.474	120.57	0.001
190729VB	Rastaman	2019	Washburn	2.924	81.1	3821.9	-	-	-	-
190729VY	Mutinous Member	2019	Washburn	6.662	64.1	1682.4	-	-	-	-
190729VZ	Toe Beanzzz	2019	Washburn	5.842	81.3	1726.7	-	-	-	-
050723H	Rastaman	2005	Washburn	3.083	81.8	4986.0	0.12	0.868	2513.69	0.069
130714SX	Rastaman	2013	Washburn	2.731	89.8	4338.0	-	-	-	-
110711P	Emerald City	2011	Washburn	3.241	84.2	4038.5	0.24	0.615	1716.00	0.099
060809B	Boomerang	2006	Washburn	-	-	-	1.41	0.301	2485.91	0.048
190729VX	Emerald City	2019	Washburn	3.04	70.6	5549.2	-	-	-	-
120717SC	Lion's Den	2012	Washburn	5.78	88.8	2719.7	0.20	22.849	1187.20	0.041
130714SY	Boomerang	2013	Washburn	5.641	79.6	6711.3	-	-	-	-

Sample ID	Sample Location	Year	Sampling area	pH	Temp °C	Sp. Cond. * (µS/cm)	Cl^- (ppm)	Cl^- %RSD	SO_4^{-2} (ppm)	SO_4^{-2} %RSD
120719TQ	Boomerang	2012	Washburn	5.774	86.1	8109.8	0.09	3.057	1808.41	0.168
110711H	Lion's Den	2011	Washburn	6.134	80.3	1733.1	-	-	-	-
120719TU	Mutinous Member	2012	Washburn	3.672	48.3	2781.7	0.10	35.786	1099.23	0.055
190729VA	Boomerang	2019	Washburn	5.555	78.3	5871.2	-	-	-	-
110711F	Triceratops	2011	Washburn	6.055	86.4	2702.0	0.92	0.406	811.00	0.172
050723E	Boomerang	2005	Washburn	5.647	86.6	6984.8	0.10	2.946	3244.11	0.038
120719TS	Top Olympics	2012	Washburn	5.688	76.8	4351.7	0.32	8.839	1646.50	0.055
120719TT	Muddy Blister	2012	Washburn	2.616	42.8	1082.6	0.16	1.489	2137.79	0.079
090801N1	Lion's Den	2009	Washburn	5.01	87.1	4558.4	0.32	0.520	1779.24	0.000
110711M	Boomerang	2011	Washburn	5.731	80.3	5831.0	0.43	0.672	4632.00	0.121
110711E	FLIP	2011	Washburn	6.037	88.7	2889.2	0.60	0.202	1060.60	0.083
110711N	Van Gogh	2011	Washburn	2.665	81.2	5546.1	0.45	0.016	2576.20	0.027
120717SE	Triceratops	2012	Washburn	5.591	85.8	2933.2	0.34	18.969	1066.87	0.105
180724SI	Just the Tip	2018	Washburn	5.51	74	2399.0	-	-	-	-
180724SJ	Steamy Windows	2018	Washburn	6.4	76	3797.0	-	-	-	-
180724SH	Jackson's Tub-o-Luv	2018	Washburn	3.226	82.8	5398.9	-	-	-	-
090726JA	Boomerang	2009	Washburn	5.771	88.9	6896.4	0.15	0.068	2906.76	0.001
120719TR	Emerald City	2012	Washburn	2.793	75.1	4545.5	4.10	1.149	1790.78	0.113
070708J	Boomerang	2007	Washburn	5.614	84.9	6860.8	-	-	3315.85	0.390
190721VQ	Triceratops	2019	Washburn	6.287	86.6	2549.3	-	-	-	-
130714SZ	Mr. Pickles	2013	Washburn	5.883	82.7	5752.1	-	-	-	-
190721VS	Jackson's Tub O' Luv	2019	Washburn	6.218	88.9	4723.4	-	-	-	-
180724SG	Mr. Clean	2018	Washburn	5.83	66.7	2726.3	-	-	-	-
050723G	Chest High Pool	2005	Washburn	5.85	78.6	6341.7	0.05	3.009	2887.72	0.062
060809E	Emerald City	2006	Washburn	6.067	78	5946.6	0.27	29.446	2653.19	0.066
180724SF	Triceratops	2018	Washburn	6.04	86	2702.7	-	-	-	-
070708L	Emerald City	2007	Washburn	4.893	89.2	4378.3	-	-	3298.56	0.012

Sample ID	Sample Location	Year	Sampling area	pH	Temp °C	Sp. Cond. * (µS/cm)	Cl^- (ppm)	Cl^- %RSD	SO_4^{-2} (ppm)	SO_4^{-2} %RSD
070708K	Clear Eye	2007	Washburn	2.255	83.9	7171.7	-	-	3644.26	0.052
190721VT	F.L.I.P.'s Kidney	2019	Washburn	5.979	83.9	4343.4	-	-	-	-
050723F	Clear Eye	2005	Washburn	2.73	83.3	8190.2	0.16	2.668	4735.97	0.068
090726KA	Rastaman	2009	Washburn	2.798	87.2	4572.2	1.22	0.351	2283.69	0.014
110711Q	Muddy Blister	2011	Washburn	3.952	38.9	4186.2	0.35	0.060	1699.70	0.003
190721VR	Mr. Clean	2019	Washburn	5.987	65.7	2724.4	-	-	-	-
090726HA	Van Gogh	2009	Washburn	2.786	86.4	7634.6	1.16	1.120	4658.55	0.004
060809D	Clear Eye	2006	Washburn	3.046	85.2	9265.0	0.42	3.755	4639.99	0.048
090801J1	Triceratops	2009	Washburn	6.225	86.6	3037.6	0.36	0.044	980.44	0.001
050723D	FLIP	2005	Washburn	6.186	81.6	2307.7	0.31	0.271	1044.20	0.082
130714SA	Goldfish Bowl	2013	Washburn	5.44	74.1	4853.7	-	-	-	-
130718SU	FLIP's Kidney	2013	Washburn	6.04	83.6	509.2	-	-	-	-
140727TW	Triceratops	2014	Washburn	5.864	87.5	3368.9	0.50	3.981	1379.97	0.003
060809A	F.L.I.P.	2006	Washburn	-	-	0.0	0.28	0.756	1304.11	0.035
070708I	Chest High	2007	Washburn	5.331	75.7	9434.0	-	-	3456.56	0.040
090726IA	Chest High	2009	Washburn	5.801	87.1	5477.3	0.47	0.340	2079.66	0.005
120717SF	FLIP	2012	Washburn	5.566	88.4	2866.0	0.22	2.577	1604.51	0.267
120717SH	Grayson's Ditch of Joy	2012	Washburn	6.75	38.6	4213.8	0.35	21.461	1796.86	0.079
120717SG	Mr. Clean	2012	Washburn	5.404	73.3	4181.1	0.41	5.238	1702.08	0.177
090801M1	F.L.I.P.	2009	Washburn	6.31	90	2760.9	0.41	0.117	1281.63	0.002
090801K1	Mr. Clean	2009	Washburn	6.145	76.4	3841.2	0.77	0.468	1219.83	0.008
090801L1	Jackson's Tub-O-Luv	2009	Washburn	3.232	73.3	6012.2	0.36	0.219	2928.34	0.001
120717SD	Jackson's Tub-O-Luv	2012	Washburn	2.62	76.7	6666.7	0.76	3.722	2461.87	0.045
140727TU	FLIP Outflow	2014	Washburn	6.448	57.6	3226.4	1.28	2.003	1473.37	0.146
140727TV	Mr. Clean	2014	Washburn	5.729	75.4	3570.7	0.45	7.752	1432.97	0.075
140727TT	FLIP	2014	Washburn	6.031	89.5	2707.4	0.49	0.145	1403.45	0.204
090725H1	White Creek at crossing spot	2009	White Creek	7.705	53.7	527.3	53.53	0.005	23.91	0.002

Sample ID	Sample Location	Year	Sampling area	pH	Temp °C	Sp. Cond. * (µS/cm)	Cl^- (ppm)	Cl^- %RSD	SO_4^{-2} (ppm)	SO_4^{-2} %RSD
090725K1	Twin Buttes Vista Source	2009	White Creek	8.474	92.8	1697.8	281.27	0.001	15.62	0.001
090725G1	Log Jam Source	2009	White Creek	7.233	80.3	1621.6	313.73	0.001	21.42	0.004
160716Q	Octopus Source	2016	White Creek	7.617	87.5	1321.3	-	-	-	-
150725WC	Spent Kleenex	2015	White Creek	8.215	85	1577.3	240.83	0.025	14.63	0.507
160716O	Log Jam	2016	White Creek	7.137	78.3	1325.3	-	-	-	-
160716R	Fallen Log Pool	2016	White Creek	7.099	91	905.2	-	-	-	-
190723ZZ	Log Jam	2019	White Creek	7.717	77.2	1663.9	-	-	-	-
170722ST	Red Sauce	2017	White Creek	6.176	83	341.7	47.80	0.054	22.65	0.026
090725X1	Octopus Source	2009	White Creek	7.808	90	1580.4	238.30	0.001	16.19	0.002
170722SV	Horneblend	2017	White Creek	6.871	79.5	556.9	52.36	0.001	27.79	0.120
180724TC	Dead Bird	2018	White Creek	6.254	80	543.8	-	-	-	-
170722SR	Green Sauce	2017	White Creek	6.65	66.4	500.0	48.47	0.144	25.95	0.028
110717D1	Spent Kleenex	2011	White Creek	8.314	87.1	1494.6	239.60	0.053	13.58	0.313
160716M	Spent Kleenex	2016	White Creek	8	82.5	1060.0	-	-	-	-
180717SY	Log Jam	2018	White Creek	7.397	80.5	1594.3	-	-	-	-
110717C1	Twin Buttes Vista	2011	White Creek	8.7	78.2	1596.4	277.00	0.495	16.00	0.000
120715SW	Fern Gully	2012	White Creek	6.747	71.9	877.2	110.04	0.154	17.09	0.440
170718SC	Bug Cemetery Source	2017	White Creek	7.222	76.1	1360.5	192.67	0.098	14.42	0.079
180724TD	Toad Shoot	2018	White Creek	6.167	76.8	421.4	-	-	-	-
180717SX	Par 5	2018	White Creek	8.726	72.7	1539.9	-	-	-	-
170718SA	Par 5	2017	White Creek	8.635	73.9	1635.5	245.22	0.563	17.69	0.075
180717SC	Fat Boi	2018	White Creek	7.95	84.1	1619.6	-	-	-	-
170722SU	Black Hole	2017	White Creek	7.672	71.3	559.2	53.10	0.012	28.18	0.006
120719HE	fallen log surface	2012	White Creek	-	92.2	1038.8	141.96	0.041	15.75	0.002
151729WF	Spent Kleenex	2015	White Creek	8.35	85.3	1589.3	238.80	0.036	14.73	0.222
180724TF	White Creek just above Dead Bird inflow	2018	White Creek	8.054	42.7	486.7	-	-	-	-
120715SX	FecToad Skin	2012	White Creek	7.344	45.1	378.0	29.80	0.005	18.34	0.178

Sample ID	Sample Location	Year	Sampling area	pH	Temp °C	Sp. Cond. * (µS/cm)	Cl^- (ppm)	Cl^- %RSD	SO_4^{-2} (ppm)	SO_4^{-2} %RSD
170722SS	Purple Drink	2017	White Creek	8.055	47.3	488.9	48.61	0.016	25.92	0.040
060806R	Octopus Source	2006	White Creek	7.67	91.4	1548.1	235.99	0.095	15.48	0.062
120719HC	spindle geyser- surface	2012	White Creek	-	-	7330.0	246.51	0.037	15.97	0.243
120715SU	Shot Drop	2012	White Creek	6.725	53.6	1574.4	241.72	0.061	21.09	0.012
130720DQ	Log Jam	2013	White Creek	6.868	79.5	1588.0	-	-	-	-
180724TB	Purple Drink	2018	White Creek	7.656	46.4	488.8	-	-	-	-
180717SZ	Spent Kleenex	2018	White Creek	8.456	83.3	1491.2	-	-	-	-
120715SY	Spent Kleenex	2012	White Creek	8.017	81	1365.6	245.62	0.247	14.99	0.053
120715SV	White Creek Scum	2012	White Creek	7.734	32.4	490.4	51.25	0.051	23.42	0.037
060809 IV	'Beal'	2006	White Creek	7.985	93.9	1563.9	227.86	0.114	17.41	0.065
060809 V	Spent Kleenex	2006	White Creek	7.868	87.4	1539.1	244.31	0.276	17.73	1.972
120719HD	fallen log deep 2	2012	White Creek	-	91.4	1059.3	141.10	0.099	15.98	0.036
120719HB	spindle geyser- deep	2012	White Creek	-	92.8	1555.6	248.11	0.167	16.16	0.130
070706A	Octopus Source	2007	White Creek	7.579	90.7	1461.5	201.59	0.097	24.16	2.372
190723ZY	Bug Heaven	2019	White Creek	8.178	21.5	1346.2	-	-	-	-
090725B1	Par 5 Source	2009	White Creek	8.482	83.5	1582.9	257.86	0.003	16.55	0.005
190723ZW	Par 5	2019	White Creek	8.728	74.6	1655.6	-	-	-	-
150725WE	Par 5	2015	White Creek	8.548	73.2	1621.2	249.21	0.259	18.07	0.097
150729WH	Par 5	2015	White Creek	8.582	73.7	1628.2	243.43	0.183	17.77	0.274
130720DR	Spent Kleenex 40cm from mouth of outflow	2013	White Creek	8	83.9	1523.0	-	-	-	-
090725Z1	Spent Kleenex Source	2009	White Creek	8.156	88.1	1430.2	257.33	0.005	14.50	0.022
190723ZV	Bug Cemetery	2019	White Creek	7.529	75	1372.5	-	-	-	-
170718SZ	Spent Kleenex	2017	White Creek	8.295	85.3	1601.5	238.58	0.004	14.44	0.055
150729WI	Bug Cemetary	2015	White Creek	7.5	73.2	1349.8	192.57	0.035	14.76	0.123
170718SY	Octopus Pink	2017	White Creek	7.964	82.6	1603.2	237.40	0.004	17.80	0.063
150725WD	Bug Cemetary	2015	White Creek	7.035	75.8	1367.6	193.71	0.032	14.93	0.062
170718SX	Octopus Beige	2017	White Creek	7.998	83	1575.0	236.98	0.024	17.81	0.126

Sample ID	Sample Location	Year	Sampling area	pH	Temp °C	Sp. Cond. * (µS/cm)	Cl^- (ppm)	Cl^- %RSD	SO_4^{-2} (ppm)	SO_4^{-2} %RSD
150725WB	Log Jam	2015	White Creek	7.32	79	1634.6	248.29	0.074	19.25	0.017
150729WG	Log Jam	2015	White Creek	7.4	79	1632.7	247.81	0.033	19.09	0.026

APPENDIX C

DIC/DOC DATA FOR HOT SPRINGS IN YNP

Sample ID	Sample Location	Year	Sampling area	DIC (µM)	DIC (µM) Std Dev	DIC δ13C VPDB (‰)	DIC Std Dev (‰)	DOC (µM)	DOC (µM) Std Dev	DOC δ13C VPDB (‰)	DOC Std Dev (‰)
160720J	Crater Hills Geyser	2016	Crater Hills	86.03	16.65	-4.71	0.49	28.05	6.66	-19.09	0.29
180714SN	Crater Hills Geyser Pool	2018	Crater Hills	-	-	-	-	31.28	16.65	-22.68	0.20
120715TW	Crater Hills Geyser Source	2012	Crater Hills	118.07	-	-4.08	-	37.03	4.26	-21.69	0.39
190719ZF	Crater Hills Geyser (Small pool for gas and bio)	2019	Crater Hills	460.33	16.65	-3.06	0.20	40.28	16.65	-21.74	0.22
160720I	Jabberwocky	2016	Crater Hills	-	-	-	-	48.58	6.66	-21.41	0.26
120713SK	Rabbit Hole	2012	Crater Hills	3567.21	16.65	-3.40	0.29	74.88	10.12	-18.11	0.41
100801YA	Rabbit Hole	2010	Crater Hills	1683.09	25.08	-2.84	0.27	76.03	5.00	-21.84	0.33
190719ZH	Cynadium Falls	2019	Crater Hills	485.63	16.65	-3.47	0.20	79.99	16.65	-21.87	0.22
180714SM	Delilah	2018	Crater Hills	562.31	21.00	-1.64	1.12	81.91	16.65	-22.51	0.22
120713SJ	Jabberwocky	2012	Crater Hills	1527.10	49.02	-3.97	0.48	88.48	3.59	-11.26	0.53
090728PA	Crumpet Spring	2009	Crater Hills	1292.41	25.85	-3.33	0.20	107.25	3.63	-17.33	0.26
140729SG	Jabberwocky	2014	Crater Hills	1049.35	18.88	-2.60	0.28	107.81	16.65	-25.84	0.28
160720H	Alice	2016	Crater Hills	301.99	16.65	-4.57	0.49	108.45	6.66	-14.96	0.26
190719ZG	Alice	2019	Crater Hills	-	-	-	-	109.56	16.65	-16.00	0.20
140729SB	Alice	2014	Crater Hills	-	-	-	-	118.98	16.65	-15.72	0.28
120713SH	Alice	2012	Crater Hills	83.70	3.76	-19.04	0.74	123.01	9.99	-16.70	0.60
110713D	Alice	2011	Crater Hills	954.60	8.84	-4.43	0.20	124.78	-	-19.09	1.06
180714SL	Alice	2018	Crater Hills	572.99	16.65	-2.79	0.20	135.69	16.65	-22.84	0.20
170724TD	Cyanidium Falls	2017	Crater Hills	83.02	6.66	7.50	0.44	140.45	16.65	-22.81	0.20
190719ZI	Rabbit Hole	2019	Crater Hills	458.76	16.65	-3.11	0.30	163.79	3.33	-14.24	0.20
090728QA	Caterpillar	2009	Crater Hills	538.04	10.76	-3.18	0.20	163.79	5.54	-16.81	0.26
180714SO	Frabjousday	2018	Crater Hills	798.39	16.65	-2.96	0.20	399.29	16.65	-19.02	0.22
160720K	Rabbit Hole	2016	Crater Hills	-	-	-	-	438.19	6.66	-8.61	0.20
170724TA	Rabbit Hole	2017	Crater Hills	309.09	6.66	0.72	0.44	525.70	16.65	-9.65	0.55

Sample ID	Sample Location	Year	Sampling area	DIC (µM)	DIC (µM) Std Dev	DIC δ13C VPDB (‰)	DIC Std Dev (‰)	DOC (µM)	DOC (µM) Std Dev	DOC δ13C VPDB (‰)	DOC Std Dev (‰)
090728OA	Alice Spring	2009	Crater Hills	676.50	13.53	-2.92	0.20	926.12	31.31	-24.65	0.26
100810R1	Mock Turtle	2010	Crater Hills	1081.70	11.74	-2.50	0.25	1144.83	41.63	-23.09	0.60
100801AA	Alice	2010	Crater Hills	1127.55	2.59	-2.53	0.25	1383.67	12.02	-21.35	0.30
120713SL	Jabberwocky After Rain/Hail	2012	Crater Hills	-	-	-	-	1671.51	-	-24.22	0.53
180714SP	White Rabbit	2018	Crater Hills	-	-	-	-	2476.47	42.22	-22.41	0.20
120715TU	Alice	2012	Crater Hills	1146.43	16.65	-3.58	0.29	3094.46	252.68	-23.86	0.49
170724TE	Crater Hills Geyser Source	2017	Crater Hills	166.03	6.66	2.06	0.44	-	-	-	-
090728NA	Crater Hills Geyser	2009	Crater Hills	233.37	4.67	-3.94	0.25	-	-	-	-
090728RA	Mockturtle	2009	Crater Hills	985.35	19.71	-3.30	0.20	-	-	-	-
160723Z	Corner Thing	2016	Geyser Creek	1444.18	37.86	-0.31	0.28	26.84	6.66	-23.95	0.29
100804WA	Bull's Eye Pool	2010	Geyser Creek	1616.72	49.65	-0.62	0.29	27.04	-	-20.46	-
190725ZI	Empress Source	2019	Geyser Creek	3641.09	110.54	0.38	0.34	27.06	3.33	-25.86	0.20
180722TS	Big Bowl Geyser ("Gucci")	2018	Geyser Creek	1003.26	47.20	0.23	0.46	28.36	16.65	-25.96	0.22
160723V	Bat Pool	2016	Geyser Creek	5205.57	53.22	-3.67	0.21	29.13	6.66	-25.87	0.29
190723VU	St. Blucia	2019	Geyser Creek	894.28	16.65	-2.80	0.30	29.55	16.65	-23.16	0.20
150724MB	Alkaline Stream	2015	Geyser Creek	6086.60	72.63	-0.05	0.26	29.96	16.65	-23.22	0.20
120719SS	Corner Thing	2012	Geyser Creek	1396.70	6.38	-0.74	0.48	31.10	3.47	-23.30	0.21
190723VY	Birthday Balloon	2019	Geyser Creek	737.87	16.65	-1.39	0.30	31.13	3.33	-24.63	0.20
110714Q	St. Blucia	2011	Geyser Creek	968.71	1.82	-5.01	0.20	32.03	-	-17.64	-
100803IA	Empress Pool Source	2010	Geyser Creek	3276.99	2.33	0.44	0.21	34.09	-	-22.50	-
120719SX	St. Blucia Source	2012	Geyser Creek	485.25	16.65	-4.23	0.29	34.31	4.26	-19.41	0.39

Sample ID	Sample Location	Year	Sampling area	DIC (µM)	DIC (µM) Std Dev	DIC δ13C VPDB (‰)	DIC Std Dev (‰)	DOC (µM)	DOC (µM) Std Dev	DOC δ13C VPDB (‰)	DOC Std Dev (‰)
180722TN	Bullseye	2018	Geyser Creek	1638.64	22.59	-0.41	0.46	34.38	16.65	-26.38	0.20
JRH110714O	Lemon Lick (Yellow Filament site emptying into Empress Pool)	2011	Geyser Creek	4968.64	36.41	-3.85	0.30	36.70	-	-25.23	-
190723VW	Corner Thing	2019	Geyser Creek	-	-	-	-	37.06	16.65	-26.57	0.22
190725ZJ	Fallen Angel Hair	2019	Geyser Creek	1413.47	27.54	0.08	0.43	37.34	16.65	-24.59	0.20
100804TA	St. Blucia	2010	Geyser Creek	769.56	8.13	-3.30	0.27	37.63	-	-20.25	-
120719K2	Bat Pool	2012	Geyser Creek	5273.09	3.23	-4.83	0.44	37.98	3.47	-21.15	0.21
190725ZH	Salami Source	2019	Geyser Creek	481.15	16.65	-2.67	0.20	39.23	16.65	-24.68	0.20
170719SF	Corner Thing	2017	Geyser Creek	1469.54	12.49	0.00	0.37	39.87	16.65	-24.56	0.42
170719SE	St. Blucia	2017	Geyser Creek	628.00	6.66	-0.81	0.44	40.68	8.33	-21.40	0.20
180713SH	Bat Pool Source	2018	Geyser Creek	4731.79	150.73	-2.57	0.22	41.01	16.65	-26.97	0.29
180722TO	Boulder Burper	2018	Geyser Creek	1788.32	92.60	0.22	0.46	41.06	16.65	-26.38	0.22
160723U	Empress Pool	2016	Geyser Creek	3035.14	125.67	0.63	0.21	41.42	6.66	-26.39	0.29
140724SB	Bat Pool	2014	Geyser Creek	4909.76	16.65	-3.67	0.20	42.39	16.65	-25.55	0.28
180722TP	Hot Hot Hot!	2018	Geyser Creek	1112.26	51.07	-0.50	0.46	43.14	16.65	-24.60	0.22
180722TM	Birthday Balloon	2018	Geyser Creek	600.87	16.65	0.57	0.46	44.37	16.65	-24.92	0.22
170718TZ	Empress Source	2017	Geyser Creek	2947.39	88.53	2.14	0.21	45.46	16.65	-25.32	0.20
180713SJ	Man-O-War	2018	Geyser Creek	6219.58	110.34	-0.31	0.46	48.22	16.65	-27.28	0.20
120719K1	Bat Pool	2012	Geyser Creek	5176.20	5.56	-4.78	0.44	50.42	3.47	-22.18	0.21
140729TZ	Empress Source	2014	Geyser Creek	3598.27	82.92	-0.20	0.23	51.26	16.65	-25.13	0.28

Sample ID	Sample Location	Year	Sampling area	DIC (µM)	DIC (µM) Std Dev	DIC δ13C VPDB (‰)	DIC Std Dev (‰)	DOC (µM)	DOC (µM) Std Dev	DOC δ13C VPDB (‰)	DOC Std Dev (‰)
170719SH	Left Ventricle	2017	Geyser Creek	-	-	-	-	52.05	16.65	-22.02	0.42
140724SF	Empress Source	2014	Geyser Creek	3868.85	102.87	-0.27	0.23	54.53	16.65	-25.41	0.28
100804VA	Pig Nose Dipped in Custard	2010	Geyser Creek	346.86	6.48	-3.78	0.27	56.56	4.48	-23.28	0.90
180722TQ	Left Ventricle	2018	Geyser Creek	-	-	-	-	57.20	16.65	-23.30	0.22
120719SY	Birthday Balloon	2012	Geyser Creek	675.66	27.52	0.24	0.29	59.74	1.87	-22.60	0.66
160723X	Spitting Croissant	2016	Geyser Creek	52.91	16.65	-6.16	0.49	60.25	6.66	-22.54	0.26
120719K5	Bat Pool	2012	Geyser Creek	5284.16	3.23	-5.05	0.44	61.66	3.47	-22.15	0.21
180722TT	Compression Slam	2018	Geyser Creek	1084.17	24.48	0.76	0.49	61.69	16.65	-25.46	0.22
160723A	Dirty Doughnut	2016	Geyser Creek	1868.72	69.22	2.84	0.28	61.74	6.66	-20.83	0.26
180713SF	Lemon Lick	2018	Geyser Creek	3075.44	37.58	1.27	0.38	64.05	16.65	-27.03	0.20
180722TR	Possible Tourette's	2018	Geyser Creek	-	-	-	-	65.59	16.65	-21.63	0.22
110714G	Hot Ice Hole	2011	Geyser Creek	2536.04	2.11	-2.10	0.27	66.69	-	-20.54	0.82
160723Y	St Blucia	2016	Geyser Creek	660.15	6.66	-3.01	0.38	66.95	6.66	-24.37	0.29
120724SB	Running Paint	2012	Geyser Creek	5490.38	77.31	2.62	0.53	67.11	4.36	-20.98	0.39
110714E	Empress Pool Source	2011	Geyser Creek	3325.94	14.45	-2.19	0.55	67.56	-	-27.20	1.39
100804NA	Geyser Creek, alkaline inflow channel	2010	Geyser Creek	5506.55	18.08	0.16	0.21	67.94	4.48	-24.88	0.90
170719SG	Spitting Croissant	2017	Geyser Creek	148.12	6.66	3.72	0.44	70.79	8.33	-22.19	0.20
120724SY	Spitting Croissant	2012	Geyser Creek	44.06	37.58	-4.46	0.74	70.79	10.12	-21.74	0.41
120719ST	Snake City	2012	Geyser Creek	1450.11	16.65	2.30	0.48	71.54	4.36	-21.09	0.66

Sample ID	Sample Location	Year	Sampling area	DIC (µM)	DIC (µM) Std Dev	DIC δ13C VPDB (‰)	DIC Std Dev (‰)	DOC (µM)	DOC (µM) Std Dev	DOC δ13C VPDB (‰)	DOC Std Dev (‰)
110714H	Spitting Croissant	2011	Geyser Creek	146.23	-	-0.92	0.88	71.98	-	-22.55	0.82
150723MC	Complete Mix	2015	Geyser Creek	2891.75	66.89	1.02	0.28	72.18	16.65	-22.93	0.20
140729TC	Salami Outflow	2014	Geyser Creek	-	-	-	-	74.46	16.65	-26.13	0.31
100804ZA	Bubblin' Hat	2010	Geyser Creek	653.49	8.93	-3.62	0.27	78.07	2.65	-14.52	0.57
190723VX	Spitting Croissant	2019	Geyser Creek	115.61	16.65	-5.08	0.20	78.19	16.65	-24.48	0.20
110714I	Dirty Donut	2011	Geyser Creek	1307.20	15.37	-1.68	0.89	80.02	-	-23.14	1.39
110714J	Doily	2011	Geyser Creek	998.74	31.56	-4.01	0.20	82.61	-	-19.20	1.06
140729TY	Spitting Croissant	2014	Geyser Creek	55.85	16.65	-	-	82.80	16.65	-23.89	0.31
100804UA	Spitting Croisant	2010	Geyser Creek	157.62	2.13	-4.45	0.42	87.40	4.48	-23.02	0.90
100804RA	Hot Icehole	2010	Geyser Creek	1342.13	26.55	1.01	0.29	95.21	4.48	-22.55	0.90
160723JN7	Geyser Creek	2016	Geyser Creek	933.85	6.66	-2.15	0.38	95.42	6.66	-26.84	0.20
120724SZ	Wild Paint Mix	2012	Geyser Creek	2183.16	29.23	0.41	0.48	106.23	4.36	-22.41	0.39
100804MA	Geyser Creek, above alkaline inflow	2010	Geyser Creek	174.84	2.02	-9.01	0.97	107.19	4.48	-24.12	0.90
150724MA	Acidic Stream	2015	Geyser Creek	180.75	16.65	-2.77	0.47	126.11	16.65	-22.29	0.20
120724SA	Mr. Toad's Wild Ride	2012	Geyser Creek	200.46	3.21	-7.53	0.54	155.21	4.36	-23.33	0.39
150723MCAR	Complete Mix After Rain	2015	Geyser Creek	1619.37	22.73	0.69	0.71	195.50	16.65	-22.60	0.20
140729TD	Spitting Croissant AR (after rain)	2014	Geyser Creek	54.50	16.65	-	-	205.14	16.65	-23.30	0.31
140729TE	Spitting Croissant AR2	2014	Geyser Creek	114.35	16.65	-	-	248.37	16.65	-21.45	0.31
170719SI	Jackhammer	2017	Geyser Creek	72.48	16.65	8.69	0.42	366.35	8.33	-1.87	0.20
190723VZ	Boiling Sombrero	2019	Geyser Creek	781.61	16.65	-4.34	0.24	381.58	16.65	-15.70	0.20

Sample ID	Sample Location	Year	Sampling area	DIC (µM)	DIC (µM) Std Dev	DIC δ13C VPDB (‰)	DIC Std Dev (‰)	DOC (µM)	DOC (µM) Std Dev	DOC δ13C VPDB (‰)	DOC Std Dev (‰)
190723VV	Jackhammer	2019	Geyser Creek	73.71	16.65	-6.17	0.20	387.83	16.65	-2.57	0.22
180713SI	The Monster	2018	Geyser Creek	86.74	16.65	-7.73	0.20	3149.63	181.83	-22.34	0.07
170718TA	Bone Pool	2017	Geyser Creek	1403.66	64.62	0.99	0.30	-	-	-	-
110714P	Corner Thing	2011	Geyser Creek	1944.30	4.24	-3.11	0.20	-	-	-	-
110714F	Bat Pool Source	2011	Geyser Creek	5363.40	22.29	-6.36	0.20	-	-	-	-
160724C	Figure 8	2016	GOPA	3073.77	36.71	-2.57	0.28	52.00	6.66	-19.00	0.26
150727U	Happy Harfter + Fig 8 Mix	2015	GOPA	147.12	-	-	-	61.04	16.65	-20.29	0.20
170713TB	Figure 8 Source	2017	GOPA	602.04	24.55	0.12	0.61	61.80	8.33	-20.43	0.20
160724E	Happy Harfer	2016	GOPA	3932.51	16.65	-0.87	0.21	68.52	6.66	-22.78	0.26
160724F	Phantom Pants	2016	GOPA	3932.51	16.65	-0.87	0.21	68.52	6.66	-22.78	0.26
100807ZA	Happy Harfer	2010	GOPA	2893.96	22.50	-0.99	0.21	68.75	7.43	-23.32	1.17
050718R	Spotted Grizzly Pool	2005	GOPA	3874.37	151.49	-3.33	1.44	69.69	1.50	-22.06	0.37
120712TA	Figure 8 Source	2012	GOPA	1857.17	16.65	-3.11	0.48	71.34	9.99	-15.64	0.60
130716DC	Figure 8 Source	2013	GOPA	1943.63	16.65	-2.92	0.58	79.90	-	-17.92	0.32
060810 XIII	Happy Harfer Pool, East Side	2006	GOPA	1267.95	9.46	-1.06	0.06	81.25	1.62	-21.55	0.47
050718W	HH Runoff Orange Mat	2005	GOPA	739.91	17.24	0.95	0.50	82.09	1.76	-19.21	0.85
050718V	HH East Pool Edge	2005	GOPA	1962.53	49.65	-0.85	0.16	82.34	1.77	-19.87	0.85
050717E	Figure 8 Source	2005	GOPA	3121.47	122.99	-2.25	0.10	84.51	1.82	-16.52	0.30
190728ZT	Happy Harfer	2019	GOPA	1873.41	48.10	-0.82	0.25	85.84	16.65	-23.38	0.20
150720I	Figure 8	2015	GOPA	-	-	-	-	86.04	16.65	-18.90	0.20
190724ZE	OB1 Heim	2019	GOPA	1134.86	19.20	-1.48	0.41	88.01	16.65	-25.27	0.20

Sample ID	Sample Location	Year	Sampling area	DIC (µM)	DIC (µM) Std Dev	DIC δ13C VPDB (‰)	DIC Std Dev (‰)	DOC (µM)	DOC (µM) Std Dev	DOC δ13C VPDB (‰)	DOC Std Dev (‰)
090802U1	Happy Harfer Source	2009	GOPA	2051.28	82.05	-0.67	0.18	88.85	3.88	-21.59	0.49
170713TC	Happy Harfer	2017	GOPA	2904.70	21.26	1.27	0.34	89.24	16.65	-23.33	0.20
180719SI	Figure 8 Source	2018	GOPA	3118.37	104.64	-0.86	0.24	96.48	16.65	-20.12	0.29
060804D	Skippy's Bathtub Source	2006	GOPA	3126.02	10.33	-3.34	0.01	96.56	1.93	-22.23	0.47
170713TD	OB1-Heim	2017	GOPA	-	-	-	-	98.33	16.65	-22.84	0.20
090725ZA	Happy Harfer Source	2009	GOPA	2712.17	108.49	-1.24	0.18	98.60	4.30	-22.76	0.49
170714SJ	Skippy's Bathtub Source	2017	GOPA	1299.83	16.65	7.76	0.42	101.70	16.65	-22.74	0.20
170714SK	Fudge Factory	2017	GOPA	1638.00	6.66	0.50	0.44	105.64	16.65	-22.57	0.20
180719SM	Happy Harfer	2018	GOPA	2911.25	29.28	0.80	0.44	117.54	16.65	-23.06	0.29
050717D	Skippy's Bathtub Source	2005	GOPA	3140.54	38.00	-2.45	0.07	122.22	2.63	-19.59	0.30
140725TI	Fudge Factory	2014	GOPA	1363.13	16.65	0.52	0.27	134.16	16.65	-22.55	0.28
190728ZQ	Spotted Grizzly	2019	GOPA	816.30	16.65	-4.45	0.24	134.57	16.65	-23.74	0.20
090723D	Dreamcicle	2009	GOPA	774.59	38.73	-2.34	0.54	136.16	5.94	-18.61	0.49
160714E	Phantom Pants	2016	GOPA	92.37	6.66	-8.31	0.76	141.73	6.66	-22.93	0.26
130716SG	Fudge Factory	2013	GOPA	1004.81	24.50	-0.58	0.50	158.87	-	-21.57	0.46
090802B1	Orpheus-in-a-bucket	2009	GOPA	173.64	8.68	-3.66	0.54	161.45	7.04	-16.41	0.49
150720K	Cuppa Muck	2015	GOPA	2993.83	88.53	-1.66	0.51	165.75	16.65	-23.23	0.20
160724G	Green Cheese	2016	GOPA	4883.05	50.30	1.09	0.21	169.98	6.66	-24.86	0.26
050718U	OP Black Mat	2005	GOPA	2727.08	71.45	-2.40	0.01	171.34	3.68	-21.74	0.37
110713S	Figure 8 Source	2011	GOPA	2349.39	66.32	-4.78	0.54	171.39	-	-20.05	1.06
090802V1	Fudge Factory	2009	GOPA	1105.52	55.28	-2.38	0.54	174.37	7.61	-21.40	0.49
190728ZR	Green Cheese	2019	GOPA	2525.58	52.37	1.40	0.45	177.98	16.65	-25.27	0.20

Sample ID	Sample Location	Year	Sampling area	DIC (µM)	DIC (µM) Std Dev	DIC δ13C VPDB (‰)	DIC Std Dev (‰)	DOC (µM)	DOC (µM) Std Dev	DOC δ13C VPDB (‰)	DOC Std Dev (‰)
050718S	Obsidian Pool	2005	GOPA	842.31	28.30	-2.56	0.15	179.84	3.87	-23.06	0.37
090723E	Spear's Latrine	2009	GOPA	2546.49	127.32	-	-	181.00	7.89	-24.23	0.49
050718T	Green Cheese	2005	GOPA	4895.85	24.48	1.44	0.07	183.25	3.94	-23.02	0.37
090725CA	Fudge Factory	2009	GOPA	894.86	26.85	-2.41	0.17	183.46	8.00	-21.84	0.49
140726SN	Green Cheese	2014	GOPA	6020.22	159.25	0.94	0.20	183.70	16.65	-25.18	0.36
090723C	Skippy's Bathtub Source	2009	GOPA	1714.98	51.45	-0.54	0.21	185.40	8.09	-23.66	0.49
090723J	Green Cheese	2009	GOPA	5254.30	210.17	1.70	0.18	194.64	8.49	-22.09	0.49
150727X	Pedro's Tarpit	2015	GOPA	128.04	16.65	-10.99	0.47	194.91	16.65	-26.09	0.20
090723F	Figure 8 Pool	2009	GOPA	1366.95	68.35	-1.96	0.54	195.41	8.52	-19.82	0.49
160714C	OB1-Heim	2016	GOPA	805.48	41.08	-3.78	0.74	196.72	6.66	-22.55	0.26
100807SA	Skippy's Bathtub	2010	GOPA	2303.73	22.78	-1.57	0.37	205.28	7.43	-27.24	1.17
160714D	Fudge Factory	2016	GOPA	577.54	16.65	-2.70	0.66	206.68	6.66	-22.25	0.26
190724ZD	Skippy's Bathtub	2019	GOPA	1119.41	16.65	-2.65	0.30	210.20	16.65	-22.96	0.20
170713TE	Spear's Latrine	2017	GOPA	3315.34	103.05	-0.72	0.20	213.14	16.65	-23.91	0.20
160714B	Skippy's Bathtub	2016	GOPA	1150.48	16.65	-2.40	0.49	215.08	-	-21.17	-
190728ZV	Phantom Pants	2019	GOPA	775.84	2.27	-2.87	0.97	216.08	16.65	-23.40	0.20
190728ZS	Muddy Pizza	2019	GOPA	1051.19	74.60	-2.91	1.56	225.35	16.65	-17.00	0.20
090725XA	South Obsidian Pool	2009	GOPA	973.62	19.47	-0.96	0.20	231.01	6.93	-25.04	1.00
190724ZB	Figure 8	2019	GOPA	2389.71	16.65	-1.93	0.30	233.06	3.33	-21.52	0.20
150720J	Obsidian Pool	2015	GOPA	1124.54	74.02	-3.24	0.55	237.93	16.65	-23.95	0.20
180719SL	South Obsidian	2018	GOPA	1340.66	16.04	0.96	0.86	240.00	16.65	-22.51	0.22
070715T	Green Cheese 57	2007	GOPA	2002.25	34.33	-2.29	1.01	244.25	40.72	-22.25	0.74
090802S1	Vomit Pool	2009	GOPA	3812.82	152.51	0.58	0.18	245.19	10.69	-21.82	0.49

Sample ID	Sample Location	Year	Sampling area	DIC (µM)	DIC (µM) Std Dev	DIC δ13C VPDB (‰)	DIC Std Dev (‰)	DOC (µM)	DOC (µM) Std Dev	DOC δ13C VPDB (‰)	DOC Std Dev (‰)
100807XA	Obsidian Pool	2010	GOPA	1010.66	22.09	-3.12	0.25	248.25	14.04	-24.44	0.56
090725BA	Vomit Pool	2009	GOPA	3637.94	145.52	0.73	0.18	248.89	10.86	-21.33	0.49
140725TK	Obsidian Pool	2014	GOPA	2070.91	16.65	0.91	0.27	250.32	16.65	-24.43	0.28
120712TD	Green Cheese	2012	GOPA	6294.32	155.22	-0.68	0.44	252.86	16.65	-21.31	1.29
170714SI	Obsidian Pool	2017	GOPA	776.08	6.66	0.78	0.44	257.74	16.65	-23.47	0.20
JRH110713N	Vomit Pool	2011	GOPA	5248.57	97.21	-1.76	0.38	259.30	5.48	-25.09	0.60
150727T	Fudge Factory (main source)	2015	GOPA	771.69	16.65	-1.57	0.42	262.94	16.65	-22.25	0.20
110713Z	Brittany's Feast	2011	GOPA	2363.48	34.26	-6.76	0.30	263.04	9.84	-23.25	0.60
070715R	Obsidian Pool	2007	GOPA	507.68	18.59	-4.63	1.01	275.71	28.66	-22.83	0.79
070715U	Obsidian Pool Black Mat (BITNB)	2007	GOPA	1722.07	21.47	-4.47	1.01	281.68	39.24	-22.88	0.92
090723K	Obsidian Pool Black Mat	2009	GOPA	1525.52	45.77	-1.32	0.16	285.60	12.46	-24.53	0.49
190724ZA	South Obsidian	2019	GOPA	913.15	43.56	-2.86	0.87	286.47	16.65	-22.49	0.20
100807OA	Submarine	2010	GOPA	1088.52	7.42	-3.11	0.27	286.97	8.18	-24.12	0.84
160724D	Obsidian Pool	2016	GOPA	-	-	-	-	296.93	6.66	-24.06	0.26
110713A	Green Cheese	2011	GOPA	5773.62	50.15	-0.41	0.57	298.94	-	-22.70	0.82
JRH110713M	Skippy's Bathtub	2011	GOPA	1501.67	11.91	-3.51	0.68	319.14	-	-22.89	0.82
140726SS	OB1-Heim	2014	GOPA	-	-	-	-	348.17	16.65	-14.10	0.28
160724H	Spotted Grizzly	2016	GOPA	7381.11	79.90	-2.16	0.21	351.23	6.66	-23.53	0.26
100807WA	Hot Shit Hill	2010	GOPA	235.44	2.19	-3.28	0.78	392.46	5.92	-19.70	0.25
100808GCL	Green Cheese	2010	GOPA	72.47	8.24	-	-	405.26	9.91	-23.86	0.30
110713U	Obsidian Pool	2011	GOPA	1594.91	11.27	-4.45	0.97	463.79	7.48	-25.61	0.60
060804E	Obsidian	2006	GOPA	722.23	8.30	-4.19	0.04	474.17	0.98	-24.35	0.05
090723I	Phantom Pants	2009	GOPA	980.51	49.03	-2.55	0.54	480.20	20.94	-24.65	0.49
090723G	Obsidian Pool	2009	GOPA	-	-	-	-	498.03	21.72	-25.74	0.49

Sample ID	Sample Location	Year	Sampling area	DIC (µM)	DIC (µM) Std Dev	DIC δ13C VPDB (‰)	DIC Std Dev (‰)	DOC (µM)	DOC (µM) Std Dev	DOC δ13C VPDB (‰)	DOC Std Dev (‰)
110713Y	Obsidian Pool Black Mat	2011	GOPA	3055.48	0.36	-4.68	0.50	507.17	19.72	-25.08	0.60
190728ZU	Dreamsicle	2019	GOPA	164.95	16.65	-5.02	0.24	531.44	16.65	-16.08	0.20
180719SN	Spotted Grizzly	2018	GOPA	6829.83	167.61	-0.88	0.22	612.57	16.65	-26.75	0.29
060804B	Green Cheese	2006	GOPA	4044.19	28.53	1.38	0.08	618.08	4.35	-19.69	0.11
140725TH	Spotted Grizzly	2014	GOPA	6607.16	33.28	-1.73	0.20	650.32	16.65	-25.64	0.33
090725AA	Foam Pool	2009	GOPA	9233.45	369.34	-0.89	0.18	674.34	29.41	-25.94	0.49
180719SO	Phantom Pants	2018	GOPA	1065.75	16.65	-2.58	0.20	696.64	16.65	-26.30	0.20
JRH110713L	Owl	2011	GOPA	254.58	69.87	-	-	737.74	30.13	-18.28	0.60
090802T1	Foam Pool	2009	GOPA	10389.74	207.79	-1.55	0.20	786.74	23.60	-26.44	1.00
110713V	Foam Pool	2011	GOPA	10609.80	103.78	-3.49	0.20	822.49	8.87	-26.40	0.60
090802Q1	Witch's Brew	2009	GOPA	2243.61	112.18	-2.75	0.54	853.85	37.24	-17.70	0.49
090725YA	Witch's Brew	2009	GOPA	2505.88	125.29	-	-	920.20	40.14	-18.00	0.49
110713T	Spotted Grizzly	2011	GOPA	9280.92	11.11	-3.95	0.16	920.83	7.74	-26.46	0.60
160724JN8	GOPA Pond North	2016	GOPA	7345.15	21.08	8.24	0.59	2363.06	15.37	-24.43	0.20
150717FB	The Gap	2015	Norris Geyser Basin	-	-	-	-	17.93	16.65	-24.72	0.20
110910G	Breathe Deep	2011	Norris Geyser Basin	-	-	-	-	18.99	-	-26.02	0.91
150728A	Log Stew	2015	Norris Geyser Basin	19.48	16.65	-	-	20.99	16.65	-24.87	0.20
160719E	Red Bubbler	2016	Norris Geyser Basin	-	-	-	-	22.08	6.66	-23.93	0.29
160719D	Perpetual Spouter	2016	Norris Geyser Basin	123.17	16.65	-2.61	0.49	23.73	6.66	-24.70	0.29
180721SV	Perpetual Spouter	2018	Norris Geyser Basin	111.90	16.65	-3.24	0.20	25.34	16.65	-28.12	0.20
180721SU	Red Bubbler	2018	Norris Geyser Basin	-	-	-	-	25.92	16.65	-25.65	0.20
150720FH	The Gap	2015	Norris Geyser Basin	109.83	16.65	-4.59	0.47	26.39	16.65	-25.32	0.20

Sample ID	Sample Location	Year	Sampling area	DIC (µM)	DIC (µM) Std Dev	DIC δ13C VPDB (‰)	DIC Std Dev (‰)	DOC (µM)	DOC (µM) Std Dev	DOC δ13C VPDB (‰)	DOC Std Dev (‰)
120718SO	Perpetual Spouter Source	2012	Norris Geyser Basin	118.74	3.76	-0.91	0.74	27.21	3.24	-24.84	0.21
110719A	Mickey Face	2011	Norris Geyser Basin	-	-	-	-	27.47	-	-20.61	-
150724FN	Beowulf	2015	Norris Geyser Basin	632.55	16.65	-0.70	0.47	27.90	16.65	-23.57	0.20
150724FO	Log Stew	2015	Norris Geyser Basin	-	-	-	-	27.93	16.65	-25.50	0.20
140804SR	Perpetual Spouter Source	2014	Norris Geyser Basin	82.40	16.65	1.74	0.91	28.21	16.65	-25.14	0.28
160719F	The Gap	2016	Norris Geyser Basin	40.21	16.65	-5.66	0.59	29.52	6.66	-27.51	0.29
180721SS	Hoku	2018	Norris Geyser Basin	432.95	14.79	-1.84	1.07	30.79	16.65	-26.24	0.22
150728Y	The Gap	2015	Norris Geyser Basin	60.20	16.65	-	-	31.80	16.65	-25.28	0.20
120714TR	Mickey Face Source	2012	Norris Geyser Basin	43.14	3.76	-4.27	0.74	31.82	3.24	-24.30	0.21
120718SQ	Don't Tell Scottie (Scottie Doesn't Know)	2012	Norris Geyser Basin	107.95	5.06	-3.71	0.49	32.03	4.26	-24.35	0.39
150728B	Dragonmail	2015	Norris Geyser Basin	-	-	-	-	32.48	16.65	-23.34	0.20
180721SR	Grendal	2018	Norris Geyser Basin	-	-	-	-	32.55	16.65	-25.92	0.22
150720FI	Ferric Tenticles	2015	Norris Geyser Basin	255.27	16.65	-1.69	0.20	32.66	16.65	-21.30	0.20
110910C	Dermatitis	2011	Norris Geyser Basin	43.99	-	-31.86	0.90	33.10	-	-24.07	0.91
190730VH	The Gap	2019	Norris Geyser Basin	204.28	16.65	-4.05	0.30	33.55	16.65	-25.20	0.20
180718SG	Arrow	2018	Norris Geyser Basin	-	-	-	-	34.11	16.65	-26.74	0.22
140725FB	Red Bubbler (source)	2014	Norris Geyser Basin	-	-	-	-	35.70	16.65	-24.58	0.28
120714TO	Red Bubbler Source	2012	Norris Geyser Basin	17.31	-	-	-	35.82	3.24	-24.91	0.62

Sample ID	Sample Location	Year	Sampling area	DIC (µM)	DIC (µM) Std Dev	DIC δ13C VPDB (‰)	DIC Std Dev (‰)	DOC (µM)	DOC (µM) Std Dev	DOC δ13C VPDB (‰)	DOC Std Dev (‰)
170725TN	Perpetual Spouter	2017	Norris Geyser Basin	87.54	6.66	3.85	0.44	35.92	16.65	-29.40	0.42
180718SH	Banana Flex	2018	Norris Geyser Basin	464.90	21.06	-1.35	0.88	36.01	16.65	-24.59	0.22
110910B	Cream of Wheat	2011	Norris Geyser Basin	-	-	-	-	36.58	-	-26.12	0.91
110719P	Cinder Pool	2011	Norris Geyser Basin	591.00	1.17	-4.24	0.20	36.69	-	-10.77	-
150722FK	Coral Snake	2015	Norris Geyser Basin	125.34	16.65	-2.59	0.47	37.10	16.65	-25.53	0.20
120718SP	Di Di Yu	2012	Norris Geyser Basin	276.29	3.76	-15.32	0.74	38.45	1.87	-25.82	0.66
110910A	Ginger Kid	2011	Norris Geyser Basin	82.96	-	-8.96	0.90	40.00	-	-25.92	0.91
180721ST	Middle Realgar Spring	2018	Norris Geyser Basin	1685.63	68.88	-1.21	0.52	41.05	16.65	-24.67	0.22
100804 E1	Don't Tell Scottie	2010	Norris Geyser Basin	137.98	0.95	-	-	41.31	4.48	-27.94	0.90
120718SK	The Gap Source	2012	Norris Geyser Basin	25.94	5.14	-4.10	0.80	42.47	1.87	-25.70	0.66
150724FP	Woodchip Beach	2015	Norris Geyser Basin	-	-	-	-	42.87	16.65	-24.49	0.20
140803FN	The Gap	2014	Norris Geyser Basin	210.86	16.65	-1.07	0.23	43.61	16.65	-26.16	0.28
160719B	Dragon Spring	2016	Norris Geyser Basin	1515.07	31.17	-2.95	0.28	44.10	6.66	-25.39	0.26
110719X	Don't Tell Scottie	2011	Norris Geyser Basin	172.51	-	-3.81	0.88	44.31	-	-24.67	1.39
150724FM	Eisentintenfis ch	2015	Norris Geyser Basin	41.22	16.65	-	-	44.86	16.65	-25.26	0.20
110910H	Something Lame	2011	Norris Geyser Basin	-	-	-	-	46.94	-	-24.47	0.91
120718DK	Cinder Pool	2012	Norris Geyser Basin	1028.85	28.33	-3.13	0.29	47.86	4.26	-20.26	0.39
110719W	Red Bubbler	2011	Norris Geyser Basin	-	-	-	-	47.90	-	-25.35	1.39
150728C	Eisentintenfis ch	2015	Norris Geyser Basin	18.11	16.65	-	-	47.94	16.65	-23.87	0.20
160719C	HFS	2016	Norris Geyser Basin	403.19	16.65	-3.67	0.49	48.33	6.66	-24.94	0.26
160719A	Eisen Tintinfisch	2016	Norris Geyser Basin	31.10	16.65	-5.86	0.59	48.97	6.66	-24.27	0.29

Sample ID	Sample Location	Year	Sampling area	DIC (µM)	DIC (µM) Std Dev	DIC δ13C VPDB (‰)	DIC Std Dev (‰)	DOC (µM)	DOC (µM) Std Dev	DOC δ13C VPDB (‰)	DOC Std Dev (‰)
180721SQ	Eisentintenfisch	2018	Norris Geyser Basin	60.14	16.65	-13.85	0.20	49.37	16.65	-25.37	0.20
130712TM	Don't Tell Scottie	2013	Norris Geyser Basin	200.80	-	-2.69	0.54	50.62	-	-26.42	0.23
120718SM	Darko's Vision	2012	Norris Geyser Basin	254.82	5.14	-1.87	0.80	50.71	1.87	-17.32	0.66
180718SD	Beowulf	2018	Norris Geyser Basin	1421.37	16.65	-2.22	0.20	51.68	16.65	-26.10	0.20
130723SY	Beowulf east source	2013	Norris Geyser Basin	921.64	16.98	-3.21	0.50	52.56	-	-25.96	0.45
140803FM	Brain	2014	Norris Geyser Basin	-	-	-	-	53.73	16.65	-26.79	0.31
170725TI	Jack Sparrow	2017	Norris Geyser Basin	-	-	-	-	53.85	16.65	-21.67	0.20
170715SN	HFS	2017	Norris Geyser Basin	535.33	6.66	-0.70	0.44	55.23	8.33	-24.90	0.20
190730VG	Eisentintenfisch	2019	Norris Geyser Basin	57.32	16.65	-4.92	0.30	55.48	3.33	-25.35	0.20
170715SO	Eisen Tintenfisch	2017	Norris Geyser Basin	74.72	1.67	-6.01	0.37	55.70	8.33	-24.15	0.20
180721SP	HFS	2018	Norris Geyser Basin	-	-	-	-	56.52	16.65	-24.50	0.20
150728Z	Woodchip Beach	2015	Norris Geyser Basin	-	-	-	-	56.58	16.65	-24.00	0.20
110910E	Coke Fiend	2011	Norris Geyser Basin	579.64	-	-3.38	0.90	57.39	-	-24.73	1.02
190730VD	HFS	2019	Norris Geyser Basin	629.39	16.65	-2.91	0.30	57.79	3.33	-24.11	0.20
180718SE	Full Cup	2018	Norris Geyser Basin	1154.23	43.11	-1.23	0.46	60.03	16.65	-26.19	0.22
140803FL	Soggy Crik	2014	Norris Geyser Basin	-	-	-	-	61.46	16.65	-22.40	0.28
130719DJ	Beowulf East	2013	Norris Geyser Basin	1023.85	28.91	-3.89	0.66	61.89	-	-24.50	0.40
130723SX	HFS	2013	Norris Geyser Basin	541.19	-	-0.45	0.69	62.02	-	-24.81	0.45
160719Z	Cinder Pool	2016	Norris Geyser Basin	502.83	16.65	-2.52	0.41	64.87	6.66	-20.75	0.29
170715SP	Dragon Spring	2017	Norris Geyser Basin	1960.40	12.49	-2.47	0.37	65.07	8.33	-22.90	0.20
130723SW	Merica	2013	Norris Geyser Basin	172.81	16.65	-4.00	0.69	67.62	-	-25.00	0.45

Sample ID	Sample Location	Year	Sampling area	DIC (µM)	DIC (µM) Std Dev	DIC δ13C VPDB (‰)	DIC Std Dev (‰)	DOC (µM)	DOC (µM) Std Dev	DOC δ13C VPDB (‰)	DOC Std Dev (‰)
110719Q	Little Cinder Pool	2011	Norris Geyser Basin	448.80	1.18	-4.89	0.25	67.85	-	-21.90	1.39
190730VE	Something Good	2019	Norris Geyser Basin	427.14	16.65	-3.58	0.30	68.45	3.33	-23.77	0.20
190730VF	Comet	2019	Norris Geyser Basin	988.87	16.65	-3.07	0.30	70.49	3.33	-23.11	0.20
140727FD	Beowulf E Iron Mat	2014	Norris Geyser Basin	174.74	16.65	-1.17	0.91	71.92	16.65	-24.53	0.31
170725TJ	Dragon East OF	2017	Norris Geyser Basin	-	-	-	-	73.30	16.65	-24.69	0.20
170725TK	Dragon East Source	2017	Norris Geyser Basin	2167.35	79.19	-1.00	0.34	75.83	16.65	-25.86	0.20
170715SM	Cinder Pool	2017	Norris Geyser Basin	773.64	6.66	-0.47	0.44	75.85	8.33	-18.73	0.20
130719DK	Dragon Tail Red	2013	Norris Geyser Basin	-	-	-	-	76.31	-	-24.99	0.40
140727FE	Flamethrower	2014	Norris Geyser Basin	554.99	16.65	-0.05	0.91	77.48	16.65	-26.15	0.28
130719DL	Dragon tail yellow surface	2013	Norris Geyser Basin	180.20	-	-2.37	0.69	77.62	-	-24.90	0.40
100803O1	Cinder Pool	2010	Norris Geyser Basin	660.69	2.44	-2.39	0.27	79.62	5.00	-17.75	0.33
140803FO	HFS after rain	2014	Norris Geyser Basin	753.41	16.65	-2.61	0.27	79.69	16.65	-24.90	0.31
140803FK	Comet	2014	Norris Geyser Basin	35.85	16.65	-	-	80.88	16.65	-24.29	0.28
130719DI	Dragon Mouth source	2013	Norris Geyser Basin	2436.08	34.74	-3.86	0.64	81.26	-	-24.33	0.40
130723SZ	Dragon Spring source	2013	Norris Geyser Basin	1837.86	16.03	-3.41	0.36	81.42	-	-26.48	0.45
140803FI	HFS	2014	Norris Geyser Basin	401.90	16.65	-3.12	0.27	81.72	16.65	-24.66	0.31
180718SF	Cinder Pool	2018	Norris Geyser Basin	552.97	13.24	-0.76	0.60	82.72	16.65	-26.49	0.29
170725TH	Tribble	2017	Norris Geyser Basin	500.02	9.99	-3.88	0.43	87.83	16.65	-24.10	0.20
140803FJ	Something good	2014	Norris Geyser Basin	-	-	-	-	89.58	16.65	-24.00	0.28
190730VC	Cinder Pool	2019	Norris Geyser Basin	1197.49	16.65	-2.15	0.30	92.69	16.65	-14.35	0.22
100804X1	Chili Blow Out	2010	Norris Geyser Basin	70.07	1.21	-	-	92.85	4.48	-21.23	0.90

Sample ID	Sample Location	Year	Sampling area	DIC (µM)	DIC (µM) Std Dev	DIC δ13C VPDB (‰)	DIC Std Dev (‰)	DOC (µM)	DOC (µM) Std Dev	DOC δ13C VPDB (‰)	DOC Std Dev (‰)
110910F	Dog Bone	2011	Norris Geyser Basin	813.56	-	-1.15	0.90	106.53	-	-15.80	0.91
120714TQ	Tantalus Creek	2012	Norris Geyser Basin	46.89	3.76	-3.81	0.74	112.41	3.24	-22.15	0.62
140727FF	Eisen Tintenfisch Mutant	2014	Norris Geyser Basin	40.17	16.65	-	-	112.44	16.65	-23.58	0.31
140804SV	Minnie Source	2014	Norris Geyser Basin	75.37	16.65	-	-	157.20	16.65	-24.81	0.28
170725TL	Mickey Face	2017	Norris Geyser Basin	262.59	1.67	-4.18	0.37	173.38	8.33	-21.50	0.20
120718SL	Dirty Dishwater	2012	Norris Geyser Basin	957.35	-	2.23	-	357.22	1.87	-18.96	0.66
100803U1	Turnadeli (Turnada Alley)	2010	Norris Geyser Basin	905.85	10.28	-8.38	0.27	1716.94	17.73	-23.46	0.24
110719Y	Perpetual Spouter	2011	Norris Geyser Basin	105.45	-	-5.34	0.73	-	-	-	-
110719Z	Di Di Yu	2011	Norris Geyser Basin	134.95	4.83	-	-	-	-	-	-
150720FJ	Honey Glazed	2015	Norris Geyser Basin	233.79	16.65	-2.34	0.47	-	-	-	-
150723M	OG Mat	2015	Rabbit Creek - North	3605.59	58.77	-1.50	0.26	24.48	16.65	-24.05	0.20
120718TO	Peekaboo	2012	Rabbit Creek - North	3100.22	60.46	-2.88	0.60	27.58	4.26	-20.20	0.39
JRH110708B	Painful Past (Now with heartbeat action!)	2011	Rabbit Creek - North	-	-	-	-	28.86	-	-22.47	-
090726R1	Painful Past	2009	Rabbit Creek - North	25.63	0.51	-	-	31.11	1.05	-24.05	0.26
090726M1	Old Blue Eyes Left Eye	2009	Rabbit Creek - North	2935.70	117.43	-1.57	0.18	31.79	1.07	-20.66	0.26
090726P1	Hammer Source	2009	Rabbit Creek - North	2620.86	104.83	-1.07	0.34	32.90	1.11	-18.77	0.26
150723L	Rabbit Creek Pink Mat	2015	Rabbit Creek - North	3567.78	57.56	-1.36	0.26	34.55	16.65	-24.95	0.20
150723N	Green Filaments	2015	Rabbit Creek - North	3547.67	89.26	-1.37	0.26	34.69	16.65	-24.11	0.20
120718TM	Tarantula Surface	2012	Rabbit Creek - North	2774.33	85.87	-2.63	0.48	37.29	1.87	-23.82	0.66

Sample ID	Sample Location	Year	Sampling area	DIC (µM)	DIC (µM) Std Dev	DIC δ13C VPDB (‰)	DIC Std Dev (‰)	DOC (µM)	DOC (µM) Std Dev	DOC δ13C VPDB (‰)	DOC Std Dev (‰)
090726S1	Nefarious Now	2009	Rabbit Creek - North	32.61	0.65	-	-	37.55	1.13	-22.47	1.00
BSC110720C	Old Blue Eyes (Right Eye)	2011	Rabbit Creek - North	2980.34	99.83	-3.95	0.20	38.15	-	-23.85	1.39
JRH110708A	Rose Terrace Pool	2011	Rabbit Creek - North	2998.01	66.64	-3.27	0.53	39.91	-	-25.96	-
130713TO	Tarantula	2013	Rabbit Creek - North	2473.81	191.70	-1.90	0.58	41.61	-	-24.51	0.23
190727ZL	Rabbit Source	2019	Rabbit Creek - North	3412.21	219.24	-0.71	0.42	44.60	3.33	-25.09	0.20
120718TK	Rum Runner	2012	Rabbit Creek - North	93.52	5.06	3.81	0.49	46.21	9.99	-21.18	0.60
170713SC	Peekaboo Source	2017	Rabbit Creek - North	2761.43	94.32	0.28	0.20	46.75	8.33	-24.53	0.20
170713SF	The Hammer (Head)	2017	Rabbit Creek - North	2667.35	83.53	0.40	0.20	49.59	8.33	-23.52	0.20
190727ZN	Chocolate Chip Cookie	2019	Rabbit Creek - North	91.59	16.65	-9.27	0.24	58.20	16.65	-23.88	0.20
110708B	Nefarious Now	2011	Rabbit Creek - North	114.52	-	-15.81	0.88	59.07	-	-24.68	0.59
BSC110720B	Old Blue Eyes (Left Eye)	2011	Rabbit Creek - North	2951.12	130.85	-4.01	0.32	62.70	-	-22.24	0.82
110708C	Sex on the Beach	2011	Rabbit Creek - North	145.28	27.32	-	-	63.09	-	-24.36	0.59
170713SD	Rum Runner	2017	Rabbit Creek - North	560.29	6.66	-4.74	0.44	64.96	16.65	-26.10	0.55
110708A	Hammer Source	2011	Rabbit Creek - North	2773.08	37.13	-3.72	0.88	66.09	-	-23.17	1.06
140805SY	No Filter	2014	Rabbit Creek - North	-	-	-	-	73.35	16.65	-24.07	0.20
140802SE	Sex on the Beach	2014	Rabbit Creek - North	407.17	16.65	-0.81	0.91	74.07	16.65	-23.55	0.20
190727ZO	Shrimp	2019	Rabbit Creek - North	4013.08	172.29	2.59	0.20	81.90	16.65	-23.62	0.20
170713SE	Sex on the Beach	2017	Rabbit Creek - North	124.69	6.66	-0.19	0.44	85.36	16.65	-21.98	0.20
120718TN	Tanantula Deep	2012	Rabbit Creek - North	2548.23	56.71	0.85	0.53	111.28	1.87	-26.82	0.66
120718TJ	Sex on the Beach	2012	Rabbit Creek - North	72.70	3.76	-10.72	0.74	114.41	10.12	-21.36	0.41
120718TL	Tiny Danza's Meat Flute	2012	Rabbit Creek - North	82.90	5.14	-8.68	0.80	126.98	1.87	-23.55	0.66

Sample ID	Sample Location	Year	Sampling area	DIC (µM)	DIC (µM) Std Dev	DIC δ13C VPDB (‰)	DIC Std Dev (‰)	DOC (µM)	DOC (µM) Std Dev	DOC δ13C VPDB (‰)	DOC Std Dev (‰)
110708D	The Rum Runner	2011	Rabbit Creek - North	183.33	35.36	-	-	189.64	-	-22.98	0.59
090726T1	Frightening Future	2009	Rabbit Creek - North	309.87	6.20	-6.24	0.20	194.38	5.83	-26.16	1.00
190727ZK	Gravy Boat	2019	Rabbit Creek - North	572.42	16.65	-1.91	0.24	199.58	16.65	-23.14	0.20
140802SD	Rum Runner	2014	Rabbit Creek - North	667.33	16.65	-6.57	0.27	267.20	16.65	-23.63	0.20
120718TI	Dew U	2012	Rabbit Creek - North	151.36	3.76	-8.24	0.74	272.82	1.87	-23.60	0.66
140805SX	Rum Runner	2014	Rabbit Creek - North	585.63	16.65	-6.57	0.27	885.26	16.65	-24.61	0.59
190727ZR	Whole Milk	2019	Rabbit Creek - North	826.33	16.65	-2.72	0.24	-	-	-	-
BSC110720A	Rabbit's Nest	2011	Rabbit Creek - North	3154.52	137.66	-4.57	0.20	-	-	-	-
JRH110708C	Rabbit Creek Source	2011	Rabbit Creek - North	3456.03	69.31	-4.02	0.20	-	-	-	-
090803YA	Hissing Cliff	2009	Rabbit Creek - South	2921.22	116.85	0.18	0.18	17.98	0.61	-21.81	0.26
090803VA	Time Bomb	2009	Rabbit Creek - South	252.84	7.59	1.66	0.64	18.91	0.64	-24.03	0.26
JRH110710E	Spitting Cobra	2011	Rabbit Creek - South	1434.11	44.17	0.49	1.01	20.76	-	-24.82	-
180718TZ	Big Filter	2018	Rabbit Creek - South	346.09	16.65	-4.43	0.20	24.99	16.65	-25.43	0.20
110720H1	Harp	2011	Rabbit Creek - South	1761.13	45.84	-0.01	0.30	25.33	-	-21.91	1.02
160725P	Shipyard	2016	Rabbit Creek - South	796.29	16.65	-2.43	0.49	26.79	6.66	-20.35	0.26
140724TE	Rogue Dead Guy	2014	Rabbit Creek - South	830.21	39.13	-1.93	0.28	28.12	16.65	-22.96	0.28
160725M	Iron Fist	2016	Rabbit Creek - South	67.27	16.65	-4.29	0.49	37.50	6.66	-21.15	0.29
110710A	Hissing Cliff	2011	Rabbit Creek - South	2939.70	7.83	-1.70	0.62	40.75	-	-24.83	-
160725O	Hissing Cliff	2016	Rabbit Creek - South	3483.29	138.92	1.04	0.28	42.52	6.66	-25.02	0.29
190718VB	Zen Garden Source	2019	Rabbit Creek - South	6032.95	229.40	1.17	0.20	43.42	3.33	-25.21	0.20
140805TM	Big Filter	2014	Rabbit Creek - South	376.29	16.65	0.69	0.76	44.49	16.65	-25.28	0.20

Sample ID	Sample Location	Year	Sampling area	DIC (µM)	DIC (µM) Std Dev	DIC δ13C VPDB (‰)	DIC Std Dev (‰)	DOC (µM)	DOC (µM) Std Dev	DOC δ13C VPDB (‰)	DOC Std Dev (‰)
090803ZA	Pau Pau Long	2009	Rabbit Creek - South	338.00	12.34	2.19	0.16	45.07	1.52	-22.37	0.26
150719D	Hissing Cliff	2015	Rabbit Creek - South	3551.78	18.00	-0.07	0.26	48.15	16.65	-24.48	0.20
140730TK	Iron Fist	2014	Rabbit Creek - South	-	-	-	-	51.34	16.65	-25.42	0.31
180718TE	Aqua Marine	2018	Rabbit Creek - South	1266.54	58.61	-0.32	0.80	52.78	16.65	-22.00	0.20
160725Q	Allagash	2016	Rabbit Creek - South	467.39	22.74	-10.03	1.16	53.90	6.66	-25.66	0.26
110710V	Zen Garden	2011	Rabbit Creek - South	5689.36	115.34	-1.48	0.20	54.86	-	-25.03	0.82
120713TL	Aqua Marine (aka PNAS Pool)	2012	Rabbit Creek - South	683.83	21.64	-2.97	0.37	58.42	11.59	-20.19	0.39
190718VD	Leinenkugels	2019	Rabbit Creek - South	534.65	16.65	-1.08	0.24	62.01	16.65	-23.94	0.20
120713TH	Harp	2012	Rabbit Creek - South	2204.88	55.65	-0.89	0.48	64.79	4.26	-24.70	0.39
140724TC	Aqua Marine (aka PNAS Pool)	2014	Rabbit Creek - South	815.26	16.65	-3.04	0.27	66.02	16.65	-23.95	0.28
190718VC	Epiphany	2019	Rabbit Creek - South	2590.40	80.74	1.80	0.20	68.45	16.65	-25.37	0.20
190727VL	Iron Fist	2019	Rabbit Creek - South	110.23	16.65	-3.49	0.20	70.96	16.65	-20.01	0.20
110710W	Hell's Gate	2011	Rabbit Creek - South	120.01	17.83	-	-	71.79	-	-22.57	0.59
140805TL	Aqua Marine (aka PNAS Pool)	2014	Rabbit Creek - South	599.66	16.65	-2.90	0.27	72.62	16.65	-22.78	0.28
180718TA	Epiphany	2018	Rabbit Creek - South	2411.11	20.72	1.50	0.23	76.00	16.65	-24.68	0.22
160725L	Aquamarine	2016	Rabbit Creek - South	762.63	14.87	-3.20	0.90	76.99	6.66	-23.81	0.29
KF180718E	Iron Fist	2018	Rabbit Creek - South	250.92	16.65	-4.55	0.20	77.20	16.65	-20.10	0.42
190727VR	Aquamarine	2019	Rabbit Creek - South	704.70	29.32	-1.65	0.99	79.68	16.65	-24.24	0.20
KF180718F	Heady Topper	2018	Rabbit Creek - South	1589.39	33.63	1.68	0.51	86.48	16.65	-23.69	0.20

Sample ID	Sample Location	Year	Sampling area	DIC (µM)	DIC (µM) Std Dev	DIC δ13C VPDB (‰)	DIC Std Dev (‰)	DOC (µM)	DOC (µM) Std Dev	DOC δ13C VPDB (‰)	DOC Std Dev (‰)
110720F1	SHIfT Hole	2011	Rabbit Creek - South	1315.96	16.66	-2.30	0.75	93.56	-	-22.83	0.59
180718TD	Monk's CafÃ©	2018	Rabbit Creek - South	1486.15	6.79	-0.31	0.34	114.63	16.65	-24.22	0.29
190727VQ	Whistilng Marmot	2019	Rabbit Creek - South	-	-	-	-	117.44	16.65	-24.96	0.20
110710X	Dragon's Belly	2011	Rabbit Creek - South	-	-	-	-	132.82	-	-25.76	0.59
140805TO	Harp	2014	Rabbit Creek - South	2082.72	16.65	0.71	0.23	143.47	16.65	-26.65	0.20
170723TR	Aqua Marine	2017	Rabbit Creek - South	492.23	16.65	-5.19	0.42	146.91	16.65	-21.79	0.20
140805TK	Bozone	2014	Rabbit Creek - South	-	-	-	-	150.51	16.65	-23.43	0.28
140730TH	Kiltlifter	2014	Rabbit Creek - South	2539.56	51.14	-2.19	0.32	159.13	16.65	-23.47	0.28
140730TI	Old Chub	2014	Rabbit Creek - South	170.22	16.65	-2.01	0.38	160.63	16.65	-24.93	0.20
170723TW	Vince's Man Cave	2017	Rabbit Creek - South	1629.38	74.57	-1.47	0.41	168.86	16.65	-26.28	0.20
190727VN	Monk's Cafe	2019	Rabbit Creek - South	938.32	32.18	-2.26	0.89	169.87	16.65	-24.94	0.20
140805TJ	Allagash	2014	Rabbit Creek - South	1002.37	16.65	-1.77	0.27	185.38	16.65	-24.06	0.28
120713TK	Kiltlifter	2012	Rabbit Creek - South	1472.88	38.60	-3.29	0.48	192.18	16.65	-23.68	0.67
140805TN	Shipyard	2014	Rabbit Creek - South	318.55	16.65	1.33	0.91	208.99	16.65	-23.80	0.31
170723TU	Allagash	2017	Rabbit Creek - South	1188.75	6.66	0.39	0.44	217.43	8.33	-22.09	0.20
110710D	Kiltlifter	2011	Rabbit Creek - South	1704.91	1.79	-2.08	0.47	217.83	-	-24.80	0.59
140730TJ	Allagash	2014	Rabbit Creek - South	1562.92	16.65	-0.61	0.27	224.43	16.65	-20.26	0.31
150719FG	Shipyard	2015	Rabbit Creek - South	645.37	16.65	0.99	0.47	228.13	16.65	-22.71	0.20
170723TT	Shipyard	2017	Rabbit Creek - South	892.41	16.65	-3.34	0.42	231.41	16.65	-21.60	0.42
170723TV	Kiltlifter	2017	Rabbit Creek - South	1589.52	12.49	-3.32	0.37	252.56	16.65	-23.09	0.20
110720G1	Aqua Marine	2011	Rabbit Creek - South	375.71	21.64	-	-	252.59	-	-26.84	0.59

Sample ID	Sample Location	Year	Sampling area	DIC (µM)	DIC (µM) Std Dev	DIC δ13C VPDB (‰)	DIC Std Dev (‰)	DOC (µM)	DOC (µM) Std Dev	DOC δ13C VPDB (‰)	DOC Std Dev (‰)
120713TI	Allagash	2012	Rabbit Creek - South	1122.43	19.82	-1.91	0.29	267.79	16.65	-20.56	0.37
160725N	Shift Hole	2016	Rabbit Creek - South	1644.89	21.66	-2.26	0.28	269.69	6.66	-25.22	0.26
190727VP	Elmo's Screech	2019	Rabbit Creek - South	1005.32	11.12	0.92	0.73	270.85	16.65	-23.01	0.22
120713TJ	SHIfT Hole	2012	Rabbit Creek - South	-	-	-	-	271.74	-	-24.40	0.41
KF180718G	Focal Banger	2018	Rabbit Creek - South	1848.32	48.41	2.42	0.48	276.64	16.65	-26.71	0.20
190727VM	Shipyard	2019	Rabbit Creek - South	1124.83	16.65	-2.73	0.20	286.07	16.65	-23.19	0.20
140805TP	Allagash (after rain)	2014	Rabbit Creek - South	595.45	16.65	-2.57	0.27	286.52	16.65	-23.58	0.28
170723TS	Monk's CafÃ©	2017	Rabbit Creek - South	-	-	-	-	290.78	16.65	-21.94	0.20
180718TY	Allagash	2018	Rabbit Creek - South	2168.92	20.55	1.12	0.48	300.44	16.65	-22.88	0.29
170723TY	SHIfT Hole	2017	Rabbit Creek - South	2746.92	35.61	-0.56	0.20	317.52	16.65	-25.44	0.20
110710B	Allagash	2011	Rabbit Creek - South	1462.31	20.82	0.57	0.72	343.48	-	-23.84	0.59
160725K	Moose Drool	2016	Rabbit Creek - South	1181.66	13.15	0.78	0.75	348.42	6.66	-24.21	0.26
160725J	Kiltlifter	2016	Rabbit Creek - South	1633.85	42.09	-3.02	0.56	348.42	6.66	-24.21	0.26
140724TF	Monk's CafÃ©	2014	Rabbit Creek - South	564.21	16.65	4.26	0.36	348.60	16.65	-19.45	0.20
110710C	Shipyard	2011	Rabbit Creek - South	1186.37	1.69	-1.95	1.12	353.01	-	-24.19	0.59
180718TB	SHIfT Hole	2018	Rabbit Creek - South	3109.17	56.11	-2.61	0.22	355.89	16.65	-25.95	0.29
180718TC	Kiltlifter	2018	Rabbit Creek - South	2084.53	43.70	-0.33	0.26	358.76	16.65	-25.74	0.29
190727VO	Shift Hole	2019	Rabbit Creek - South	3113.26	10.80	-2.18	0.21	379.40	16.65	-25.85	0.20
170723TZ	Moose Drool	2017	Rabbit Creek - South	1344.12	16.65	3.32	0.42	392.54	16.65	-23.35	0.20
140724TB	SHIfT Hole	2014	Rabbit Creek - South	3085.52	41.97	-2.97	0.20	392.95	16.65	-25.09	0.36
140724TD	Moose Drool	2014	Rabbit Creek - South	1250.98	22.67	-2.59	0.22	395.13	22.96	-23.44	0.20

Sample ID	Sample Location	Year	Sampling area	DIC (µM)	DIC (µM) Std Dev	DIC δ13C VPDB (‰)	DIC Std Dev (‰)	DOC (µM)	DOC (µM) Std Dev	DOC δ13C VPDB (‰)	DOC Std Dev (‰)
140730TG	Monk's CafÃ©	2014	Rabbit Creek - South	3084.61	16.65	-1.96	0.27	395.22	16.65	-20.10	0.31
110710Y	Moose Drool Pool	2011	Rabbit Creek - South	1001.85	4.96	-2.97	0.77	440.73	-	-22.64	-
110720D1	Mr. Toad	2011	Rabbit Creek - South	1858.12	5.08	-2.67	0.29	471.78	-	-19.18	-
170723TX	Big Filter	2017	Rabbit Creek - South	255.25	6.66	3.74	0.44	-	-	-	-
090803UA	Spitting Cobra	2009	Rabbit Creek - South	1410.07	42.30	2.96	0.16	-	-	-	-
150719F	Spitting Cobra	2015	Rabbit Creek - South	1426.29	16.65	3.88	0.42	-	-	-	-
150719E	Ironfist	2015	Rabbit Creek - South	39.97	16.65	-	-	-	-	-	-
090724PA	Mound Spring Source	2009	Sentinel Meadows	2659.48	53.19	-2.44	0.20	17.03	1.29	-22.72	0.56
090724T1	Flat Cone Spring Source	2009	Sentinel Meadows	4590.13	91.80	-2.22	0.20	18.06	1.37	-17.83	0.56
150729H	Bison Mouth Waterfall	2015	Sentinel Meadows	5585.91	167.88	0.30	0.26	20.79	16.65	-25.08	0.20
120716DD	Bison Pool	2012	Sentinel Meadows	5467.23	146.21	-0.91	0.44	29.40	-	-	-
140725SH	Mound Source	2014	Sentinel Meadows	2710.87	49.70	-2.31	0.23	31.84	16.65	-25.91	0.31
120717DX	Mound Spring	2012	Sentinel Meadows	2788.41	90.16	-3.50	0.48	32.20	3.47	-22.52	0.21
120720DC	Bison Pool	2012	Sentinel Meadows	5541.44	208.43	-0.81	0.60	32.33	-	-19.06	-
120712SB	Mound Source	2012	Sentinel Meadows	2765.34	62.98	-3.52	0.60	33.64	3.47	-25.69	0.21
120720DD	Bison Pool	2012	Sentinel Meadows	5704.21	126.10	-0.96	0.60	34.10	-	-19.40	-
120714DC2	Bison Pool	2012	Sentinel Meadows	5407.48	168.09	-0.65	0.44	34.44	-	-18.77	-
090724TA	Iron Pot	2009	Sentinel Meadows	2709.77	54.20	0.58	0.20	36.35	2.75	-21.91	0.56
110716E	Bison Pool Source corresponds to 110712E, 110713E	2011	Sentinel Meadows	5548.68	165.18	-1.70	0.23	36.52	-	-19.61	-

Sample ID	Sample Location	Year	Sampling area	DIC (µM)	DIC (µM) Std Dev	DIC δ13C VPDB (‰)	DIC Std Dev (‰)	DOC (µM)	DOC (µM) Std Dev	DOC δ13C VPDB (‰)	DOC Std Dev (‰)
120720DB	Bison Pool	2012	Sentinel Meadows	5313.98	397.78	-0.79	0.60	36.81	-	-19.74	-
090724M1	Bison Source	2009	Sentinel Meadows	5646.66	112.93	0.19	0.20	37.47	2.83	-21.06	0.56
140730SL	Bison Source	2014	Sentinel Meadows	5576.77	43.83	0.29	0.20	40.52	16.65	-24.66	0.28
JRH110720H	Bison Pool Source	2011	Sentinel Meadows	5559.47	107.99	-1.87	0.56	40.94	-	-24.09	-
120714DC1	Bison Pool	2012	Sentinel Meadows	5459.83	113.29	-0.70	0.44	41.82	9.99	-20.39	0.60
120716DE	Bison Pool	2012	Sentinel Meadows	5360.93	60.27	-0.99	0.44	46.42	9.99	-21.44	0.60
180712SD	Bison Source	2018	Sentinel Meadows	5486.57	103.76	1.47	0.22	46.50	16.65	-26.51	0.29
120714DE2	Bison Pool	2012	Sentinel Meadows	5630.79	96.17	-0.96	0.44	46.95	9.99	-21.46	0.60
120714DE1	Bison Pool	2012	Sentinel Meadows	5635.09	124.71	-0.99	0.44	52.96	9.99	-21.21	0.60
130718DE	Mound Spring Source	2013	Sentinel Meadows	2641.95	16.65	-2.98	0.64	56.02	-	-23.42	0.40
120720DE	Bison Pool	2012	Sentinel Meadows	5678.24	158.91	-1.14	0.60	57.58	9.99	-21.15	0.60
060807E	Mound Source	2006	Sentinel Meadows	2539.39	58.33	-2.95	0.05	58.08	1.16	-23.80	0.47
140730SM	Flat Cone	2014	Sentinel Meadows	4167.97	123.60	-1.97	0.20	62.41	16.65	-33.94	0.28
120717DD	Bison Pool	2012	Sentinel Meadows	5685.46	76.32	-0.93	0.60	64.45	9.99	-21.34	0.60
060807B	Bison Source	2006	Sentinel Meadows	5292.76	83.02	-0.20	0.12	66.91	1.34	-23.23	0.47
060812B	Bison Source, Shallow	2006	Sentinel Meadows	5300.01	68.51	-0.15	0.08	68.28	2.58	-20.63	1.00
120716DE2	Bison Pool	2012	Sentinel Meadows	5559.00	151.98	-1.02	0.44	71.52	9.99	-22.12	0.60
060812A	Steep Cone Source	2006	Sentinel Meadows	4419.28	59.85	-1.64	0.12	74.43	2.81	-20.17	1.00
060807C	Flatcone Source	2006	Sentinel Meadows	4326.63	87.01	-2.66	0.20	81.77	1.72	-25.53	0.39
060812C	Iron Pot	2006	Sentinel Meadows	2497.53	31.12	0.32	0.01	85.93	3.24	-25.56	0.15
070711B	Mound Cone Source	2007	Sentinel Meadows	2610.58	54.48	-3.46	0.48	96.98	2.00	-26.14	0.13

Sample ID	Sample Location	Year	Sampling area	DIC (µM)	DIC (µM) Std Dev	DIC δ13C VPDB (‰)	DIC Std Dev (‰)	DOC (µM)	DOC (µM) Std Dev	DOC δ13C VPDB (‰)	DOC Std Dev (‰)
160715K	Cole's Coffee	2016	Sentinel Meadows	509.51	16.65	-21.40	0.49	102.08	6.66	-27.95	0.20
160715JN4	Sentinal Spring 3	2016	Sentinel Meadows	609.15	6.66	-10.56	0.38	102.08	6.66	-27.95	0.20
070710I	Bison Source	2007	Sentinel Meadows	5441.77	32.30	-0.48	0.42	117.92	3.41	-23.65	0.41
110712E	Bison Pool at edge of Source	2011	Sentinel Meadows	5275.06	86.97	-1.75	0.20	123.85	-	-25.12	1.39
100808HA	Milk Chocolate	2010	Sentinel Meadows	194.94	4.25	-4.76	0.78	606.40	15.01	-23.38	0.24
190718ZB	Milk Chocolate	2019	Sentinel Meadows	710.51	16.65	-5.42	0.20	912.95	16.65	-25.57	0.20
100808IA	Special Dark	2010	Sentinel Meadows	2333.37	33.04	-1.87	0.28	1275.20	41.63	-28.21	0.32
160715G	Special Dark	2016	Sentinel Meadows	-	-	-	-	2101.62	111.95	-25.77	0.39
190718ZD	Special Dark	2019	Sentinel Meadows	412.90	16.65	-13.89	0.20	2917.45	114.19	-26.63	0.20
150729D	Mound Spring	2015	Sentinel Meadows	2697.66	99.84	-2.31	0.26	-	-	-	-
150729F	Flat Cone	2015	Sentinel Meadows	4599.54	140.80	-2.15	0.26	-	-	-	-
150729E	Steep Cone	2015	Sentinel Meadows	4760.06	123.19	-1.57	0.26	-	-	-	-
150717A	Colony Flats	2015	Sentinel Meadows	5679.30	75.71	0.24	0.26	-	-	-	-
090730ZA	The Dryer	2009	Sylvan	560.85	17.07	2.82	0.40	17.25	1.38	-	-
090730WA	Evening Primrose	2009	Sylvan	772.56	23.18	1.15	0.16	22.45	1.80	-	-
190729ZB	Tidepool	2019	Sylvan	9060.03	61.75	1.29	0.20	26.45	16.65	-26.48	0.20
110715S	The Dryer	2011	Sylvan	-	-	-	-	28.58	-	-18.74	-
180723TZ	The Dryer	2018	Sylvan	30.14	16.65	-22.04	0.20	32.12	16.65	-22.31	0.20
160721Q	The Dryer	2016	Sylvan	38.88	16.65	1.10	0.59	32.68	6.66	-20.32	0.29
190729ZA	The Dryer	2019	Sylvan	-	-	-	-	34.02	16.65	-22.50	0.20
120721TB	Evening Primrose	2012	Sylvan	1473.31	16.65	-1.37	0.48	36.64	-	-12.93	-
090730YA	Sylvan Spring	2009	Sylvan	1609.09	48.27	0.18	0.16	36.97	2.96	-	-

Sample ID	Sample Location	Year	Sampling area	DIC (µM)	DIC (µM) Std Dev	DIC δ13C VPDB (‰)	DIC Std Dev (‰)	DOC (µM)	DOC (µM) Std Dev	DOC δ13C VPDB (‰)	DOC Std Dev (‰)
120722SN	The Dryer	2012	Sylvan	743.64	-	6.67	-	37.21	3.47	-24.52	0.21
100730GA	The Dryer	2010	Sylvan	972.10	20.27	2.66	0.25	38.57	-	-21.10	-
140731SV	The Dryer	2014	Sylvan	-	-	-	-	38.99	16.65	-19.50	0.28
180723TX	Burning Eye	2018	Sylvan	185.34	16.65	-7.70	0.20	43.26	16.65	-23.07	0.20
110715L	Avocado Source	2011	Sylvan	8407.54	17.87	-2.26	0.16	43.73	-	-13.82	1.06
160717U	Evening Primrose	2016	Sylvan	1971.93	47.31	-1.28	0.28	45.88	6.66	-18.13	0.26
190720ZL	Sylvan Spring	2019	Sylvan	2112.64	5.98	-0.79	0.42	51.50	3.33	-19.01	0.20
190720ZK	Burning Eye	2019	Sylvan	99.53	16.65	-3.82	0.30	55.09	3.33	-22.01	0.20
170720SK	Evening Primrose	2017	Sylvan	1811.06	1.97	0.63	0.29	56.50	8.33	-18.37	0.20
110715U	Sylvan Spring	2011	Sylvan	3511.64	10.97	-4.34	0.20	59.20	-	-7.38	1.06
100730FA	Sylvan Spring	2010	Sylvan	2555.20	30.77	-1.35	0.21	60.09	7.43	-17.41	1.17
050721P	Avocado Pool	2005	Sylvan	9357.51	114.16	-0.54	0.27	60.44	1.30	-18.80	1.31
190720ZO	Evening Primrose	2019	Sylvan	1829.31	7.22	-0.92	0.42	60.59	3.33	-16.49	0.20
090730W1	Gunter's Fancy	2009	Sylvan	1316.85	39.51	-0.55	0.16	60.65	4.85	-	-
170720SO	Burning Eye	2017	Sylvan	147.05	6.66	1.17	0.44	60.94	16.65	-19.34	0.20
160721P	Little Red Head	2016	Sylvan	86.93	16.65	-6.18	0.49	60.99	6.66	-15.00	0.26
170716TR	Avocado	2017	Sylvan	9110.48	348.76	1.07	0.26	63.06	16.65	-21.13	0.20
170720SM	Sylvan Spring	2017	Sylvan	2678.11	39.52	0.28	0.24	63.89	16.65	-18.24	0.20
060805L	Avocado Source	2006	Sylvan	7907.45	101.56	-0.03	0.14	64.03	1.28	-21.07	0.47
110715Q	Roman Bath	2011	Sylvan	578.02	-	0.10	-	64.57	-	-16.35	1.06
100730HA	Go Bears!	2010	Sylvan	1260.99	32.95	-0.03	0.25	65.33	7.43	-25.90	1.17
100730KA	Roman Bath	2010	Sylvan	350.48	1.75	-3.34	0.27	69.26	7.43	-19.12	1.17
190729ZW	Avocado	2019	Sylvan	9740.63	214.23	0.66	0.42	69.28	3.33	-21.73	0.20
190720ZN	Roman Bath	2019	Sylvan	791.08	16.65	-3.55	0.30	71.25	3.33	-18.23	0.20
090730XA	Lobster Claw	2009	Sylvan	244.12	12.21	-2.15	0.54	71.33	5.71	-	-

Sample ID	Sample Location	Year	Sampling area	DIC (µM)	DIC (µM) Std Dev	DIC δ13C VPDB (‰)	DIC Std Dev (‰)	DOC (µM)	DOC (µM) Std Dev	DOC δ13C VPDB (‰)	DOC Std Dev (‰)
160721N	Avocado	2016	Sylvan	6339.16	128.35	0.88	0.21	71.67	6.66	-17.36	0.26
120722SO	Avocado	2012	Sylvan	7143.01	115.79	-0.59	0.44	74.87	4.26	-14.47	0.39
120721TA	Gunter's Fancy	2012	Sylvan	1464.81	13.32	-1.93	0.29	75.38	10.12	-17.64	0.41
140802TW	Evening Primrose	2014	Sylvan	1759.94	23.99	-1.28	0.23	75.57	16.65	-17.38	0.31
110715N	Danny Boy	2011	Sylvan	1653.35	62.02	-4.55	0.67	80.56	-	-19.38	0.82
160717X	Roman Bath	2016	Sylvan	371.64	16.65	-4.19	0.49	82.37	6.66	-19.99	0.29
140731ST	Go Bears!	2014	Sylvan	3072.68	45.83	-2.84	0.23	84.62	16.65	-22.75	0.20
090730X1	Barfing Boulder	2009	Sylvan	458.59	22.93	-3.44	0.54	85.57	6.85	-	-
120721TC	Go Bears!	2012	Sylvan	2163.13	41.28	-3.64	0.29	85.62	9.99	-22.54	0.60
150718FE	Sylvan Spring	2015	Sylvan	2506.14	39.16	-1.02	0.26	87.38	16.65	-15.33	0.20
190720ZM	Lobster Claw	2019	Sylvan	308.76	16.65	-3.22	0.30	87.44	16.65	-17.49	0.22
090730VA	Go Bears!	2009	Sylvan	814.19	24.43	-2.65	0.19	89.41	7.15	-	-
130721SF	Rice Milk (Little Read Head)	2013	Sylvan	-	-	-	-	89.84	-	-16.37	0.24
090730UA	Lil' Hottie	2009	Sylvan	65.67	3.28	-2.31	0.54	90.64	7.25	-	-
090730TA	Acid Pants	2009	Sylvan	307.67	15.38	-2.13	0.54	91.87	7.35	-	-
130714TU	Goldilocks Source	2013	Sylvan	3262.40	24.30	-4.75	0.58	93.98	-	-23.77	0.23
140802TT	Lil' Red Head	2014	Sylvan	130.97	16.65	-1.07	0.38	95.54	16.65	-14.45	0.20
120721TW	Goldilocks Source	2012	Sylvan	2300.70	40.53	-5.01	0.44	96.86	9.99	-23.98	0.60
100805GA	Goldilocks Source	2010	Sylvan	2787.62	9.06	-3.61	0.27	98.68	7.43	-26.66	1.17
110715T	Go Bears!	2011	Sylvan	938.19	27.74	-1.64	0.20	99.17	-	-24.11	0.82
150718FC	Little Red Head	2015	Sylvan	222.62	16.65	-16.61	0.47	99.67	16.65	-18.16	0.20
190729ZY	Goldielocks	2019	Sylvan	7170.00	76.50	-2.64	0.20	99.72	16.65	-24.22	0.20
JRH110715Y	Goldilocks Source	2011	Sylvan	5730.95	69.12	-5.49	0.20	101.14	-	-25.28	-
160721R	Goldilocks	2016	Sylvan	4123.28	60.24	-3.23	0.21	101.30	6.66	-26.56	0.26

Sample ID	Sample Location	Year	Sampling area	DIC (µM)	DIC (µM) Std Dev	DIC δ13C VPDB (‰)	DIC Std Dev (‰)	DOC (µM)	DOC (µM) Std Dev	DOC δ13C VPDB (‰)	DOC Std Dev (‰)
050721K	Sylvan Spring	2005	Sylvan	3092.00	41.74	-1.45	0.08	103.41	2.22	-18.07	0.62
180723TU	Roman Bath	2018	Sylvan	-	-	-	-	107.68	16.65	-20.42	0.20
100809I1	Danny Boy	2010	Sylvan	1301.47	32.23	-3.54	0.27	108.26	7.43	-22.01	1.17
090730U1	Goldilocks Source	2009	Sylvan	-	-	-	-	108.98	8.72	-	-
060805K	Goldilocks Source	2006	Sylvan	5689.32	40.62	-4.62	0.07	109.16	4.12	-22.13	0.15
050721M	Goldielocks Source	2005	Sylvan	2689.53	101.66	-3.86	0.14	109.73	2.36	-25.02	0.57
140731SU	Avocado	2014	Sylvan	8229.03	185.26	-0.04	0.20	114.81	16.65	-19.46	0.28
160721O	Little Hottie	2016	Sylvan	191.48	16.65	-5.05	0.49	117.56	6.66	-14.56	0.26
160717V	Sylvan Spring	2016	Sylvan	2424.52	41.75	-0.67	0.28	119.94	6.66	-13.27	0.26
170716TS	Gunter's Fancy	2017	Sylvan	1145.39	34.37	-0.51	0.25	120.47	16.65	-20.40	0.20
120722SM	Roman Bath	2012	Sylvan	182.68	16.65	-4.64	0.61	120.63	10.12	-20.72	0.41
140731SW	Gunter's Fancy	2014	Sylvan	2541.19	85.84	-2.15	0.20	121.65	16.65	-20.84	0.20
180723TW	Lobster Claw	2018	Sylvan	-	-	-	-	123.02	16.65	-20.08	0.20
170720SN	Lobster Claw	2017	Sylvan	516.48	6.66	-0.70	0.44	123.12	16.65	-17.77	0.20
160721JN5	Sylvan Stream	2016	Sylvan	-	-	-	-	124.08	6.66	-27.97	0.20
110715K	Lobster Claw	2011	Sylvan	651.12	-	0.07	-	124.63	-	-15.67	1.06
180723TY	Sylvan Spring	2018	Sylvan	2498.18	60.47	1.09	0.22	126.30	16.65	-13.24	0.29
090730C1	Blondie Source	2009	Sylvan	-	-	-	-	126.65	10.13	-	-
070714D	Evening Primrose	2007	Sylvan	2097.19	23.50	-4.30	1.01	127.43	44.43	-21.49	1.46
120722SP	Sylvan Spring	2012	Sylvan	2127.69	26.64	-2.47	0.60	127.57	10.12	-14.26	0.41
140802TR	Little Hottie	2014	Sylvan	109.40	16.65	0.08	0.91	134.57	16.65	-12.95	0.28
110715W	Little Hottie	2011	Sylvan	205.57	-	-2.87	0.88	136.60	-	-16.44	0.82
170716TT	Goldilocks Source	2017	Sylvan	6872.46	90.81	-1.91	0.24	137.00	16.65	-23.88	0.20
120722SK	Little Hottie	2012	Sylvan	113.13	3.76	-3.66	0.74	143.51	10.12	-15.33	0.41
140731SX	Blondie Fringe	2014	Sylvan	4930.65	99.92	-2.77	0.20	144.76	16.65	-23.98	0.28

Sample ID	Sample Location	Year	Sampling area	DIC (µM)	DIC (µM) Std Dev	DIC δ13C VPDB (‰)	DIC Std Dev (‰)	DOC (µM)	DOC (µM) Std Dev	DOC δ13C VPDB (‰)	DOC Std Dev (‰)
050721N	Burning Eye	2005	Sylvan	719.01	45.23	-3.77	0.02	146.70	3.15	-21.24	0.38
120721TY	River Styx	2012	Sylvan	-	-	-	-	150.76	9.99	-20.79	0.60
190720ZJ	Acid Pants	2019	Sylvan	744.17	16.65	-3.37	0.20	151.44	16.65	-10.98	0.20
190729ZX	Blondie	2019	Sylvan	6875.98	9.47	-2.27	0.20	157.49	16.65	-26.92	0.20
140802TX	Goldilocks	2014	Sylvan	7235.40	207.59	-3.14	0.20	159.20	16.65	-28.47	0.20
160717T	Lobster Claw	2016	Sylvan	177.89	16.65	-4.45	0.49	159.25	6.66	-20.70	0.26
140802TS	Acid Pants	2014	Sylvan	-	-	-	-	163.71	16.65	-8.59	0.28
KF120721L	GoldiStyx Myx	2012	Sylvan	600.73	16.65	-4.15	0.29	172.21	9.99	-22.58	0.60
180723TV	Acid Pants	2018	Sylvan	205.28	16.65	-4.50	0.20	176.30	16.65	-10.35	0.20
070714C	Goldielocks Source	2007	Sylvan	7516.32	109.31	-0.95	0.37	179.31	97.59	-22.48	0.83
190729ZZ	Gunter's Fancy	2019	Sylvan	1385.39	16.65	-2.03	0.20	180.92	16.65	-19.88	0.20
110715O	Blondie	2011	Sylvan	3622.20	116.35	-5.00	0.31	183.45	-	-25.90	0.82
150718FF	Lobster Claw	2015	Sylvan	107.98	16.65	-	-	187.82	16.65	-20.87	0.20
060810T	Lobster Claw	2006	Sylvan	559.82	2.07	-4.57	0.19	190.93	3.82	-22.99	0.47
140802TV	Sylvan Spring	2014	Sylvan	2379.82	43.02	-1.35	0.20	201.41	16.65	-14.76	0.31
160717W	Go Bears	2016	Sylvan	2641.54	34.58	-3.01	0.28	202.98	6.66	-23.28	0.26
100805CA	River Styx, before Goldistyx myx	2010	Sylvan	552.71	5.98	-1.90	0.34	210.93	7.43	-19.91	1.17
120722SL	Lobster Claw	2012	Sylvan	523.00	15.11	-4.27	0.29	214.60	9.99	-21.16	0.60
140731SY	Biting Moth	2014	Sylvan	-	-	-	-	218.88	16.65	-10.25	0.28
160721S	Acid Pants	2016	Sylvan	293.30	6.66	-4.05	0.76	218.92	6.66	-8.05	0.26
140731SS	Acid Pants	2014	Sylvan	494.33	16.65	-3.56	0.27	224.33	16.65	-10.09	0.28
170716TU	Lil' Hottie	2017	Sylvan	128.19	6.66	0.76	0.44	248.54	16.65	-17.46	0.20
090730Y1	3 Bears - Water (pool 'B')	2009	Sylvan	-	-	-	-	295.19	23.62	-	-
130714TY	River Styx	2013	Sylvan	518.93	-	-0.23	0.54	295.55	-	-16.44	0.32

Sample ID	Sample Location	Year	Sampling area	DIC (µM)	DIC (µM) Std Dev	DIC δ13C VPDB (‰)	DIC Std Dev (‰)	DOC (µM)	DOC (µM) Std Dev	DOC δ13C VPDB (‰)	DOC Std Dev (‰)
170720SP	Go Bears!	2017	Sylvan	5164.93	149.95	-1.84	0.20	312.43	16.65	-23.52	0.20
100805KA	Sulfur Island	2010	Sylvan	134.92	0.63	-	-	350.44	8.66	-12.51	0.24
130714TZ	Nap Cap	2013	Sylvan	1298.62	72.97	-3.75	0.99	419.03	-	-22.95	0.46
120722SQ	Peaceful Pool	2012	Sylvan	-	-	-	-	615.62	-	-19.32	-
140802TU	Lobster Claw	2014	Sylvan	648.14	65.69	-3.15	0.28	667.02	16.65	-24.36	0.20
170716TQ	Blondie Zygo Mat	2017	Sylvan	3083.28	90.52	-0.68	0.27	1129.14	16.65	-19.29	0.20
090730T1	Avocado Source	2009	Sylvan	7830.50	313.22	1.27	0.18	-	-	-	-
090801O1	Sulfur Creek	2009	Washburn	-	-	-	-	135.40	10.24	-24.60	0.56
190729VB	Rastaman	2019	Washburn	40.52	16.65	-9.11	0.20	175.23	16.65	-18.97	0.22
190729VY	Mutinous Member	2019	Washburn	8075.77	16.65	1.54	0.24	180.15	16.65	-20.11	0.20
190729VZ	Toe Beanzzz	2019	Washburn	731.67	7.49	-1.84	0.64	185.79	3.33	-16.32	0.20
050723H	Rastaman	2005	Washburn	102.57	4.42	-10.16	0.62	200.23	4.31	-17.87	0.37
130714SX	Rastaman	2013	Washburn	58.03	-	-4.87	0.54	202.19	-	-18.07	0.23
110711P	Emerald City	2011	Washburn	605.84	39.32	-	-	235.46	3.71	-15.48	1.06
060809B	Boomerang	2006	Washburn	262.68	6.66	-6.76	0.15	238.16	11.91	-13.19	0.41
190729VX	Emerald City	2019	Washburn	336.86	16.65	-5.78	0.20	241.33	16.65	-17.44	0.22
120717SC	Lion's Den	2012	Washburn	236.30	16.65	-2.27	0.37	261.05	16.65	-18.75	0.37
130714SY	Boomerang	2013	Washburn	737.69	18.04	-3.09	0.50	269.79	16.65	-15.28	0.32
120719TQ	Boomerang	2012	Washburn	722.27	17.24	-2.72	0.29	277.31	16.65	-16.83	0.37
110711H	Lion's Den	2011	Washburn	419.41	-	2.43	1.06	294.44	5.49	-21.08	0.60
120719TU	Mutinous Member	2012	Washburn	467.48	5.14	5.00	0.80	300.94	1.87	-17.56	0.66
190729VA	Boomerang	2019	Washburn	686.74	16.65	-3.52	0.20	301.44	16.65	-16.08	0.22
110711F	Triceratops	2011	Washburn	1586.29	46.39	-2.38	0.20	301.62	2.87	-22.26	0.60
050723E	Boomerang	2005	Washburn	929.65	14.50	-2.84	0.15	311.38	3.18	-11.73	0.17
120719TS	Top Olympics	2012	Washburn	1073.54	-	-	-	332.27	1.87	-16.25	0.66
120719TT	Muddy Blister	2012	Washburn	275.70	5.06	-2.32	0.49	338.64	16.65	-17.14	0.37

Sample ID	Sample Location	Year	Sampling area	DIC (µM)	DIC (µM) Std Dev	DIC δ13C VPDB (‰)	DIC Std Dev (‰)	DOC (µM)	DOC (µM) Std Dev	DOC δ13C VPDB (‰)	DOC Std Dev (‰)
090801N1	Lion's Den	2009	Washburn	162.44	4.87	-0.62	0.78	355.22	19.85	-15.16	0.28
110711M	Boomerang	2011	Washburn	764.20	15.52	-4.32	0.21	359.44	2.46	-17.32	0.60
110711E	FLIP	2011	Washburn	912.82	23.34	-	-	366.06	5.14	-23.84	0.60
110711N	Van Gogh	2011	Washburn	344.49	-	-3.58	0.73	371.94	9.64	-13.98	0.60
120717SE	Triceratops	2012	Washburn	1183.84	21.95	-0.20	0.29	391.10	16.65	-21.41	0.37
180724SI	Just the Tip	2018	Washburn	2477.11	16.65	1.45	0.20	391.46	16.65	-22.94	0.22
180724SJ	Steamy Windows	2018	Washburn	975.32	16.65	-0.96	0.44	399.36	16.65	-14.30	0.20
180724SH	Jackson's Tub-o-Luv	2018	Washburn	927.46	18.13	0.03	0.47	403.37	16.65	-17.28	0.29
090726JA	Boomerang	2009	Washburn	451.14	13.53	-1.42	0.16	411.71	8.23	-15.73	0.13
120719TR	Emerald City	2012	Washburn	808.91	24.13	-5.74	0.29	416.44	16.65	-19.38	0.37
070708J	Boomerang	2007	Washburn	726.47	64.13	-4.77	0.77	422.49	23.70	-15.44	1.30
190721VQ	Triceratops	2019	Washburn	1553.29	60.59	-1.13	0.70	434.07	16.65	-20.89	0.22
130714SZ	Mr. Pickles	2013	Washburn	414.60	-	-0.17	0.69	456.16	16.65	-14.93	0.32
190721VS	Jackson's Tub O' Luv	2019	Washburn	1214.59	10.87	-1.27	0.96	459.85	46.74	-19.71	0.30
180724SG	Mr. Clean	2018	Washburn	6705.31	62.58	0.77	0.22	479.99	16.65	-23.56	0.29
050723G	Chest High Pool	2005	Washburn	1954.46	15.05	-2.33	0.06	485.64	9.03	-13.35	0.08
060809E	Emerald City	2006	Washburn	1427.75	11.16	-3.60	0.49	490.68	8.04	-14.47	0.04
180724SF	Triceratops	2018	Washburn	1561.42	21.36	0.78	0.34	496.01	16.65	-21.53	0.29
070708L	Emerald City	2007	Washburn	228.81	18.59	-	-	509.72	43.68	-17.14	1.24
070708K	Clear Eye	2007	Washburn	497.03	18.59	-6.72	1.01	512.87	29.28	-13.98	1.07
190721VT	F.L.I.P.'s Kidney	2019	Washburn	1686.80	16.65	-1.43	0.20	526.39	20.27	-23.74	0.20
050723F	Clear Eye	2005	Washburn	506.62	21.53	-5.29	0.14	526.68	4.06	-11.63	0.01
090726KA	Rastaman	2009	Washburn	104.25	2.08	-	-	530.73	10.61	-21.06	0.13
110711Q	Muddy Blister	2011	Washburn	182.47	23.07	-	-	536.09	-	-11.95	-
190721VR	Mr. Clean	2019	Washburn	5486.88	120.21	0.05	0.42	543.98	17.59	-23.14	0.43

Sample ID	Sample Location	Year	Sampling area	DIC (µM)	DIC (µM) Std Dev	DIC δ13C VPDB (‰)	DIC Std Dev (‰)	DOC (µM)	DOC (µM) Std Dev	DOC δ13C VPDB (‰)	DOC Std Dev (‰)
090726HA	Van Gogh	2009	Washburn	325.18	6.50	-5.10	0.20	546.94	10.94	-12.12	0.13
060809D	Clear Eye	2006	Washburn	382.45	4.30	-5.75	0.20	583.45	0.62	-14.89	0.05
090801J1	Triceratops	2009	Washburn	1135.64	100.11	1.26	0.16	588.54	54.14	-21.34	0.21
050723D	FLIP	2005	Washburn	4336.11	4.77	-0.46	0.27	647.41	6.28	-21.83	0.11
130714SA	Goldfish Bowl	2013	Washburn	496.96	-	1.36	0.69	653.84	-	-26.00	0.50
130718SU	FLIP's Kidney	2013	Washburn	2471.17	42.74	0.13	0.64	824.99	16.65	-24.70	0.32
140727TW	Triceratops	2014	Washburn	996.25	20.24	-0.91	0.20	845.37	16.65	-21.10	0.20
060809A	F.L.I.P.	2006	Washburn	2491.47	7.32	-0.35	0.14	912.52	61.53	-24.41	0.26
070708I	Chest High	2007	Washburn	1962.06	57.69	-5.26	1.01	933.08	11.74	-15.20	0.57
090726IA	Chest High	2009	Washburn	407.49	12.22	-1.63	0.16	955.55	49.93	-15.44	0.31
120717SF	FLIP	2012	Washburn	980.40	21.66	-0.89	0.29	1508.97	16.65	-22.22	0.37
120717SH	Grayson's Ditch of Joy	2012	Washburn	688.11	5.06	5.46	0.49	1649.41	69.52	-22.81	0.53
120717SG	Mr. Clean	2012	Washburn	2859.59	18.81	-3.30	0.60	2085.85	126.39	-23.09	0.71
090801M1	F.L.I.P.	2009	Washburn	865.74	25.97	-0.84	0.80	2384.22	73.49	-22.60	0.13
090801K1	Mr. Clean	2009	Washburn	3738.05	112.14	0.35	0.23	2654.08	53.08	-22.23	0.13
090801L1	Jackson's Tub-O-Luv	2009	Washburn	1641.96	32.84	-3.76	0.20	3537.95	70.76	-20.57	0.13
120717SD	Jackson's Tub-O-Luv	2012	Washburn	1580.21	51.28	-5.30	0.60	3675.48	130.28	-21.32	0.48
140727TU	FLIP Outflow	2014	Washburn	813.03	16.65	-6.25	0.27	4405.14	34.45	-22.78	0.21
140727TV	Mr. Clean	2014	Washburn	2596.41	32.88	-0.74	0.20	4819.66	23.09	-22.72	0.21
140727TT	FLIP	2014	Washburn	1163.71	23.73	-1.76	0.23	-	-	-	-
090725H1	White Creek at crossing spot	2009	White Creek	2305.80	69.17	4.04	0.16	18.48	1.48	-	-
090725K1	Twin Buttes Vista Source	2009	White Creek	3816.14	114.48	-1.39	0.28	18.89	1.51	-	-
090725G1	Log Jam Source	2009	White Creek	5424.98	162.75	-0.13	0.20	19.85	1.59	-	-
160716Q	Octopus Source	2016	White Creek	5293.48	62.72	-1.05	0.21	23.05	6.66	-25.03	0.29

Sample ID	Sample Location	Year	Sampling area	DIC (µM)	DIC (µM) Std Dev	DIC δ13C VPDB (‰)	DIC Std Dev (‰)	DOC (µM)	DOC (µM) Std Dev	DOC δ13C VPDB (‰)	DOC Std Dev (‰)
150725WC	Spent Kleenex	2015	White Creek	4744.19	56.25	0.04	0.26	23.74	16.65	-24.48	0.20
160716O	Log Jam	2016	White Creek	5627.99	23.21	-0.39	0.21	24.35	6.66	-24.76	0.29
160716R	Fallen Log Pool	2016	White Creek	4067.77	20.40	-0.18	0.21	24.69	6.66	-25.85	0.29
190723ZZ	Log Jam	2019	White Creek	5532.08	232.44	0.03	0.20	25.03	16.65	-24.81	0.20
170722ST	Red Sauce	2017	White Creek	3338.87	102.58	2.49	0.21	25.95	16.65	-23.96	0.20
090725X1	Octopus Source	2009	White Creek	4986.84	149.61	-1.03	0.29	27.79	2.22	-	-
170722SV	Horneblend	2017	White Creek	2422.20	12.49	2.00	0.37	28.06	16.65	-25.95	0.20
180724TC	Dead Bird	2018	White Creek	2472.60	90.92	0.88	0.46	29.47	16.65	-27.17	0.20
170722SR	Green Sauce	2017	White Creek	2864.61	74.89	1.89	0.26	29.95	16.65	-26.17	0.20
110717D1	Spent Kleenex	2011	White Creek	4527.95	63.02	-2.09	0.26	30.75	-	-24.24	-
160716M	Spent Kleenex	2016	White Creek	4578.01	57.71	0.16	0.21	32.07	6.66	-25.23	0.29
180717SY	Log Jam	2018	White Creek	5664.03	179.20	0.48	0.22	32.15	16.65	-25.94	0.29
110717C1	Twin Buttes Vista	2011	White Creek	4034.58	17.16	-3.79	0.32	32.17	-	-25.02	-
120715SW	Fern Gully	2012	White Creek	3864.75	46.01	-0.78	0.48	32.60	3.24	-23.04	0.62
170718SC	Bug Cemetery Source	2017	White Creek	5240.72	315.65	-0.17	0.26	33.65	16.65	-25.38	0.42
180724TD	Toad Shoot	2018	White Creek	2361.56	47.11	1.06	0.46	34.42	16.65	-26.69	0.20
180717SX	Par 5	2018	White Creek	4151.35	123.33	-0.71	0.22	34.93	16.65	-26.86	0.29
170718SA	Par 5	2017	White Creek	4206.87	122.83	-1.69	0.26	35.44	16.65	-24.75	0.42
180717SC	Fat Boi	2018	White Creek	5294.70	190.95	0.24	0.23	36.02	16.65	-25.65	0.22
170722SU	Black Hole	2017	White Creek	2214.35	12.49	2.77	0.37	36.22	16.65	-27.11	0.20
120719HE	fallen log surface	2012	White Creek	4142.53	102.24	-1.46	0.60	37.30	-	-24.34	-
151729WF	Spent Kleenex	2015	White Creek	4718.59	65.88	0.13	0.26	37.90	16.65	-25.07	0.20
180724TF	White Creek just above Dead Bird inflow	2018	White Creek	-	-	-	-	38.21	16.65	-24.58	0.20
120715SX	FecToad Skin	2012	White Creek	2043.02	33.93	1.50	0.48	39.62	1.87	-19.98	0.62

Sample ID	Sample Location	Year	Sampling area	DIC (µM)	DIC (µM) Std Dev	DIC δ13C VPDB (‰)	DIC Std Dev (‰)	DOC (µM)	DOC (µM) Std Dev	DOC δ13C VPDB (‰)	DOC Std Dev (‰)
170722SS	Purple Drink	2017	White Creek	1928.23	12.49	1.68	0.37	40.19	16.65	-25.62	0.20
060806R	Octopus Source	2006	White Creek	5143.77	52.54	-1.42	0.05	46.61	0.98	-25.22	1.00
120719HC	spindle geyser-surface	2012	White Creek	4434.62	59.18	0.98	0.53	50.99	1.87	-24.25	0.66
120715SU	Shot Drop	2012	White Creek	5719.78	149.35	1.52	0.48	55.80	3.24	-21.33	0.62
130720DQ	Log Jam	2013	White Creek	5448.63	109.16	-1.21	0.64	57.72	-	-22.79	0.40
180724TB	Purple Drink	2018	White Creek	2022.55	60.47	2.49	0.23	57.84	16.65	-27.41	0.29
180717SZ	Spent Kleenex	2018	White Creek	4567.09	150.23	1.27	0.22	68.35	16.65	-27.11	0.29
120715SY	Spent Kleenex	2012	White Creek	4690.18	123.61	-1.27	0.60	71.55	4.26	-22.06	0.39
120715SV	White Creek Scum	2012	White Creek	2355.98	72.00	0.57	0.48	76.26	3.24	-22.13	0.62
060809 IV	'Beal'	2006	White Creek	3764.50	100.49	-0.22	0.16	98.81	3.73	-23.35	0.15
060809 V	Spent Kleenex	2006	White Creek	4443.93	108.77	0.13	0.05	102.75	3.88	-22.72	0.15
120719HD	fallen log deep 2	2012	White Creek	4126.90	133.13	-1.52	0.60	125.25	10.12	-27.60	0.41
120719HB	spindle geyser- deep	2012	White Creek	3968.76	57.02	1.03	0.53	140.16	1.87	-26.59	0.66
070706A	Octopus Source	2007	White Creek	5273.39	21.65	-1.80	0.21	157.66	3.41	-25.97	0.41
190723ZY	Bug Heaven	2019	White Creek	4417.78	131.37	0.38	0.20	294.83	16.65	-25.51	0.20
090725B1	Par 5 Source	2009	White Creek	3907.17	117.22	-1.92	0.51	-	-	-	-
190723ZW	Par 5	2019	White Creek	4126.37	148.17	-1.40	0.20	-	-	-	-
150725WE	Par 5	2015	White Creek	4162.60	132.15	-1.84	0.26	-	-	-	-
150729WH	Par 5	2015	White Creek	4170.12	87.07	-1.91	0.26	-	-	-	-
130720DR	Spent Kleenex 40cm from mouth of outflow	2013	White Creek	4337.22	67.43	-0.50	0.64	-	-	-	-
090725Z1	Spent Kleenex Source	2009	White Creek	4626.53	92.53	0.01	0.20	-	-	-	-
190723ZV	Bug Cemetery	2019	White Creek	4684.48	217.08	-0.74	0.20	-	-	-	-
170718SZ	Spent Kleenex	2017	White Creek	4695.64	166.83	0.34	0.26	-	-	-	-

Sample ID	Sample Location	Year	Sampling area	DIC (µM)	DIC (µM) Std Dev	DIC δ13C VPDB (‰)	DIC Std Dev (‰)	DOC (µM)	DOC (µM) Std Dev	DOC δ13C VPDB (‰)	DOC Std Dev (‰)
150729WI	Bug Cemetary	2015	White Creek	5207.48	72.63	-0.44	0.26	-	-	-	-
170718SY	Octopus Pink	2017	White Creek	5270.55	157.52	-0.90	0.26	-	-	-	-
150725WD	Bug Cemetary	2015	White Creek	5317.84	83.03	-0.41	0.26	-	-	-	-
170718SX	Octopus Beige	2017	White Creek	5409.56	221.18	-0.74	0.26	-	-	-	-
150725WB	Log Jam	2015	White Creek	5708.57	20.88	-0.45	0.26	-	-	-	-
150729WG	Log Jam	2015	White Creek	5866.04	37.61	-0.94	0.26	-	-	-	-